CONFORMATIONAL EQUILIBRIA OF RENIN INHIBITORY PEPTIDES IN SOLUTION.

by

GRAEME JAMES ANDERSON

A thesis submitted in partial fullfillment of the requirements for the degree of

DOCTOR OF PHILOSOPHY

at the

University of London

1989

Abstract

Linear peptides exhibit a wide range of conformations in solution at room temperature, all or none of which may be important in receptor recognition. Resolving these conformations may be a first step towards understanding which conformation(s) is important for binding to receptors, and can lead to the synthesis of more potent conformationally constrained analogues. Spectroscopic methods were used to investigate the conformations adopted by Renin Inhibitory Peptide (RIP), a linear inhibitor of the enzyme renin; renin is an important factor in the regulation of blood pressure, and an attractive target for antihypertensive therapy.

Circular dichroism spectra were recorded as a function of solvent polarity, pH, salt concentration and temperature. The low temperature spectra in particular, were useful in resolving the conformational equilibrium - at the lowest temperatures recorded cis amide Pro bonds were 'frozen out'. The room temperature CD spectrum was found, by solvent titrations, to exist as a mixture of two predominant conformations, with cis and trans Pro bonds, the percentage of each conformational component varying as a function of solvent polarity.

^{1}H NMR studies were used to further define the conformational components of RIP in solution. Assignments were made in the same

solvents in which CD spectra were recorded, and structural and 2-D NMR chemical exchange information interpreted in the light of CD results. Low temperature spectra were recorded to attempt to 'freeze out' cis peptide bonds.

Energy minimisation and molecular dynamics routines were used to further refine the structures adopted by RIP, based on NMR distance constraints.

Overall, the results were consistent with RIP existing as two predominant conformations in equilibruim with one another. This equilibrium was slow relative to the NMR timescale which allowed both conformations to be resolved and the structures of each determined. The low temperature CD studies were crucial for interpretation of the data and can be used quite generally for resolving the conformational components of small flexible peptides.

Table of contents

This thesis is dedicated to my mother and father, in the hope that in some small way, it will go towards repaying them the great debt I owe them.

Acknowledgements

I am grateful to my supervisor Professor William A Gibbons for his encouragement, stimulating ideas and support throughout the course of my Ph.D.

I am also especially indebted to Colin James and Dr's Paolo Mascagni and Rino Esposito for their guidance and useful dicussions which helped the project get off the ground.

My fellow students Cali Hyde and Rita Lim have been a constant source of good humour and helped put the setbacks into perspective. Dr Rita Lim also helped in the proof reading, for which I am especially grateful.

Mrs Gill Patterson has my admiration and great appreciation for the cheerful way in which she handled the many troubles I gave her during the typing of this thesis.

My girlfriend Yvonne has helped to keep me sane (!), cheerful, and made the difficult times seems that little bit better. My parents deserve special credit for the unwavering support and love they have shown me.

Chapter 1

Introduction

1.1 Hypertension and mechanisms of blood pressure control.

Research over the last few decades has elucidated the mechanisms by which blood pressure control is exerted via different neural, renal, vascular and hormonal pathways (W.H. Birkenhager and J.L. Reid, 1984). A number of mechanisms control blood pressure directly by reacting to changes in arterial pressure. Reflex signals are then sent to the heart and vasculature to return pressure to original levels. Other mechanisms exert control by more indirect methods.

Neural mechanisms of blood presure control involve several pathways, mostly using the autonomic nervous system. The sino aortic baroreceptor reflex is the most important of these neural pathways. Stretch-sensitive receptors detect a change in arterial blood pressure, which results in changes of nerve impulse firing patterns. This information is then transferred to the central nervous system (CNS), where it is processed and acted upon accordingly.

The cardiopulmonary baroreceptor reflex, using so-called 'low-pressure' receptors has its mode of action by sensing the 'degree of filling' of the circulation. The chemoreceptor reflex detects changes in blood oxygen and carbon dioxide concentrations. The CNS ischemic reflex is only activated when blood flow drops to a critical level, and rapidly returns blood pressure to normal.

A number of hormonal mechanisms regulate blood pressure.

Adrenal catecholamines (eg. adrenalin, noradrenaline) act as circulating vasoconstrictor agents, and higher than normal concentrations have been cited in several studies of hypertensive agents. (R. Franco-Morselli et al, 1977).

Another endocrine mechanism is anti-diuretic hormone (ADH). Various factors influence the release of ADH, the most important of which is the hypothalmic osmoreceptor (which responds to changes in water pressure) (R.W. Schriver et al, 1979). ADH increases renal tubular permeability, to water, and causes vascoconstriction.

The kidney is a source of several vasoactive substances, including the renin-angiotensin-aldosterone-system, the kallikrein-kinin system and prostaglandins (M.B. Vallotton, 1987).

Prostaglandins are thought to act as 'tissue hormones', regulating filtration rate and the reabsorption of salt and water.

Kinins are formed from kininogens by the action of the kallikrein enzymes. Kinins affect blood vessels and influence the reabsorption of sodium and water in the tubule.

The renin-angiotensin-system results in the formation of angiotensin II, which has several effects on the cardiovascular

system. It is a potent vasoconstrictor, and also promotes sodium and water retention, increases permeability of blood cells and stimulates aldosterone synthesis and release. Aldosterone exerts its action by effecting sodium reabsorption in the kidney tubules.

Atrial natriuretic factor, ANF, is synthesised in the heart, and has an effect on active membrane transport of sodium, including renal tubular transport. (E.H. Blaine, 1986). It has been suggested that ANF provides a parallel and opposite system to that of the renin-angiotensin system.

Renal control of blood pressure, part of which is exerted by neural and hormonal mechanisms, is also directly controlled by the kidney itself. Small increases in perfusion pressure cause this renal mechanism to come into effect, which rapidly increases salt and water excretion. This results in a lowering of blood pressure via changes in blood volume.

Vascular mechanisms are exerted at the local level as well as by endocrine and neural systems. The kidneys, heart and brain regulate this flow over a range of pressure related to chemical factors and stretching of muscle.

1.2 Interaction of drugs with blood pressure control mechanisms.

Antihypertensive drugs can be divided into eight categories:

(1) Ganglion blockers - These inhibit transmission across synapses in nerve endings, by preventing acetylcholine from binding to its receptor. Examples are trimetaphen and pentolinium

(2) Adrenergic neurone blockers - Drugs such as

bethanidine prevent the release of noradrenaline at the nerve-endings and produce vasodilation.

(3) α-Adrenoreceptor antagonists - These substances block the activation of α_1 receptors by catecholamines, causing vasodilation of the blood vessels (eg. prazosin).

(4) Direct vasodilators - These have a direct mode of action on the smooth muscle, dilating arterioles preferentially to veins eg. hydralazine.

(5) β-Blockers - These are some of the most widely used antihypertensive drugs (propanolol, labetolol), often in conjunction with other hypotensives. They produce a gradual decrease in blood pressure, although their exact mode of action is not known. It is postulated to include reduction of cardiac output and inhibition of renin production.

(6) Centrally acting hypotensives - These circulatory factors act primarily on receptors in the brain (central regulation). The mechanism of action is primarily through antagonism of α_2 receptors. Methyldopa and clonidine are the most widely used examples.

(7) Diuretics - The main drugs in this category are thiazide and frusemide. They act by direct vasodilation of peripheral blood vessels, and

by promoting Na^+ and H_2O secretion in the kidney.

(8) Renin-angiotensin system inhibitors and antagonists - Interfering with this system produces antihypertensives. Captopril and enalapril inhibit angiotensin-converting enzyme (ACE), and thus stop the production of angiotensin II, a potent vasoconstrictor.

1.3 The Renin-Angiotensin System.

The renin-angiotensin system is one of the most important of the various mechanisms implicated in the regulation of blood pressure (M.B. Vallotton, 1987). The end product of the system, the octapeptide angiotensin II, is one of the most important vasoconstrictor agents known.

Below is shown an outline of the system as it is presently understood, and its interaction with the kallikrein-kinin system.

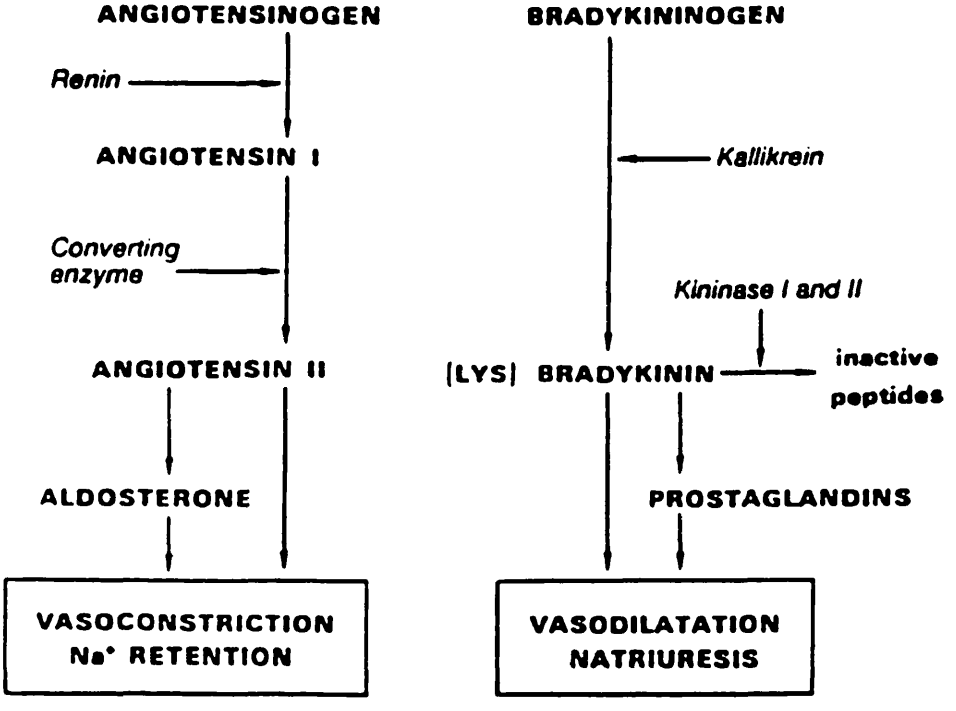

Renin and kallikrein are enzymes which split the circulating liver produced substrates antiotensinogen and kininogen.

Angiotensin converting enzyme (ACE) transforms the inactive angiotensin I, and is the same enzyme which is responsible for the degradation of bradykinin. The octapeptide angiotensin II and the nonapeptide [Lys] bradykinin exert direct and opposite vasoactive action on vessels. They also stimulate the release of aldosterone and prostaglandins, which mediate sodium retention and natriuresis respectively.

1.3.1 Biological action of the Renin-Angiotensin System.

The active form of renin has a molecular weight of approximately 36,000, and is released by the kidneys in repsonse to decreased renal perfusion. (J.C.S. Fray, 1980). The cleavage of the α-2 globulin angiotensinogen by renin, is the rate limiting step in the process of angiotensin II formation. ACE then cleaves the C-terminal dipeptide from angiotensin I to form angiotensin II. This short-lived peptide (it is rapidly cleaved to inactive fragments) acts via its receptors to constrict the blood vessels directly, to stimulate aldosterone release, and also to inhibit further renin release by a feedback loop (J.D. Swales, 1979).

1.3.2 The Enzyme Renin

Renin is a highly specific peptidase, the only known natural substrate for which is angiotensinogen. Although other aspartic

proteinases have little specificity, renin will cleave only a single bond in angiotensinogen. The human substrate scissile bond is Leu-Val, while it is Leu-Leu for other mammals. Even this minimum substrate difference is important, in that while the human enzyme cleaves human and other mammallian substrates, human angiotensinogen is cleaved only by human renin. (M.A. Ondetti and D.W. Cushman, 1982). Partial hydrolysis of angiotensinogen with trypsin releases on N-terminal tetradecapaptide which is cleaved to angiotensin I on incubation with renin.

Since angiotensin I has very high biological activity, because of its ready conversion to angiotensin II, the very first assays developed for renin were biological assays (A.B. Gold et al, 1966). This assay was very sensitive and allowed the measurement of very small quantities of renin normally present in plasma.

Nowadays, human plasma renin assays involve measuring the angiotensin I cleaved from angiotensinogen by renin, by radioimmunosassay (E. Haber et al, 1969; A.E. Freelander and T.L. Goodfriend, 1979). Commercial kits for renin assays are now available.

All aspartic proteinases so far examined share the functional presence of carboxyl residues in the active site, have striking sequence homology and many common structural features. The three dimensional structure of renin has not yet been determined, although structure-activity relationships show the active-site aspartic acid residues centred in a long cleft which is capable of

binding at least eight amino-acids (L.T. Skeggs et al, 1980; E. Haber and J. Burton, 1979).

The aspartic acids are hydrogen-bonded to each other and to either a water molecule or an ammonium ion (M.N. James and A.R. Sielecki, 1985; R. Bott et al, 1982). The ionisation state of the catalytic acid residues is not known, but one may remain protonated. Renin, like all aspartic proteinases has a flap region which can open and close upon substrates or inhibitors. The unique specificity and pH optimum of renin (pH 7, as compared to pH 3) has yet to be explained, in spite of the sequence homology to other aspartic proteinases.

The general features of cleavage of amide bonds by renin and related enzymes is not yet fully established. The two carboxyl groups and the tyrosine residue at the active site are assumed to play a similar role to that proposed in pepsin. The protonated carboxyl polarises the carbonyl group of the scissile amide bond (D.H. Rich, 1986). In pepsin this polarisation facilitates attack by the carboxylate of the ionised residue either directly or through the action of a water molecule, forming a detectable tetrahedral intermediate. (D.H. Rich et al, 1982).

The tyrosine present in the active site protonates the leaving amino group (J. Tang, 1979).

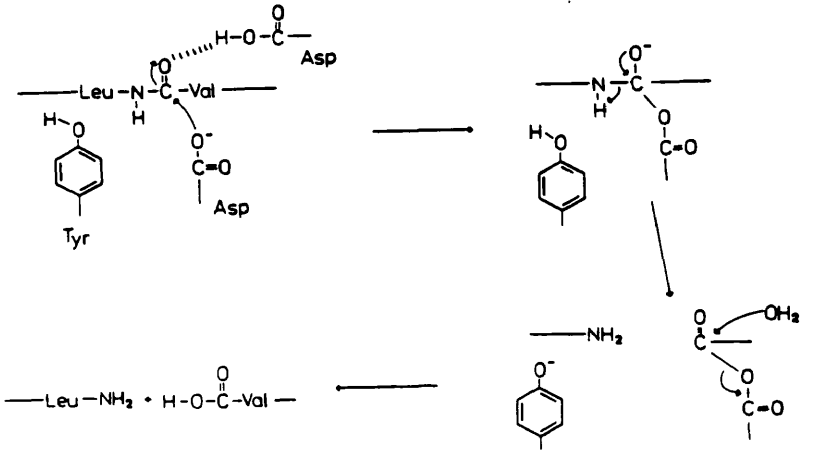

1.3.3. Antihypertensive agents from inhibition of the Renin-Angiotensin-System

The development of ACE inhibitors such as captopril, enalapril and lisinopril, (M.A. Ondetti et al, 1983; M.J. Wyvratt and A.A. Patchett, 1985) has shown that interfering with the Renin-Angiotensin System can provide potent hypotensives, as well as providing important tools for the study of this system.

ACE inhibitors were developed by initially studying synthetic substrates and natural peptide inhibitors extracted and sequenced from snake venom. A systematic search was then made for soluble ACE inhibitors which were active in vivo. This approach led to the isolation of the nonapeptide teprotide and culminated in the design of clinically useful ACE inhibitors and bradykinin potentiators. Captopril (D.W. Cushman et al, 1977) was designed to bind specifically to the active site of carboxypeptidase A which has similar substrates specificity to ACE but whose mechanism of action is better understood. Enalapril (J. Biollaz et al, 1981) is an improvement over captopril in that it has no sulphydryl group and therefore fewer side-effects (no skin rashes and loss of taste). An equally potent inhibitor to enalapril has recently become commercilaly available, lisinopril (H.H. Rotmensch, 1984). This compound is more slowly and less completely absorbed than enalapril, and has a longer duration of action. It also does not require metabolic activation, unlike enalapril (formation of free acid from ethoxide).

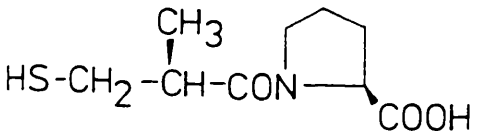

Captopril

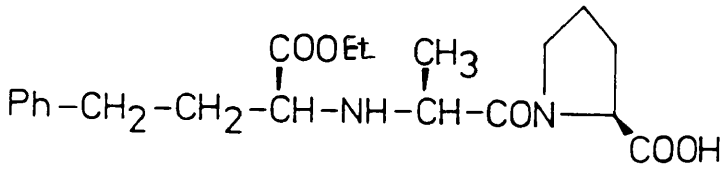

Enalapril

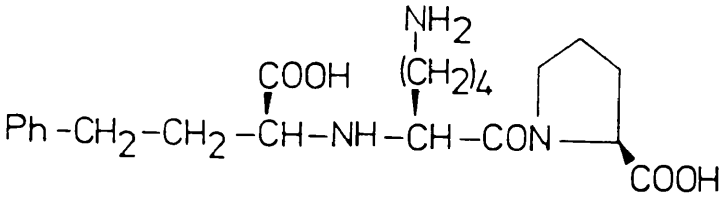

Lisinopril

The inhibition of ACE has therefore proved to be an important addition to hypertensive drug therapy and has aided the investigation investigation of the Renin-Angiotensin-System. However, the main disadvantage of ACE inhibitors is their interaction with the kallikrein-kinin system, by inhibition of kinase II, which stops degradation of the hypotensive agent bradykinin. (O. Iimura et al, 1986). Designing in vivo inhibitors of renin may result in hypotensive agents with fewer side-effects than their ACE counterparts and provide more specific probes to investigate the role of the Renin-Angiotensin-System in blood pressure regulation.

1.4 Renin Inhibitors.

A knowledge of substrate sequence, mechanistic hypotheses based on studies of similar aspartic proteinases and the discovery of pepstatin (a naturally occurring aspartic proteinase) have all aided the development of potent renin inhibitors. (M.A. Ondetti

and D.W. Cushman, 1982) In recent years the trend has been towards the development of lower molecular weight inhibitors which are more likely to become useful antihypertensive agents. Renin inhibition has been achieved with substrate analogues, several types of transition state analogues, renin antibodies and phospholipids.

1.4.1 Substrate Analogues

The minimum sequence required for an efficient renin substrate was defined by Skeggs et al (1968) and this laid down the basis of specific substrate analogue inhibitors capable of interacting with the renin active site. The minimal sequence octapeptide, H-His-Pro-Phe-His-Leu-Leu-Val-Tyr-OH, was studied and a number of analogues prepared (J. Burton et al, 1980; R.J. Cody et al, 1980). Problems were initially encountered with lack of solubility at neutral pH; increasing solubility by replacing hydrophobic groups with hydrophi lic residues led to much reduced binding to renin. The central residues were increased in lipophilicity and a Pro added to the N-terminal to increase solubility. The analogue with best activity was H-Pro-His-Pro-Phe-His-Phe-Phe-Val-Tyr-OH. The further addition of a Lys residue reduced clearance from circulation in vivo, by up to a factor of ten. This decapeptide, H-Pro-His-Pro-Phe-His-Phe-Phe-Val-Tyr-Lys-OH, called renin inhibitory peptide (RIP), had a K_i of 2μM. Its hypotensive effect in vivo (J. Burton et al, 1980) has been tested in monkeys, and found to block the hypertensive effect

of infused human renin without affecting responses to angiotensins I and II.

A similar approach the to above has led to a shorter sequence, H-Phe-Phe-(4,I)-Val-Tyr-Lys-OH, with potency comparable to RIP (J. Burton et al, 1983).

1.4.2 Transition-State Analogue

Pepstatin is a naturally occurring acyl pentapeptide which inhibits a number of aspartyl proteinases, including renin. Pepstatin inhibits pepsin by virtue of its action as a transition-state analogue, since the carbon bearing the hydroxyl group in the 4(S)-amino-3(S)-hydroxyl-6-methyl heptanoic acid residue (statine, Sta) in position three, mimics the transition-state form of the amide carbonyl during peptide hydrolysis (See 1.3.2). The 3(S) configuration is very important for binding, as demonstrated by 1000-fold drop in potency upon changing to the 3(R) form (J. Boger et al, 1983). It has been proposed that the enzyme-bound water molecule is displaced by the hydroxyl group of statine upon binding of the inhibitor (D.H. Rich, 1985).

Derivatives of pepstatin with increased solubility have been prepared as inhibitors of human renin, the most potent being pepstatin-Glu with an inhibitory constant of 5.8μM (M. Eid et al, 1981).

Since renin is such a highly specific enzyme, Boger et al (1983) incorporated statine into the angiotensinogen sequence hoping to find more potent inhibitors. By noting similarities

between pepstatin and substrates of aspartic proteinases, it has been suggested (J.Powers et al, 1977) that statine replaces both amino-acids around the cleavage site. Peptides which were synthesised according to this hypothesis are potent inhibitors, and were selective for human renin over other aspartic proteinases (J. Boger et al, 1983). IC_{50}'s of 1nM can be obtained (J.M. Wood et al, 1985) using statine analogues eg. Z-Arg-Arg-Pro-Phe-His-Sta-Ile-His-Lys-(Boc)-OCH_3.

An analogue of statine in which the hydroxyl group is replaced by an amino group (aminostatine) has been synthesised and tested (M. Jones et al, 1985; R.J. Arrowsmith et al, 1986). The amino group was expected to interact favourably with the acidic groups in the active site; however no increase in potency over statine inhibitors was found. The favourable interaction with the active site aspartic acids may be balanced by the energy required to desolvate the ammonium ion when the inhibitor binds to renin. Also, the fact that the 3(R) isomer is slightly more potent than the 3(S) form (cf statine) is suggestive of a different mode of binding (R.J. Arrowsmith et al,1986).

By fitting theoretical inhibitors into a proposed active site model, Iizuka et al (1988) synthesised a statine analogue (norstatine, 3(S)-amino 2(R)-hydroxy-5-methylhexanoic acid) with one less carbon in the backbone, which had a better fit to their model. Inhibitors with a K_i of 8nM were obtained.

Boger et al, (1985a) used molecular modelling to predict that statine analogues containing a cyclohexyl side-chain (ACPHA, 5-cyclohexyl-4(S)-amino-3(S)-hydroxy pentanoic acid) would be more

potent than statine analogues. This was found to be the case and many recently reported renin inhibitors have included this cyclohexyl addition (J. Boger et al, 1985b; H. Sham et al, 1986).

Analogues of statine or ACPHA with 2(R) or 2(S) alkyl substituents have been synthesised, to replace the S_1' side-chain which is absent when statine or ACPHA is used as a dipeptide mimic. This has been found to increase potency in some cases (H. Stein et al 1986) but not in others (D.F. Veber et al, 1984).

Inhibition of renin by a peptide containing a ketone analogue of statine ('statone') has been synthesized (S. Thaisrivongs et al, 1986).

The binding of similar analogues to pepsin was studied, and the ketone found to bind in the ketal form, by enzyme catalysed addition of water. The statone analogue was found to be 20 times less potent than the corresponding statine analogue, which may be a reflection of the energy required to hydrate the ketone. Difluoroketone analogues which exist predominantly in the hydrated form ('difluorostatone') are 65 times more potent than the statone analogues (K. Fearon et al, 1987).

Phosphostatine analogues (J.F. Dellaria, Jr and R.G. Maki, 1986), in which the hydroxyl group is replaced by a phosphinic acid moiety were potent inhibitors of pepsin (P.A. Bartlett and W.B. Kezer, 1984), but were not active for human renin. It has been suggested that at the higher pH's at which inhibitor binding to renin is tested the acidic group is completely ionised , which may be unfavourable for binding.

Szelke et al (1983) have designed transition-state analogue inhibitors of renin which are not based on statine-like compounds. The scissile amide bond of substrate analogues has been replaced by a 'reduced peptide' isostere.

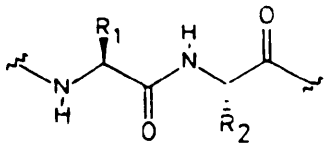

Peptide

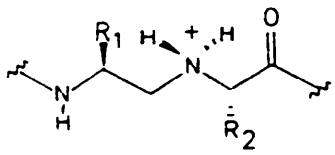

Reduced peptide

This was intended a mimic the tetrahedral intermediate for amide bond hydrolysis and presumed to approximate the structure of the transition-state. Although the 'reduced peptide' isostere has tetrahedral geometry, it lacks both hydroxyl groups; the high potency observed for inhibitors of this type may be due to an electrostatic interaction between the active site aspartic acids and the basic amine. H-142, H-Pro-His-Pro-Phe-His-Leu^{R}-Val-Ile-His-Lys-OH is 30,000 times more potent (B.J. Leckie et al, 1985), than the human octapeptide substrate on which it was based. The peptide Boc-Phe-His-Val^{R}Val-NH-2(S)-methylbutyl (J.J. Plattner et al, 1986), IC_{50}=8.6nM, shows the effectiveness of the reduced peptide bond in the design of low molecular weight inhibitors.

A second transition-state design which Szelke and co-workers have introduced is the 'hydroxy' isostere of the Leu-Val bond (M. Szelke et al, 1983).

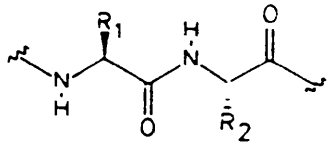

peptide

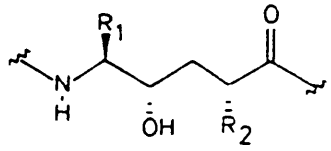

'hydroxy' isostere

The Leu-Val side-chains are correctly orientated to interact with the enzyme subsites, while the hydroxy groups might mimic the tetrahedral intermediate which is formed during hydrolysis of the amide bond. Boc-Pro-Phe-(N-Me)His-Leu-$\overset{OH}{}$Val-Ile-NH-CH_2(2Pyr) (IC_{50}=0.39nM) and the 'dipeptide' tBuCO(CH_2Ph)CO-His-Val-Cal-Val-NH-CH_3 (IC_{50} = 2nM) show that small molecular weight inhibitors with this modification have high potency. The former has been tested in vivo and found to be orally active (D.T. Pals et al, 1986).

Several reports have appeared in which peptides, with the 'hydroxy' isostere, served as the basis for the introduction of conformational constraints.

In one case, the introduction of α-methylproline in place of a Pro residue resulted in the peptide having stability to various degrading enzymes in vivo, and furnished an inhibitor of IC_{50} = 1.6nM (S. Thaisrivongs et al, 1987).

Another study used the proposed enzyme-bound inhibitor conformation to suggest the possibility of a γ-lactam restriction at the P2-P3 site (S. Thaisrivongs et al, 1988). A peptide with this lactam constraint and a hydroxy ethylene isostere at the cleavage site inhibited renin with an IC_{50} of 6.5nM.

Several types of inhibitors which use binding sites only towards the amino-terminal end of the cleavage site have been reported.

Peptide glycols, such as

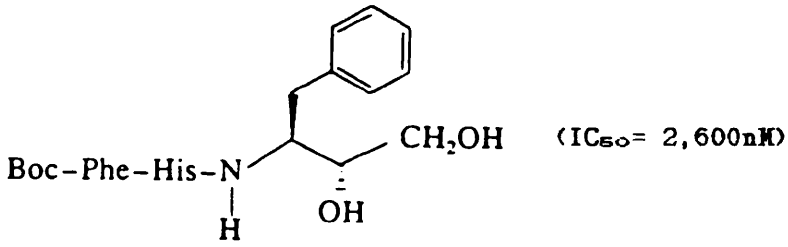

(IC_{50}= 2,600nM)

bind to these sites and position a metabolically stable diol group which interacts with the catalytic site aspartic acids (G.J. Hanson et al, 1985). Diols which have an additional alkyl substituent in the subsite toward the C-terminal end of the cleavage site have been patented (J.R. Luly et al, 1986).

Peptide aldehydes are another class of potent inhibitors activity which bind only to N-terminal portions of the active site (J.A. Fehrentz et al, 1984; T. Kobuka et al, 1984). These aldehydes were the first low molecular weight inhibitors to be reported in the literature. They may bind in the hydrated form, and as such mimic the transition-state, although they are not

expected to have any potential as in vivo inhibitors because the aldehyde function is rapidly metabolised.

Renin inhibitors which contain a ketone function have been reported (B.J. Leckie et al, 1985), and many are more potent than the corresponding aldehyde, reflecting the fact that they are able to make binding interactions on both sides of the cleavage site.

Several classes of inhibitor have incorporated non-peptide C-terminal elements. Inhibitors such as

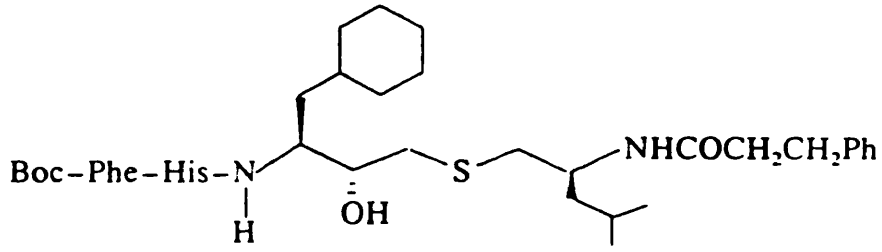

(J.R. Luly et al, 1987)

with a thiol linkage and retroamides (S.H. Rosenberg et al, 1987).

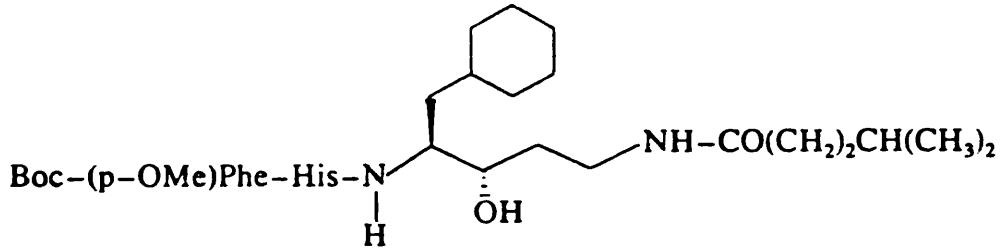

derive their potency by positioning the side-chain groups in the S_2' and/or S_3' subsites of renin.

Inhibitors in which sulphide and sulphoxide groups mimic the amide bond have been studied (C.W. Smith et al, 1988), but were

found to be less potent than corresponding statine analogues, presumably because of the removal of the hydrogen-bonding capabilities.

Olefinic compounds which replace the amide bond of the cleavage site have been synthesised and are extremely potent and specific inhibitors of renin (R.L. Johnson, 1984). Dehydrostatine analogues have also been prepared (C.W. Smith et al, 1988).

Ether linkages, where the amide bond is replaced by a $-CH_2O-$ moiety, are disappointing as renin inhibitors presumably because the fit of the peptide to the enzyme is destroyed. However, replacing the P4-P3 amide bond of a peptide based on the angiotensinogen sequence with the 'ether peptide' linkage afforded a peptide (a hydroxy isostere) with an IC_{50} of 1.6nM (R.E. Tenbrink et al, 1988).

1.4.3 Renin Antibodies

Inhibitory renin antibodies provided the first evidence that interfering with the Renin-Angiotensin-System had therapeutic potential (G.E. Wakerlin, 1958). More recently, mono and polyclonal antibodies, prepared using purified renins, have shown potent inhibition in vitro (V.J. Dzau et al, 1984; J.M. Wood et al, 1986; J. Bouhnik et al, 1987), and hypotensive effects in vivo.

Antibodies have also been prepared against specific regions of renin, to investigate the structures of the flap region (C.F.

Liu et al, 1988) and the prorenin prosegment (I. Gaillard et al, 1986).

1.4.4 Phospholipids

A number of investigations have reported the renin inhibitory effects of phospholipids, lysophospholipids and analogues (M.A. Ondetti and D.W. Cushman, 1978).

Sen et al (1967, 1968), first isolated a phosphatidylethanolamine from renal extract and investigated its inhibitory properties.

Derivatives have been developed (the two most studied shown below) which show a low level of inhibitory activity in vitro, with K_i's (IC_{50}'s) in the millimolar range.

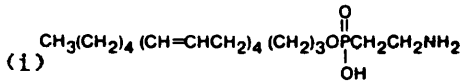

(J.G. Turcotte et al, 1975)

(H. Hosoki et al, 1977)

Despite the moderate activity in vitro, (i) lowers blood pressure in the hypertensive rat. (ii) has a K_i of 2mM and is a competitive and reversible inhibitor of dog renal renin.

1.5. Molecular Modelling in Renin Inhibitor Design

A crystal structure for renin is not yet available to serve as a basis for modelling studies, although progress has been made towards this goal. Navia et al (1984), have described preliminary crystallographic data on mouse renin and inhibitor complexes. Crystals of renin, and inhibitor complexes, derived from recombinant DNA techniques, have been reported (R.A. Poorman et al, 1986), but no crystal structure data has been forthcoming. X-ray crystal structures for related aspartic proteinases pepsin (N.S. Andreava et al, 1984), penicillopepsin (M.N. James and A.R. Sielecki, 1985), and endothiapepsin (L.H. Pearl and T.L. Blundell, 1984) have been determined. Inhibitor H-142 complexed to endothiapepsin has been crystallised and the structure determined (S.I. Foundling et al, 1987), as has the structure of a pepstatin-analogue renin inhibitor (Iva-Val-Val-Sta-OEt) with penicillopepsin. These structures and their similarity to human renal renin have been used to derive models for mouse renin (T.L. Blundell et al, 1983) and human renin (B.L. Sibanda et al, 1984; V. Carlson et al, 1985).

These models of the enzyme have played an important part in the design of inhibitors. Boger et al (1985a) used the pepsin/pepstatin structure (R. Bott et al, 1982) to predict that statine would best serve as a dipeptide mimic, and to design two classes of constrained cyclic statine inhibitors which would better fit the active site.

A network of proposed hydrogen-bonds between the inhibitor and renin has been derived from a human renin model by J.J. Plattner and co-workers (1986),

However, at no point in these studies has there been a direct observation by any physical techniques (such as NMR or X-ray crystallography) of the 3-D structure of renin, or it s inhibitors, either in solution or bound to the enzyme.

Models of the active site of renin have been used to predict the conformation of the inhibitor when bound, and in general indicated an extended type of inhibitor conformation (T.K. Sawyer et al, 1988a; K.Y. Hui et al, 1987; T.K. Sawyer et al, 1988b), instead of the postulated β-turn previously reported for the P2-P5 sequence (I. Leipina et al, 1984). The peptide H-142 when bound to the aspartic proteinase endothiapepsin has an extended type of structure (S.I. Foundling et al, 1987), although the author themselves admit 'it would be unwise to establish rigid definitions of enzyme subsites on the basis of one inhibitor'. This dilemma may be resolved when a human renin X-ray structure becomes available, but until then the question of the active site structure must remain open.

1.6 NMR and Circular Dichroism Based Structure Determination

1.6.1 Circular Dichroism Studies of Peptides.

Circular Dichroism (CD) uses circularly polarised light rather than isotropic light to cause electronic transitions within

molecules. Only asymmetric molecules can exhibit a CD spectrum, and it is a particularly useful technique as it is sensitive to the conformation of a molecule (W.C. Johnson Jr, 1978; S. Brahms and J. Brahms, 1980). It has thus been applied to the study of biological molecules such as peptides, proteins, nucleic acids and polysaccharides.

In peptides (R.W. Woody, 1985), the amide chromophore is the most abundant and generally dominates the spectrum at wavelengths below 250nm.

There are two distinct electronic transitions associated with this chromophore above 180nm. The $n-\pi^*$ transition is characteristic of carbonyl compounds, and involves the promotion of a non-bonding electron on the carbonyl oxygen to an antibonding π^* orbital of the amide group. This transition lies between 230-210nm.

The $\pi-\pi^*$ transition is observed at 210-190nm, involving promotion of an electron from the highest filled orbital (HOMO) to the lowest unfilled antibonding (π^*) orbital (LUMO).

The amide region (250-190nm) can have interferences from aromatic chromophores (Tyr,Phe and Trp), although the extent and importance of these transitions is not known and is a matter of some controversy (R.W. Woody, 1978).

Each conformation adopted by a peptide has a highly distinctive CD spectrum. The CD spectrum of α-helical polypeptides are qualitatively independant of side-chain and solvent (W.C. Johnson Jr and I. Tinoco Jr., 1972); the β-sheet conformation is much more variable in its CD spectrum, presumably

because of the broader range of structures available as compared to helices (J. Applequist, 1982); the β-turn conformations (I, II, III, IV and their mirror-images) have been calculated by R.W. Woody (1974), and agree well with experimental work. The so-called 'random-coil' CD spectrum has been reinterpreted (A.F. Drake et al, 1988) and does not represent a disordered peptide structure, but an equilibrium between two conformations. The CD spectrum resulting from a peptide in solution is a summation of each conformation which it adopts. Resolving these conformational components is an important step in relating 3-D structures to activity and can lead in many instances to conformationally constrained analogues with enhanced biological activity (R.F. Freidinger et al, 1980).

Cyrogenic CD (G.Siligardi et al, 1987) in particular 'freezes out' the most thermodynamically stable conformation at the lowest temperatures, and aids in the interpretation of room temperature CD spectra.

1.6.2 NMR Studies of Peptides

Circular Dichroism can provide a simple and sensitive means for determining the conformations adopted by peptides in solution, but at best it provides only crude and ill-defined structures. Much more detailed information can be obtained from proton (^{1}H) high-field Nuclear Magnetic Resonance (NMR) spectroscopy, since the ^{1}H NMR spectra of most organic compounds contain signals from all parts of the molecule. Furthermore, the resonance signals are

particularly sensitive to interactions between protons and to molecular motion, and so can provide a wealth of information concerning the conformation and dynamics (I.D. Campbell, 1985). ^1H NMR studies can therefore complement the many X-ray crystallographic studies of peptides (and proteins). In solution, environmental conditions are easily varied and provide information in environments which are much more similar to the biologically relevant state of the peptide.

For peptide and protein conformational studies (K. Wuthrich, 1986), the three most important parameters are the chemical shift (δ) of resonances, the spin-spin coupling constant for protons separated by three bonds (^3J) and the nuclear Overhauser effect (NOE) between specific pairs of protons.

The chemical shift of a proton resonance is normally obtained directly from the NMR spectrum very accurately. These chemical shifts are very sensitive to the peptide structure and are used to characterise a given conformational state and to detect any conformational changes. The dominant factor determining the chemical shift of a proton resonance is usually the nature of the group concerned.

The contributions of interest to the chemical shift are those arising from the spatial environments of an atom in a peptide. This can be estimated from the differences between chemical shifts observed in a peptide and those observed for the same amino-acid in an unstructured peptide (A. Bundi and K. Wurthrich, 1979). One important effect is the shift induced by aromatic rings, the ring current shift. The shift depends on θ, the angle between the

perpendicular to the ring and the vector which joins the centre of the ring and the nucleus being observed (R.A. Dwek, 1973). There is a r^{-3} distance dependence with ring current shift.

The situation is less straightforward when considering CαH protons, as these are strongly affected by nearby carbonyl groups; NH proton chemical shifts are also heavily influenced by hydrogen-bonding.

Spin-spin coupling is transferred via the electrons of chemical bonds, and falls off rapidly with the number of bonds involved. Three bond couplings are the most important in the study of peptides, as these can be related to dihedral angles by an equation of the form -

$$^3J = A \cos^2\theta + B \cos\theta + C$$

(V.F. Bystrov, 1976), where θ is the torsional angle H-X-Y-H, and A,B, and C are constants, normally 8.5, - 1.1 and 0.4 respectively for ^3JNH-CαH.

The nuclear Overhauser effect (NOE) is the change in the intensity of a resonance in the NMR spectrum caused by the saturation of another resonance (J.H. Noggle and R.E. Schirmer, 1974). This is a relaxation effect which depends on dipolor coupling between protons. Detecting this effect can be achieved by selective irradiation or by observing cross-peaks in two-dimensional experiments (G. Wider et al, 1984). The magnitude of NOE effects are dependent on the distance (r) between pairs of protons, in the simplest form as r^{-6}. Using geminal protons as standard distance, quantitative estimates of distance can be made

(K. Wuthrich, 1986), providing the time dependency of the effect has been studied.

Two dimensional NMR techniques are widely used, both to assign proton resonances to specific atoms within the peptide and to obtain structural information (distance constraints etc). The idea of 2-D NMR was first introduced by J. Jeener (1971) and involved spreading the NMR spectrum into two frequency dimensions and generally observing cross-peaks between protons which are scalar coupled (or dipolar coupled) (A.Bax and L. Lerner, 1986).

The most frequently used experiment is the COSY (COrrelated SpectroscopY) method (W.P. Aue et al, 1976), which shows scalar coupling between two protons A and X, with a cross-peak centred about the diagonal at (A, X) and (X, A), where A and X are the chemical shift frequencies of spins A and X respectively. New methods have recently been introduced which provide net transfer of magnetisation between spins, giving correlations throughout the whole of the spin system and allowing complete assignment of each amino-acid in a peptide. This is known as the Homonuclear Hartmann-Hahn (HOHAHA) experiment (A. Bax and D.G. Davies, 1985).

Another commonly used 2-D experiment is the NOESY (Nuclear Overhauser Effect SpectorscopY) method (F. Wider et al, 1984). Here, cross-peaks indicate which protons are in close proximity to one another (dipolar coupled). These protons may be far apart in terms of peptide sequence, but are brought together by folding of the peptide chain. It is possible to quantify NOEs to give approximate distances (M-C Kuo and W.A. Gibbons, 1980; E.T. Olejniczak et al, 1981). Recently a new variation of the NOESY

experiment has been introduced (A.A. Bothner-By et al, 1984; H. Kessler et al, 1987), and is known as the ROESY experiment (Rotating frame nuclear Overhauser Effect SpectroscopY). This has the advantage of the ROE being positive for all values of the correlation time, τ_c, whereas for medium sized (10-20 amino-acids) peptides in the NOESY experiment, the NOE is either $\simeq 0$ or very small (positive or negative). Aside from allowing conformational studies of medium sized peptides, chemical exchange peaks can be distinguished from ROEs (by difference in phase), which is useful for interpreting multiple conformations.

There are nowadays a great deal of 2-D NMR experiments available (H. Kessler et al, 1988) such as J-resolved, multiple quantum filters, heteronuclear correlations etc.

Chapter 2

Material and Methods

2.1 Circular Dichroism

Instrumentation:

All studies were carried out on a JASCO J40CS spectrometer with dedicated Apple Microcomputer for processing and plotting, in the CD facility at University College, London.

Spectra in the range 320 - 260nm were recorded in a 10mm quartz cell, and from 260 to 190nm in a 0.2mm cell. A spectrum of solvent only was subtracted from each spectrum of peptide, to remove any effects from slight absorbances from solvent molecules.

Reagents:

The methanol used was of HPLC grade (Rathburn); Trifluoroethanol (TFE, Aldrich) was distilled and stored in sealed vials under nitrogen until used. Solvent water was distilled and de-ionised before use.

Salt solutions used to test ion-binding properties were freshly prepared from distilled, de-ionised water.

0.5M solutions of HCl (Fisons) and NaOH (BDH), which were used to alter pH during the pH titration, were also freshly prepared with dd H_2O.

2.2. Peptide Synthesis.

Instrumentation:

Synthesis of peptides was carried out either on a semi-automated Synthor 2000 Peptide Synthesiser (Peptides International) or a fully automated ABI Peptide Synthesiser.

Reagents:

For use with the Synthor instrument, dichloromethane (DCM, BDH) dimethylformamide (DMF, Aldrich) dicyclohexylcarbodiimide (DCC, Aldrich), and diisopropylethylamine (DIPEA, Aldrich) were freshly distilled before use, and for the ABI synthesiser DCM, DCC and DIPEA were used as supplied by ABI; the DCC and DIPEA were dissolved in DCM.

Hydroxybenzotriazole (HOBt, Aldrich) and trifluoroacetic acid (TFA, Halocarbon) were used with no purification.

Hydrogen fluoride (HF, ICI) cleavage was carried out using the Peninsula Laboratories teflon vacuum system with a low/high HF procedure. The scavengers p-cresol and thiocresol were obtained from Aldrich, dimethylsulphide (DMS) from Aldrich and triflouromethanesulphonic acid (when needed) from Fluorochem.

Derivatized amino acids were used without further purification: Boc-L-Pro, Boc-L-Phe and Boc-L-Val were purchased from Bachem, Boc-L-His (BOM) from Cambridge Biochemicals and Boc-L-Lys(2-chlorocarboxybenzyl) and Boc-L-Tyr(2,6-dibromobenzyl) from the Peptide Institute Ltd.

Synthetic Strategy:

The general stragety for coupling amino acids was as outlined by J.W. Stewart and J.D. Young (1984).

Chloromethylated polystyrene resin with attached Boc-L-Lys(2-chlorocarboxybenzyl) was initially swollen in DCM. The coupling procedure outlined below was then repeated for each residue. TFA was added to remove the Boc protecting group; the DIPEA/DCM solution was then used to convert the peptide from the basic to neutral form. A sample was then removed (automatically in the ABI synthesiser), and a ninhydrin test carried out to test the percentage of coupling (V.K. Sarin et al, 1981). A double coupling procedure was normally used; the first utilized a symmetrical anhydride (from DCC + amino-acid) and the second used HOBt active ester (from DCC + HOBt + amino-acid). These reagents were prepared outside the vessel and added manually to the Synthor reaction vessel, whereas the anhydrides and esters were generated in situ in the ABI synthesizer.

Cleavage from the 1g resin was by low/high HF procedure, stirring with a low (25%v/v) then high concentration of HF(100%) at 0°C, using p-cresol and thiocresol as scavengers. The resin cleaved peptide was washed several times with 50% acetic acid in

(a) Analytical reverse phase (C_{18}) HPLC profile of RIP, using a gradient of 100% H_2O + 0.1% TFA to 100% of CH_3CN(60%) + H_2O (40%) + 0.1% TFA. over a period of 75 minutes.

(b) FAB mass spectrum of purified RIP, showing the correct molecular weight. The small peak to the right is from M+23(Na), from the sodium/glycerol matrix used.

(c) Table showing the result of the amino acid analysis of purified RIP. The value for Tyr is rather low as expected, because of degradation during hydrolysis. These values were within the 10% experimental error and consistent with the correct RIP configuration.

RIP was stable if stored in a freezer at -30°C. In solution gradual decomposition occurred, as witnessed by the appearance of several very small spurious peaks, not originally present, during NMR analysis.

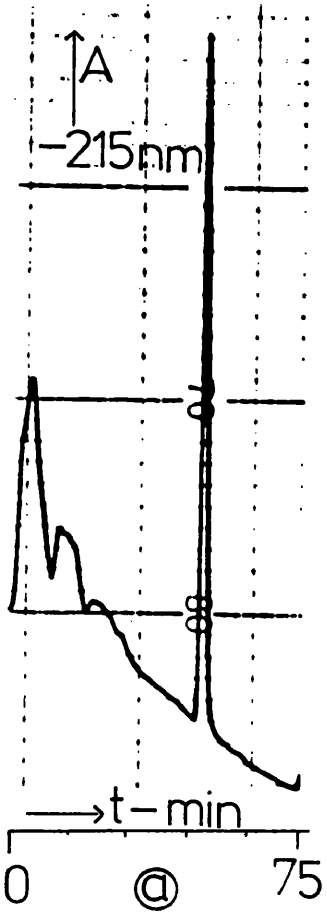

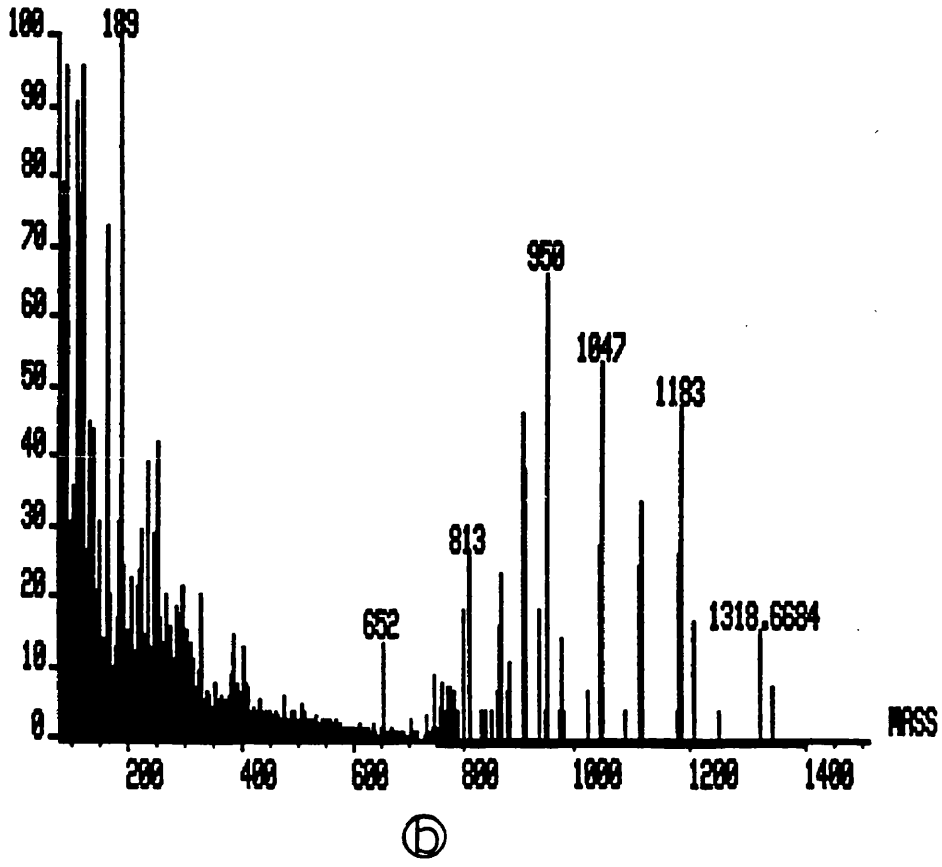

ⓒ

Standard	Height (2.5 nmoles)	Sample Height	No. of nmoles	Ratio
Pro	10.5	28.5	6.97	2.23
Val	74	73	2.47	0.81
Tyr	49	45	2.29	0.75
Phe	41	155	9.45	3.10
His	24	60	6.25	2.05
Lys	104	135	3.23	1.06

dd H_2O, filtered and freeze-dried, and the yield recorded (generally 90%).

Purification:

The peptide(s) were purified by passing down a C18-ODS reverse phase HPLC column (Whatman) at 39°C. Solvents ddH_2O + 0.1% TFA, and 60% CH_3CN (Rathburn) + 40% ddH_2O +0.1% TFA were filtered and degassed before use. Peptide samples were dissolved in ddH_2O + 0.1% TFA, centrifuged, then added to the columns. The purified samples were collected, the CH_3CN/TFA blown off with nitrogen, and lyophylysed.

Quality Control:

HPLC purified samples were submitted for Fast Atom Bombardment (FAB) Mass Spectrometry, 300MHz or 500MHz ^1H NMR, amino-acid analysis and analytical HPLC.

2.3 Nuclear Magnetic Resonance.

Instrumentation:

All spectra, both 1-D and 2-D, were recorded on a Varian 300MHz with XL-300 computer, or a Bruker 500MHz spectrometer, with dedicated Aspect 3000 computer.

Reagents:

Renin Inhibitory Peptide (RIP) was synthesized as described in the Peptide Synthesis Materials and Methods section.

Denterium oxide (D_2O, 99.8%) was purchased from MSD, as was methanol-D^3 (CD_3OH, 99.8%). Trifluoroethanol-D^3 was obtained

from Fluorochem and distilled from ddH_2O, to obtain TFE-D^2 (CF_3CD_2OH).

Samples were recorded in 5mm OD tubes (Wilmad).

One-dimensional NMR Methods:

Experiments were performed using the Fourier transform mode with a field frequency lock on the solvent deuterium signal.

Decoupling of solvent resonance was generally carried out with a presaturation routine, with the decoupler switched off during acquisition. The power level was set to the minimum value necessary for complete saturation of solvent signal.

When multiplets of first order spin systems were clearly discernable in normal 1-D spectra, coupling constants were extracted and tabulated. For overlapping, non first order systems, coupling constants were obtained by observing cross-peaks in 2-D COSY type experiments. These coupling constants were then converted to the relevant dihedral angles.

Spin-lattice relaxation time measurements (T_1) were performed using the inversion recovery technique, 180°_x - t_1 - 90°_x - acquisition (T.C. Farrar and E.D. Becker, 1971). Calculation of T_1 values was performed on the Varian XL-300, using the available microprogramme.

Two dimensional NMR Methods:

2-D NMR plots are most effectively presented as computer-generated contour plots of the 2-D array of data points. In this representation, the central horizontal axis (normally bottom left to top right) corresponded to the normal 1-D spectrum. Cross-peaks at frequency (ν_x, ν_y) represented connections between

NMR Experimental Conditions

(a) Samples of RIP for NMR studies were first degassed (bubbled gently with nitrogen) to remove traces of dissolved paramagnetic oxygen. Care was taken during purification to avoid contamination with paramagnetic ions - the presence of these along with oxygen would have greatly reduced any NOEs present.

(b) 90° pulse widths for the transmitter (and decoupler where appropriate) were calibrated prior to the running of 2-D experiments.

Typical 90° values were:

6-7 μsec for the transmitter

30-35μsec for the decoupler at power = 5H(HOHAHA)

40-45μsec for the decoupler at power = 8H (ROSEY)

* D3= delay to switch decoupler powers (5 msec).

protons X and Y at their respective frequencies. These cross-peaks represented either scalar coupling between protons (as in the COSY, Long-range COSY, DQF COSY, HOHAHA), or NOEs between diploar coupled protons (NOESY, ROESY), or protons in chemical exchange (ROESY).

For accurate determination of chemical shift values, coupling constants, NOEs (or ROEs) etc, 'slices' through the 2-D matrix were normally inspected and plotted. These spectra corresponded to one of the Dø increments and gave the connectivities from the resonance frequency on the diagonal to all other parts of the spectrum. For weak scalar coupling or small NOEs which were below the contour levels this method was invaluable and was routinely used in this project.

Typically, the number of increments varied between 256 and 512, the data set at each containing either 1K or 2K data points. No zero-filling was applied in the F2 frequency domain; the F1 data set was normally zero-filled to 512 W (from 256W) or 1K (from 512W).

The 2-D data matrix was processed using either a sine-bell (or sine-bell squared) apozidation, shifted by $\pi/_{x}$ (x = 0,1,2....) (Bruker Software) in both domains, or a combination of resolution enhancement and guassian apozidation (Varian Software).

COSY:

(HG(S1) - (S2).....D.O.)

D1 - *D3 - 90 - Dø - 90 - FID

This homonuclear (^1H - ^1H) chemical shift correlation experiment (A. Bax et al, 1981a) used gated presaturation (HG) of solvent during both preparation and evolution. A high power level (S1) was used during preparation, with a lower level (S2) for evolution. Normally, S1 = 15L, S2 = 30L was sufficient.

Dø was varied in equidistant increments using a relaxation delay (D1) of between 0.5 and 1.0 seconds.

Phase-cycling was used to remove the axial artifacts.

Long-range COSY:

(HG(S1) - (S2)..... .....D.O.)

D1 - D3 - 90 - Dø - D2 - 90 or 45 - D2 - FID

(A. Bax et al, 1981b)

For presaturation of solvent resonance, two power levels were applied, S1 = 15L, S2 = 30L. with S2 low enough to avoid loss of resolution but still give good enough suppression.

The delay D2 was added to allow transfer of magnetisation to occur throughout more of the spin-system. D2 was set to 0.25/J, where J was the coupling constant to be emphasised.

Double Quantum Filtered COSY:

(HG(S1) - (S2).....D.O.)

D1 - 90 - Dø - 90 - D3 - 90 - FID

(A. Marion et al, 1983)

Single quantum transitions were suppressed in this experiment, which helped in solvent suppresiion, particularly for methanol which gave two strong resonance signals. The phase cycling employed (in which the radiofrequency phase was varied, with all other parameters remaining unchanged) used the fact that double quantum transitions were twice as sensitive to radiofrequency phase shifts as single quantum. By rotating the phase of the excitation pulse in small steps, it was possible to rotate the signal phase twice as fast. Single quantum transitions were therefore filtered out by programming the receiver reference phase to follow at just the required rate (R. Freeman, 1988).

Two power levels, as previously, were used to saturate the solvent resonance.

NOESY:

(HG(S1) - (S2).....D.O.)

D1 - 90 - Dø - 90 - D9 - 90 - FID

(J. Jeener et al, 1979)

A phase sensitive cycling routine was used to suppress interferences from axial peaks. The delay D9, the mixing time, was set, as a good first approximation, to the average T_1 value for backbone protons. A solvent suppression routine was added to the pulse sequence once again with two decouplers power levels.

Homonuclear Hartmann-Hahn:

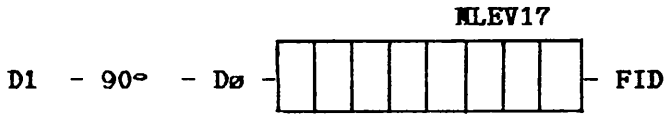

(A. Bax and D.G. Davies, 1985)

In this case, magnetisation was transfered between each proton in a spin-system, by applying a 90° pulse to the sample, a variable delay Dø, followed by the application of a spin-locking field. Net magnetisation transfer then occurred between coupled spins, because now

$$H_{1S} = H_{1I}$$

where H_{1S} and H_{1I} are the effective field strengths experienced by spins S and I. To stop dephasing of spins, the phase of the spin-lock was changed to the -y axis (causing re-focussing). The MLEV17 cycle was therefore used, to phase alter the spin-lock along the ±y axis, allowing Hartmann-Hahn magnetisation to occur. This experiment was performed in the inverse mode, the decoupler being used to apply the spin-lock instead of the transmitter; this was because the duty cycle of the transmitter was not sufficient for the phase alternation needed.

DANTE solvent suppression (G.A. Morris and R. Freeman, 1978) was incorporated into the pulse sequence, using the main transmitter for the solvent presaturation.

ROESY:

90° - Dø - MIX - FID

(A.A. Bothner-By et al, 1984).

This method has two main advantages over the conventional NOESY type of experiment.

(i) The NOE in the rotating frame (ROE) was always positive, irrespective of the correlation time, τc, of the molecule.

(ii) Chemical exchange cross-peaks can be distinguished from ROEs.

A spin-locking field was applied after the variable delay Dø, for a period corresponding to the mixing time, during which rotating frame cross relaxation occurred. In order to suppress transfer of magnetisation between coupled spins (as in the HOHAHA experiment) a rapid series of small flip angles for mixing was used. This procedure effectively suppressed J-coupling in the ROESY experiment (H. Kessler et al, 1987), and has been incorporated into the pulse sequence.

Inverse mode detection was again used to apply the spin-locking field. Solvent suppression was by the DANTE pulse sequence using the transmitter to pulse.

2.4. Molecular Modelling.

Instrumentation:

The building of approximate peptide structure from NMR distance data, energy minimisation and molecular dynamics calculations were all carried out using the QUANTA and CHARMm programmes on the Silicon Graphics (4D Series) facility, with an IRIS computer.

The QUANTA programme was used to generate an initial peptide structure based on standard bond lengths and angles for amino-acids. The structure was then interactively modified to agree with NMR and CD data, by manually rotating about covalent bonds, satisfying one distance constraint and dihedral angle at a time.

This initial structure was then subjected to Energy Minimisation, using the CHARMm programme. The Steepest Descent algorithm was used for an initial cycle, followed by the Powell method of minimisation. This procedure resulted in a more refined structure, with energetically unfavourable reactions removed.

Molecular Dynamics:

The CHARMm programme was used to perform molecular dynamics simulations, based on the energy minimised structures generated from NMR distance constrains, after an initial heating and equilibration step. These calculations gave information on the relative flexibility of different parts of the peptide.

Chapter 3

RIP CD Studies.

3.1 Conformation as a function of solvent.

The CD spectra of RIP in H_2O, CH_3OH and CF_3CH_2OH at room temperature (~ 25°C) are shown in Figure 3.1.

The CD spectrum of RIP in water was not consistent with a single conformation. It closely resembled a type III' β-turn reference curve (R.W. Woody, 1974), but the intensity of the absorption was only approximately one third of that calculated, and so the spectrum cannot result from this type of conformation alone.

In methanol solution, the spectrum did not result from a single conformation, either in terms of wavelength or absorption.

The spectrum in TFE did not resemble any reference spectra, and so resulted from a mixture of conformers. In each solvent therefore, it appeared RIP adopted different conformations, or different percentages of each conformational component.

* RIP concentration was 1mg per ml.

In general, the CD spectrum recorded experimentally was a summation of each conformation which existed in solution, the intensities and wavelengths of the maxima and minima dependant on the percentage of each conformation. In this instance, the spectrum in each solvent was likely to result from (and was later shown to result from) the conformational equilibrium between several conformations.

3.2. Membrane and Ion Binding Studies.

To RIP in water, 10µl of SDS (sodium dodecycl sulphate) was added, to simulate an approximate membrane environment. This resulted in precipitation of the peptide at all concentrations studied. No further work was carried out in this area.

The CD spectrum of RIP in H_2O with a 10-fold excess of salts (Mg,K and Na chlorides, 1:1:1) is shown in Figure 3.2, along with the CD spectrum in the absence of these salts. No difference between the two spectra was discernible, indicating the lack of ion binding to this peptide.

3.3. Variable Temperature Study.

CD spectra* were recorded as a function of temperature, in methanol/glycerol (9:1), over the range +45°C → -142°C. The spectra in methanol only were exactly the same over the range

+45°C → -110°C. The lowering of temperature induced 'freezing' of the equilibruim mixture into a single conformation or related set of conformers (G. Siligardi et al, 1987).

The variation of CD spectra with temperature, between 260nm and 185nm, is shown in Figure 3.3; also shown is a plot of $\Delta\epsilon$ at 222nm (the absorption of the peptide chromophore) versus temperature.

At the highest temperatures, the curve levelled off, indicating the presence of a high temperature conformation state; the lowest temperatures measured also showed a levelling-off of the curve - here the low temperature state has been 'frozen out'. At intermediate temperatures the plot indicated a fairly co-operative transition between the two states, with Tm, the 'melting temperature' ~-55°C. This conformation equilibrium can be represented as

State A (HIGH T) $\longleftrightarrow$ State B (LOW T)

At the lowest temperature measured (-142°C), the spectrum was similar to that of N-acetyl-L-Proline-N,N'-dimethylamide (V.Madison and J. Schellman, 1970). They assigned this to the presence of cis Pro peptide bonds (see Figure 3.4). It thus seemed likely that at lower temperatures in methanol/glycerol (9:1) solution, there was a preference for the peptide to adopt a conformation with a cis peptide bond at Pro(3). The high temperature spectrum was a mixture of conformers; an NMR study later helped to prove cis amide bonds were present (Chapter 6).

Figure 3.5. shows the CD spectrum as a function of temperature for the region 320 - 240nm and also the temperature variation of $\Delta\epsilon$ for the Phe and Tyr absorbances (Lb bands), at 257.5nm and 280nm respectively. These showed a different temperature behaviour, the Phe rings showing little change in environment until ~ -100°C, whereupon their absorption began to increase strongly. The Tyr on the other hand began to rapidly change at -60°C. This observation indicated that the Phe rings had a quite different chemical environment from the Tyr ring, and the tendancy towards a cis Pro(3) amide bond was not reflected in their environment until much later than the Tyr residue.

Figures 3.6, 3.7 and 3.8 show the change in $\Delta\epsilon$ with temperature at 210nm, 215nm and 230nm respectively. The plot at 210nm (where any interference from the Phe rings was manifest) had striking resemblance to that obtained for Phe at 257.5nm. A plot of $\Delta\epsilon$ at 257.5nm versus $\Delta\epsilon$ at 210nm, which gave a straight line, confirmed that these absorbances were from the same chromophore (Figure 3.9). The room temperature spectrum therefore contained some contribution from the Phe chromophores, but only a negligible amount, as seen by the very weak absorbance at 210nm.

At 215nm, the plot of $\Delta\epsilon$ versus T was very similar to that at 222nm. There was a high correlation when $\Delta\epsilon$ (215nm) versus $\Delta\epsilon$ (222nm) was plotted at each temperature (Figure 3.10), which indicated that the same chromophore, in this case the peptide bond, was responsible for the absorption. The maximum absorbance in this region (222nm) was therefore confirmed as being exclusively from the peptide chromophore ($n - \pi^*$).

Figure 3.8 shows the temperature variation of the absorption, $\Delta\epsilon$, at 230nm. There was expected to be a contribution from the Tyr chromophore at this wavelength, and the curve did not resemble that at 215nm and 222nm, where there was no aromatic interference with the peptide chromophores. It appeared therefore that contributions from both Tyr and peptide chromphores gave rise to this shape of curve, which remembled neither.

3.4. Resolution of the Components of the Conformational Equilibrium

The fact that CD spectra were additive was used to decipher the predominant conformations which existed in solution equilibria.

Using the spectrum at room temperature in methanol/glycerol (or the identical methanol spectrum) as one state, and the lowest temperature methanol/glycerol spectrum as the other, it was possible (Figure 3.11) to calculate spectra corresponding to different percentages of each state; these calculated spectra corresponded almost exactly to the experimental results (Figure 3.3). This is further evidence that a two-state equilibruim existed, that position of equilibrium shifting as the temperature was varied. It was also possible to assign each spectrum at intermediate temperatures to an approximate percentage of State A (HIGH T) and State B (LOW T).

By the use of this additivity principle a much more striking result was obtained. The room temperature TFE CD spectrum and the

lowest temperature methanol/gylcerol spectrum were used to calculate spectra resulting from an equilibrium mixture of these two conformations. (Figure 3.12).

With 75% of the TFE spectrum, and 25% of the spectrum from the cryogenic mixture it was possible to generate an approximate methanol spectrum ie the methanol spectrum at room temperature can be represented as

~ 75% TFE structure $\longleftrightarrow$ ~ 25% structure with cis Pro(3) amide bond

At percentages of 75% of the TFE component, the calculated spectra mirror the low temperature experiment where State B was being 'frozen out'.

The TFE spectrum itself was a mixture of conformers, having less cis Pro(3) amide and more percentage of a structure with a trans amide bond, than RIP in methanol solution. From NMR data (Chapter 5), the percentage of each component in TFE was 37% cis Pro(3), 63% trans Pro(3).

A CD spectrum corresponding to 100% of the trans form in TFE/MeOH was then calculated using the low temperature methanol/glycerol and room temperature TFE spectra (Figure 3.13). The intensities and the approximate positions of maxima and minima indicated that the spectrum may bear some rememblance to a β-turn of type III (R.W. Woody, 1974).

The fraction of each component in methanol was also calculated once the ratio in TFE was known; the room temperature

methanol spectrum could be generated from 75% of the TFE and 25% of the spectrum from State B. (Figure 3.12) In methanol at room temperature the equilibrium therefore was of the form:

47% trans conformation $\longleftrightarrow$ 53% cis conformation

This was very close to the ratio calculated from NMR data (Chapter 6).

Considering the errors inherent in the 'synthesis' of CD spectra, the agreement of all these spectra with experimental results was very satisfying.

3.5 Solvent titration.

The conformational equilibrium which existed for RIP was dependent on solvent, both for the position of equilibrium, and the structures of the conformational components. To prove that TFE/MeOH was predominantly a two state system and TFE/H_2O, MeOH/H_2O was not, a solvent titration was carried out from 100% of one solvent to 100% of the other. Figure 3.14 shows the results obtained when RIP was titrated between TFE and methanol. Two isodichroic (isosbestic) points were obtained, at 195nm and 235nm. This was indicative of a two state system, as predicted from previous CD results, one state with cis peptide bonds and the other trans peptide bonds.

The TFE-H_2O solvent titration (Figure 3.15) in contrast, showed no isosbestic points. In this case, a two state system

did not exist. Titrating between H_2O and MeOH (Figure 3:16) also showed no isodichroic points, indicating that RIP in these solvents mixtures did not exist as a two-state system. NMR studies later proved that states A and B were present in H_2O. The absence of isodichroic points was best explained by the existence of a third state, C. This may have been present in TFE and MeOH solutions, but in lesser amounts than in H_2O. These results were invaluable in interpretation of ^1H NMR data.

3.6 pH Titration.

The behaviour of RIP over a range of pH values is shown on Figures 3.17 and 3.18 (320-230nm and 260-200nm respectively).

In the region 260-200nm there was a small variation in the intensity of the bonds centred at 222nm ($n-\pi^*$) and 205nm ($\pi-\pi^*$), with a greater intensity at lower pH, indicating a shifting in the position of equilibrium.

This pH induced conformational change was also reflected in an isosbestic point at 210nm, this being characteristic of a conformational equilibrium between two states, in this instance:

$$X \underset{OH^-}{\overset{H^+}{\rightleftharpoons}} Y$$

The plot of $\Delta\epsilon$, at 205nm, versus pH is shown in Figure 3.19.

At pH values lower than 1.98 the peptide precipitated, and so an approximate pKa value of the C-terminal Lys carboxyl and the influence which its ionisation state had on the conformation, could not be determined.

The shape of the pH versus $\Delta\epsilon$ curve showed there was no effect upon the conformation or position of equilibrium when the two His imidazole rings underwent protonation/deprotonation.

Although the two imidazole rings were undoubtedly important in the binding of RIP to renin, they appeared to play little role in stabilising the predominant conformations in an aqueous environment.

Figure 3.20 shows the CD spectrum (from 260-200nm) at pH values 9.44 and 11.31. The former was the situation in which the Tyr aromatic hydroxyl was unionised and in the latter the Tyr hydroxyl was in the charged form, resulting in a red shift in the absorbance of the La band of the Tyr moiety, to ~ 245nm, from ~225nm. Thus it no longer overlapped the absorbance from the peptide chromophore and the contribution the Tyr residue made to the absorption could be assessed. However, upon changing the pH from 9.44 to 11.31, the Lys side-chain amino and the N-terminal Pro(1) lost their positive charges. The changes observed in the spectrum may also be a reflection of the change in conformation resulting from either of these three ionisations/deionisation. There were a number of explanations:-

(i) The change in CD from pH 9.44 to 11.31 was a reflection of the contribution which Tyr made to the spectrum at ~ 225nm at lower pH values.

(ii) The de-ionisation of either the N-terminal Pro residue or the Lys side-chain removed an important stabilising ionic interaction resulting in this characteristic CD spectrum. This had originally been assigned to a 'random coil' structure, but has been recently re-interpreted as having a significant amount of polyproline II type of conformation (A.F. Drake et al, 1988).

(iii) A combination of (i) and (ii).

In the range 320-230nm (Figure 3.21) RIP had only Tyr and Phe Lb bands with no interference from the peptide chromophore. Upon ionisation, the Tyr absorbance shifted from ~280nm to ~295nm, and ~225nm to ~245nm, as expected; there was also a significant change in the environment experienced by at least one of the three Phe rings, as reflected in the change in intensity of the absorption at 260nm. Changing the pH over the range 9.44 to 11.31 therefore may have had an effect on the Phe rings, presumably because of a disruption of the peptide backbone. It was also possible that the large intensity increase was due to the movement of the Tyr La band to ~245nm, and not due to the Phe rings.

In general however, the changes in peptide backbone conformation with pH (as reflected in any absorbance changes) were very slight in comparison to the effects observed when the temperature was varied.

Figure 3.1 Room temperature CD spectra of RIP as a function of solvent polarity.

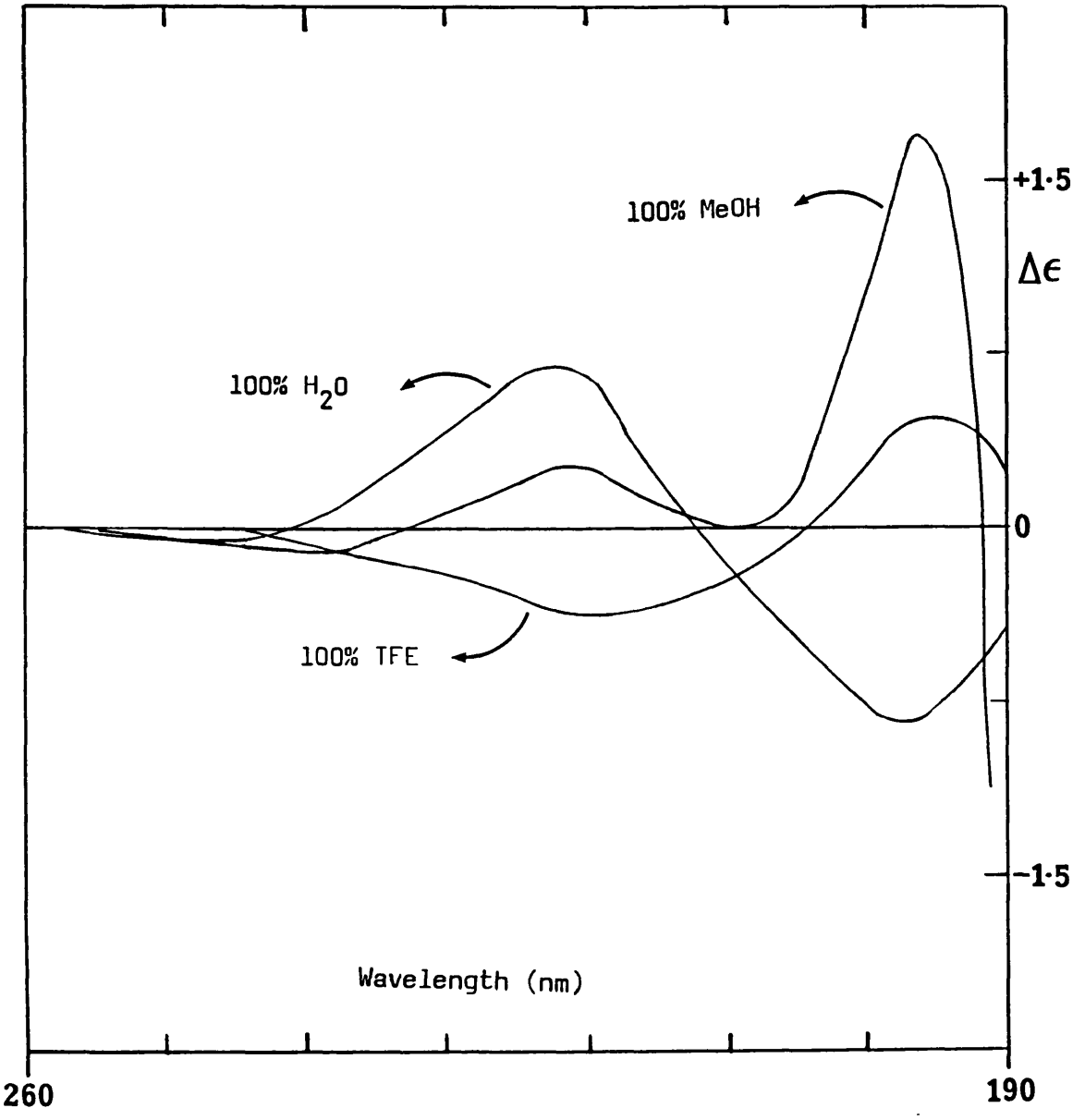
100% MeOH
100% H_2O
100% TFE
+1·5
Δϵ
0
-1·5
Wavelength (nm)
260
190

Figure 3.2 CD spectra of RIP recorded in the presence of, and in the absence of, a ten-fold excess of salts, to determine if ion-binding was occuring.

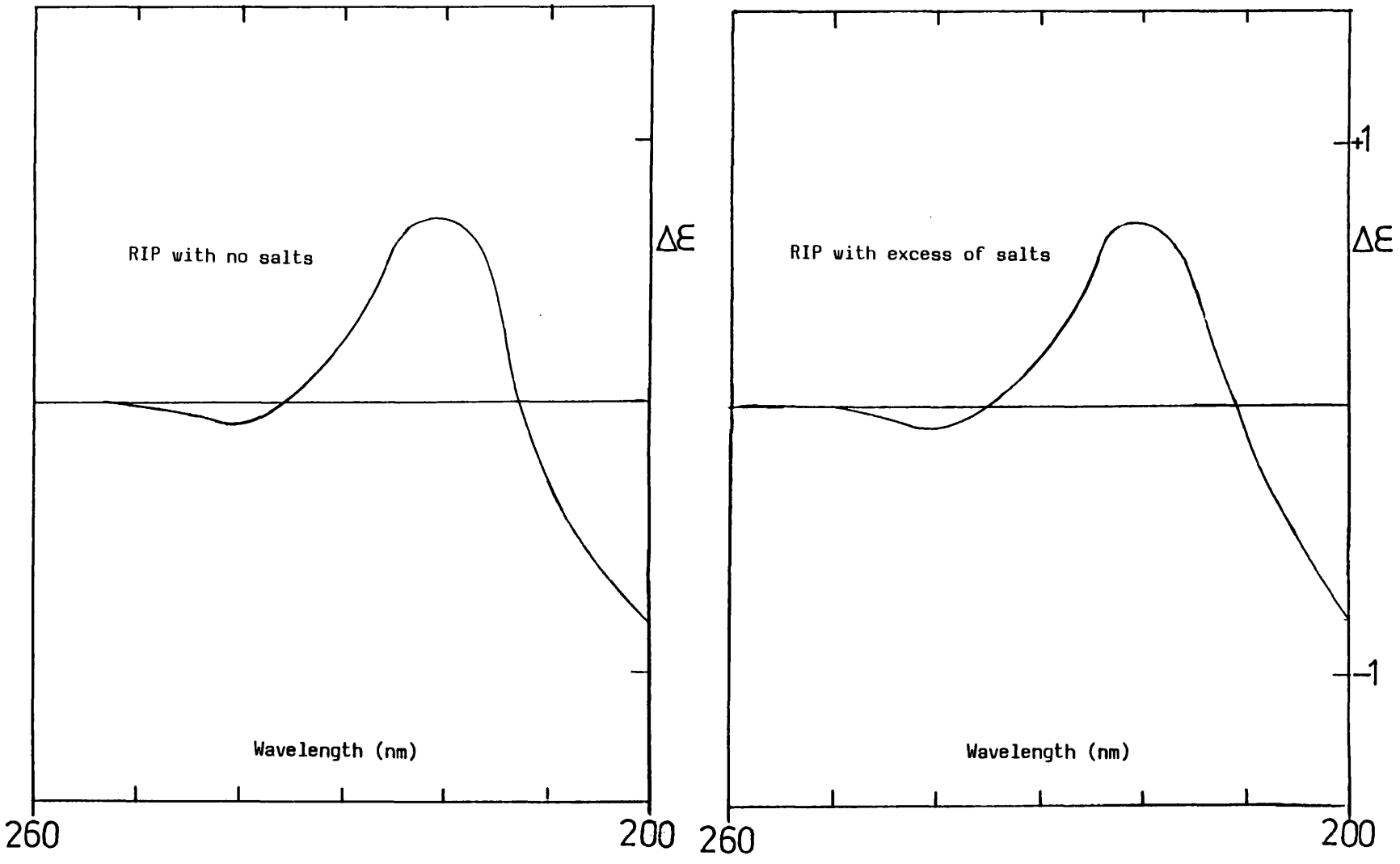
RIP with no salts
ΔE
Wavelength (nm)
260
200
RIP with excess of salts
+1
ΔE
−1
Wavelength (nm)
260
200

Figure 3.3 CD spectra of RIP recorded as a function of temperature, in methanol/glycerol (9:1) solution, from 260nm to 185nm. a = +17°C; b = -3°C; c = -13°C; d = -30°C; e = -54°C; f = -73°C; g = -108°C; h = -142°C.

Also shown is a plot of $\Delta\epsilon$ at 222nm versus temperature to indicate the 'freezing out' of the low temperature state.

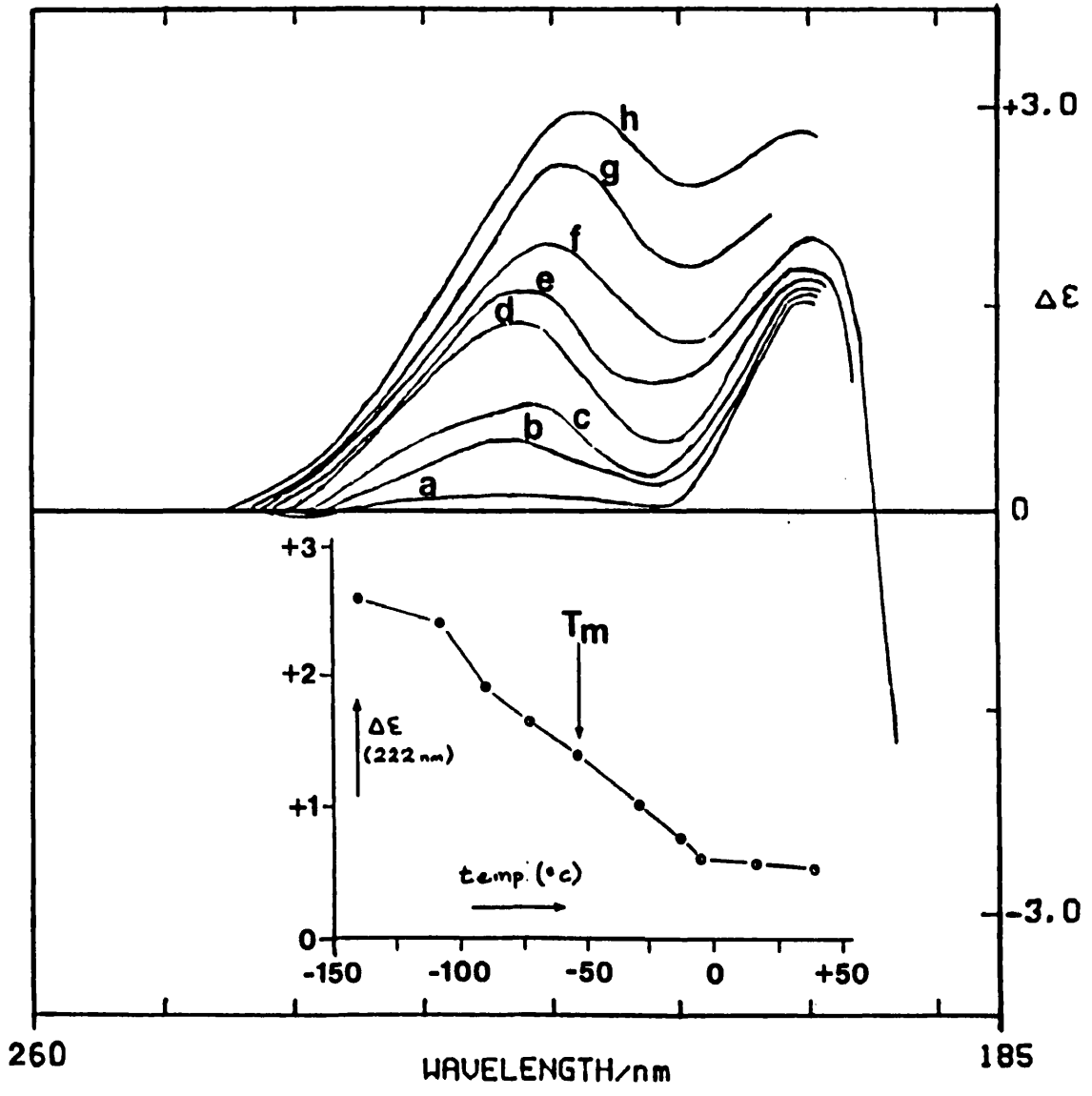
+3.0
Δε
0
-3.0
h
g
f
e
d
c
b
a
+3
+2
+1
0
Tm
Δε
(222 nm)
temp (°c)
-150
-100
-50
0
+50
260
WAVELENGTH/nm
185

Figure 3.4 Diagram to indicate the cis and trans orientations of the amide bond in peptides.

trans ⇌ cis

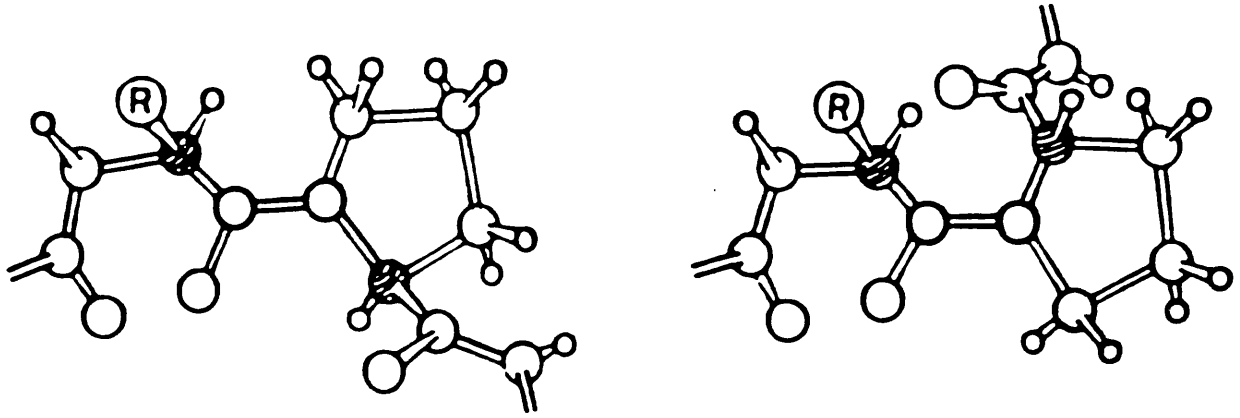

Figure 3.5 CD spectrum of RIP recorded as a function of temperature, in methanol/glycerol (9:1) solution, from 320nm to 240nm.

Also shown is a plot of $\Delta\epsilon$ versus temperature at 257.5nm and 280nm, to observe the temperature behaviour of the Phe and Tyr residues respectively.

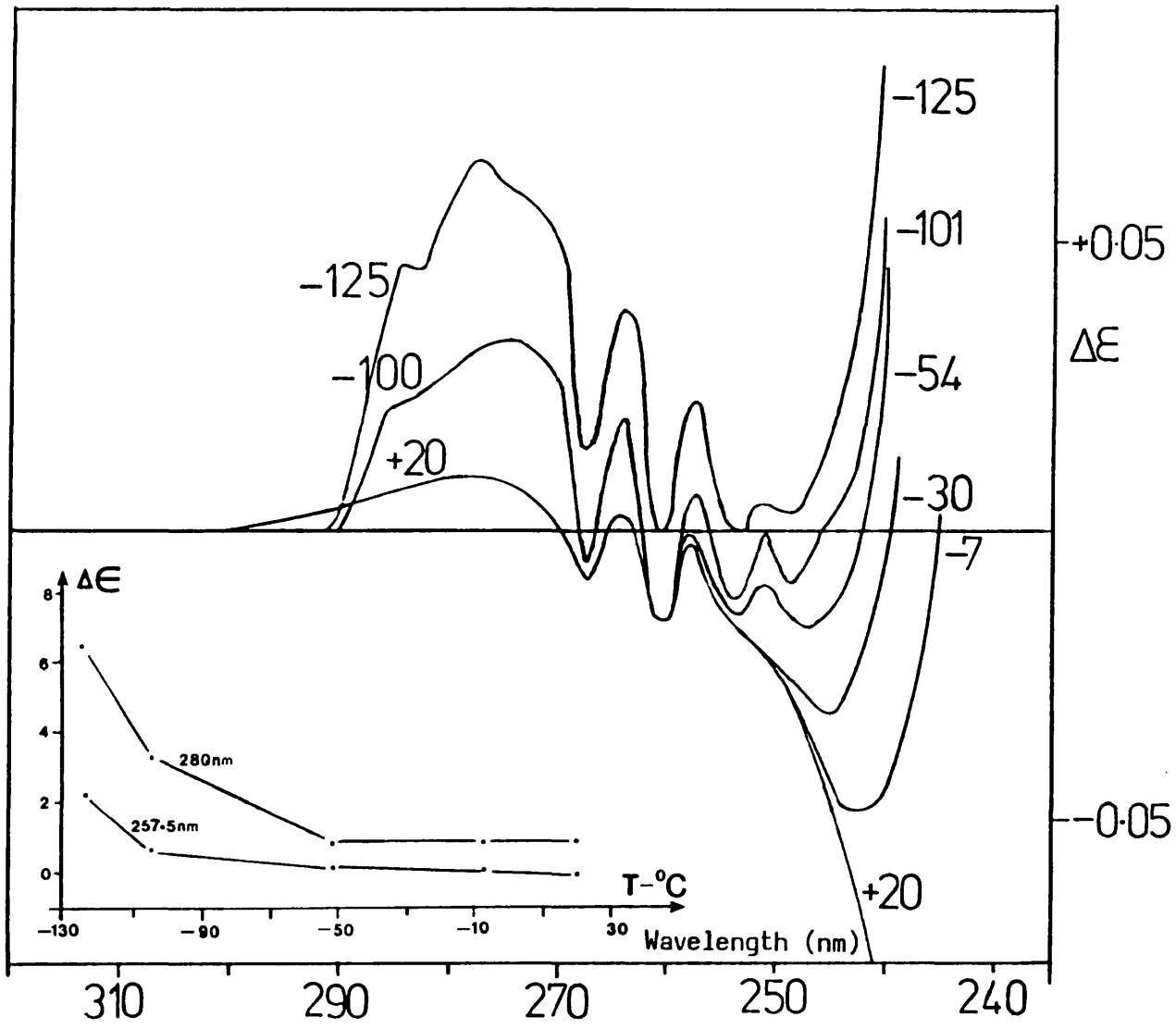
-125
-101
-54
-30
-7
+20
-125
-100
+20
+0·05
ΔE
-0·05
ΔE
8
6
4
2
0
280nm
257·5nm
T-°C
-130
-90
-50
-10
30
Wavelength (nm)
310
290
270
250
240

Figure 3.6 Plot of $\Delta\epsilon$ versus temperature at 210nm, for RIP, in methanol/glycerol (9:1) solution.

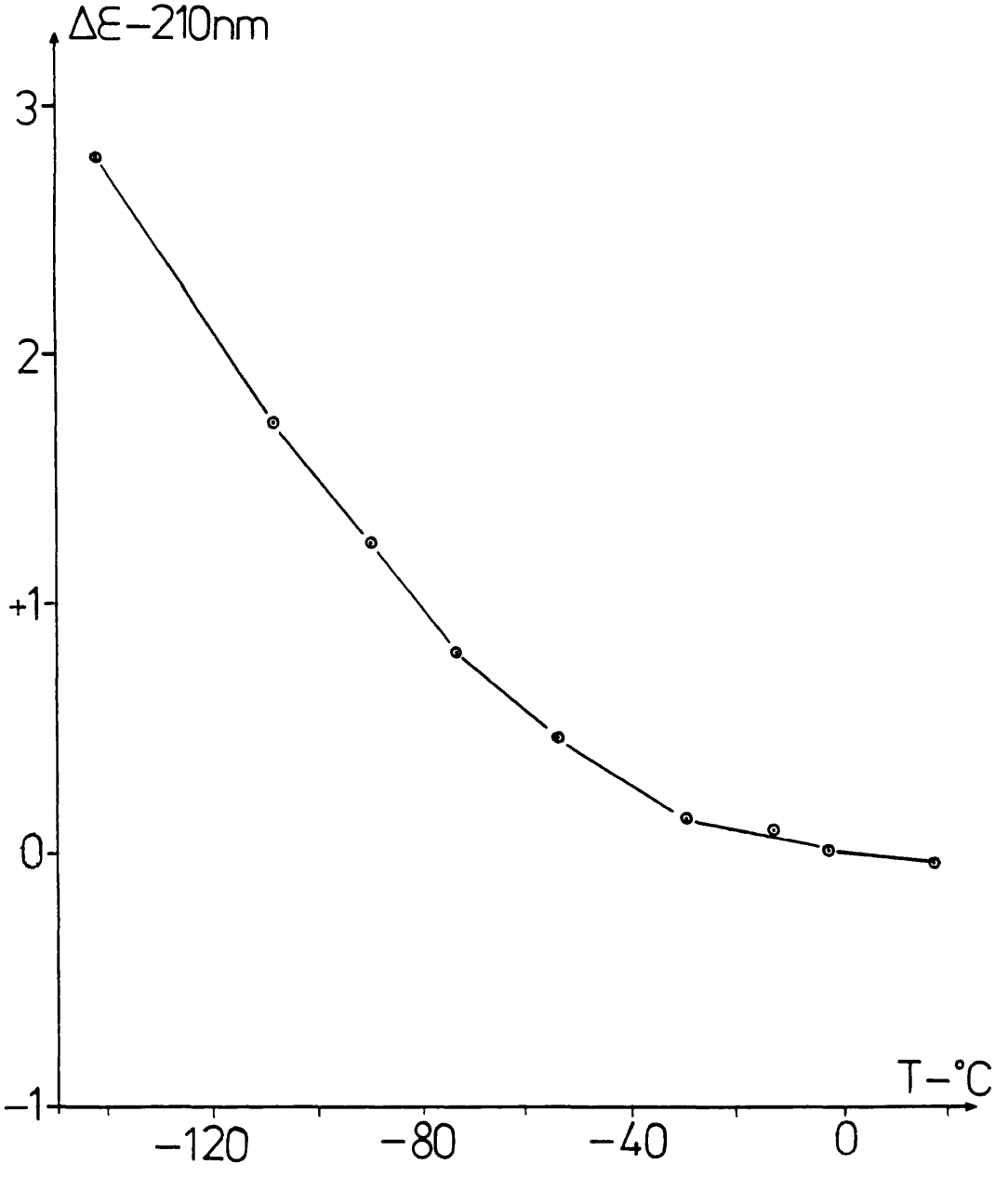
ΔE–210nm
3
2
+1
0
–1
T–°C
–120
–80
–40
0

Figure 3.7 Plot of $\Delta\epsilon$ versus temperature at 215nm, for RIP, in methanol/glycerol (9:1) solution.

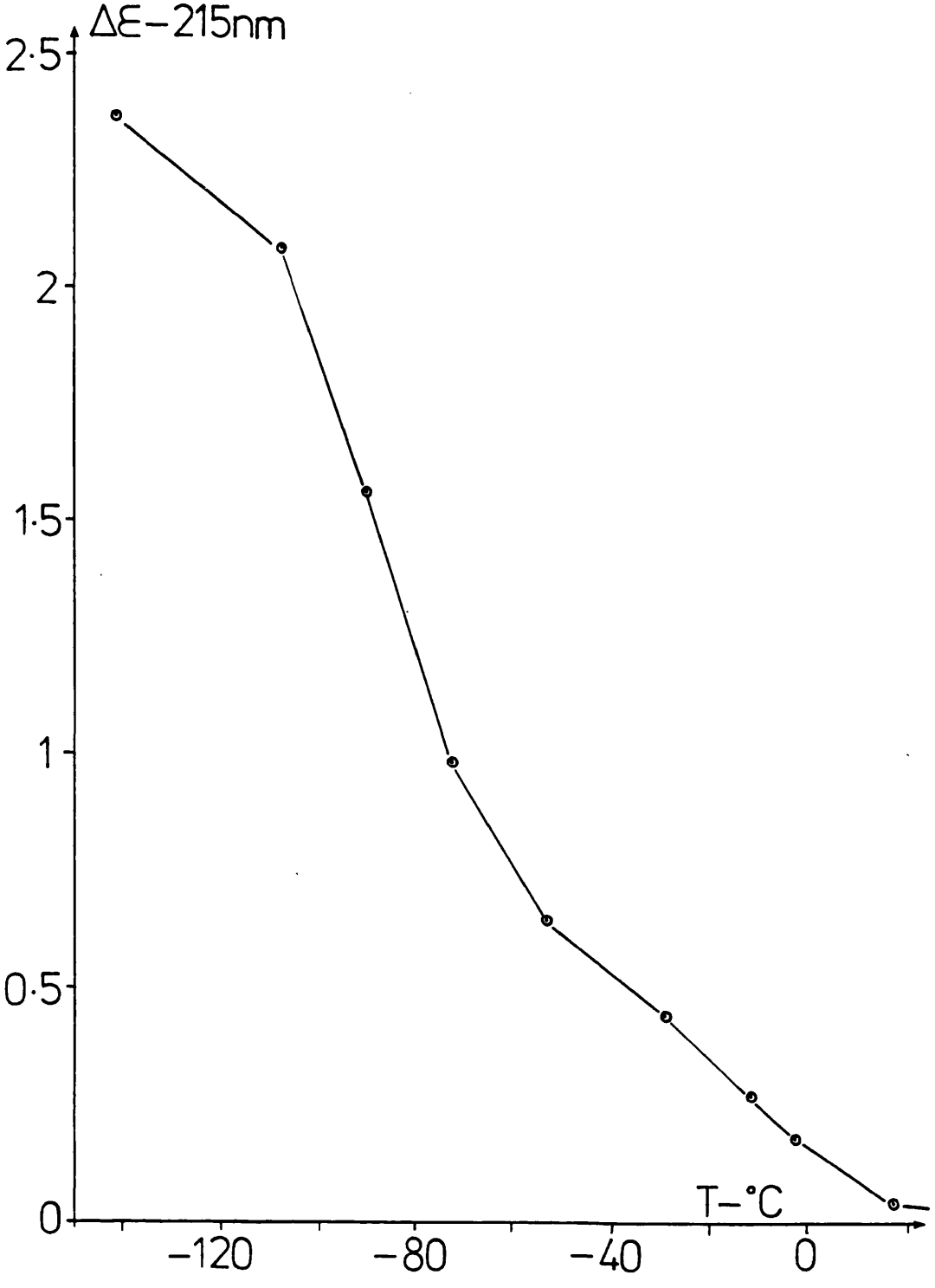
ΔE–215nm
2·5
2
1·5
1
0·5
0
T–°C
–120
–80
–40
0

Figure 3.8 Plot of $\Delta\epsilon$ versus temperature at 230nm, for RIP, in methanol/glycerol (9:1) solution.

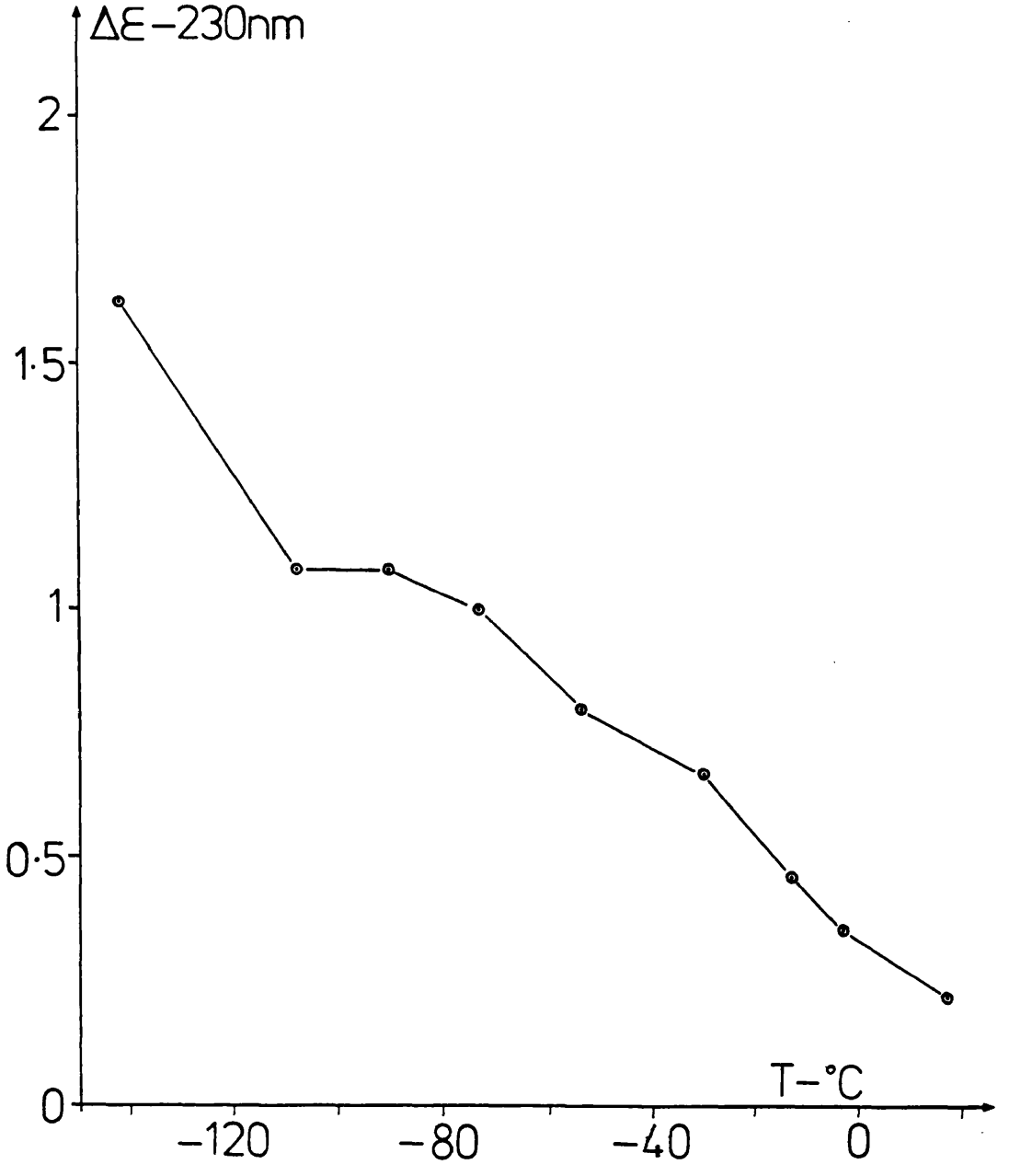
ΔE−230nm
2
1·5
1
0·5
0
T−°C
−120
−80
−40
0

Figure 3.9 Plot of $\Delta\epsilon$ at 257.5nm versus $\Delta\epsilon$ at 210nm, at different temperatures.

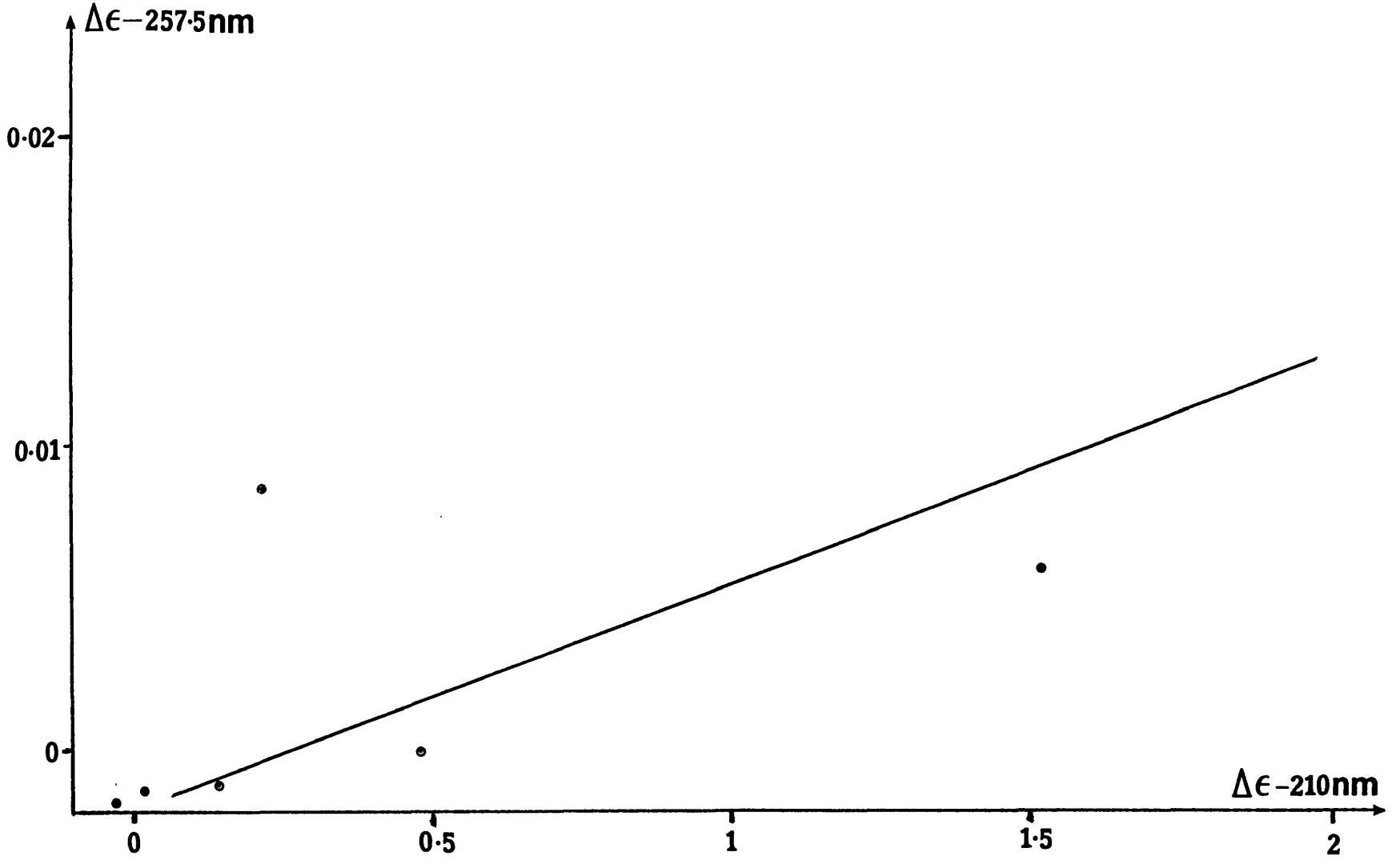
Δε−257·5nm
0·02
0·01
0
Δε−210nm
0
0·5
1
1·5
2

Figure 3.10 Plot of $\Delta\epsilon$ at 215nm versus $\Delta\epsilon$ at 222nm, at different temperatures.

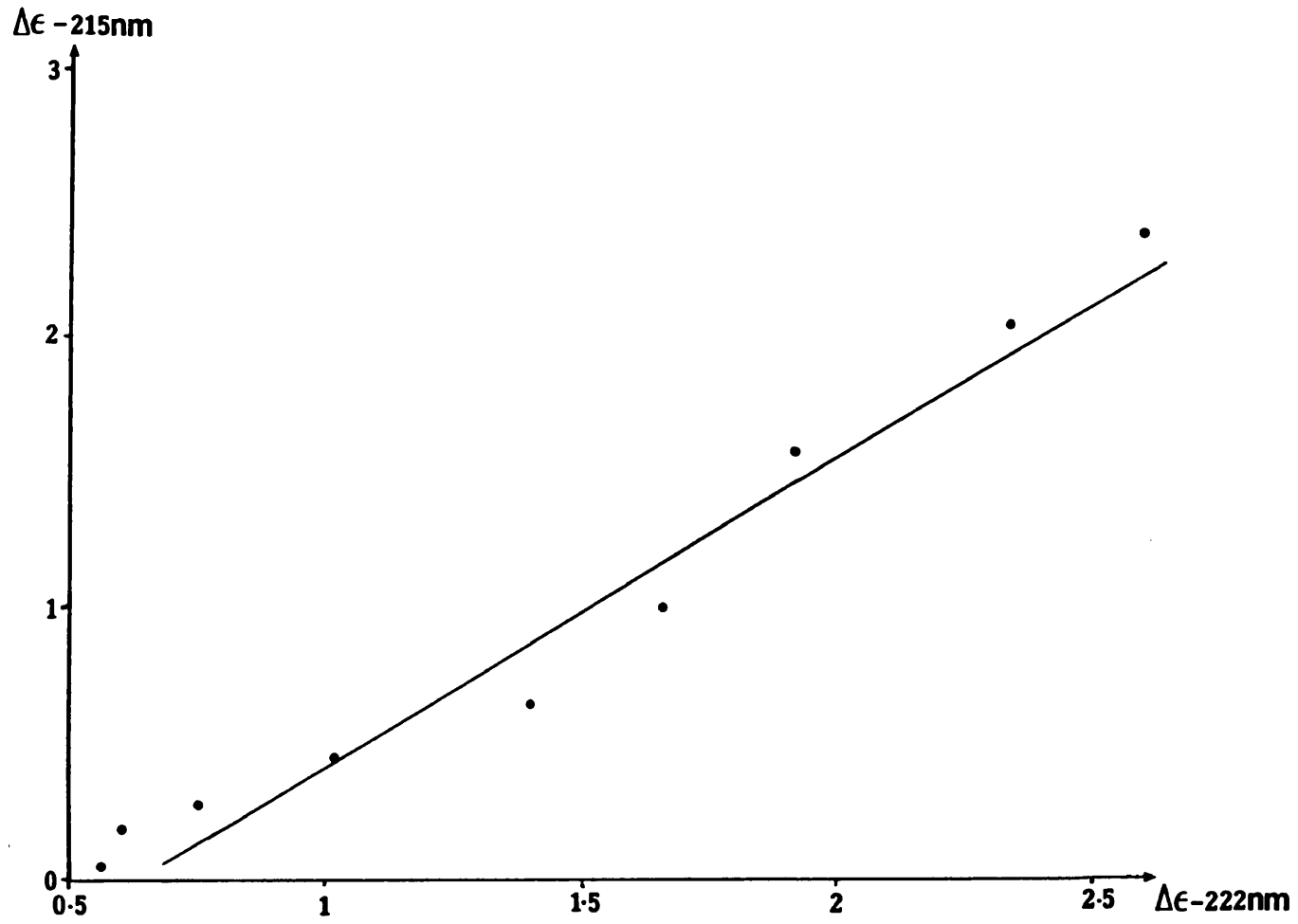
Δε -215nm
3
2
1
0
0·5
1
1·5
2
2·5
Δε-222nm

Figure 3.11 Shown are the CD spectra which were calculated from the room temperature methanol spectrum and the lowest temperature methanol/glycerol spectrum.

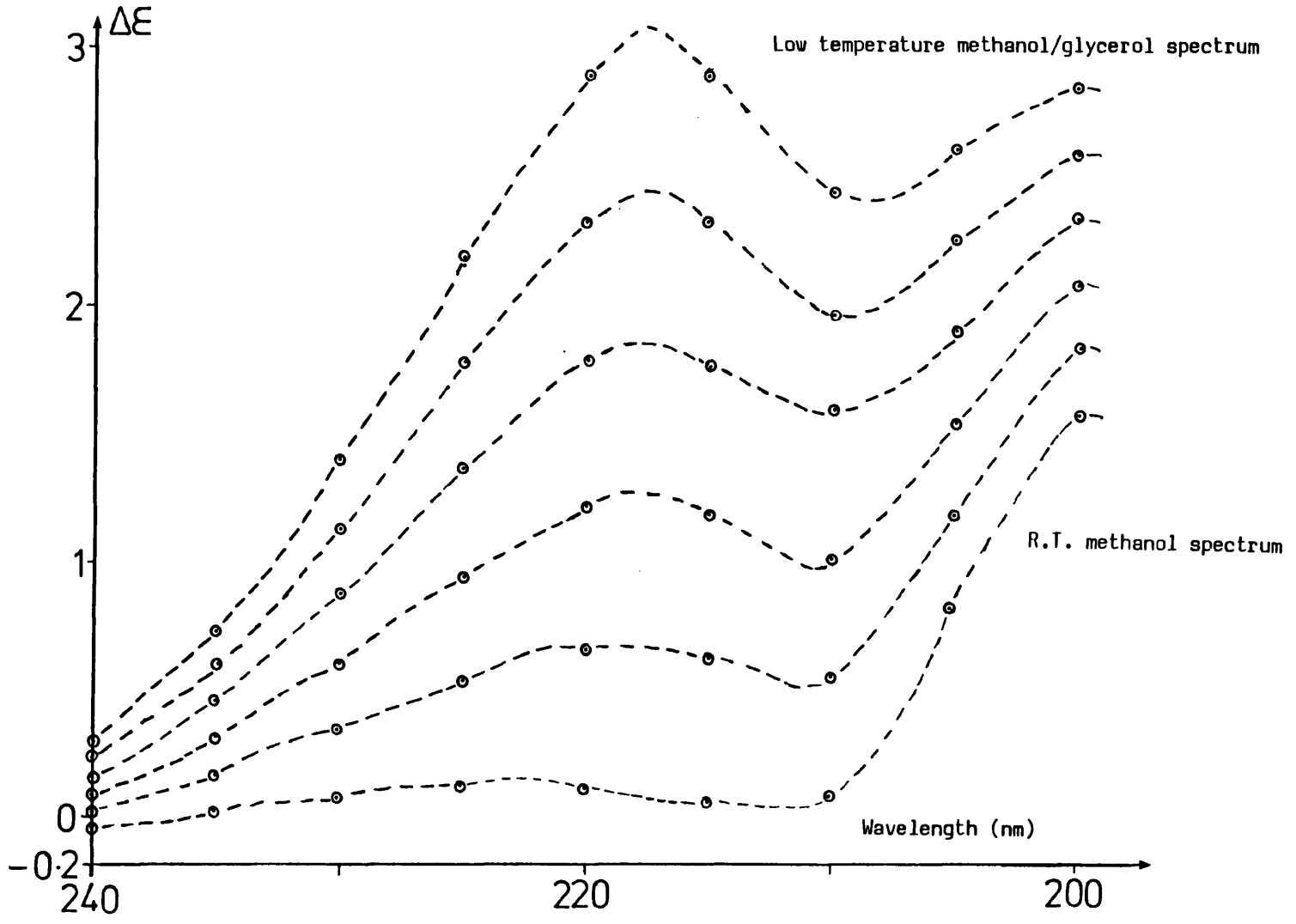
ΔE
3
2
1
0
-0·2
240
220
200
Wavelength (nm)
Low temperature methanol/glycerol spectrum
R.T. methanol spectrum

Figure 3.12 Shown are the CD spectra which were calculated from the room temperature trifluoroethanol spectrum and the lowest temperature methanol/glycerol spectrum.

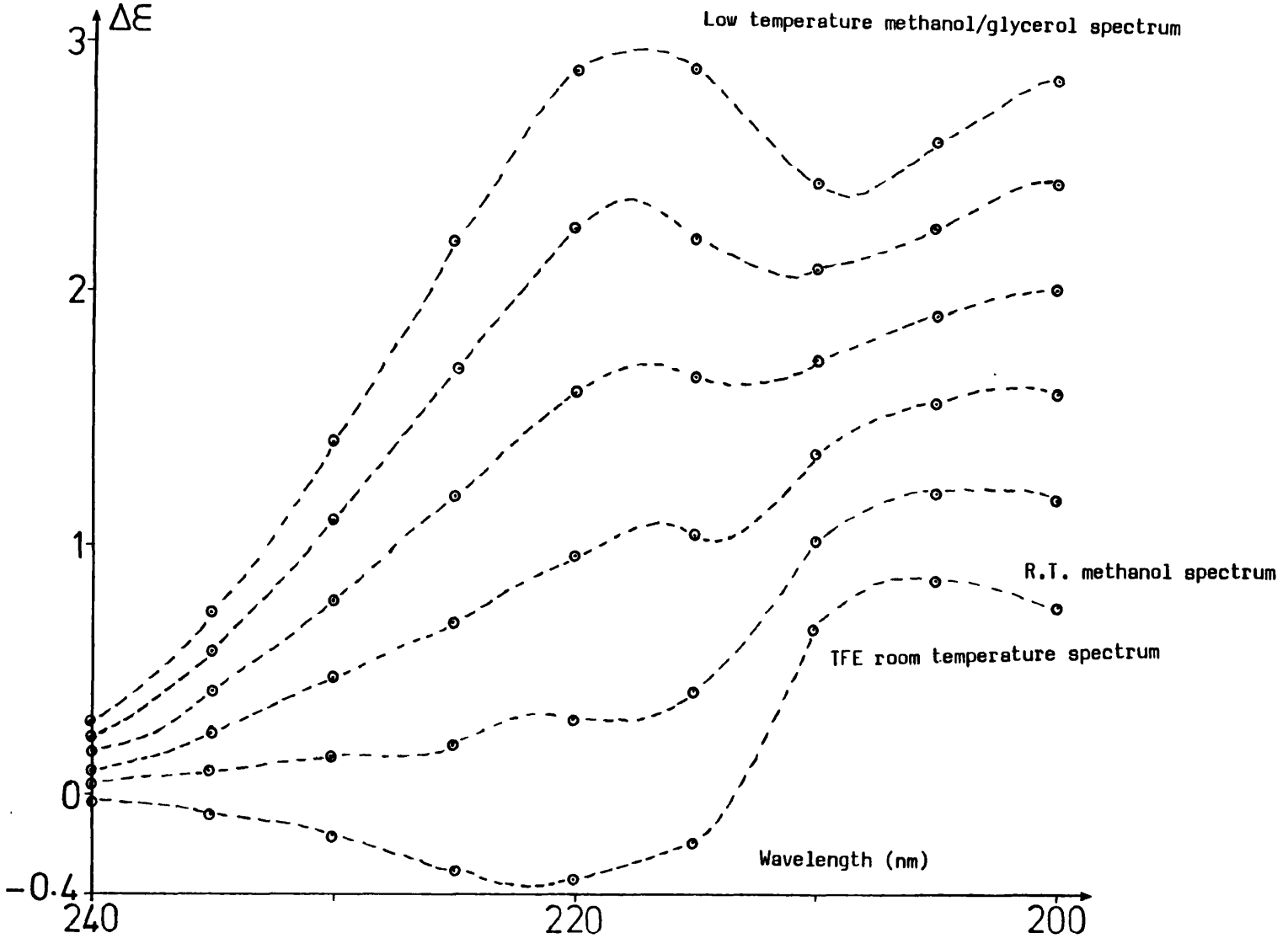
ΔE
3
2
1
0
-0.4
240
220
200
Low temperature methanol/glycerol spectrum
R.T. methanol spectrum
TFE room temperature spectrum
Wavelength (nm)

Figure 3.13 Calculated CD spectrum for the 'trans form' of the conformational equilibrium existing for RIP using NMR data to determine the percentage of each form in trifluoroethanol.

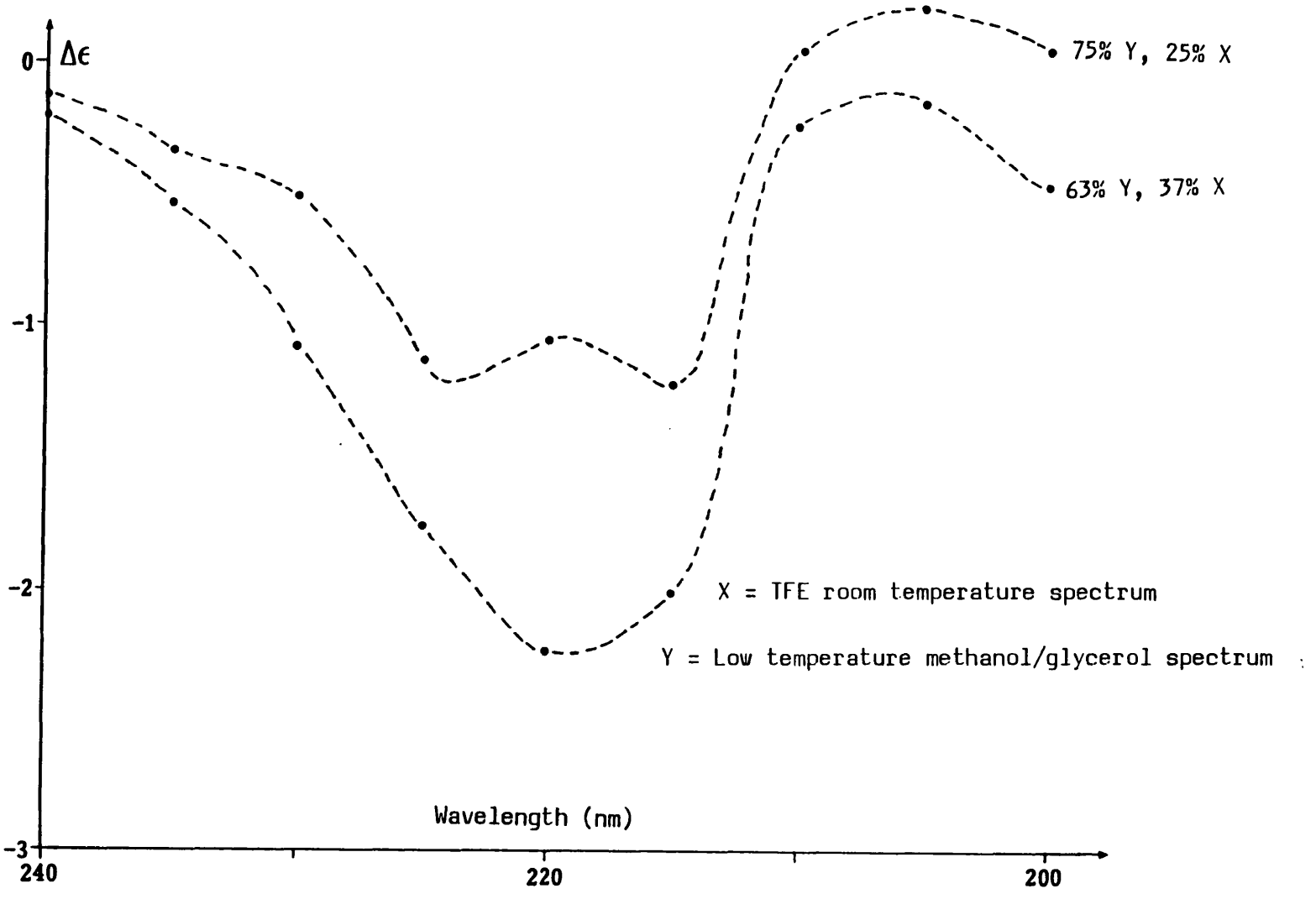
0
Δε
-1
-2
-3
240
220
200
Wavelength (nm)
75% Y, 25% X
63% Y, 37% X
X = TFE room temperature spectrum
Y = Low temperature methanol/glycerol spectrum

Figure 3.14 CD solvent titration for RIP, between MeOH and TFE. The percentage of each form is indicated. Note the presence of two isodichroic points in this plot.

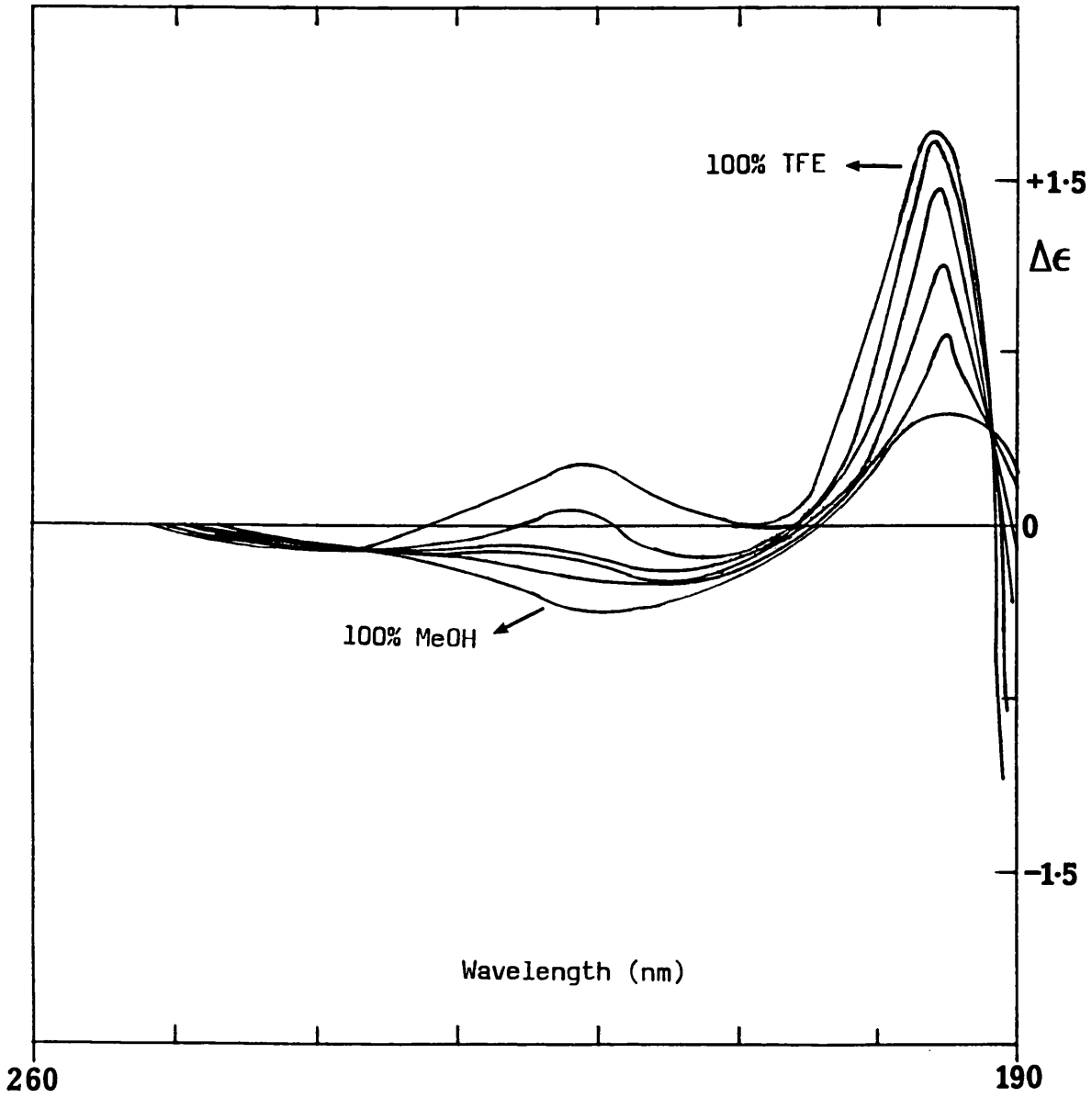
100% TFE
+1·5
Δϵ
0
100% MeOH
-1·5
Wavelength (nm)
260
190

Figure 3.15 CD solvent titration for RIP, between TFE and H_2O. The percentages of each form is indicated. Note the absence of any isodicroic points in this plot.

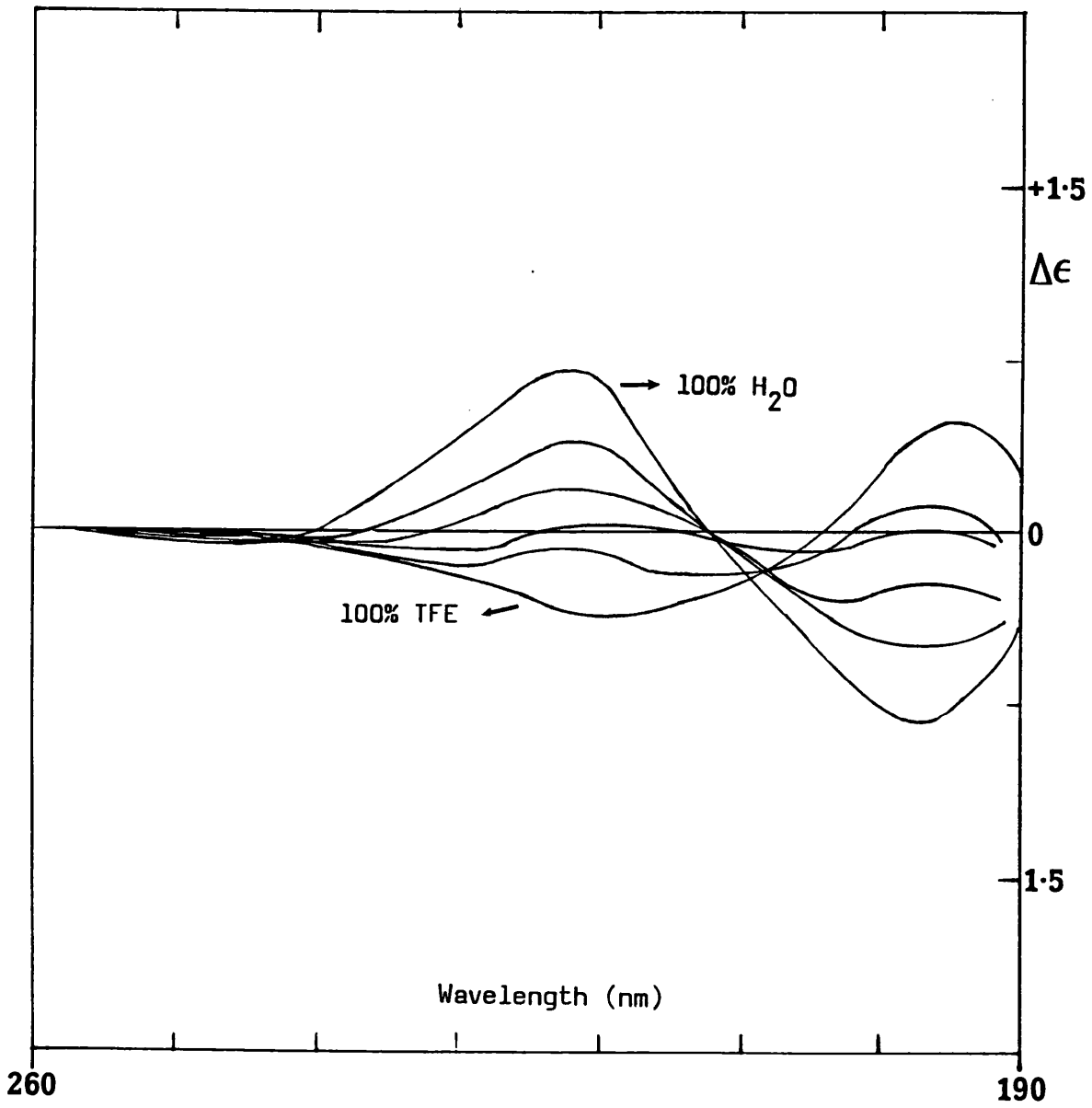
+1·5
Δε
100% H_2O
0
100% TFE
1·5
Wavelength (nm)
260
190

Figure 3.16 CD solvent titration for RIP, between MeOH and H_2O. The percentage of each form is indicated. Note the absence of any isodichroic points in this plot.

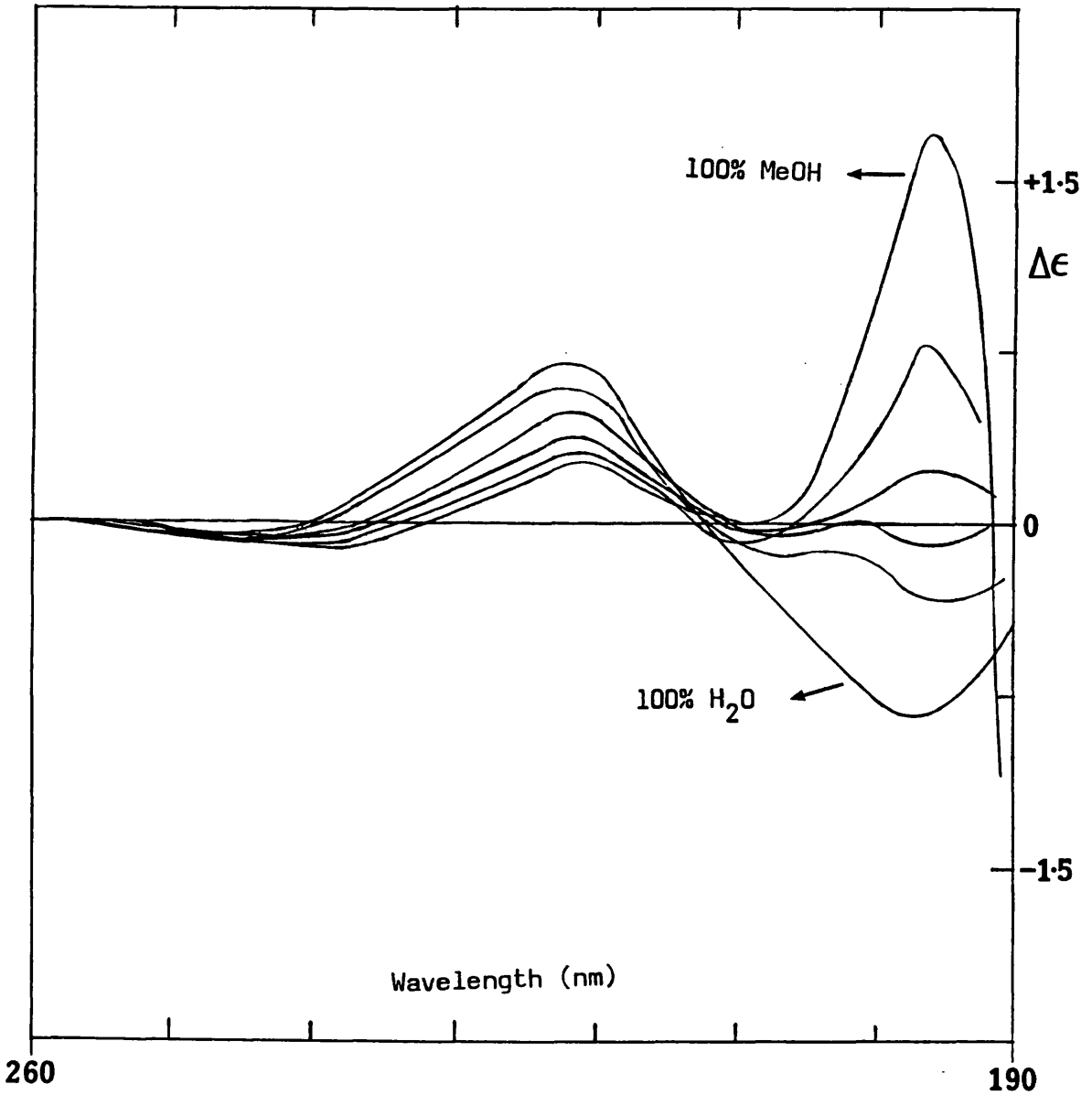
100% MeOH
+1·5
Δϵ
0
100% H2O
-1·5
Wavelength (nm)
260
190

Figure 3.17 CD spectra of RIP recorded as a function of pH, between 320nm - 230nm, to observe any effects on the Tyr and Phe side-chains.

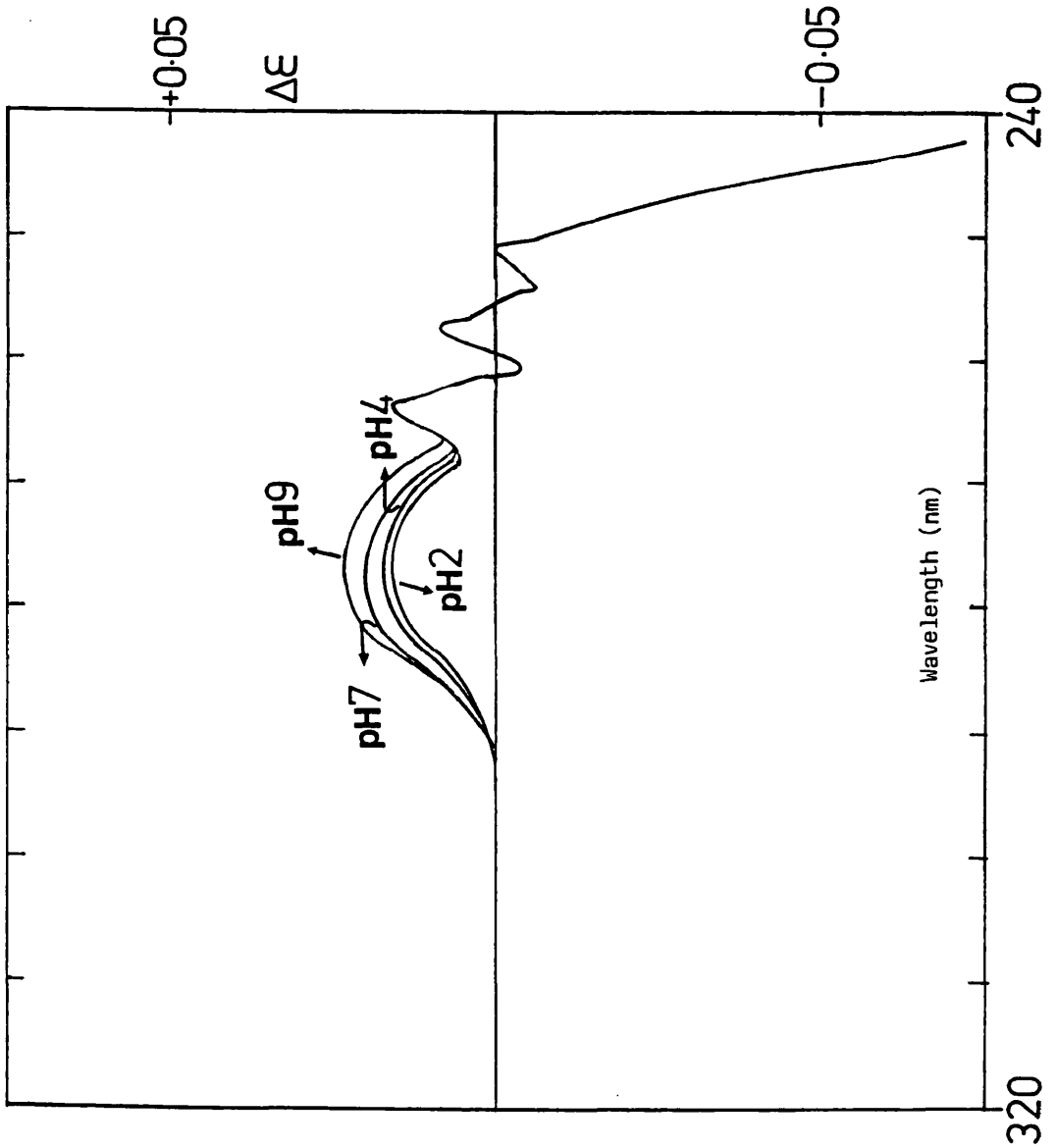
+0·05
Δε
−0·05
240
320
Wavelength (nm)
pH9
pH4
pH2
pH7

Figure 3.18 CD spectra of RIP recorded as a function of pH, between 260nmmm 200nm, to observe any effects on the peptide backbone (and aromatic side-chains).

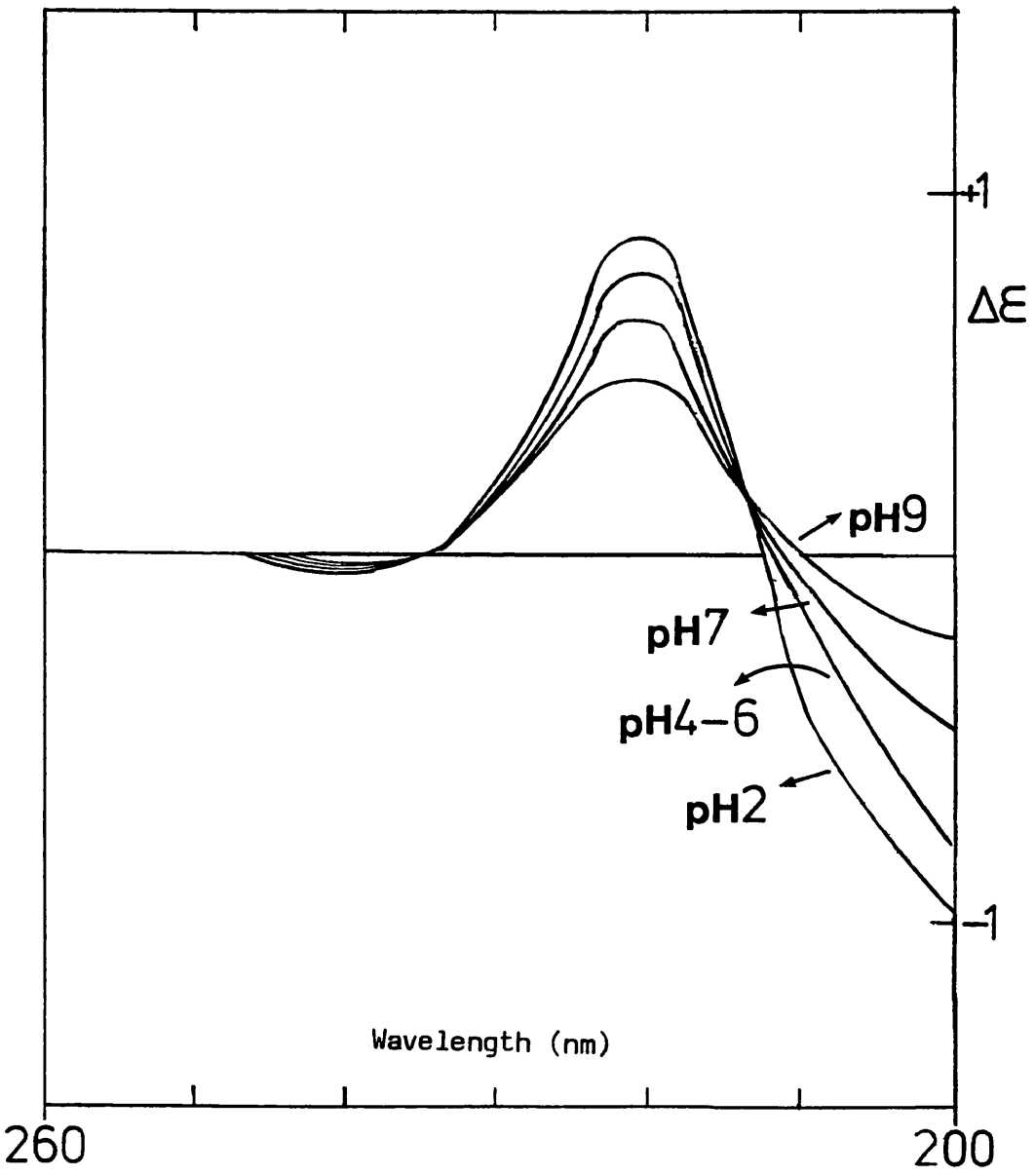
+1
ΔE
pH9
pH7
pH4–6
pH2
–1
Wavelength (nm)
260
200

Figure 3.19 Plot of $\Delta\epsilon$ at 205nm versus pH, for RIP, between pH 2 and 9.

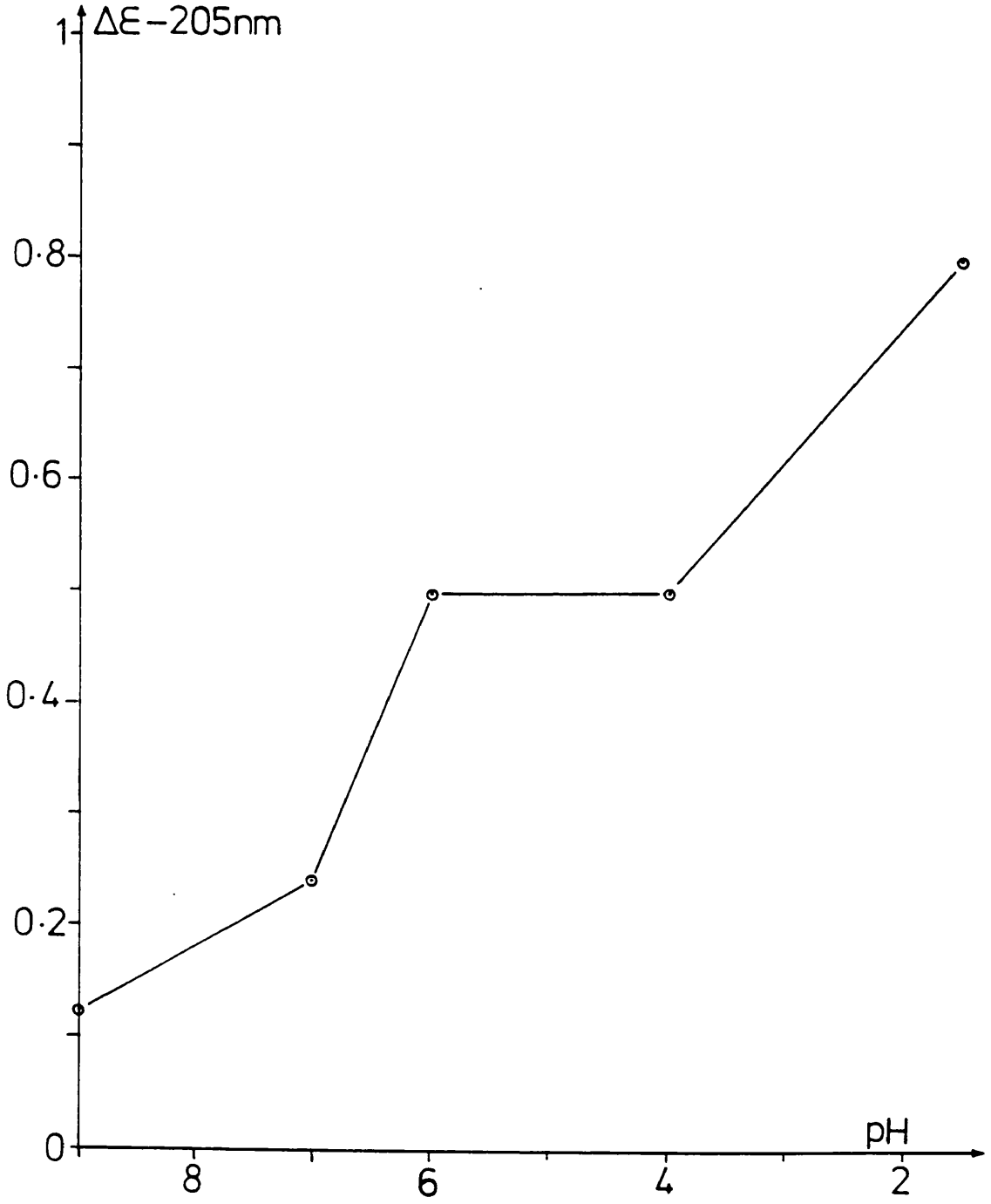
ΔE −205nm
1
0·8
0·6
0·4
0·2
0
8
6
4
2
pH

Figure 3.20 CD spectra of RIP, between 260nm and 200nm, at pH's 9.44 and 11.31, to observe any changes in conformation resulting from ionisation of Tyr residue, Lys side-chain and Pro N-terminus.

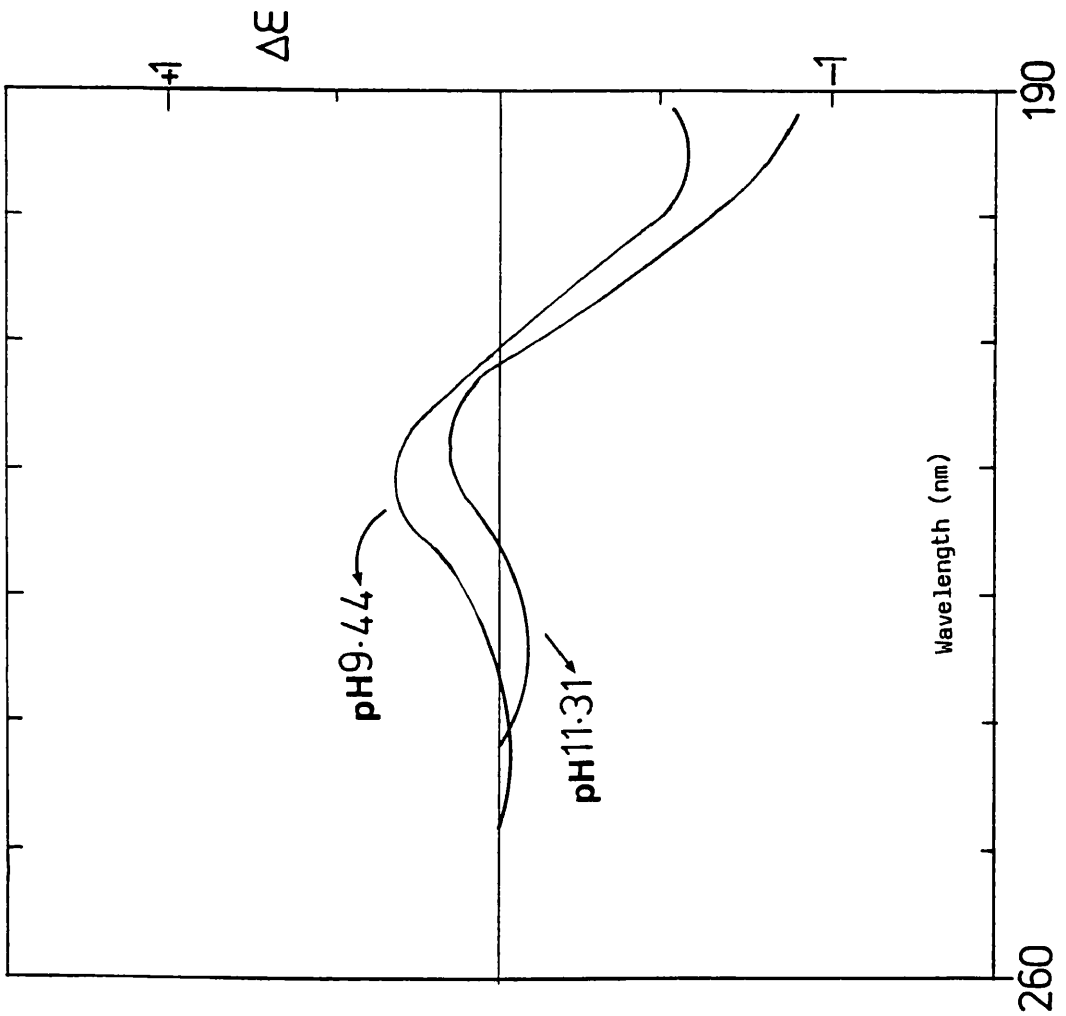
ΔE
+1
−1
190
260
Wavelength (nm)
pH9·44
pH11·31

Figure 3.21 CD spectra of RIP, between 320nm and 230nm, at pH's 9.44 and 11.31, to observe if Tyr ionisation has occurred.

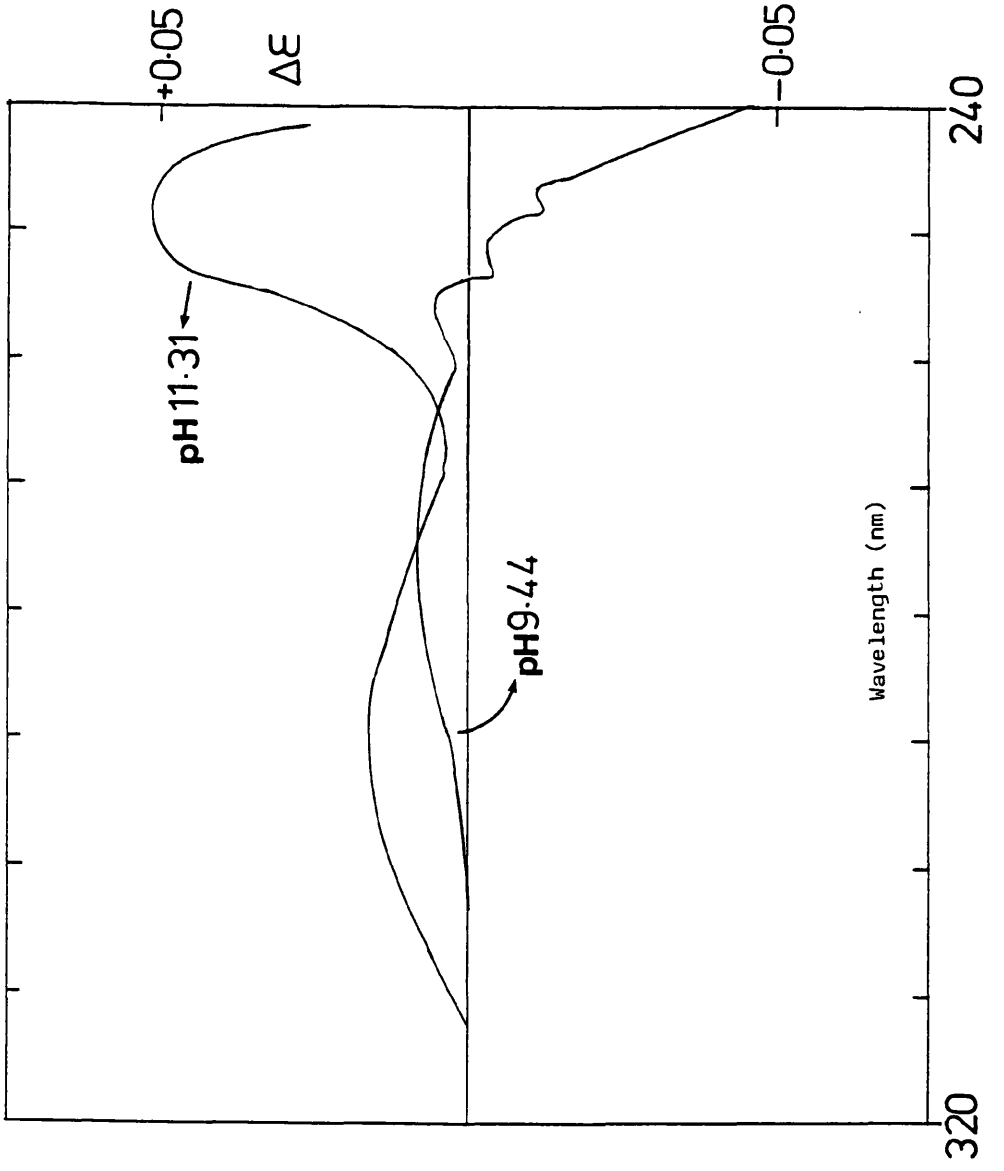
+0·05
Δε
−0·05
240
320
pH 11·31
pH 9·44
Wavelength (nm)

Chapter 4

NMR STUDIES OF RIP IN H_2O/D_2O

4.1 Assignment and Coupling Constants

The proton spectrum of a 10mM solution of RIP in an H_2O/D_2O mixture (60:40), at pH 3.31, is shown in Figure 4.1. To define the conformations adopted by the peptide, assignments for every proton in the molecule had first to be obtained.

To determine the pH value at which T_2 was a maximum for the water signal, so that the water peak had the minimum width, a Carr-Purcell-Meiboom-Gill (CPMG) sequence was employed (T.C. Farrar and E.D. Becker, 1971). At pH values between 5 and 2, the value of c for which the FID was not truncated was determined (c was the number of times the $(D2\text{-}180_y\text{-}D2)\text{-}_c$ procedure was carried out). The value of c was directly related to the T_2 of the water signal. Figure 4.2. shows the results of the experiment, where c was plotted against pH. The T_2 maxima occurred at pH ~3.3. This pH was maintained throughout all the NMR studies described in this chapter.

A Homonuclear Hartmann-Hann experiment (HOHAHA) was then performed, using MLEV-16 composite phase cycles for mixing in the inverse mode, and the Dante sequence for solvent supression. The experiment was optimised to observe coupling from J=0.5Hz upwards, by adjusting the time of the spin-lock. (Figure 4.3)

By taking sections through the F2 axis, it was possible to obtain assignments for 7 of the 8 amide protons (Figure 4.4.) Proline (3) had no amide proton, and the N-terminal proton of Pro (1) was exchange broadened and therefore not visible. Sections were thus taken through the α-protons of these residues.

The only α-proton not accounted for by these cross-sections appeared at 4.76ppm and was assigned to a His residue (Figure 4.4) (later assigned to His(2)).

The remaining NH proton, at 8.59 ppm also showed no cross-peaks and was therefore also assigned to His(2). These assignments were later confirmed by NOE experiments.

Although the HOHAHA gave assignments for each individual amino-acid within the peptide, more information was needed to make sequence specific assignments within RIP.

Using Nuclear Overhauser Enhancements (NOEs), whereby magnetisation was transferred between nuclei which were 1.5 to 5 Angstroms apart, (J.H. Noggle and R.E. Schirmer, 1971), their sequence specific assignments and information on the peptide's conformation were obtained.

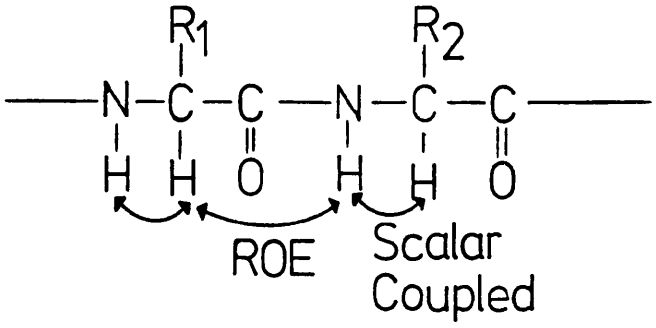

As CH_i and NH_{i+1} were close in space, a cross-peak in a 2-D NOESY experiment (See Materials and Methods) allowed connectivities between adjacent amino-acids to be established. In conjunction with the HOHAHA experiment, which showed scalar coupling, total assignment of each proton resonance to an exact position within the peptide was achieved.

In this instance, a NOESY experiment gave no cross-peaks between CH_i and NH_{i+1} on adjacent residues for mixing times, τm, between 100-400msec.

Figure 4.5 shows the dependence of the maximum NOE on the correlation time, τc, which is a measure of molecular motion. Small molecules tumble rapidly and have very small τc, of the order of 10^{-11} sec; for large macromolecules with much slower tumbling, τc, is of the order of 10^{-7} sec. The NOE changes from positive for small values of τc, to negative for larger τc values, passing through zero for intermediate sized molecules (800-2000 MWt). RIP falls within this region, and hence gave no observable NOEs,

However, spin-locked NOE methods have been developed (A.A. Bothner-By et al, 1984; H. Kessler et al, 1987; A. Bax and D.G.

Davies, 1988), known as the ROESY or CAMELSPIN experiment, in which the NOE is positive for all values of τc (Figure 4.5).

It was now possible to assign RIP totally, as well as determine which protons, far apart in the sequence, were spatially within 5Å of each other, thus helping to define the three-dimensional structure.

Shown in Figure 4.6 are sections through the F2 axis of the ROESY experiment. The rotating frame NOEs (ROEs) were negative with respect to peaks on the positive diagonal, and those which allowed assignments to be made were starred (*) eg. in the first cross-section shown, the Lys NH (easily recognised from its characteristic coupling pattern in the HOHAHA experiment), showed connectivity to the α proton of the adjacent residue of Tyr; a reference to the HOHAHA experiment showed protons to which the Tyr α proton was coupled (β,NH), and a cross section through its amide proton in the ROESY experiment gave a connectivity to the next amino-acid, in this case Val α.

Couplings between aromatic β protons (Tyr, 3 Phe's) and the protons at the 2 and 6 positions were not observed in the HOHAHA experiment; however these were observed in the ROESY experiment. The geometry of the system dictated that these ROEs were between protons from within the same amino-acid, their large intensities being an indication of their relative proximity in space. Figure 4.7 shows these β-aromatic connectives, which allowed sequence specific assignments of these aromatic protons. Once these 2 and 6 ring protons were assigned their connectitivies to other phenyl

* The Karplus relationships were derived from studies of hydrocarbons; the effect of the electronegativity of the nitrogen atom thus needs to be taken in to account.

Bystrov (1976) calculated this correction as

$$^{3}J_{NH-C\alpha} = 1.09J_{OBS}$$

ring protons were found, by reference to the HOHAHA experiment. (Figure 4.8).

The chemical shift values of each proton are listed in Table 4.1; also listed is the chemical shift difference between the observed value and that expected for the amino-acid in a totally non-folded peptide (A. Bundi and K. Wuthrich, 1979); also calculated was the distance to an aromatic residue. Hydrogen-bonding, or close proximity to aromatics both result in anomalous chemical shifts.

It should also be noted that certain residues had a multiplicity of peaks which were not expected from consideration of coupling. For Pro(3) δ protons, four peaks were observed (two intense, two less intense) (Figure 4.9).

The NH proton assigned to His(2) was broadened to such an extent that it was almost lost in the baseline. It was likely that because of its close proximity to Pro(1) NH_2^+, it was broadened by base catalysed exchange at intermediate rate. The positive charge of Pro(1) attracted hydroxide ions near to His(2)NH where it could undergo exchange as follows:

$$-NHCO- + OH^- \rightleftharpoons NCO^- + H_2O$$

NH-Cα coupling constants were corrected for electronegativity effects, and related to a quadratic equation (V.F. Bystrov, 1976) to give information concerning the preferred orientation(s) around the $-CH_i-NH_i$ bond, the ϕ_i dihedreal angle (Figure 4.10). In

conjunction with the ROE distance constraints, these were used to determine a 3-D structure for the peptide in solution, by computer calculations. Table 4.2 shows the coupling constants obtained and the calculated ϕ_i angles for $-NH_i-CH_i-$. The values for $J(NH_i-CH_i)$ for an α-helical type stucture are between 2-4Hz; for a 'random' type structure $J(NH_i-CH_i) \approx$ 5-7Hz; for a β-turn type of structure $J(NH_i-CH_i) \approx$ 8-11Hz (K. Wuthrich, 1986). Most of the corrected values were within this latter range, correlating well with CD results.

The percentages of gauche and trans rotamers were also determined (Table 4.2), from $J(C_{\alpha i}-C_{\beta i})$ coupling constants.

In general, the results here showed a lack of rotational freedom, as would be expected from a fairly rigid and folded structure.

4.2 ROEs and Structural Information

As mentioned previously, the ROESY experiment not only gave information which led to a full assignment, but indicated which protons were close together in space, and the approximate distance between them (J.H. Noggle and R.E. Schirmer, 1971). However, there were additional considerations in the ROESY experiment - the intensity of the ROE could not be directly transformed to distance by calibration, as in the NOESY experiment. When measuring the spin-locked NOE between coupled spins, the cross-peaks may have had contributions from Hartmann-Hahn type of transfer (A. Bax and D.G. Davies, 1988). In most cases this will not be important, but

measurement of ROEs between protons which were close in chemical shift may have been seriously affected.

Figure 4.11 shows sections through the F2 frequency of many nuclei where intramolecular ROEs were seen. There were indicative of folding and used in determination of the 3-D structure. Also indicated is the approximate strength of the ROE between the protons concerned. As mentioned above, it was not possible to determine absolute distances; however the intensity of the cross-peaks were still indicative of distances between protons. Therefore, ROEs were classified as follows, according to their intensities:

Strong - 2.75 ± 0.5Å

Medium - 3.5 ± 0.5Å

Weak - 4.5 ± 0.5Å

A large number of ROEs were observed between the three residues at the C-terminal end of the peptide (-Val(8)-Tyr(9)-Lys(10)-COO^-) and the three residues at the N-terminal (-Pro(3)-His(2)-Pro(1)-NH_2^+). One possible explanation for the N and C termini being brought together was an interaction between the positive charge and negative charge to form a salt-bridge (A similar situ ation has been reported for bradykinin, in which a C-terminal Arg forms a salt-bridge with the guanidino group of the N-terminal Arg. (V.T. Ivanov et al, 1975)). This 'cyclisation' would necessitate the formation of a β-turn (either with or

without the formation of a hydrogen-bonded structure), in order that the peptide backbone turned back on itself. The CD results in H_2O (See Chapter 3) were consistent with this observation; the CD pH titration also showed that removal of the stabilising influence of the ionic interaction, by raising the pH to above the pK of the N-terminal Pro, resulted in a drastic change in the peptide conformation. This interaction seemed therefore to be very important in stabilising structure.

Much fewer NOEs were observed from the region of RIP where the turn was expected to occur (4 → 7). This may indicate that this region was much less rigid than the N and C termini region. There were ROE cross-peaks indicating an interaction between the phenyl rings of residues 4 and 7, and the His(5) imidazole ring with these two rings (Figure 4.11). The protons of both benzenoid rings were ring-current shifted (R.A. Dwek, 1973) (See Table 4.1), as compared with protons in a non-structured environment. The shielding of the aromatic rings indicated that each spent a significant amount of time above and below the plane of the other aromatic ring, and not in the plane.

This interaction was of the form:-

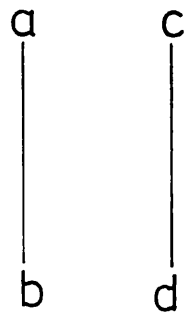

(This results in a shielding of the protons in both rings).

and not:-

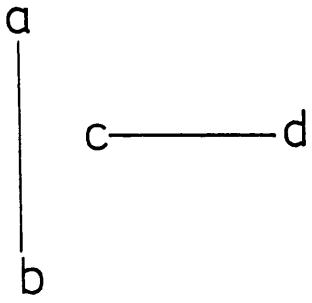

(This results in a deshielding of the protons on one of the rings, and shielding in the other).

4.3. Temperature Variation of Amide Chemical Shifts.

RIP amide chemical shifts are shown as a function of temperature in Figure 4.12. The slope of the plot helped to distinguish between protons which were in different environments, and may also indicate which protons were involved in hydrogen-bonding, in conjunction with other techniques (NOEs, IR), or shielded from solvent by steric effects. A fairly arbitary range for the gradients for the protons in hydrogen-bonded and non hydrogen-bonded environments is $+1 \rightarrow -5 \times 10^{-3}$ ppm/°C for the former, and $-6 \rightarrow -10 \times 10^{-3}$ ppm/°C for the latter.

The behaviour of the RIP amide protons were therefore divided into two different categories,

a) Protons corresponding to Val(8)NH, Lys(10)NH, PheNH(6), PheNH(7) and His(5)NH, which had gradients of -6.5×10^{-3} ppm/°C $\rightarrow$ -5×10^{-3}ppm/°C.

b) Protons corresponding to Tyr(9)NH and Phe(4)NH, with gradients of -8×10^{-3}ppm/°C → -9×10^{-3}ppm /°C.

It should be noted that the shallowest gradients corresponded to the protons which were furthest displaced in chemical shift, from values expected for a non-structured peptide (Table 4.1).

Conversely, the two amide protons which gave the steepest gradients, and therefore reflected a much more variable environment, also showed least deviation from these standard chemical shift values for amide protons.

Although the first category of protons had gradients just outside the generally accepted range for involvement in hydrogen-bonding and/or solvent shielding effects, their values may be indicative of either one of, or both of, these phenomena.

4.4 T_1 Measurements.

T_1 measurements were recorded using the Inversion Recovery method (T.C. Farrar and E.C. Becker, 1971), 180°_x -t_1- 90°_x - acquisition (See Materials and Methods). (Figure 4.13).

It was possible there would be a correlation between the T_1 experiment value and the amide temperature gradient. In the previous section the difference between the two sets of amide protons were accounted for by solvent shielding effects and/or some hydrogen-bonding character.

T_1 measurements were a reflection of the interaction between the nuclear spin and the lattice, and so the protons least exposed to solvent molecules lost their longitudinal magnetisation much

slower (longer T_1, lower rate) than those protons which, for a large percentage of their time, felt the effects of the surrounding lattice (short T_1, faster rate). The calculated T_1 values for RIP protons are shown in Table 4.3.

The data obtained again showed two classes of amide protons, designated as before. The two protons which showed most variation in chemical shift with temperature, Tyr(9) and Phe(4), had the longest T_1, showing their relative shielding from solvent lattice, compared to the second class of protons Val(8), Lys(10), Phe(6), Phe(7) and His(5), which were exposed to the solvent to a greater extent.

The good correlation between T_1 values and temperature gradients (Figure 4.14) indicated that long T_1 values, and hence less exposure to the surrounding lattice, were correlated with no hydrogen-bonding characteristics; short T_1 values, more exposure of the peptide backbone to solvent, correlated with some possible hydrogen-bonding character.

Though T_1 measurements gave valuable information, it was not possible to know beforehand if a hydrogen-bonded proton would have been more or less exposed to solvent than a proton in a non-hydrogen bonded region. Measurements were best used to define classes of protons, then other experiments were done to define structures much more precisely.

4.5. RIP Concentration Studies.

The aggregation of peptides at high concentrations is somewhat of a nuisance when studying solution conformations, and may tend to blur any folded structures which are present, or give anomalous NOE results . A ^{1}H NMR study of RIP at low and high concentrations was undertaken and the following NMR parameters monitored.

(1) Chemical Shift -

Aggregation of RIP to form, in effect, large polymers would affect the chemical/magnetic environment of specific protons such that they experienced a different effective magnetic field, and exhibited a change in chemical shift.

(2) Coupling Constants -

As aggregation proceeded the rotational freedom of parts of the molecule would change, and different rotamers become populated (V.F. Bystrov, 1976). The coupling constant, J, a direct measure of these rotamer populations, would change as a consequence of aggregation.

(3) Line-Width at Half-Height -

The observed line-width at half-height, inclusive of magnetic field inhomogeneities, $\nu_{1/2}$, is related to the 'effective T_2', T_2^* (T.L. James, 1975), by the equation

$$\nu_{1/2} = \frac{1}{\pi \; T_2^*}$$

If aggregation occurred, the T_2 value would decrease as the correlation time of the molecule decreased, resulting in a broadening of the resonances.

Spectra at four different concentrations of RIP, ranging from 0.74 to 12.20 mM were recorded at 500MHz. The results are shown in Table 4.4, listing the variation of chemical shifts, coupling constants and line-widths.

A comparison of each of these parameters in turn indicated that within experimental error, there was no variation with concentration. The chemical shift and coupling constant may not have shown any significant variation with aggregation. However, assuming little or no variation in the inhomogeneities of each of the samples, a significant decrease in T_2^* and a corresponding increase in line-width would have accompanied aggregation.

The absence of any such effects was evidence that no aggregation was occuring at these concentrations studies. Any ROEs or NOEs at these concentrations were therefore designated as intramolecular, and not intermolecular, in origin.

4.6. Chemical Exchange and Cis-Trans Isomerisation.

CD data indicated the likelihood of an equilibrium between cis and trans forms of the amide bond of Pro(3), with the trans form much more prevalent in aqueous solution. Indeed, four separate resonances were recognised for Pro(3) δ protons, where the isomerisation was expected to occur (Figure 4.9). The most intense two of these gave ROEs to the adjacent His(2) α-proton,

and so must, by a consideration of the geometry, have resulted from a trans orientation of the amide bond. The ratio of trans : cis was found to be approximately 82:18, by integration. The two resonances corresponding to a cis orientation were well separated from those of the trans form, and so it was possible to view cross-sections through all four Pro(3) δ resonances in the ROESY experiment (Figure 4.15). Figure 4.16 shows these cross-section in the F2 direction, at 3.44ppm and 3.29ppm, corresponding to the cis form, and 3.52ppm and 3.33ppm for the trans form.

The cross section through 3.44ppm showed an ROE to the Pro(3) proton at 3.33ppm, and a positive chemical exchange peak to the proton at 3.52ppm. This indicated immediately that the resonances at 3.52ppm and 3.44ppm were from the same proton which was in slow (by the NMR timescale) exchange between two different chemical environments, in this case trans (3.52ppm) and cis (3.44ppm) forms of the amide bond. The ROE observed at 3.33ppm was to the other δ proton, in the trans form. No ROE was found between the two protons when in the cis form; this was not too surprising because the signals were weak in intensity and any ROE would most likely not be seen above spectral noise.

The cross-section through 3.29ppm showed a chemical exchange cross-peak to the same proton in the trans form, at 3.33ppm. There were ~ 2.8Hz/pt. in the spectrum and so it seemed unlikely that this was due merely to overlap with the more intense signal at 3.33ppm. This again was more evidence supporting cis-trans isomerisation about Pro(3).

Cross-sections taken through Pro(3) δ protons at 3.33ppm and 3.52ppm revealed neither ROEs nor chemical exchange peaks to either of the cis forms at 3.29ppm and 3.44ppm respectively. As previously, any cross-peaks to these very weak signals may have been lost in the baseline.

The existence of cis-trans isomerisation about the Pro(3) peptide bond can be used as an explanation for the anomalous T_1 and amide temperature variation of Phe(4) and Tyr(9)NH.

The movement and flexibility of the peptide backbone in this region would not allow any hydrogen-bonding character at Phe(4)NH, and may have had the effect of exluding water molecules from close proximity to this proton, hence giving a longer T_1 value than anticipated. For Tyr(9)NH, it was possible that the movement of the adjacent His(2)-Pro(1) moiety affected it in a similar manner to Phe(4)NH, but to a lesser extent, as reflected in the shorter T_1 value and shallower amide temperature gradient.

TABLE 4.1

Residue	Chemical Shift (ppm)		ΔObs.-Lit.	Distance to Aromatics (Å)
	α	4.12	-0.351	
	βu	1.80)	-0.181)	
	βD	2.23)	+0.249)	
Pro(1)	γ	1.80	-0.230	
	δu	3.22)		
	δD	3.22)	-0.433	5.00
	α	4.76	+0.130	
	βu	2.96)	-0.238)	
	βu	2.99)	-0.263)	
His(2)	NH	8.60	+0.185	
	1m2	8.36	+0.240	
	1m4	7.06	-0.08	
	α	4.21	-0.261	
	βu	1.58)	-0.401)	5.13
	βD	2.06)	-0.235)	
Pro(3)	γ	1.77	-0.260	
	δut	3.34)	-0.313)	
	δDt	3.52	-0.133)	
	δuc	3.29)	-0.363)	
	δdc	3.44)	-0.213)	
	α	4.29	-0.373	
	βu	2.69)	-0.443)	4.96
	βD	2.78)	-0.301)	
Phe(4)	NH	8.17	-0.058	
	2.6	6.94	-0.349	
	3.5	7.02)	-0.370)	
		7.05)	-0.340)	
	4	7.09	-0.249	
	α	4.32	-0.310	
	βu	2.86)	-0.363)	
	βD	2.90)	-0.338)	
His(5)	NH	7.98	-0.435	
	1m2	8.29	+0.170	
	1m4	6.80	-0.340	

Residue	Chemical Shift (ppm)		ΔObs-Lit .	Distance to Aromatics (Å)
	α	4.26	-0.403	5.11
	βu	2.71)	-0.281)	
	βD	2.76)	-0.463)	4.88
Phe(6)	NH	7.83	-0.398	
	2.6	6.94)	-0.349)	
		6.96)	-0.329)	
	3.5	7.08)	-0.310)	
		7.11)	-0.280)	
	4	7.04	-0.299	
	α	4.30	-0.363	
	βu	2.67)	-0.321)	4.69
	βD	2.70)	-0.523)	
Phe(7)	NH	7.91	-0.318	
	2.6	6.90	-0.389	
	3.5	7.03	-0.360	
	4	7.09	-0.249	
	α	3.77	-0.414	5.07
	β	1.69	-0.440	4.97
Val(8)	γu	0.60)	-0.342)	
	γD	0.62)	-0.349)	
	NH	7.60	-0.836	4.01
	α	4.29	-0.314	
	βu	2.75)	-0.172)	
	βD	2.82)	-0.307)	
Tyr(9)	NH	7.99	-0.193	
	2.6	6.95	-0.199	
	3.5	6.61	-0.247	
	α	3.97	-0.388	
	βu	1.58)	-0.167)	
	βD	1.77)	-0.100)	
Lys(10)	γ	1.12	-0.351	
	δ	1.44	-0.268	
	ε	2.76	-0.263	
	NH	7.64	-0.768	4.13

TABLE 4.2

Residue	Coupling constant (Hz)	Rotational Angle (degrees)
Lys (10)	J(NH-Cα) = 7.55 corrected = 8.23	θ = 14° and 149°; ϕ= 46°, 74°, -89°, -151°
	J(α - β_1) = 5.3) J(α - β_2) = 5.3)	67% gauche, 33% trans
Tyr (9)	J(NH-Cα) = 7.65 corrected 8.34	θ = 11°, 149° ϕ = 49°, 71°, -89°, -151°
Val (8)	J(NH-Cα) = 8.45, corrected = 9.21	θ = 156°; ϕ = -96° -144°, -151°
	J(α-β) = 8.3	48% gauche, 52%trans
Phe (8)	J(NH-Cα) = 7.50, corrected 8.18	θ = 14°, 148°; ϕ = 46°, 74°, -88°, -152°
Phe(6)	J(NH-Cα) = 7.10, corrected = 7.74	θ = 20°. 146°; ϕ = 40°, 80°, -84°, -154°

Residue (degrees)	Coupling Constants (Hz)	Rotational Angle
His (5)	$J(NH - C\alpha) = 7.95$	θ = o°, 152°
		ϕ = 60°, -92°
	corrected = 8.67	-148°
	$J(\alpha - \beta_1) = 8.4$)	
	$J(\alpha - \beta_2) = 8.4$)	28% gauche, 72% trans
Phe (4)	$J(NH - C\alpha) - 6.55$	θ = 24°, 142°;
		ϕ = 36°, 84°
	corrected = 7.14	-82°, -158°
Pro (3)	$J(\alpha - \beta_1) = 8.8$	θ = 20°, 146°
	$J(\alpha - \beta_2) = 9.0$	θ = 180°, 147°
His (2)	$J(NH - C\alpha) = 8.30$	θ = 154°; ϕ = -94°
	corrected = 9.04	-146°
	$J(\alpha - \beta_1) = 8.5$)	
	$J(\alpha - \beta_2) = 8.5$)	26% gauche, 74% trans
Pro (1)	$J(\alpha - \beta_1) = 8.8$	θ = 20°, 146°
	$J(\alpha - B_2) = 8.8$	θ = 20°, 146°

TABLE 4.3

Proton	T_1 value (seconds)
Phe (4) NH	0.39
His (5) NH	0.32
Phe (7) NH	0.26
Phe (6) NH	0.31
Tyr (9) NH	0.33
Lys (10) NH	0.28
Val (8) NH	0.27
Tyr (9) 3,5	1.15
Val (8) α	0.17
Pro (3) δdt	0.11
Pro (3) δut	0.12
Pro (1) δ	0.37
Pro (1) β	0.16
Pro (3) βd	0.18
Val (8) β	0.28
Lys (10) δ	0.37
Lys (10) γ	0.29
Val (8) γ	0.32

TABLE 4.4

(1) = 16mMolar; (2) = 9mMolar; (3) = 3mMolar; (4) = 0.8mMolar

All samples at pH 4.1

Proton		Chemical Shift (ppm)	J (Hertz)	Width at half Height (Hertz)
Lys (10) NH	(1)	7.60	(1) 7.40	(1) 3.1
	(2)	7.60	(2) 7.42	(2) 3.4
	(3)	7.61	(3) 7.42	(3) 3.3
	(4)	7.60	(4) 7.44	(4) 3.1
Tyr (9) NH	(1)	7.97	(1) 7.51	(1) 3.6
	(2)	7.97	(2) 7.48	(2) 3.8
	(3)	7.96	(3) 7.52	(3) 3.8
	(4)	7.96	(4) 7.49	(4) 3.6
Val (8) NH	(1)	7.66	(1) 8.52	(1) 3.0
	(2)	7.66	(2) 8.50	(2) 3.3
	(3)	7.65	(3) 8.49	(3) 3.1
	(4)	7.64	(4) 8.49	(4) 3.2
Phe (7) NH	(1)	8.03	(1) 8.04	(1) 3.8
	(2)	8.02	(2) 8.06	(2) 3.9
	(3)	8.00	(3) 8.07	(3) 3.9
	(4)	8.02	(4) 8.07	(4) 3.9
Phe (6) NH	(1)	7.88	(1) 7.02	(1) 4.1
	(2)	7.88	(2) 7.07	(2) 4.1
	(3)	7.88	(3) 7.02	(3) 3.9
	(4)	7.87	(4) 7.03	(4) 3.8
His (5) NH	(1)	8.06	(1) 7.68	(1) 3.4
	(2)	8.06	(2) 7.72	(2) 3.4
	(3)	8.05	(3) 7.66	(3) 3.6
	(4)	8.06	(4) 7.69	(4) 3.4
Phe (4) NH	(1)	8.25	(1) 6.52	(1) 3.8
	(2)	8.26	(2) 6.52	(2) 3.6
	(3)	8.24	(3) 6.50	(3) 3.8
	(4)	8.25	(4) 6.51	(4) 3.8

Proton	Chemical Shift (ppm	J (Hertz)	Width at half Height (Hertz)
	(1) 4.12	(1) 8.8	(1) 3.5
	(2) 4.12	(2) 8.9	(2) 3.5
Pro (1) α	(3) 4.12	(3) 8.8	(3) 3.6
	(4) 4.12	(4) 8.8	(4) 3.5
	(1) 4.20	(1) 8.9	(1) 3.4
	(2) 4.20	(2) 8.8	(2) 3.5
Pro (3) α	(3) 4.20	(3) 8.7	(3) 3.5
	(4) 4.20	(4) 8.8	(4) 3.4
	(1) 3.89	(1) 8.4	(1) 3.0
	(2) 3.89	(2) 8.4	(2) 3.1
Lys (10) α	(3) 3.89	(3) 8.3	(3) 3.1
	(4) 3.89	(4) 8.4	(4) 3.1
	(1) 3.74	(1) 8.3	(1) 3.0
	(2) 3.74	(2) 8.3	(2) 3.0
Val (8) α	(3) 3.73	(3) 8.2	(3) 3.0
	(4) 3.73	(4) 8.3	(4) 3.0
	(1) 3.18		(1) 3.8
	(2) 3.18		(2) 3.7
Pro (1) δ	(3) 3.18		(3) 3.7
	(4) 3.17		(4) 3.8
	(1) 3.34		(1) 3.7
	(2) 3.34		(2) 3.6
Pro (3) δ	(3) 3.34		(3) 3.7
	(4) 3.33		(4) 3.7
	(1) 2.99	(1) 8.4	(1) 3.5
	(2) 2.99	(2) 8.3	(2) 3.5
His (5) βd	(3) 2.99	(3) 8.3	(3) 3.6
	(4) 2.99	(4) 8.3	(4) 3.6
	(1) 2.19		(1) 3.4
	(2) 2.19		(2) 3.5
Pro (1) β	(3) 2.19		(3) 3.4
	(4) 2.20		(4) 3.5

Proton	Chemical Shift (Hertz) J (Hertz)	Width at half Height (Hertz).
	(1) 2.03	(1) 3.8
	(2) 2.03	(2) 3.8
Pro (3) βd	(3) 2.03	(3) 3.9
	(4) 2.02	(4) 3.8
	(1) 1.64	(1) 3.2
	(2) 1.64	(2) 3.1
Val (8) β	(3) 1.64	(3) 3.1
	(4) 1.64	(4) 3.2
	(1) 1.10	(1) 2.9
	(2) 1.09	(2) 3.0
Lys (10) γ	(3) 1.09	(3) 3.0
	(4) 1.10	(4) 3.0

Figure 4.1 1-D ^1H NMR spectrum of RIP in H_2O/D_2O solution (60:40) at pH 3.31.

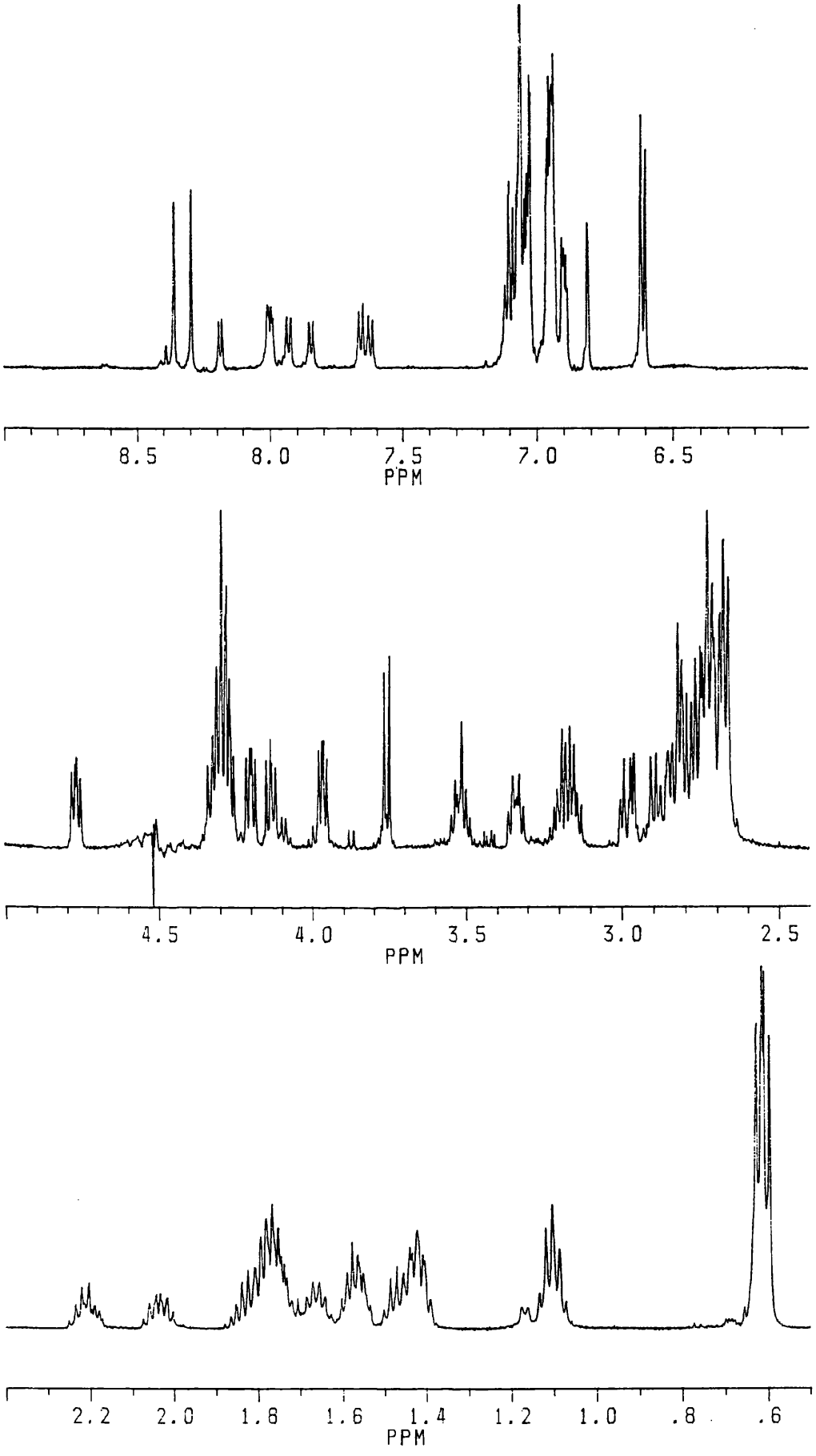
8.5
8.0
7.5
7.0
6.5
PPM
4.5
4.0
3.5
3.0
2.5
PPM
2.2
2.0
1.8
1.6
1.4
1.2
1.0
.8
.6
PPM

Figure 4.2 Plot of pH versus c, to determine the pH at which T_2, the spin-spin relaxation time, was maximum and the solvent peak a minimum width. c was the number of times the (D2-180$_y^o$ - D2)c sequence was carried out.

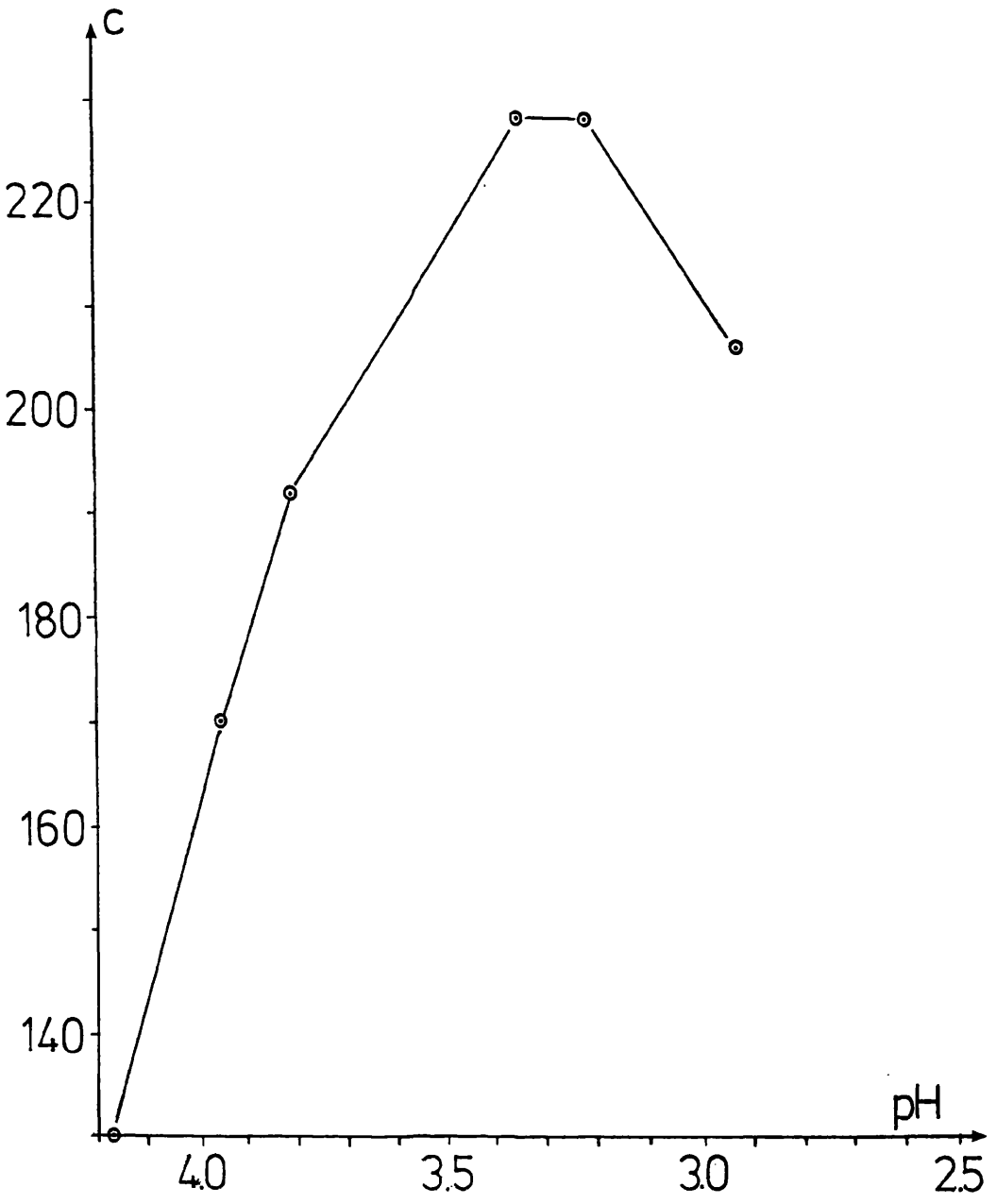
c
220
200
180
160
140
pH
4.0
3.5
3.0
2.5

Figure 4.3 Contour plot of the HOHAHA experiment performed on RIP. The diagonal (bottom left to top right) represents the 1-D spectrum; cross-peaks from the diagonal show coupling between protons from within the same amino-acid residue.

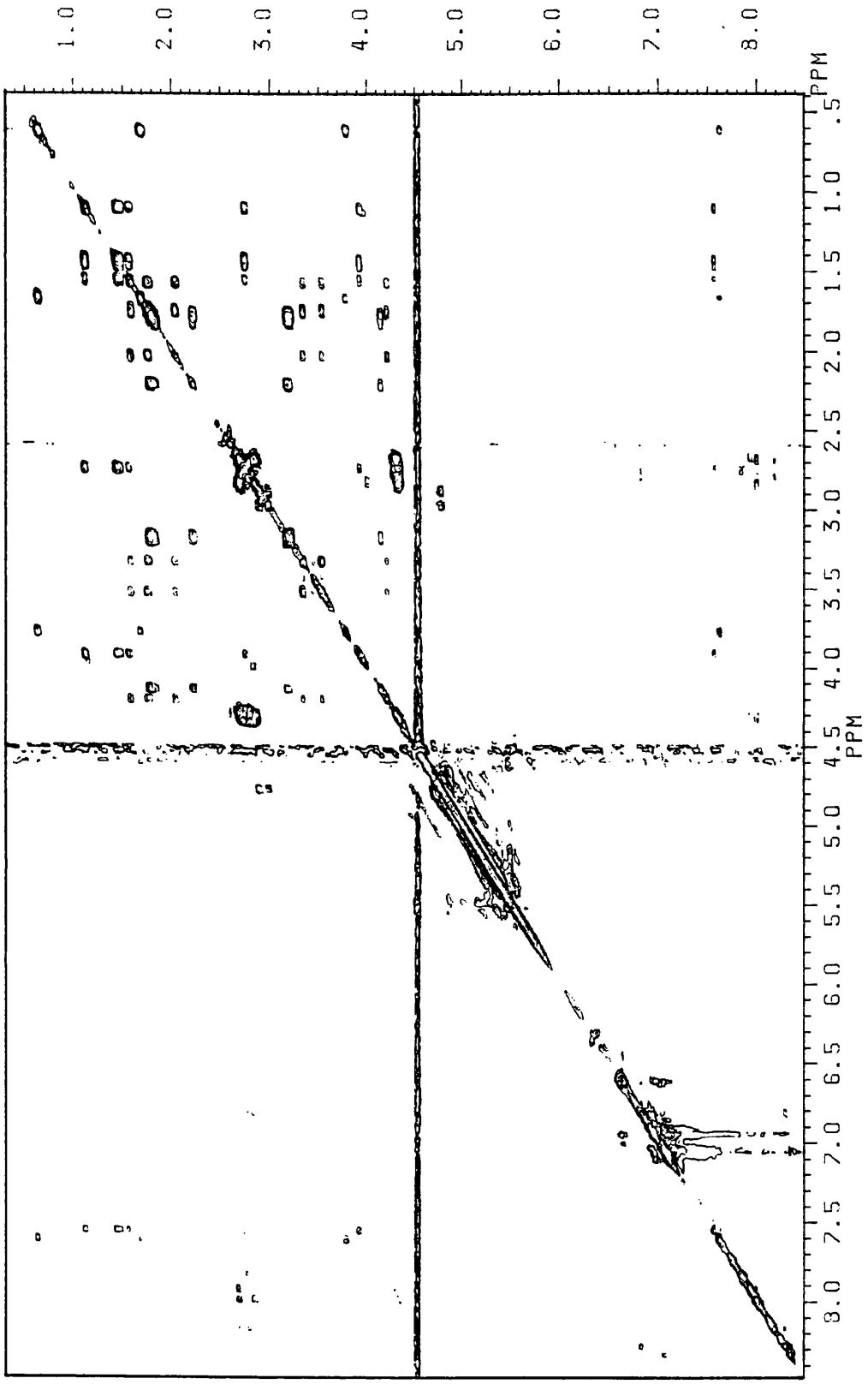
1.0
2.0
3.0
4.0
5.0
6.0
7.0
8.0
PPM
.5
1.0
1.5
2.0
2.5
3.0
3.5
4.0
4.5
PPM
5.0
5.5
6.0
6.5
7.0
7.5
8.0

Figure 4.4 Cross sections through the amide protons of the HOHAHA experiment. For Pro(1), His(2) and Pro(3), cross sections were taken through the alpha protons.

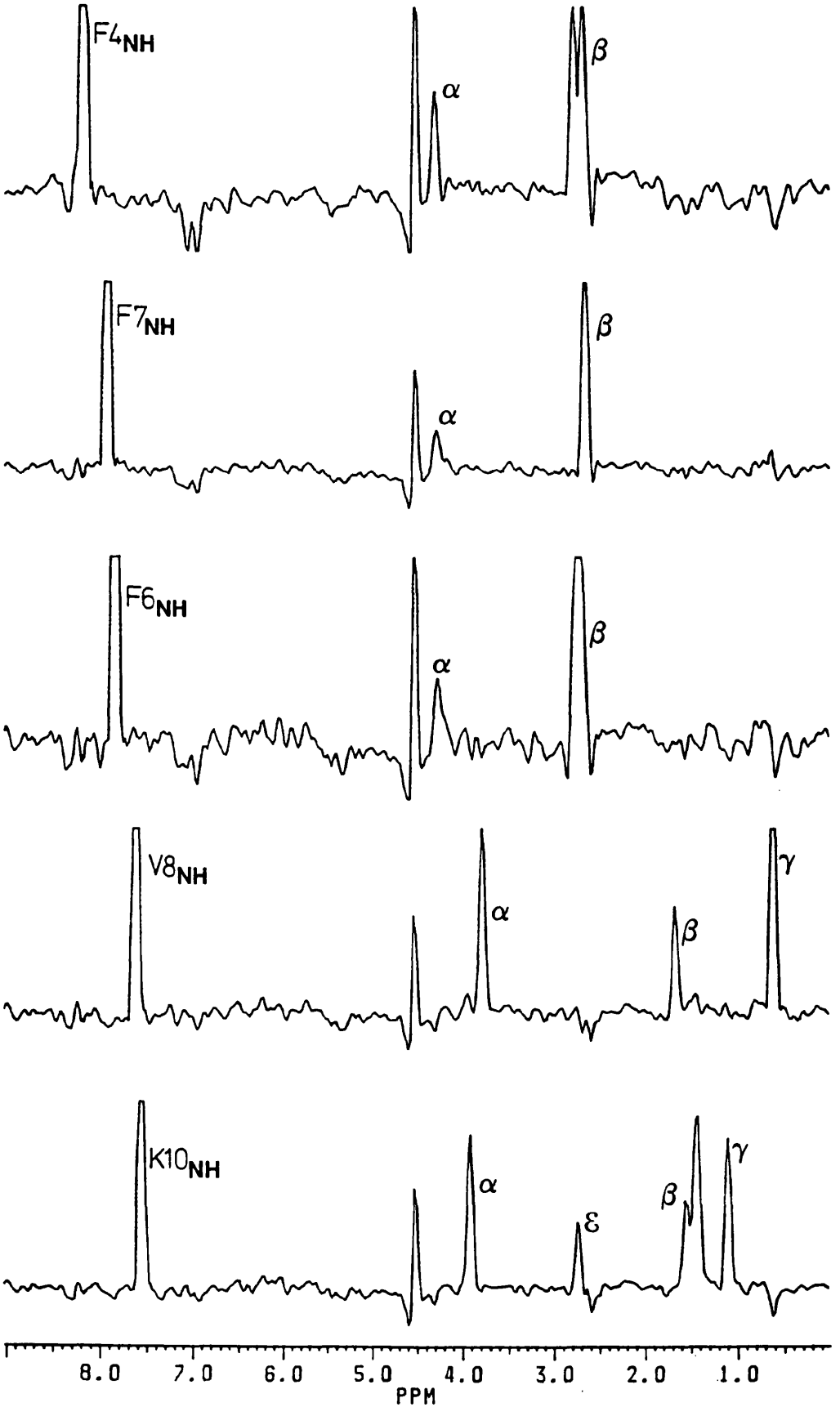
F4NH
α
β
F7NH
α
β
F6NH
α
β
V8NH
α
β
γ
K10NH
α
ε
β
γ
8.0
7.0
6.0
5.0
4.0
3.0
2.0
1.0
PPM

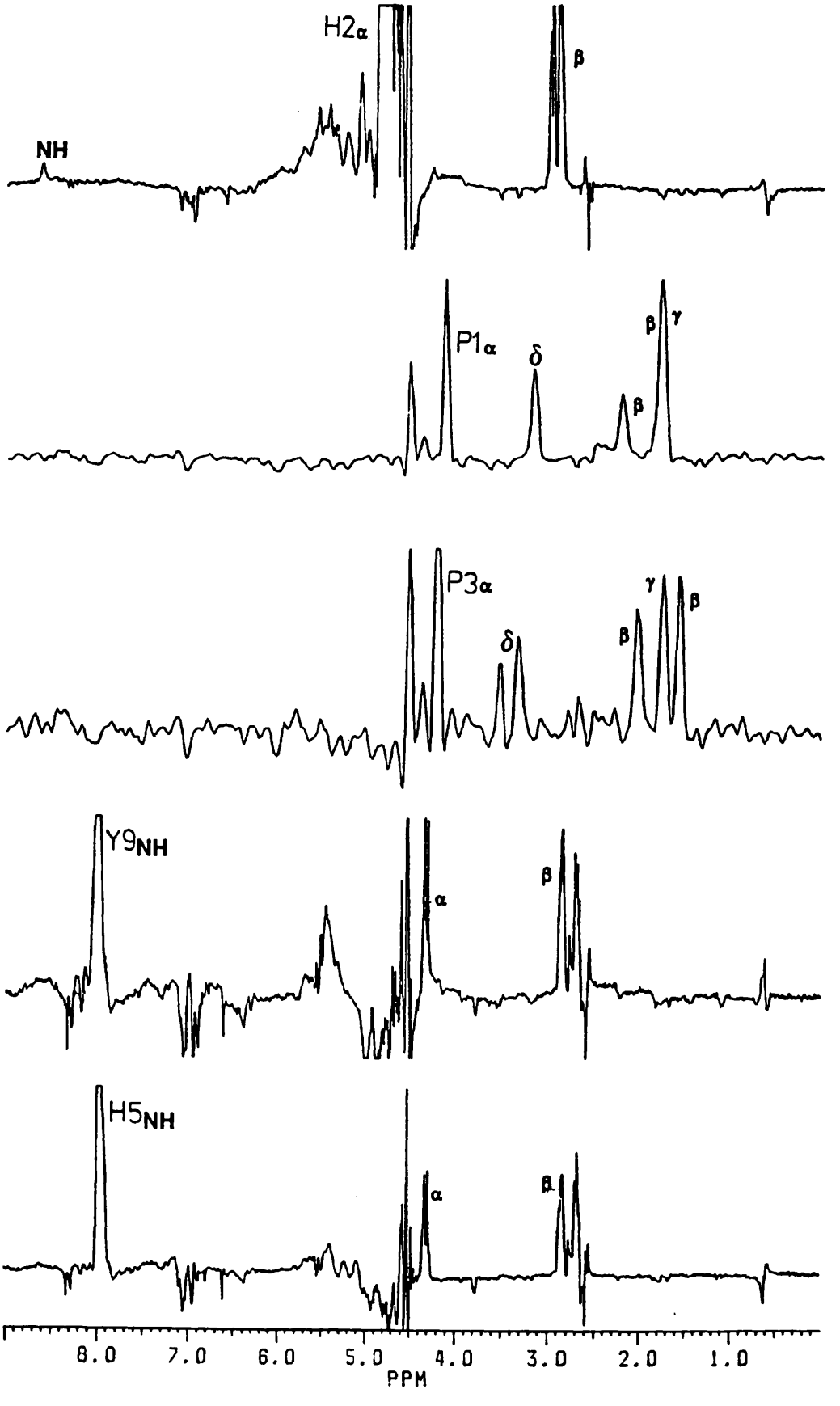
H2α
β
NH
P1α
δ
β
β
γ
P3α
δ
β
γ
β
Y9NH
α
β
H5NH
α
β
8.0
7.0
6.0
5.0
4.0
3.0
2.0
1.0
PPM

Figure 4.5 Plot of the maximum NOE and the maximum ROE as a function of correlation time, τ_c.

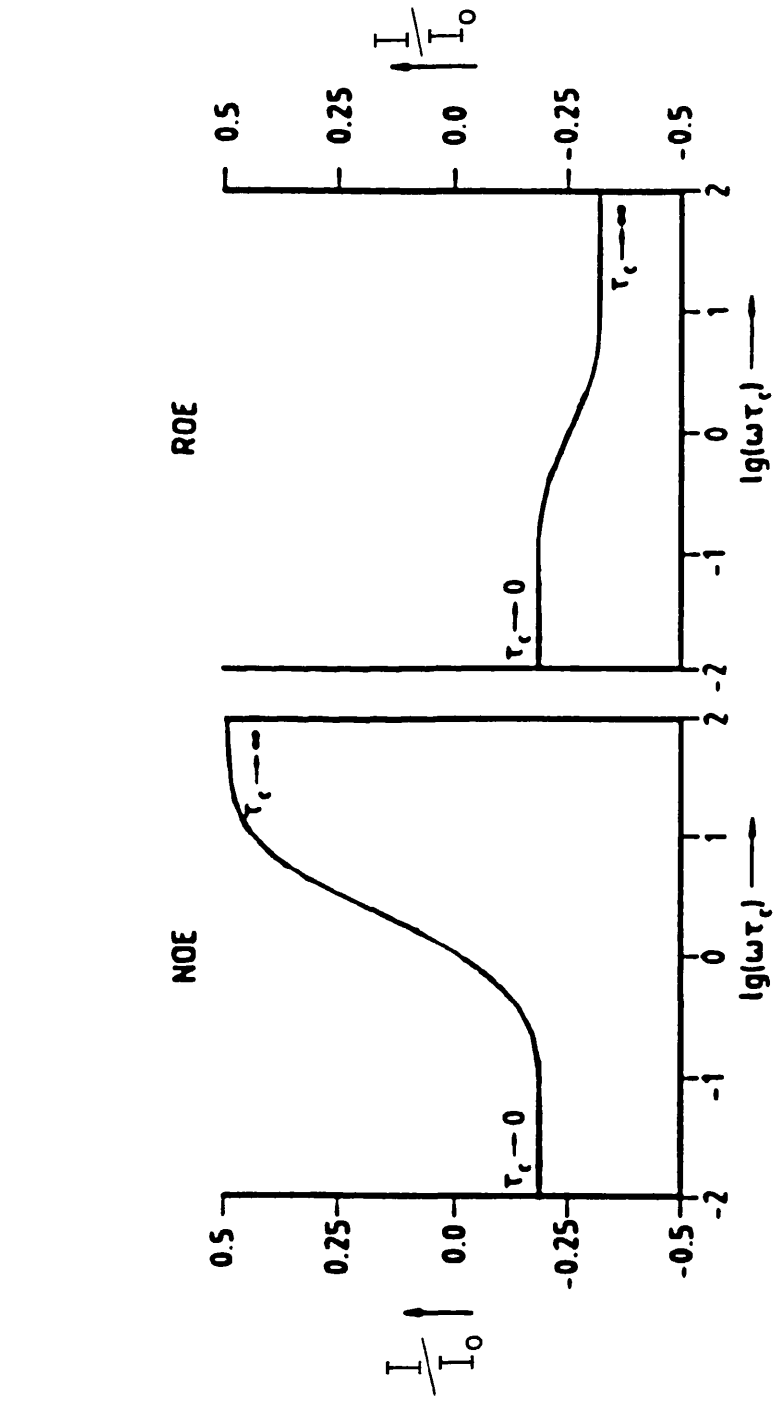
NOE
ROE
0.5
0.25
0.0
-0.25
-0.5
I/I0
2
1
0
-1
-2
lg(ωτc)
τc→∞
τc→0

Figure 4.6 Cross sections through amide and alpha protons in the ROESY experiment which show connectivities between adjacent amino-acids. The ROEs which show this connection are starred *.

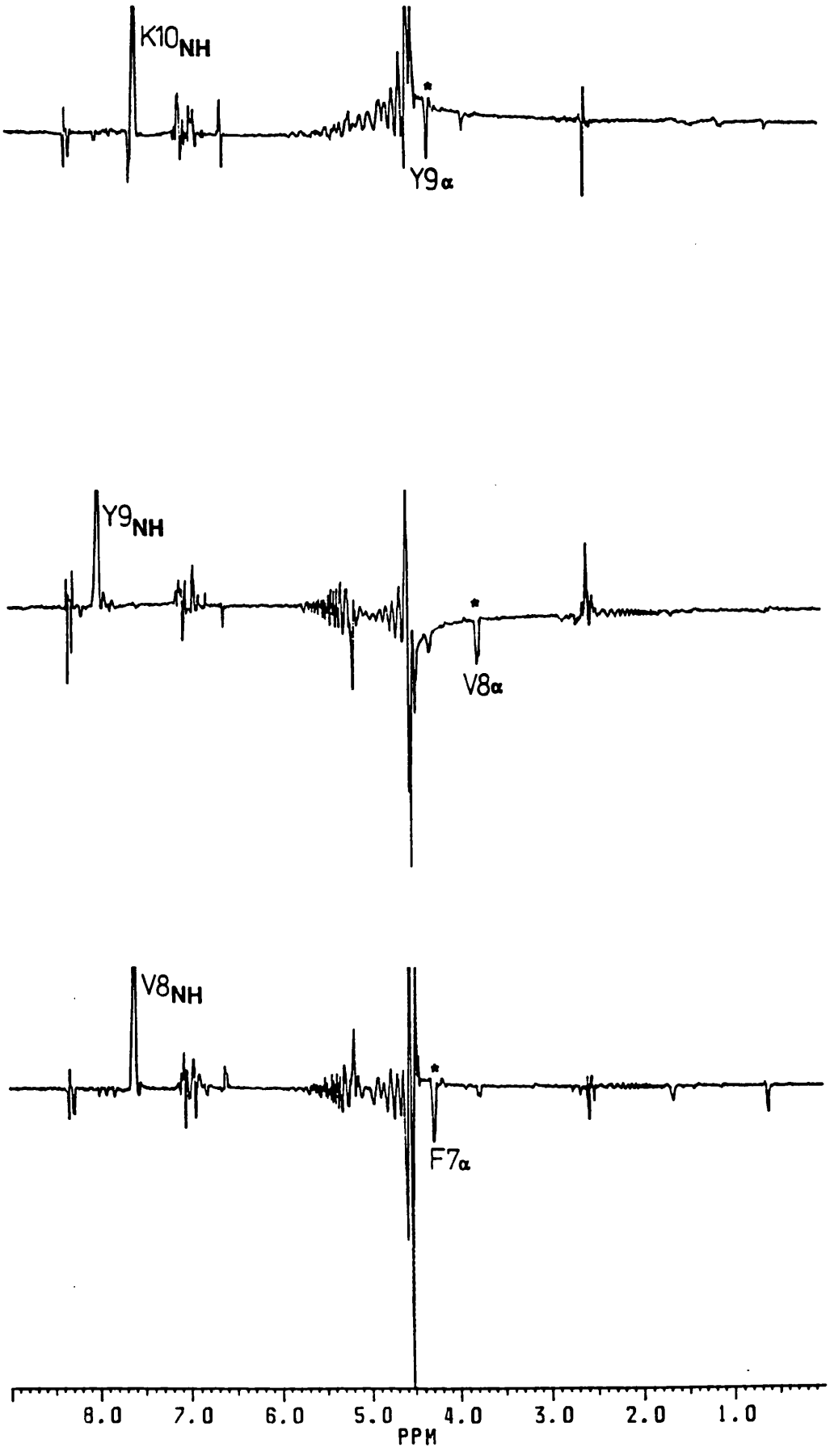
K10NH
Y9α
Y9NH
V8α
V8NH
F7α
8.0
7.0
6.0
5.0
4.0
3.0
2.0
1.0
PPM

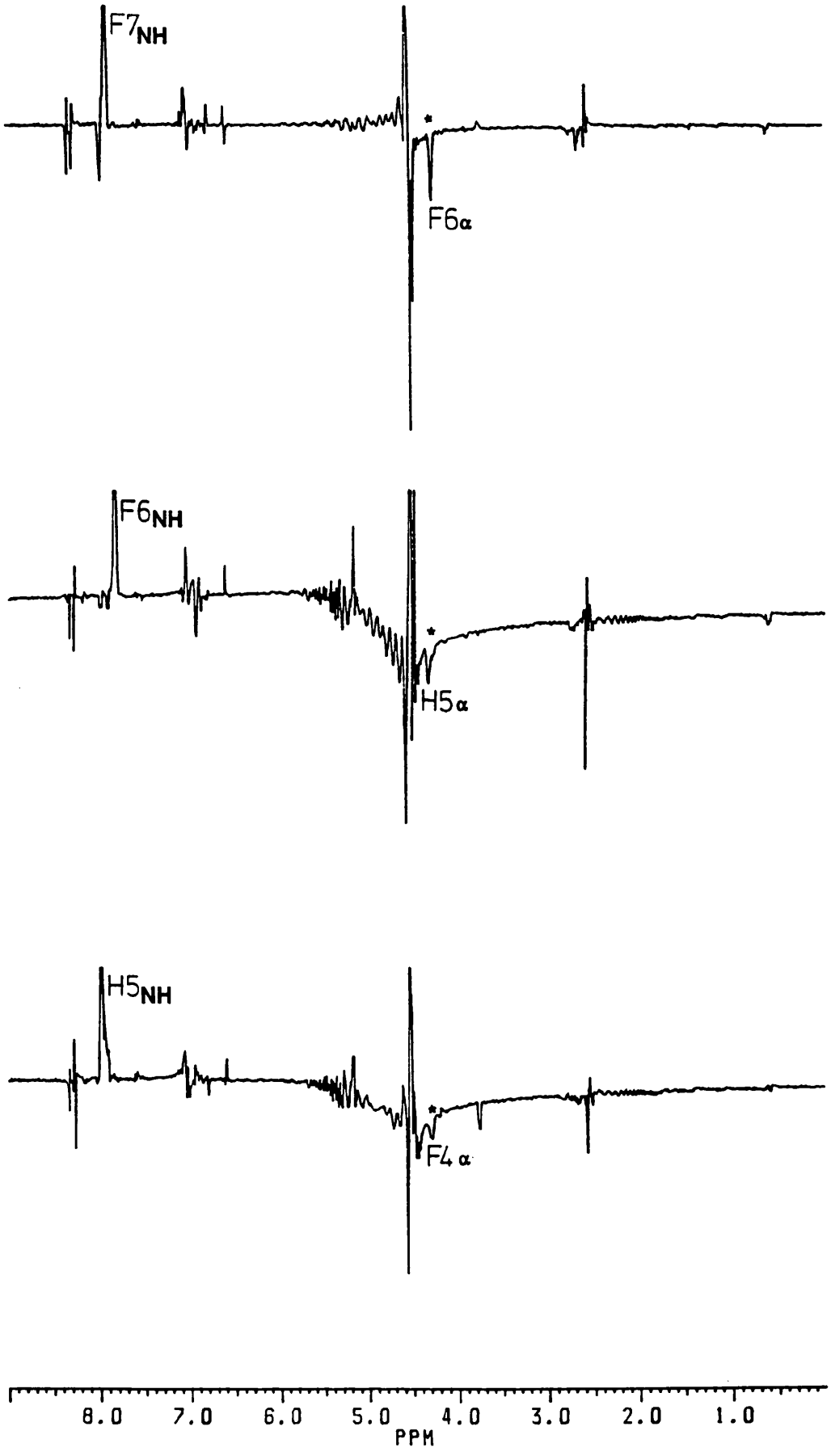
F7NH
F6α
F6NH
H5α
H5NH
F4α
8.0
7.0
6.0
5.0
4.0
3.0
2.0
1.0
PPM

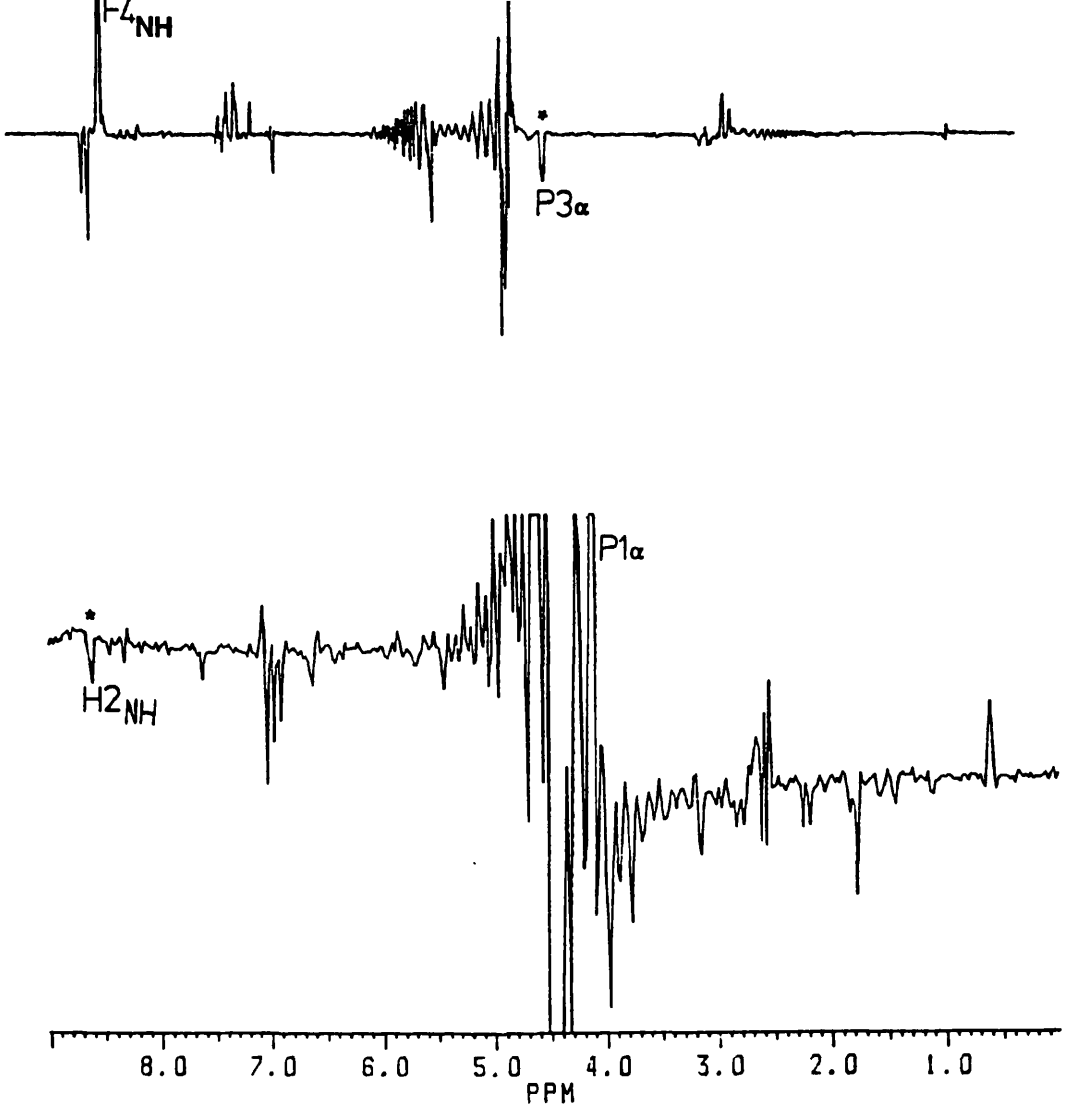
F2NH
P3α
P1α
H2NH
8.0
7.0
6.0
5.0
4.0
3.0
2.0
1.0
PPM

Figure 4.7 Contour plot of part of the ROESY experiment, showing connections from aromatic ring protons to their β protons, for residues 4,6 and 7 (Phe) and 9 (Tyr).

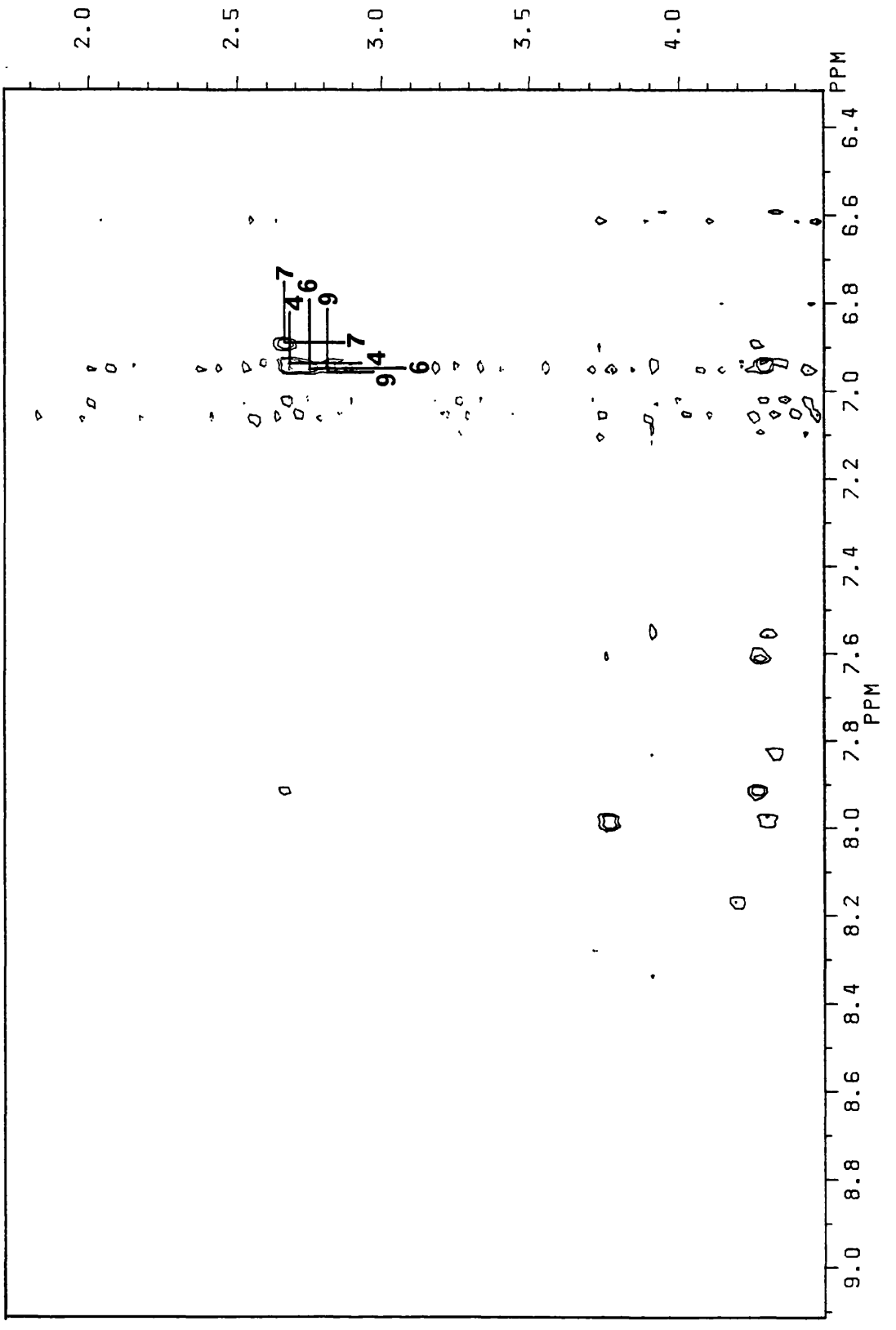
2.0
2.5
3.0
3.5
4.0
PPM
6.4
6.6
6.8
7.0
7.2
7.4
7.6
7.8
8.0
8.2
8.4
8.6
8.8
9.0
PPM

Figure 4.8 Contour plot of the HOHAHA experiment, showing cross-peaks from the Phe 2,6 protons to their 3,5 and 4 ring protons.

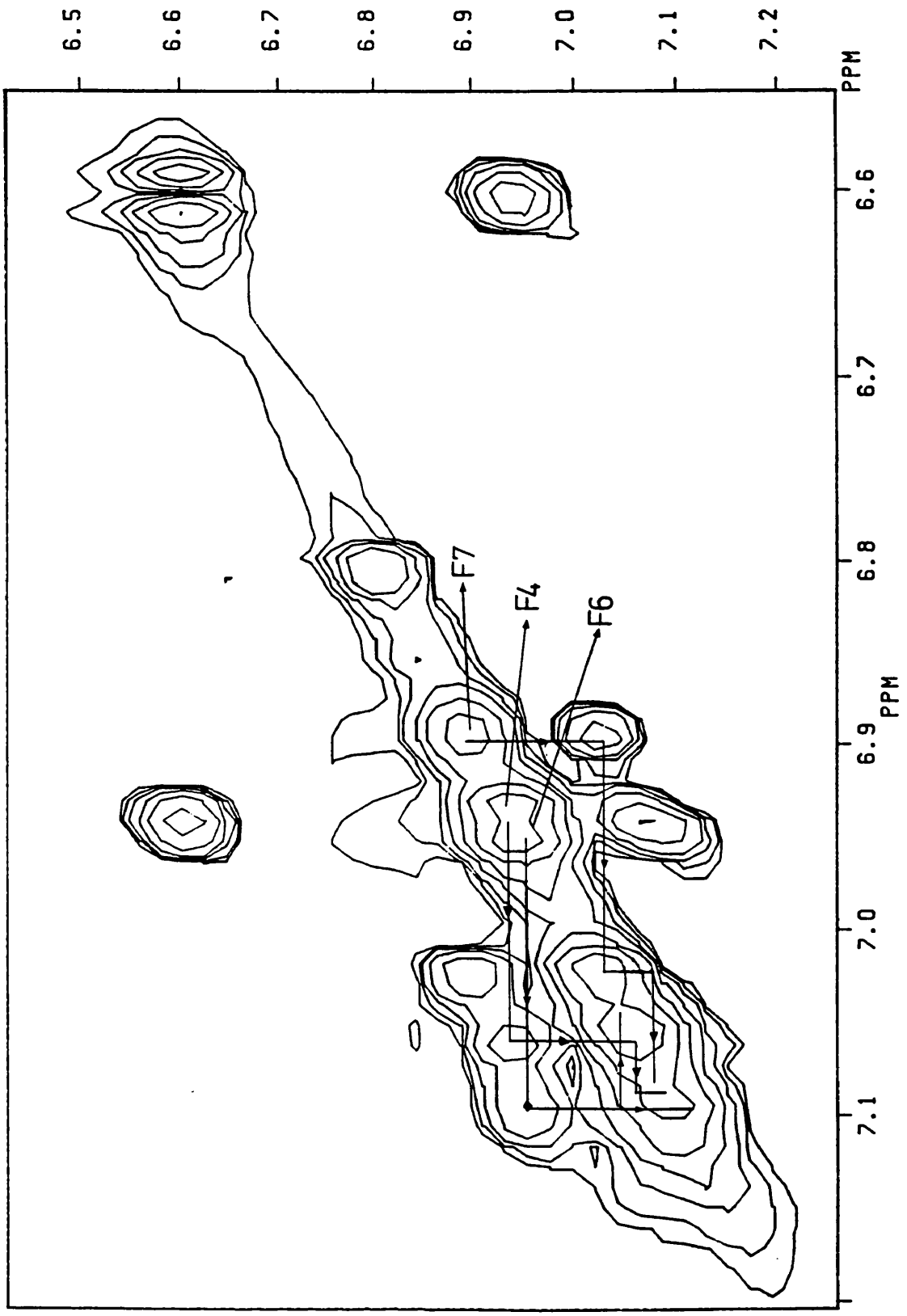
6.5
6.6
6.7
6.8
6.9
7.0
7.1
7.2
PPM
6.6
6.7
6.8
6.9
7.0
7.1
PPM
F7
F4
F6

Figure 4.9 1-D ^{1}H NMR spectrum of the Pro δ region of RIP. Note that for Pro(3), four resonances are found, corresponding to cis and trans forms of the peptide bond.

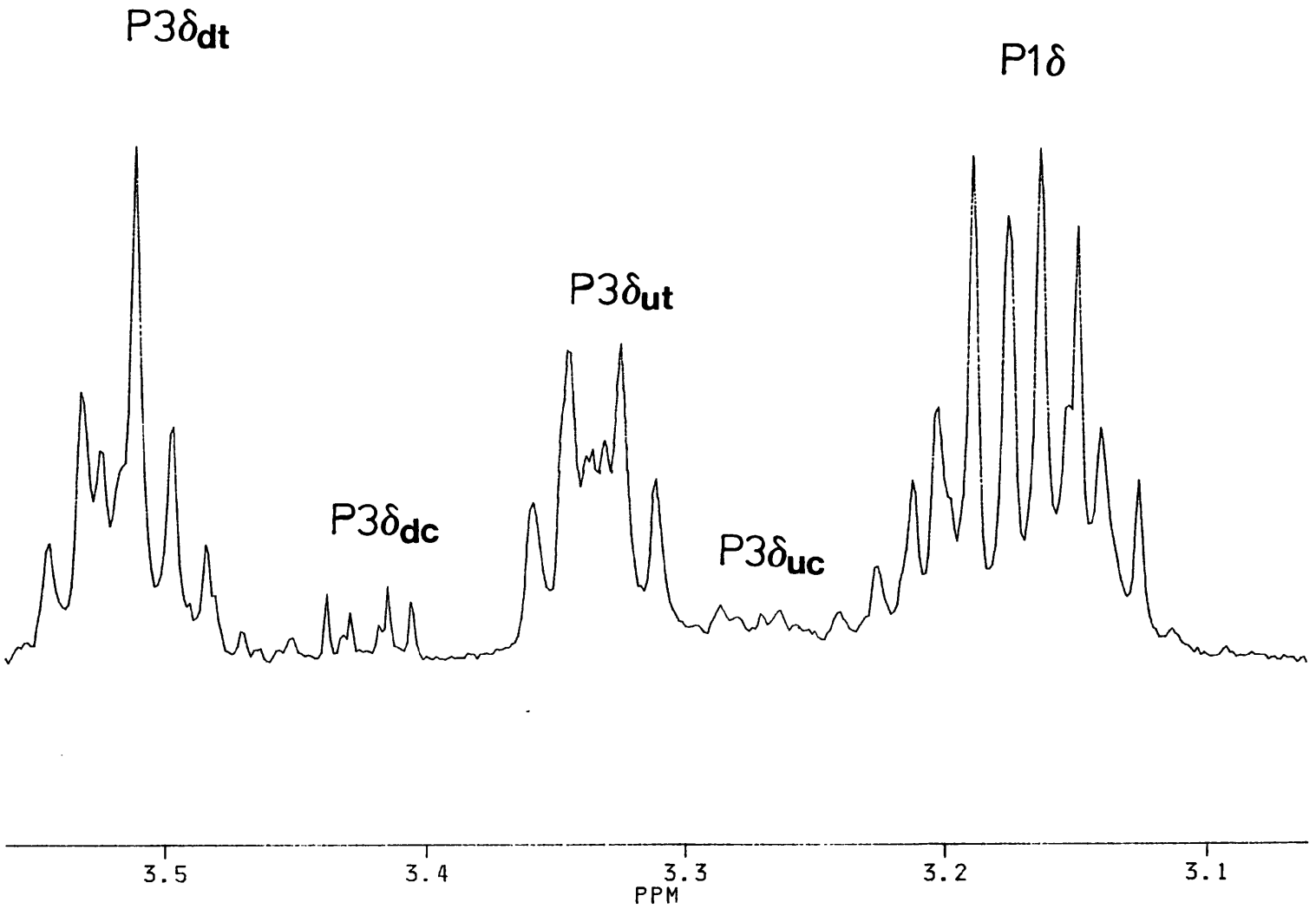
P3δdt
P1δ
P3δut
P3δdc
P3δuc
3.5
3.4
3.3
3.2
3.1
PPM

Figure 4.10 Diagram defining the three basic angles of the peptide backbone. ø, ¥ and ω.

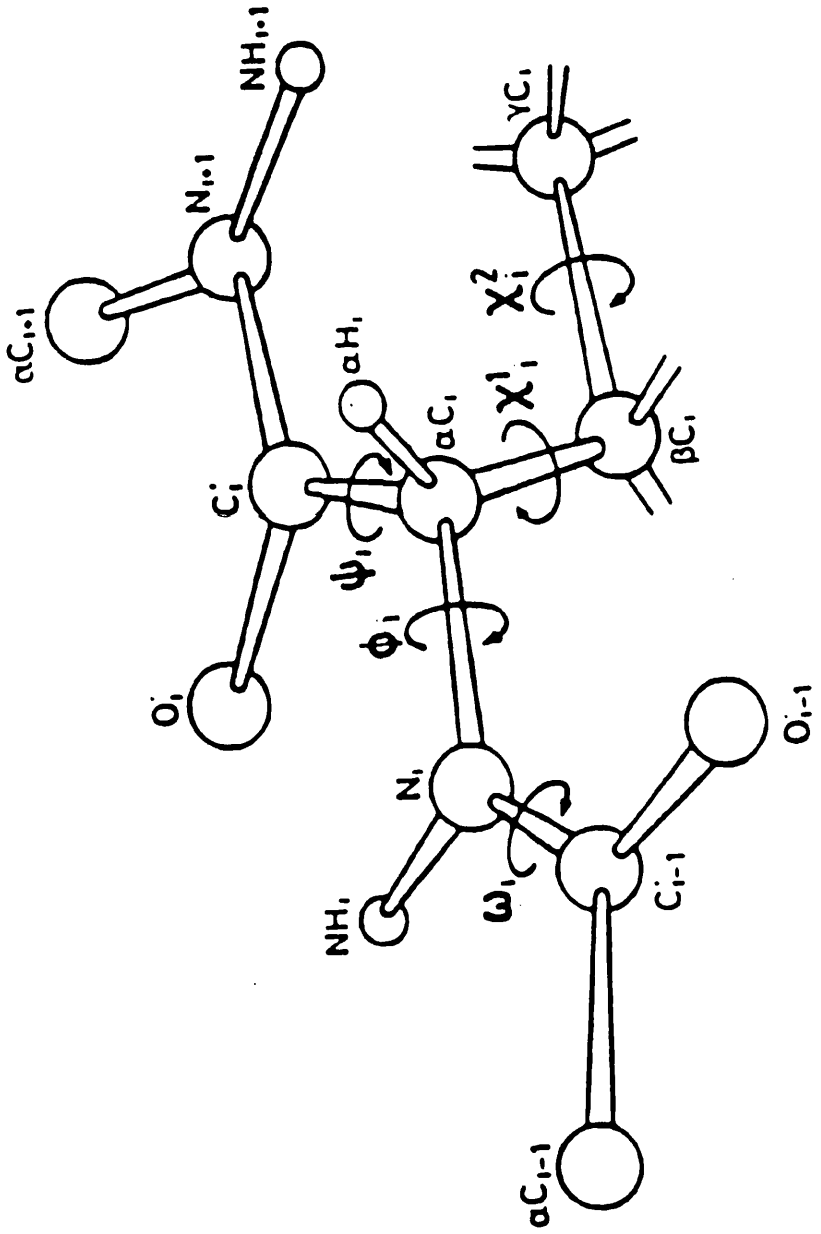
NH$_{i+1}$
N$_{i+1}$
αC$_{i+1}$
YC$_i$
χ^2_i
αH$_i$
αC$_i$
χ^1_i
βC$_i$
C$_i$
ψ_i
ϕ_i
O$_i$
N$_i$
O$_{i-1}$
NH$_i$
ω_i
C$_{i-1}$
αC$_{i-1}$

Figure 4.11 Cross sections through selected protons in RIP, showing intramolecular ROEs. These ROEs are used in determining a three-dimensional structure, and are negative with respect to the positive peak on the diagonal. The strength of the ROE is also indicated (S, M or W).

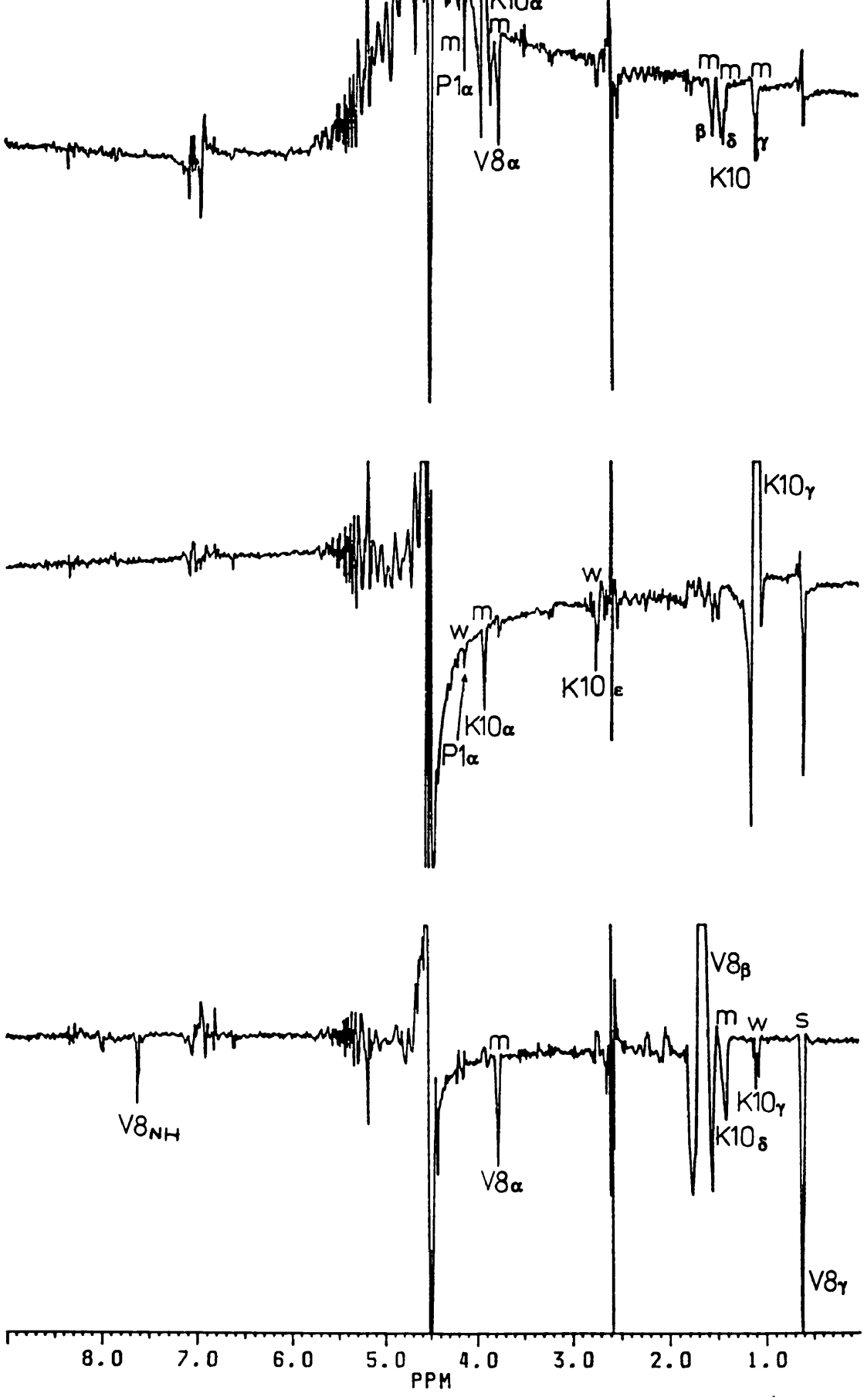
m
P1α
V8α
m
m m m
β δ γ
K10
K10γ
w
m
w
K10ε
K10α
P1α
V8β
m w s
K10γ
K10δ
V8NH
m
V8α
V8γ
8.0 7.0 6.0 5.0 4.0 3.0 2.0 1.0
PPM

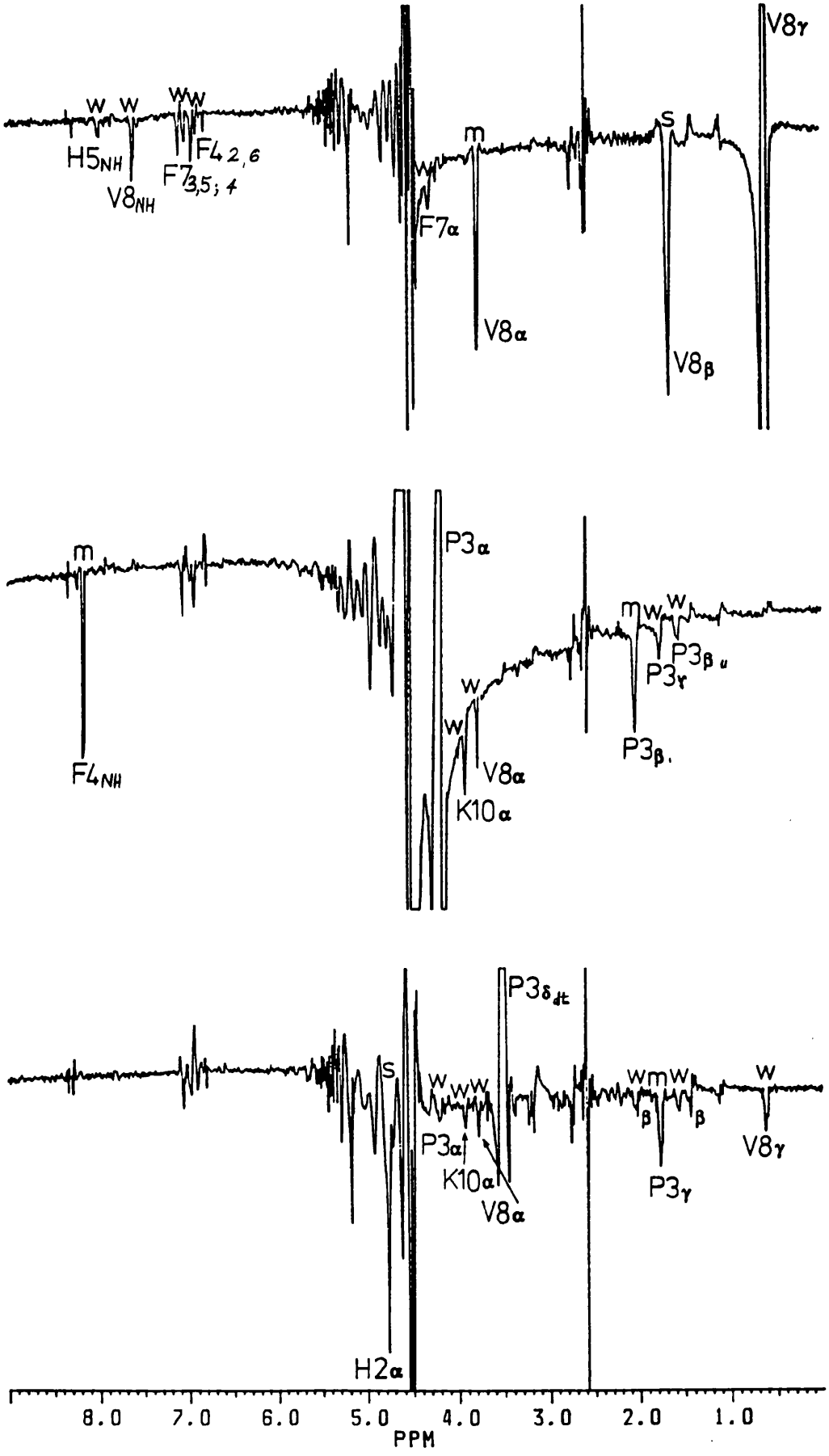
V8γ
w w
ww
H5NH
V8NH
F4 2,6
F7 3,5; 4
m
F7α
V8α
s
V8β
m
F4NH
P3α
m w w
P3γ
P3β u
w
w
V8α
K10α
P3β.
P3δ dt
s
w w w
P3α
K10α
V8α
H2α
w m w
β
β
P3γ
V8γ
8.0
7.0
6.0
5.0
4.0
3.0
2.0
1.0
PPM

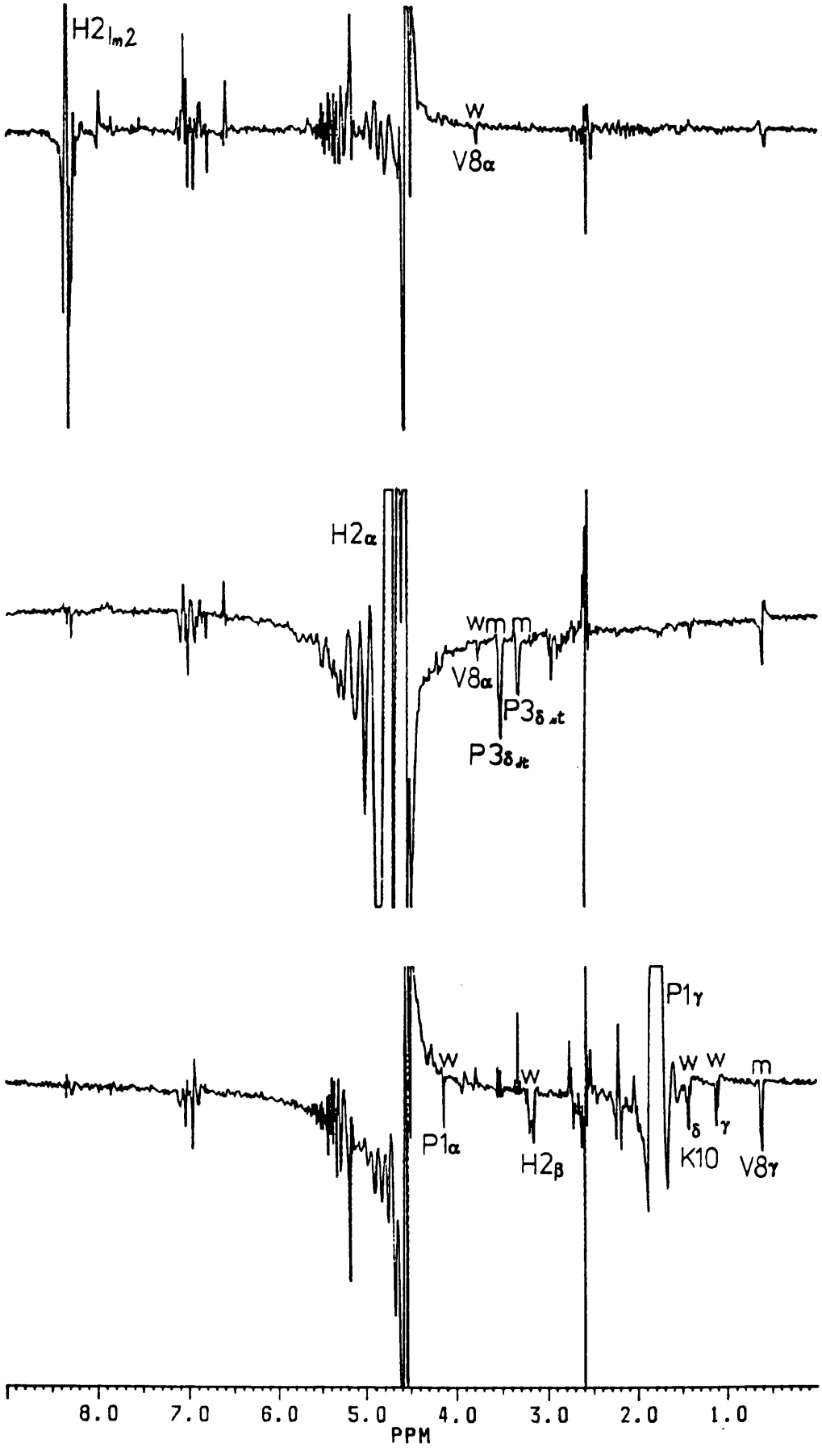
H2Im2
w
V8α
H2α
wm
m
V8α
P3δ,t
P3δ,t
P1γ
w
w
w
m
P1α
H2β
δ
γ
K10
V8γ
8.0
7.0
6.0
5.0
4.0
3.0
2.0
1.0
PPM

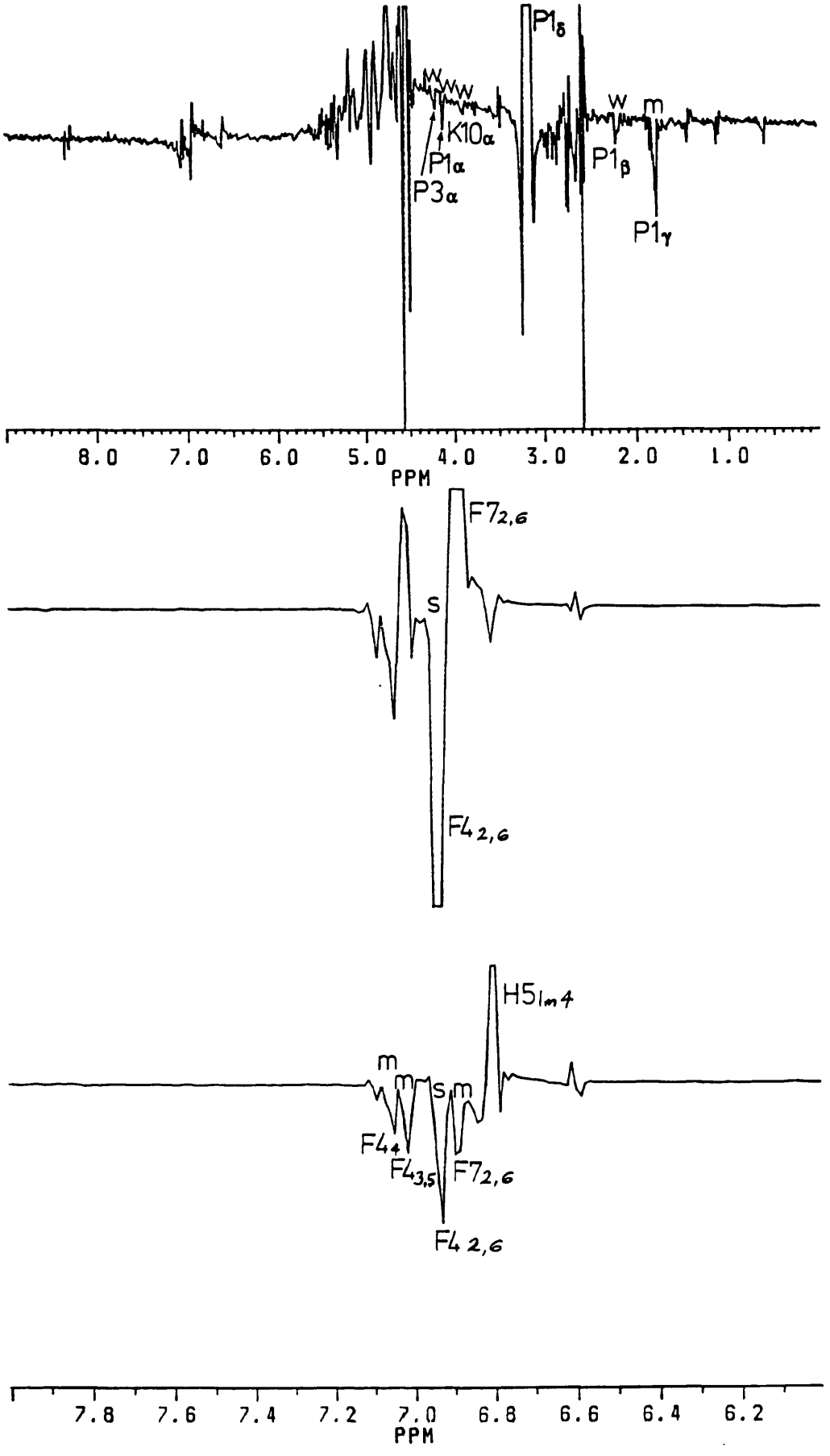
P1δ
w
w
w
K10α
P1α
P3α
w
m
P1β
P1γ
8.0
7.0
6.0
5.0
4.0
3.0
2.0
1.0
PPM
F72,6
s
F42,6
H5Im4
m
m
s
m
F44
F43,5
F72,6
F42,6
7.8
7.6
7.4
7.2
7.0
6.8
6.6
6.4
6.2
PPM

Figure 4.12 Plot of chemical shift versus temperature amide protons of RIP, in H_2O/D_2O. The gradients (in ppm/°C) are as follows:

F(4) = -9.05×10^{-3}
Y(9) = -8.04×10^{-3}
H(5) = -5.03×10^{-3}
F(7) = -6.53×10^{-3}
F(6) = -6.03×10^{-3}
K(10)= -6.03×10^{-3}
V(8) = -6.03×10^{-3}

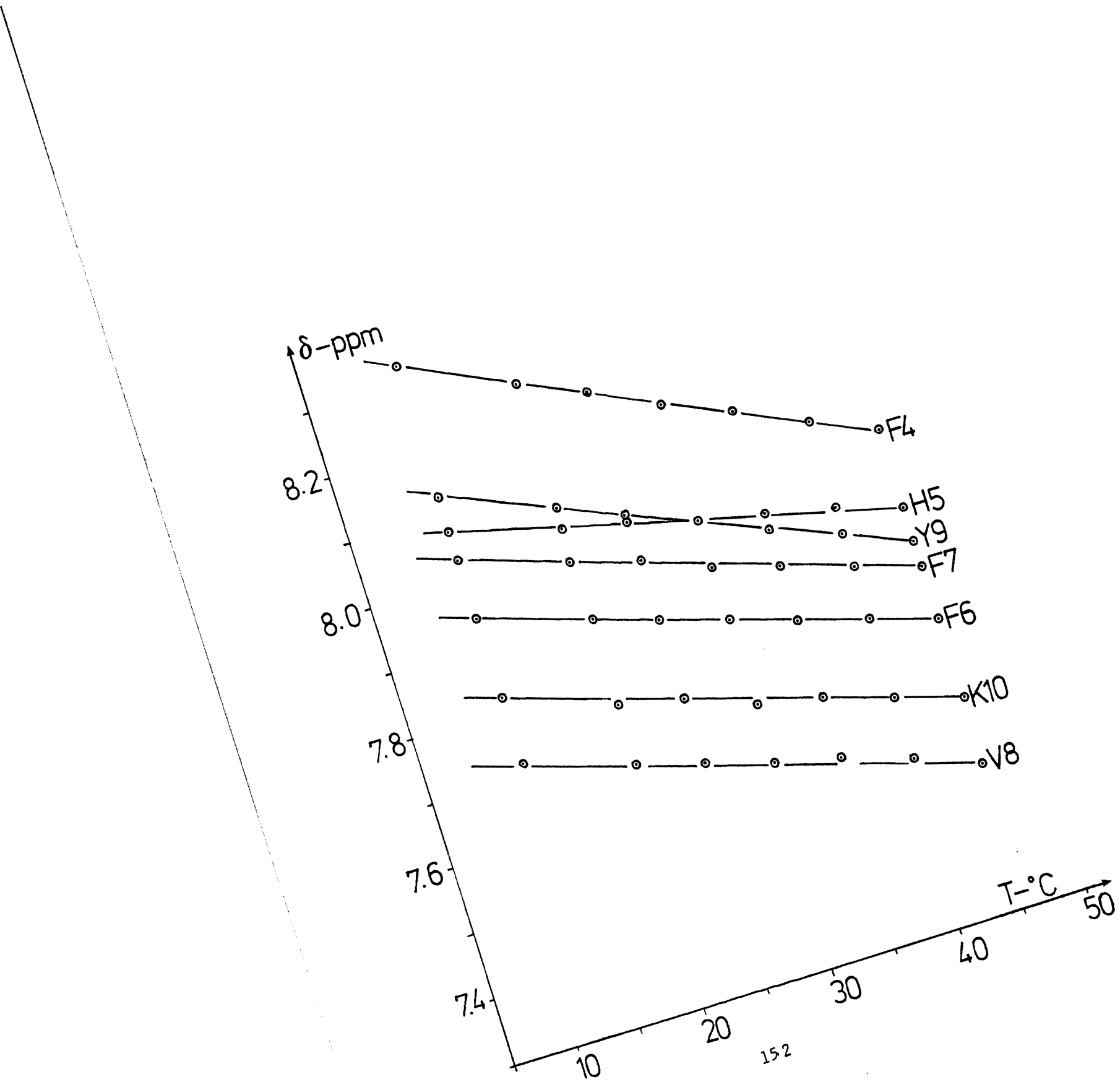
δ-ppm
8.2
8.0
7.8
7.6
7.4
F4
H5
Y9
F7
F6
K10
V8
T-°C
10
20
30
40
50

Figure 4.13 T_1 measurement of amide protons. The delay t_1 was varied between 0.1 and 0.9 seconds; the change in intensity of each proton with t_1 allows the value of T_1 to be calculated.

The experiment was recorded at pH 3.6 in this instance, at slightly lower pH than used in other experiments, because of alteration of sample with time. Only Lys(10) NH moved significantly as a result of this slight change.

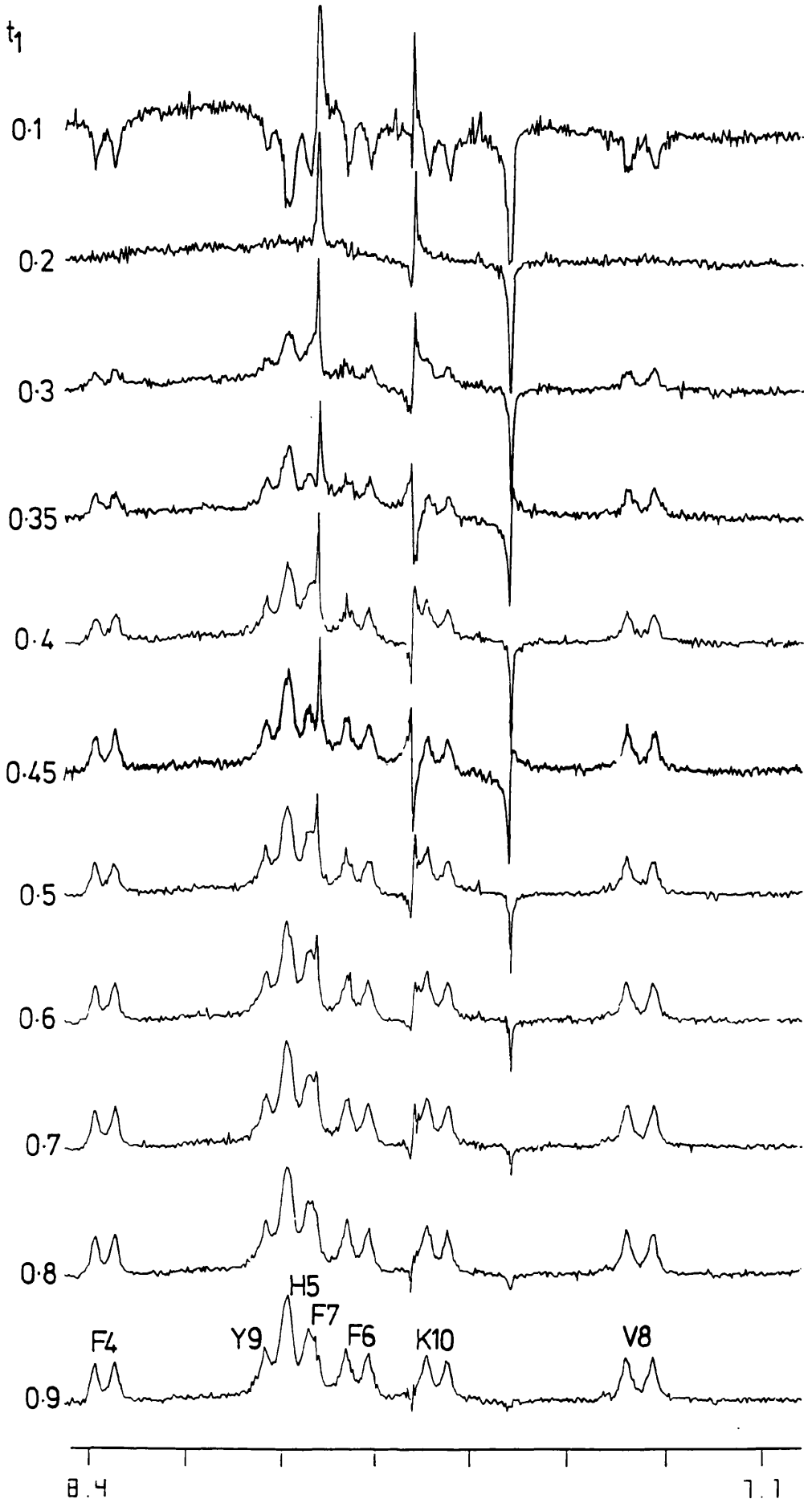
t1
0·1
0·2
0·3
0·35
0·4
0·45
0·5
0·6
0·7
0·8
0·9
F4
Y9
H5
F7
F6
K10
V8
8.4
7.1

Figure 4.14 Plot to show correlations between amide temperature gradients and T_1 values for amide protons of RIP.

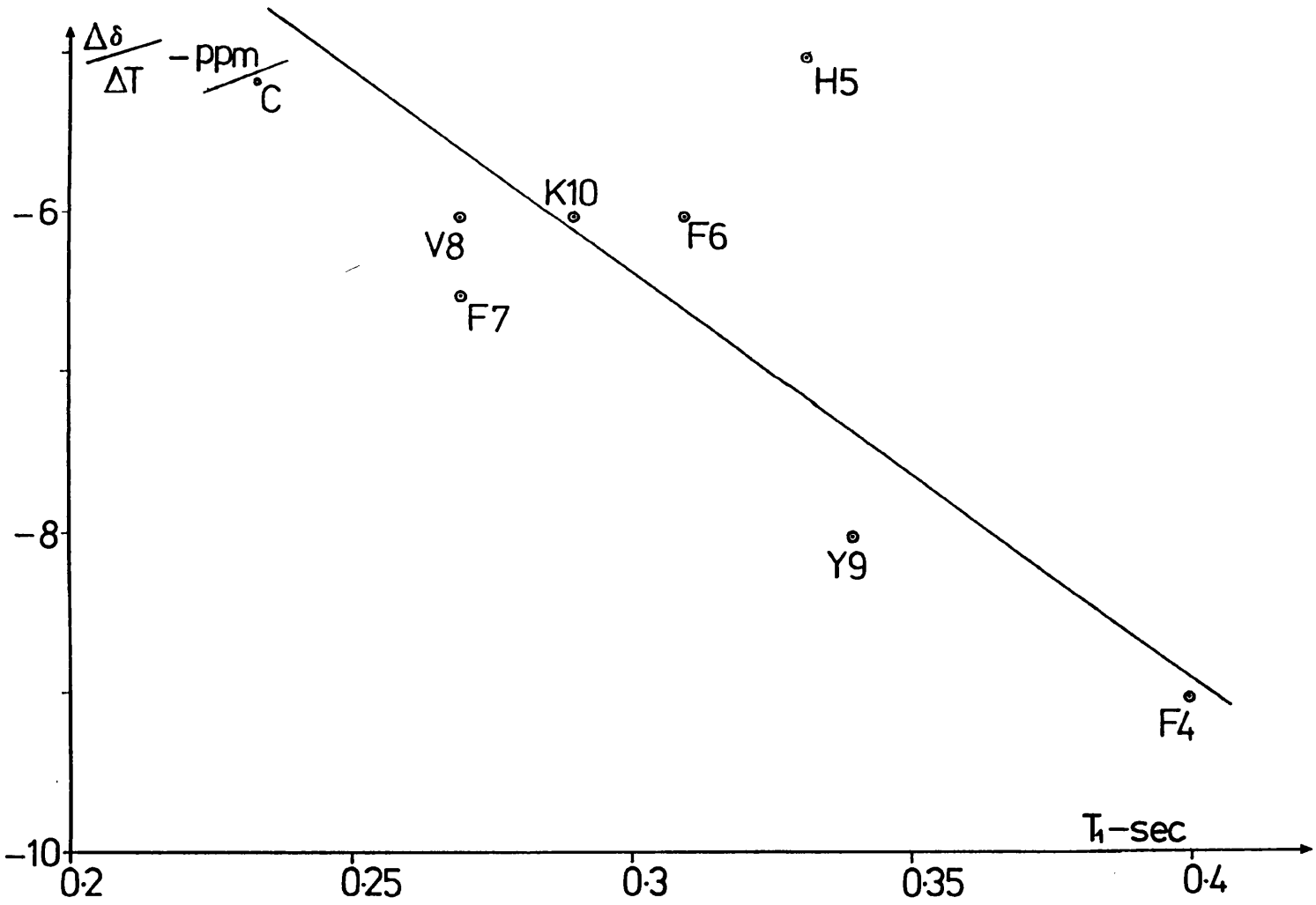
Δδ/ΔT – ppm/°C
H5
K10
V8
F6
F7
Y9
F4
−6
−8
−10
T1 – sec
0·2
0·25
0·3
0·35
0·4

Figure 4.15 ROESY contour plot showing the region of Pro(3)δ protons. ROE and chemical exchange (C.E.) cross peaks are indicated, proving the existance of cis-trans isomerisation at Pro(3).

The ROE cross-peaks have positive phase in this plot and the chemical exchange negative. These are represented by + and - respectively.

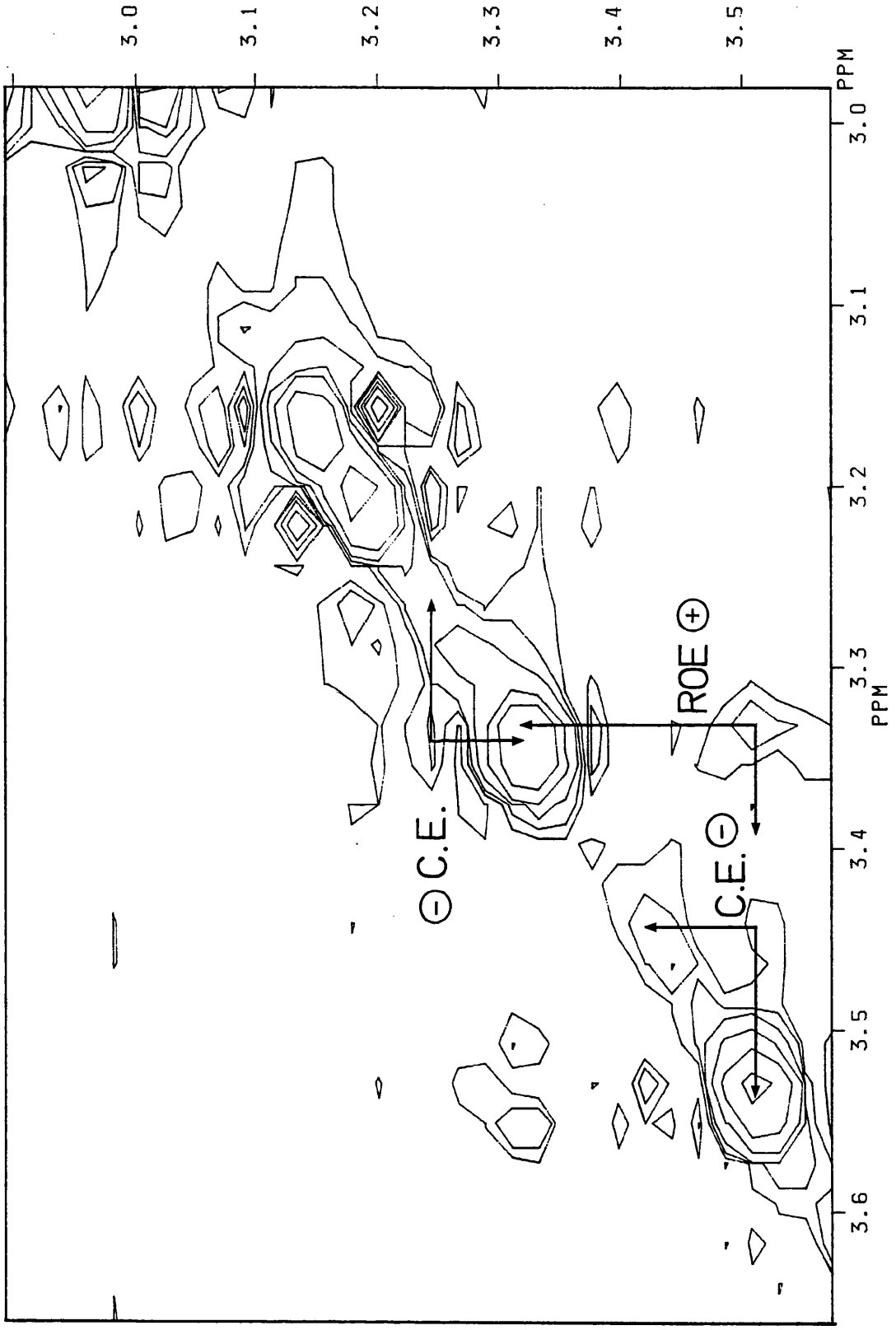
3.0
3.1
3.2
3.3
3.4
3.5
3.6
PPM
ROE ⊕
⊖ C.E.
C.E. ⊖

Figure 4.16 Cross sections through the δ protons of Pro(3), indicating the negative phase ROEs between the two trans forms, and positive phase chemical exchange peaks between cis and trans forms.

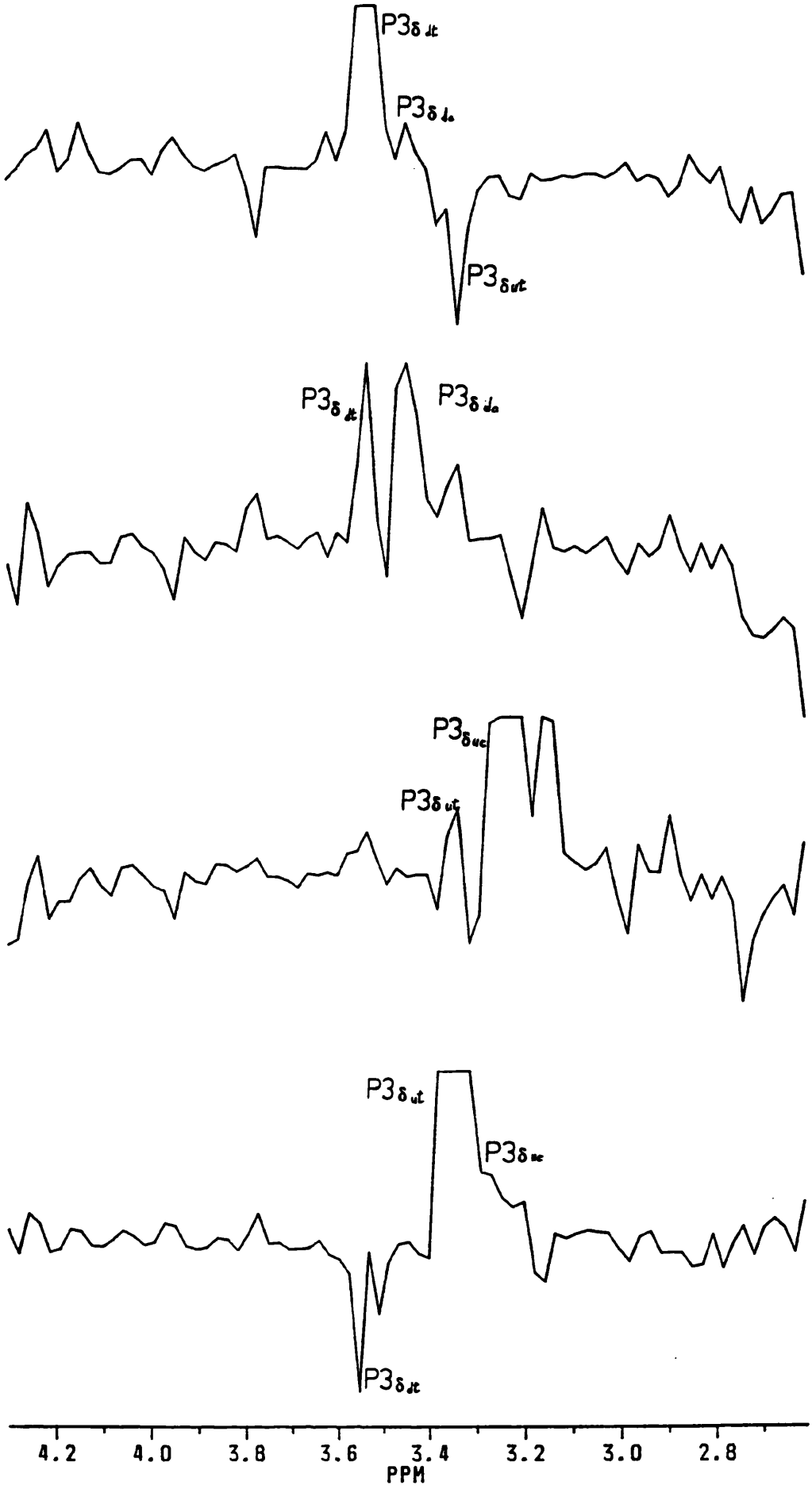
P3δ dt
P3δ da
P3δ ut
P3δ dt
P3δ da
P3δ uc
P3δ ut
P3δ ut
P3δ uc
P3δ dt
4.2
4.0
3.8
3.6
3.4
3.2
3.0
2.8
PPM

Chapter 5

NMR Studies of RIP in Trifluoroethanol

5.1. Assignment of Proton Resonance

The 1-D spectrum of a 3.2mM solution of RIP is shown in Figure 5.1.

The assignment strategy for RIP in TFE was similar to that employed for studies in H_2O/D_2O. A Homonuclear Hartmann Hahn (HOHAHA) experiment (A. Bax and D.G. Davies, 1985) was performed, with a spin locking field applied during mixing, allowing magnetisation to transfer across the whole spin system.

Cross-sections through each amide proton (Figure 5.2) allowed connectivities of seven of the ten amino-acids to be distinguished. Two of the eight amide protons were broadened (at 8.37ppm and 7.95ppm, later assigned to Phe(4) and His(5) respectively), but these still gave cross-peaks to their α and β protons. The remaining NH proton, at 8.60ppm, was very broad and showed no cross-peaks. The α-proton of this amino-acid

(assigned later in conjunction with the ROESY as His(2)) gave a cross-peak to this amide proton, allowing assignments to be made.

The N-terminal proline residue had no observable amine protons, because of exchange broadening; and Pro(3) had no amide proton. Sections were taken through the α-proton for the two Pro residues, to give connectivities through the whole of the spin-system. (Figure 5.2).

Figure 5.3 shows the contour plot of the aromatic region; the cross-peaks led to the assignments of the three Phe ring protons. However, no aromatic to β cross-peaks were observed in this case.

A ROESY experiment was then performed (A.A. Bothner-By et al, 1984). An initial experiment with a mixing time, τ_m, of 150msec gave little or no cross-peaks; increasing τ_m to 250msec gave cross-peaks which were used to obtain sequence specific asssignments and information on the conformations adopted by RIP. Sections through the F_2 axis at the frequency of the amide protons and α protons (Figure 5.4) showed these connectivities. The negative ROE cross-peaks to the α-proton region connected adjacent amino-acids; a reference to the HOHAHA results then gave the sequence specific assignments.

Aromatic to β connectivities, from within the same residue, were found. These permitted assignments (Figure 5.5.) to specific residues within the sequence.

The chemical shift value of each proton (with reference to TMS) is listed in Table 5.1. The chemical shift differences between the observed values, and those found for protons in a non-structured amino-acid environment (A. Bundi and K. Wuthrich,

1979), were also calculated . Protons which showed significant chemical shift differences may have been either involved in hydrogen bonding and/or near to aromatic rings, resulting in ring current shifts (R.A. Dwek, 1973). The distance to aromatic rings was also calculated, using the $1/r^3$ distance relationship

The NH-Cα coupling constants were determined, and related to the dihedral angle ϕ_i. Cα-Cβ coupling constants were also determined where appropriate and related to the percentage of gauche and trans rotamers. Table 5.2. summarised these results.

5.2. Chemical Exchange and cis-trans isomerisation.

If the interpretation of CD was correct, cis-trans isomerisation about the amide bond of Pro(3) should be observed, and reflected in several resonances for the δ protons. Indeed, four resonances were observed (Figure 5.6) for these protons.

The most intense resonances, at 3.68ppm and 3.31ppm, showed ROEs to His(2) α proton, and so must have resulted from a trans orientation of the amide bond. An expansion of the Pro(3) region in the HOHAHA experiment allowed connectivities between the trans to the cis forms to be established, at 3.61ppm, and 3.53ppm (Figure 5.7)

An expansion of this same region in the ROESY experiment is shown in Figure 5.8. A negative ROE, as expected, was observed between 3.68ppm and 3.31ppm for the two δ protons in the trans orientation. A weak ROE was also found between protons in the cis orientation at 3.53ppm and 3.611ppm. Positive chemical

exchange cross-peaks were seen between 3.68ppm and 3.62ppm, and 3.50ppm a nd 3.31ppm respectively. These indicated that the resonance signals at 3.68ppm and 3.61ppm, and 3.53ppm and 3.31ppm, were from the same proton which was undergoing exchange between two different chemical environments, the cis and trans forms of the Pro(3) peptide bond.

These observations confirmed the interpretations from CD work, that RIP in TFE existed in two predominant forms, with more of the trans amide bond present than the cis. The peak integration of the trans; cis ratio could not be determined because the solvent interferred with the resonance signals.

Other chemical exchange peaks were observed between the resonances at 7.53ppm and 7.47ppm (figure 5.9); these were assigned to Phe(7) 4-ring proton by the HOHAHA experiment. Because positive exchange peaks were found, these resonances must have resulted form the proton in two different environments. The ratio of peaks areas, 7.53/7.47ppm was approximately 65/35. This was the approximate ratio calculated from CD results, for the extent of cis:trans isomerism. It was likely therefore that the conformational change at Pro(3) was the cause of the benzene ring at Phe(7) experiencing two different chemical environments, on the same time-scale as the Pro(3) isomerisation.

This interaction indicated that Pro(3) and Phe(7) residues were close in space, or that the interaction was mediated by relay effect from a third part of the molecule. The ROEs obtained (see section 5.3) showed that the predominant conformation(s) brought these residues within 5A of each other. For example, in the cis

form, a cross-section through 7.47ppm gave an ROE to Pro(3)δuc at 3.53ppm; both Proδuc and Proδdc gave ROEs to an aromatic ring at 7.31ppm, which corresponded to one of the 2,6 protons of the Phe(7) ring.

The two protons Pro(3)δut and δdt gave ROEs to Val(8), but showed none to Phe(7), and vice-versa. In the trans form, although folded, Phe(7) appeared to have moved away from the vicinity of Pro(3) protons.

Both Phe(4) and His(5) NH protons were found to be broadend in the 1-D spectrum. One possible explanation for this was their presence at the region of conformational change, which resulted in exchange broadening.

His(2)NH was much broader than Phe(4) and His(5), perhaps because of its proximity to both Pro(3) and Pro(1). It could have undergone both chemical (cis-trans) and base catalysed (proximity to Pro(1) NH_2^+) exchange respectively, and so have been correspondingly broadened.

5.3. Intramolecular ROEs and RIP conformations.

Section 5.2 has establised that RIP in TFE existed in two different forms, each of which gave ROEs characteristic of the structure in that form. The predominant form in aqueous solution had a trans Pro(3) amide bond and ROEs showed it to exist with a β-turn about residues 4 → 7, with the N and C termini interacting. In TFE, the predominant (trans) form was expected to

be similar to that in H_2O, but perhaps with small local variations.

The ROEs from Pro(3)δt were similar to those in H_2O, whereas those from Pro δc characterized the conformation when the peptide bond had a cis orientation.

A number of ROEs were found, in TFE, from residues for apart in terms of the sequence. These were classified according to whether the same (or similar) ROEs were found in H_2O. Figure 5.10 shows cross sections, through the ROESY experiment, at various chemical shift values. These ROEs were also found in H_2O solution and were likely to have arisen from a conformation very similar to that which existed predominantly in water.

In TFE however, there was no detectable interaction between the N and C termini. This could be explained if the interaction had been removed, either because the HN_2^+ and CO_2^- were uncharged or the conformational equilibrium moved Pro(1) from the vicinity of Lys(10), for a significant percentage of the time.

Cross-sections through Pro(3)δut gave ROEs to the Val(8) residue, as did similar cross-sections in the ROESY experiment in H_2O. No ROEs between the Phe rings of residues 4 and 7 were found, indicating that these did not 'stack' one upon the other, as was the case previously. His(5) imidazole ring also showed no cross-peaks to either of the two rings.

These facts may be a reflection of the more polar nature of H_2O, the hydrophilic groups having a greater tendency to cluster together in this situation than in TFE.

Overall, the conformation appeared to be generally similar between the two trans forms in TFE and H_2O, in spite of these differences in backbone and side-chain orientations.

In the cis form, ROEs were found between the Pro(3) δdc and δuc protons and the Phe(7) 2,6 ring protons. These two residues were therefore within 5Å of each other, the C4 resonance of Phe(7) being modulated by the changes at Pro(3).

TABLE 5.1

Residue		Chemical Shift (ppm)		ΔObs.-Lit.		Distance to Aromatics (Å)
	α	4.38		-0.091		
	βu	2.03	)	+0.049	)	
	BD	2.45	)	+0.165	)	
Pro(1)	γ	2.03		0.000		
	δu	3.39	)	-0.263	)	
	δD	3.44	)	-0.213	)	
	α	4.95		+0.320		
	βu	3.10	)	-0.098	)	
His(2)	βD	3.13	)	-0.133	)	
	NH	-		-		
	1m2	8.04		-0.08		
	1m4	7.18		+0.04		
	α	4.45		-0.021		
	Bu	1.92	)	-0.061	)	
	βD	2.25	)	-0.045	)	
Pro(3)	γ	1.95		-0.080		
	δut	3.31	)	-0.343	)	5.40
	δDt	3.68	)	+0.027	)	
	δuc	3.53	)	-0.123	)	
	δDC	3.61	)	-0.043	)	
	α	4.63		-0.033		
	βu	3.09	)	-0.133	)	
	βD	3.09	)	+0.099	)	
Phe(4)	NH	8.37		+0.142		
	2.6	7.19		-0.099		
	3.5	7.32		-0.070		
	4	7.28		-0.059		
	α	4.57		-0.060		
	βu	3.14	)	-0.054	)	
	βD	3.17	)	-0.093	)	
His(5)	NH	7.95		-0.465		
	1m2	8.21		-0.090		
	1m4	7.00		-0.140		

Residue	Chemical Shift (ppm)	ΔObs. -Lit.	Distance to Aromatics (Å)
	α 4.50	-0.163	
	βu 2.98)	-0.011)	
	βD 3.05)	-0.173)	
Phe(6)	NH 7.73	-0.498	4.77
	2.6 7.17	-0.119	
	3.5 7.30	-0.090	
	4 7.26	-0.079	
	α 4.56	-0.103	
	βu 3.03)	+0.039)	
	βD 3.11)	-0.113)	
Phe(7)	NH 7.70	-0.520	4.70
	2.6 7.20)	-0.089)	
	7.30)	-0.090)	
	3.5 7.35	-0.04	
	4 7.47)	+0.131)	
	7.53	+0.191	
	α 4.04	-0.144	
	β 2.00	-0.130	
	γu 0.82)	-0.122)	
Val(8)	γD 0.82)	-0.149)	
	NH 7.25	-1.186	3.57
	α 4.59	-0.014	
	βu 2.96)	+0.038)	
	βD 3.11)	-0.017)	
Tyr(9)	NH 7.62	-0.563	4.58
	2.6 7.13	-0.019	
	3.5 6.84	-0.017	
	α 4.24	-0.108	
	βu 1.72)	-0.027)	
	βD 1.86)	-0.010)	
Lys(10)	γ 1.41	-0.061	
	δ 1.72	+0.012	
	ε 3.00	-0.023	
	NH 7.40	-1.008	3.77

TABLE 5.2

Residue	Coupling Constants (Hertz)	Rotational Angle
Lys (10)	J(NH-Cα) = 7.19, corrected = 7.84	θ = 18°, 146°; ϕ = 42°, 78°, -86°. -154°
Tyr (9)	J(NH-Cα) = 7.68 corrected = 8.37	θ = 11°, 149° ϕ = 49°, 71° -89°, -151°
Phe (7)	J(NH-Cα) = 6.70 corrected 7.30	θ = 23°, 143° ϕ = 37°, 83°, -83°, -157°
Phe (6)	J(NH-Cα) = 5.97 corrected = 6.31	θ = 32°, 138° ϕ = 28°, 92°, -78°, -162°
His (5)	J(NH-Cα) = 6.50 corrected = 7.10	θ = 26°, 142°; ϕ = 34°, 86°, -82°, - 158°

Figure 5.1 1-D spectrum of RIP in TFE-d^2, at 298K (3.2mM).

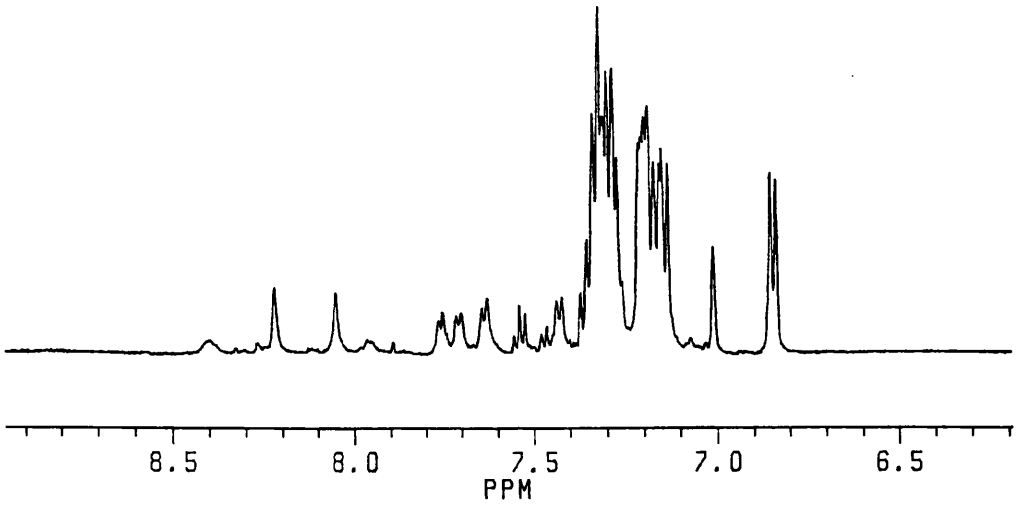
8.5
8.0
7.5
7.0
6.5
PPM

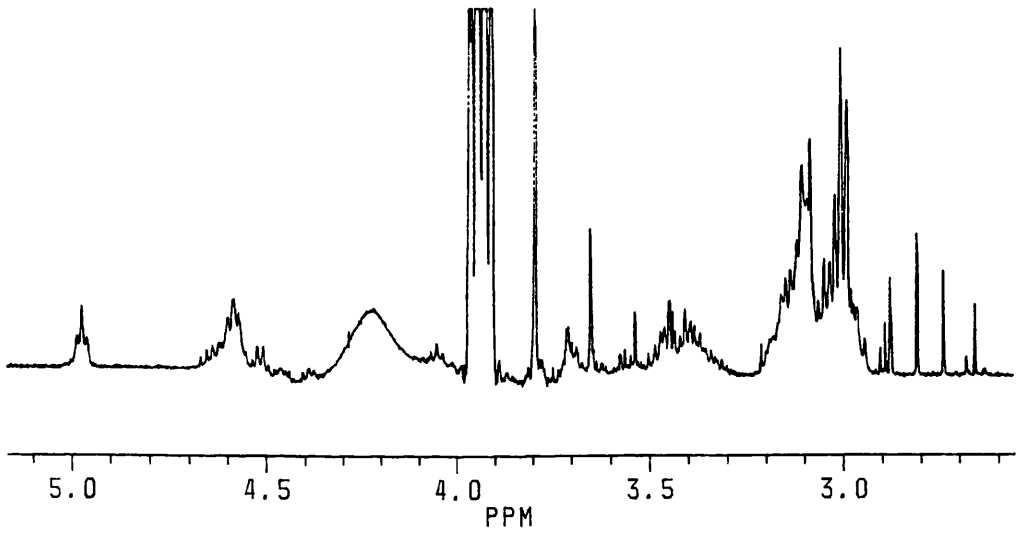
5.0
4.5
4.0
3.5
3.0
PPM

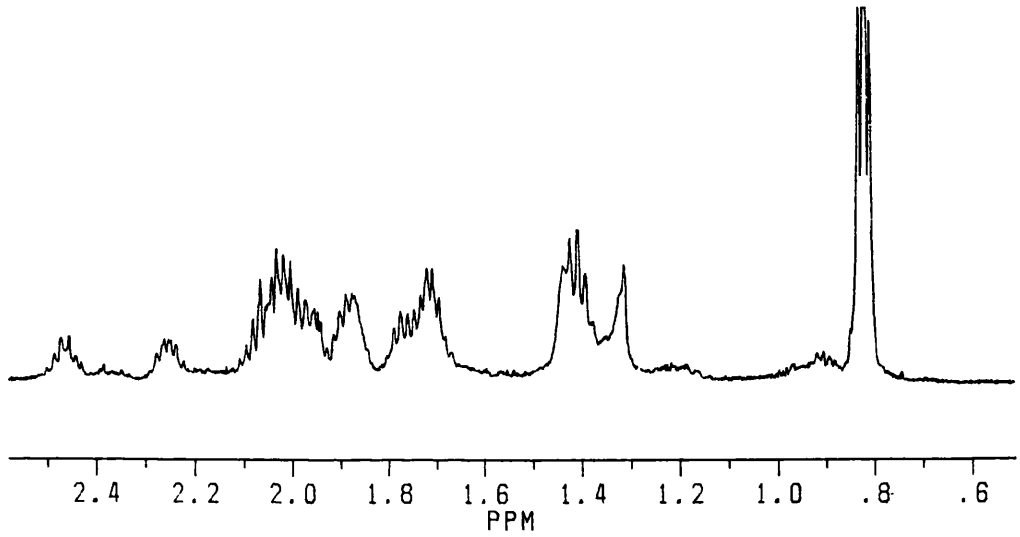
2.4
2.2
2.0
1.8
1.6
1.4
1.2
1.0
.8
.6
PPM

Figure 5.2 Cross sections through amide or alpha protons of each amino acid residue in the HOHAHA experiment, giving connectivities throughout the whole of the spin system.

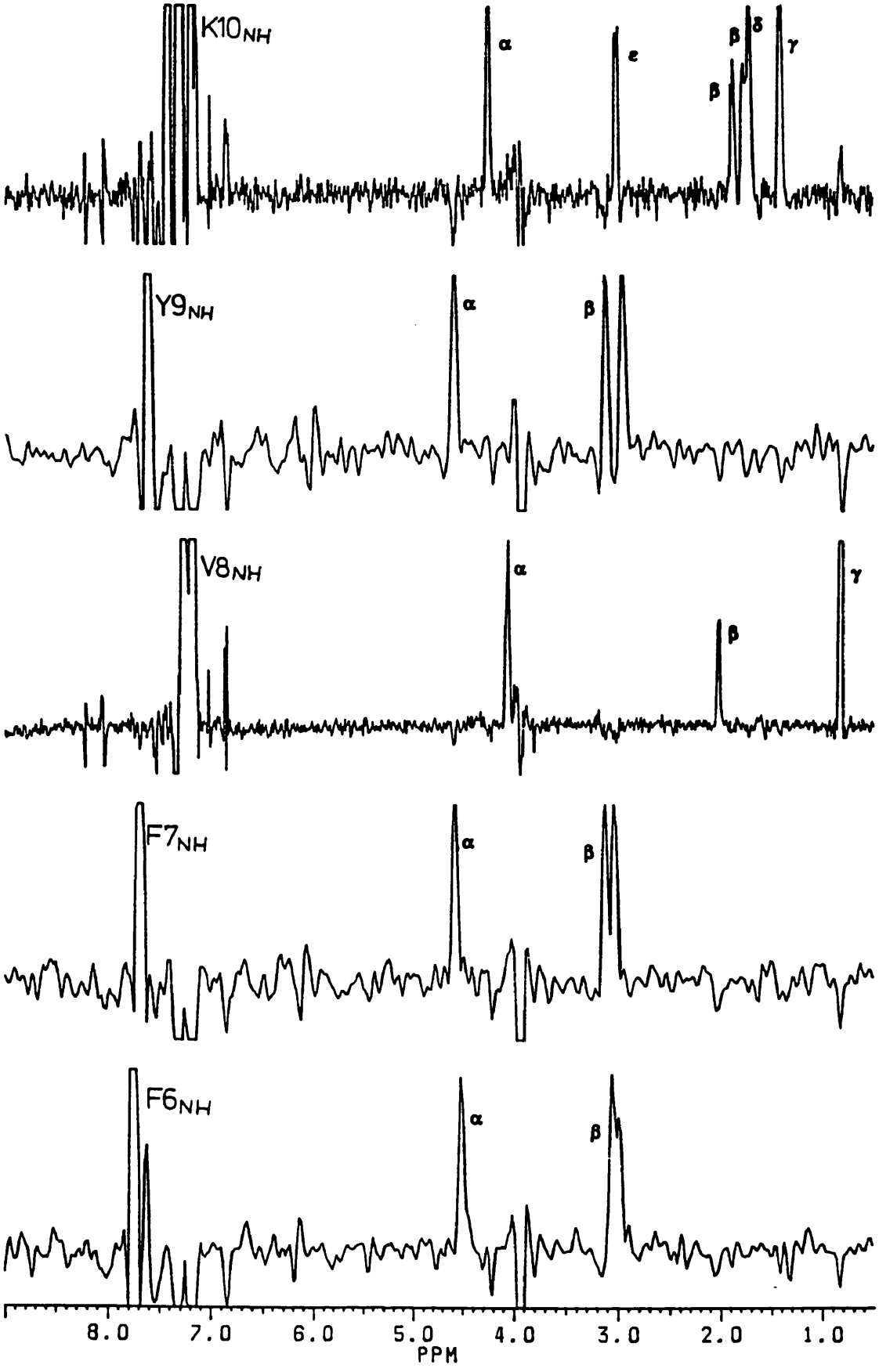
K10NH
α
ε
β
β
δ
γ
Y9NH
α
β
V8NH
α
β
γ
F7NH
α
β
F6NH
α
β
8.0
7.0
6.0
5.0
4.0
3.0
2.0
1.0
PPM

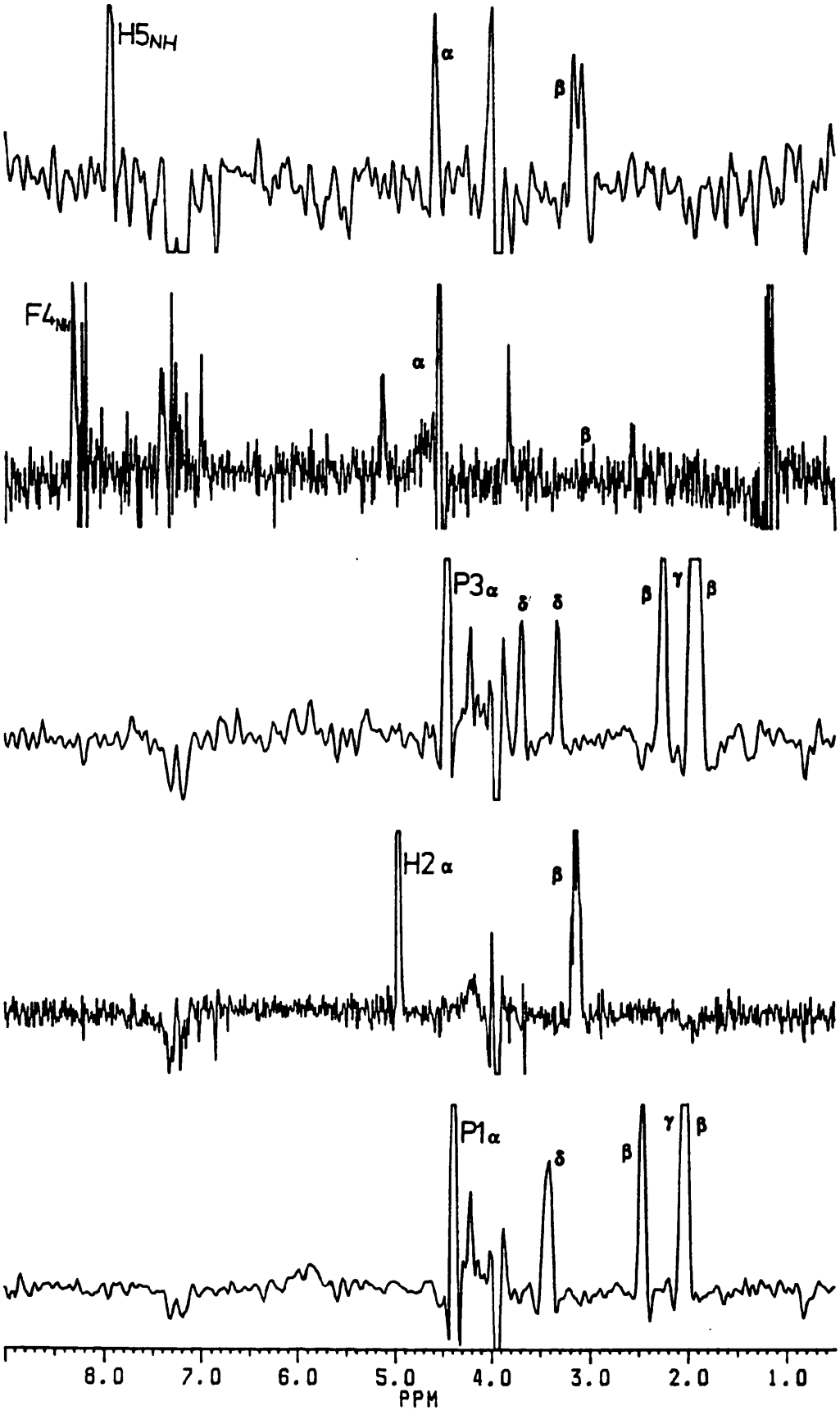
H5NH
α
β
F4NH
α
β
P3α
δ
δ
β
γ
β
H2α
β
P1α
δ
β
γ
β
8.0
7.0
6.0
5.0
4.0
3.0
2.0
1.0
PPM

Figure 5.3 Contour plot of the aromatic region of the HOHAHA experiment, showing assignments around each of the three Phe rings.

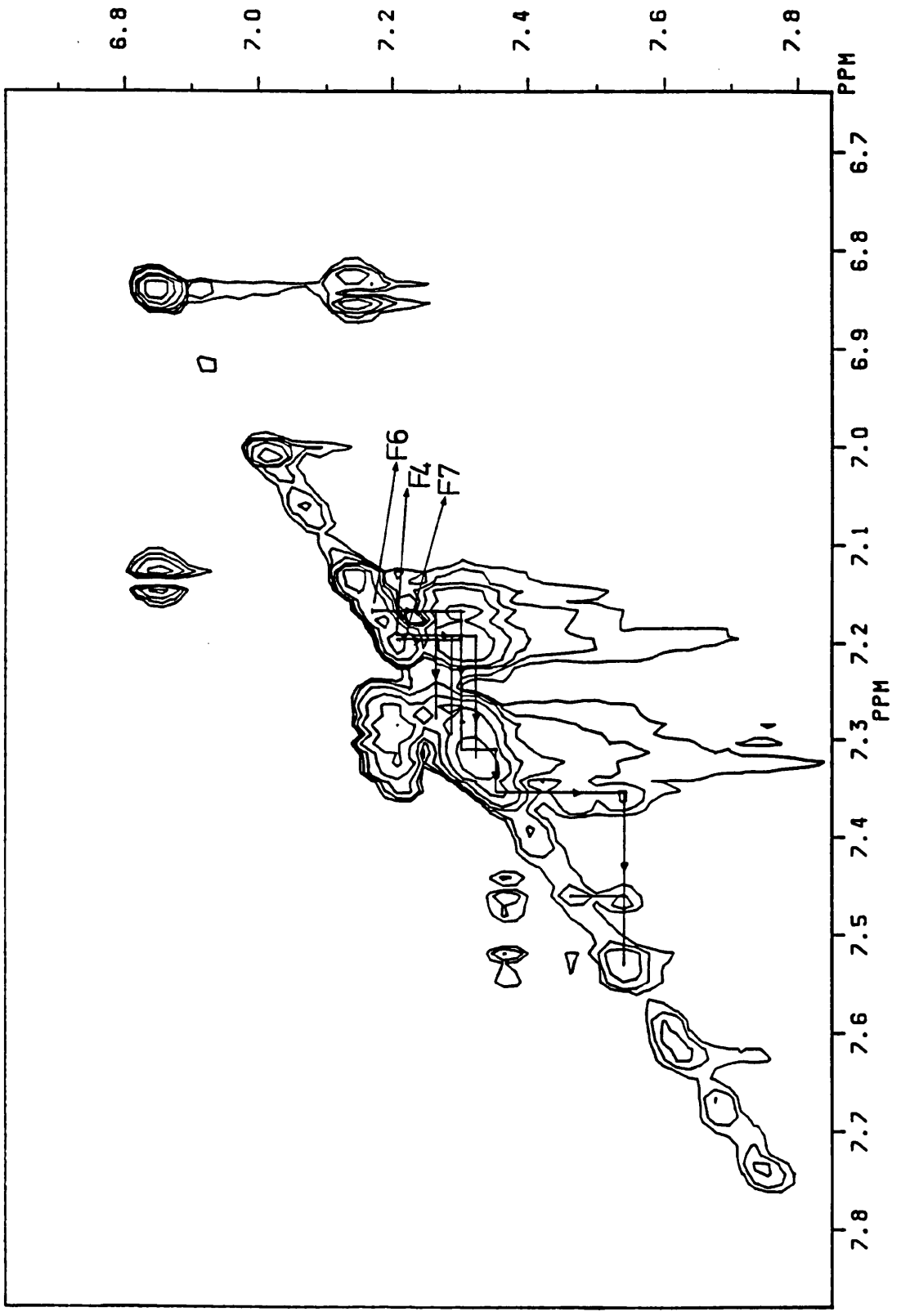
6.8
7.0
7.2
7.4
7.6
7.8
PPM
F6
F4
F7
6.7
6.8
6.9
7.0
7.1
7.2
7.3
7.4
7.5
7.6
7.7
7.8
PPM

Figure 5.4 Cross-sections through amide or alpha protons of each amino acid residue in the ROESY experiment, to give connectivities between adjacent residues.

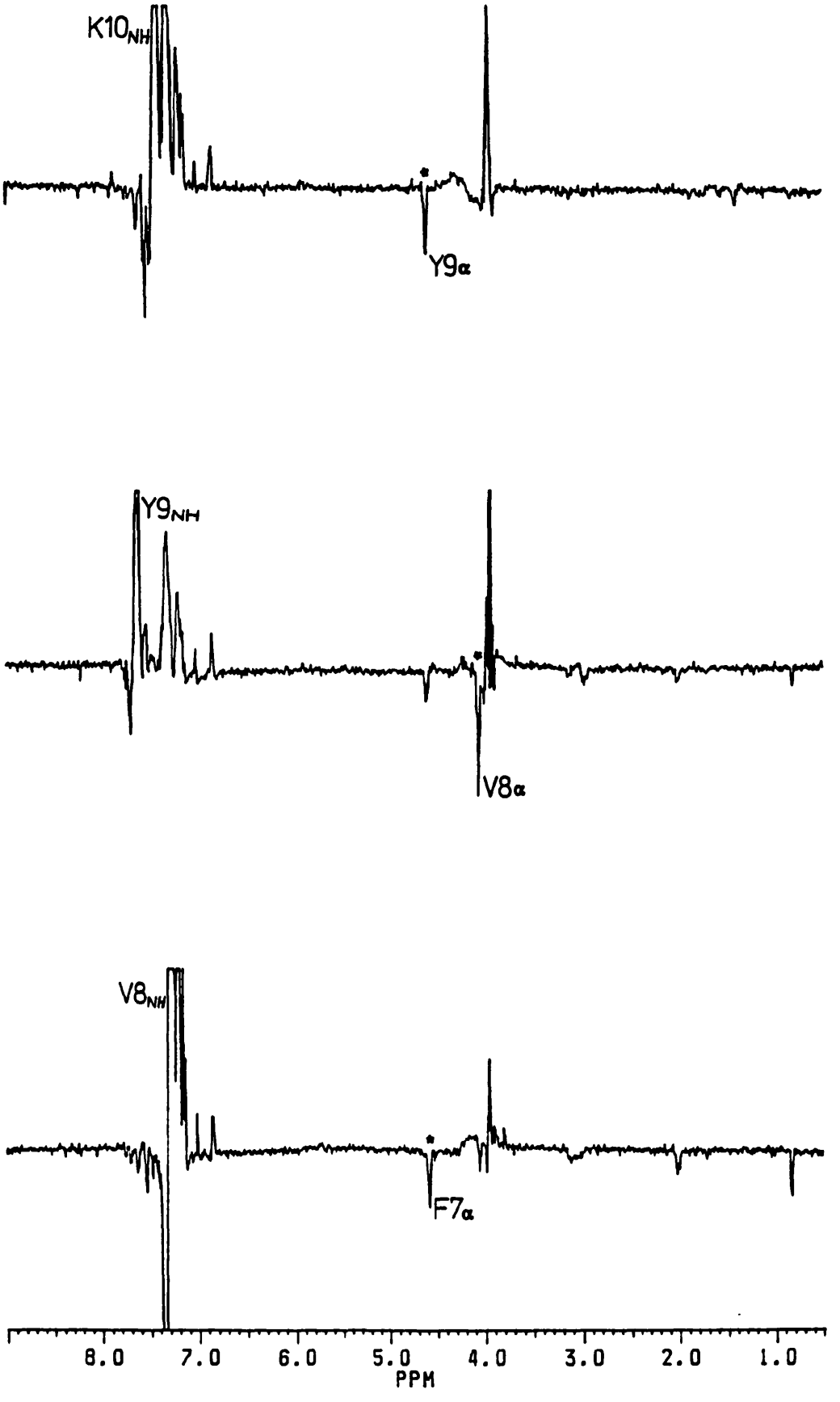
K10NH
Y9α
Y9NH
V8α
V8NH
F7α
8.0
7.0
6.0
5.0
4.0
3.0
2.0
1.0
PPM

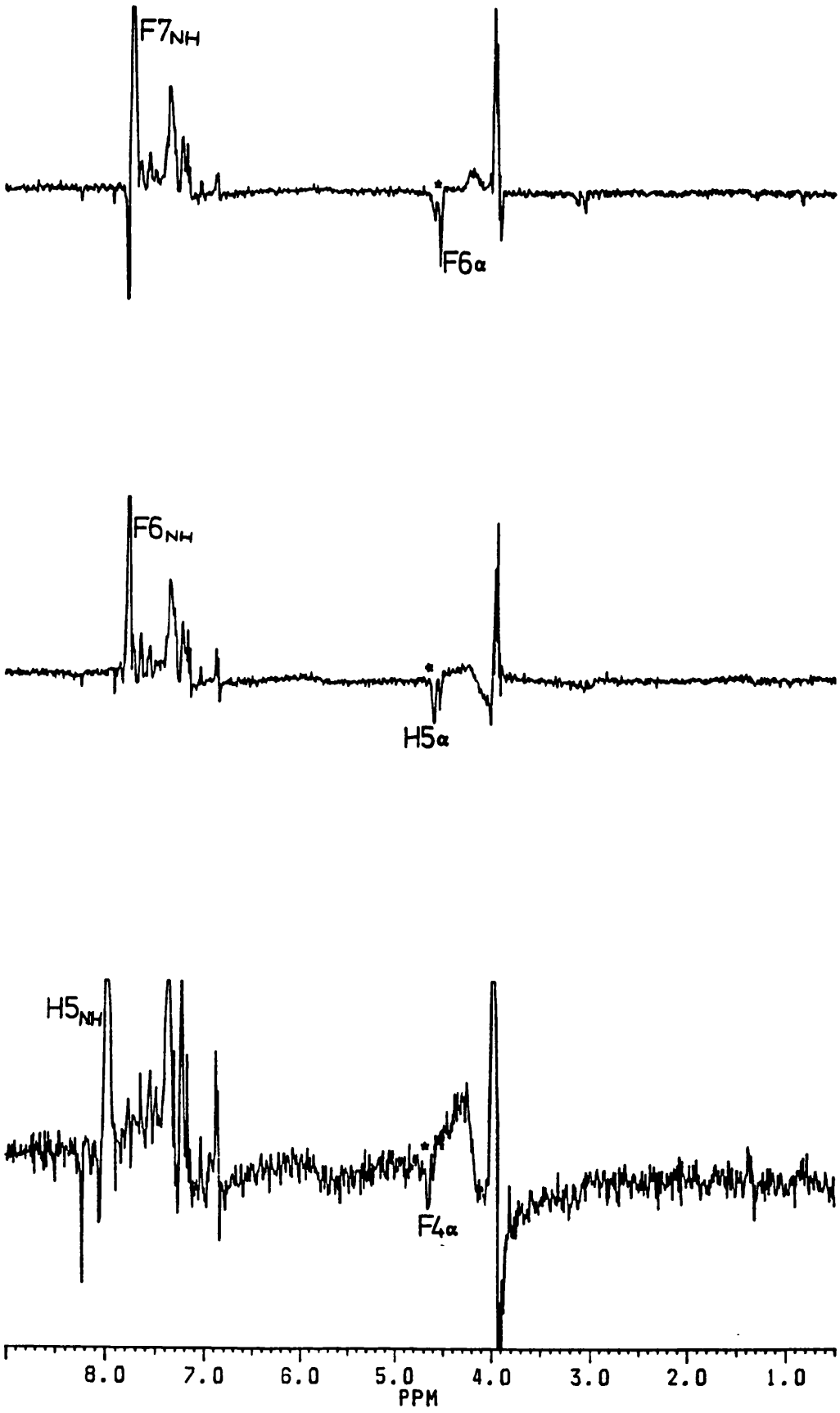
F7NH
F6α
F6NH
H5α
H5NH
F4α
8.0
7.0
6.0
5.0
4.0
3.0
2.0
1.0
PPM

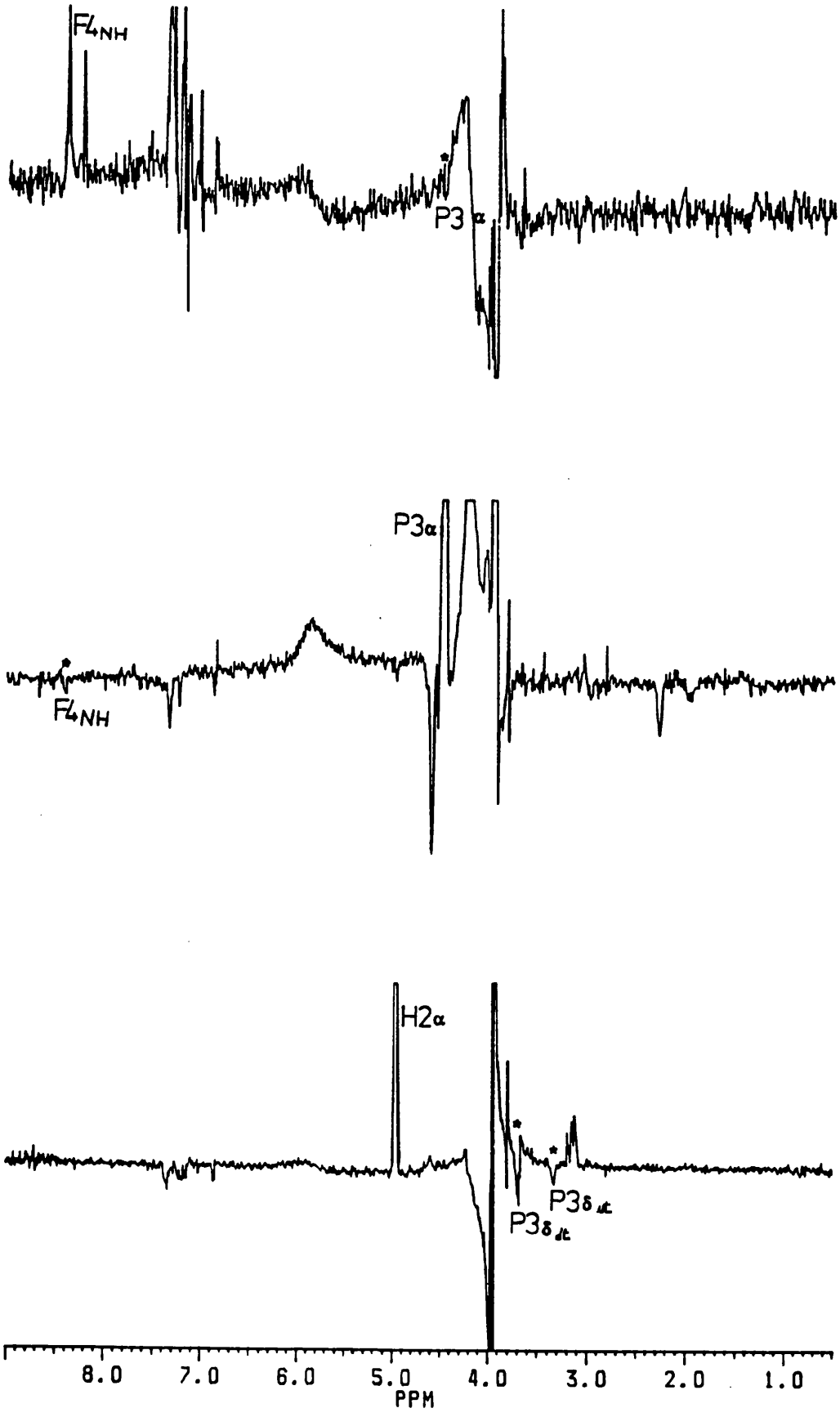
F4NH
P3α
P3α
F4NH
H2α
P3δdl
P3δdl
8.0
7.0
6.0
5.0
4.0
3.0
2.0
1.0
PPM

Figure 5.5 Contour plot of the ROESY experiment, which shows the aromatic to β proton connectivities for the residues Phe (4), Phe (6), Phe (7) Tyr (9) and His (5).

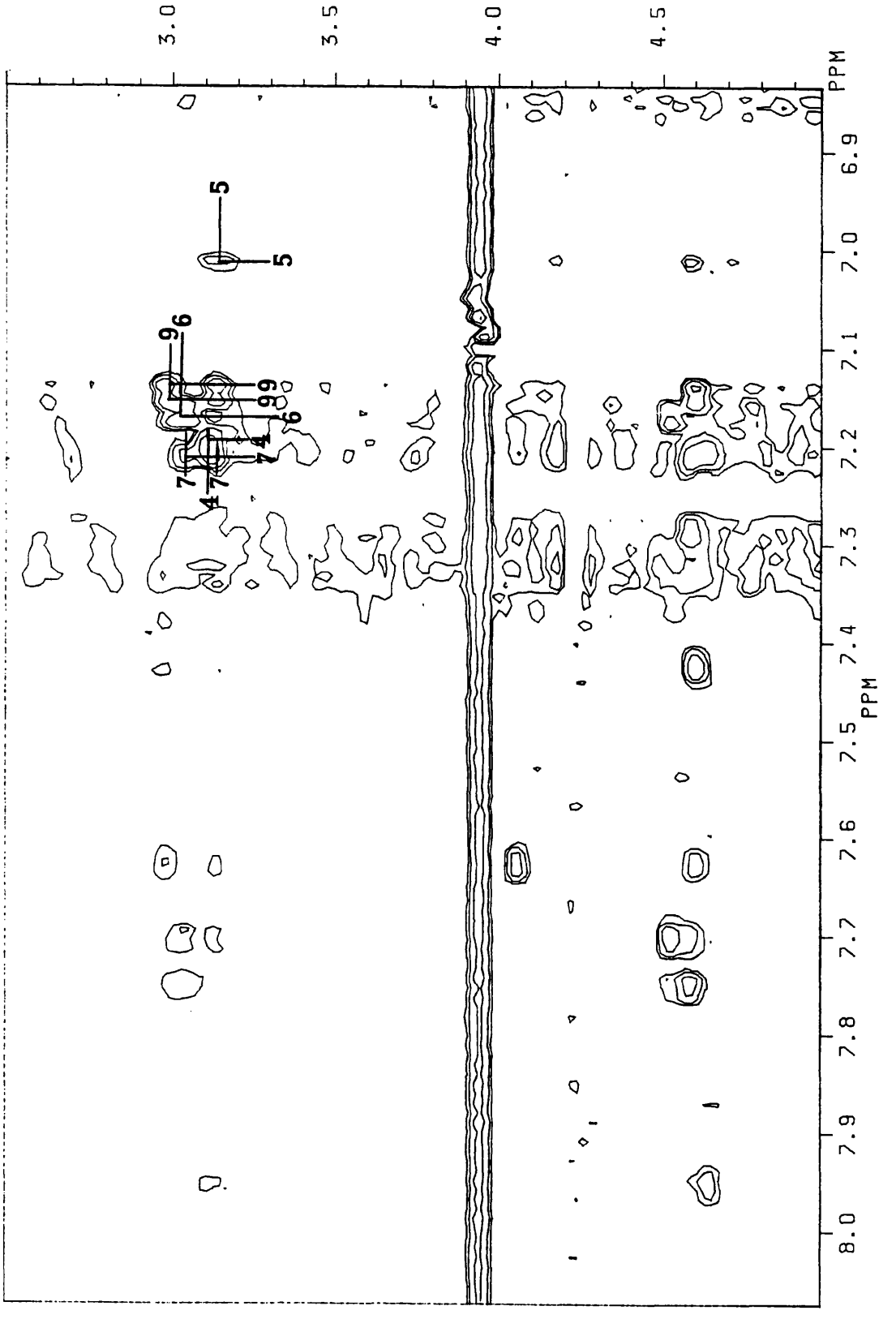
3.0
3.5
4.0
4.5
PPM
6.9
7.0
7.1
7.2
7.3
7.4
7.5
7.6
7.7
7.8
7.9
8.0
PPM
5
5
9
6
9
9
6
7
4
7
7
4

Figure 5.6 1-D plot of the Pro δ proton region, showing four resonances for residue Pro (3), indicating the presence of cis-trans.

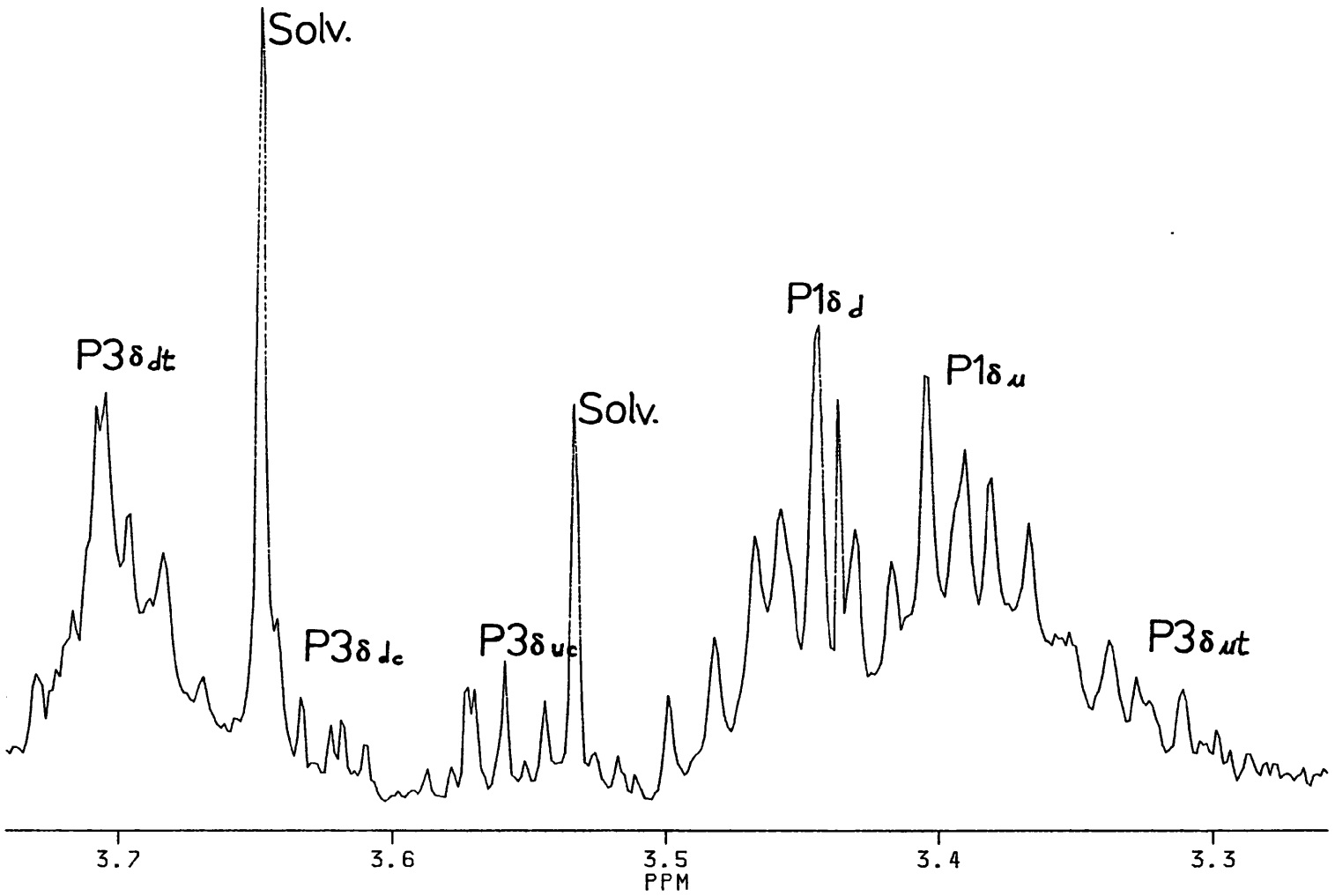
Solv.
P3δ dt
P3δ dc
P3δ uc
Solv.
P1δ d
P1δ u
P3δ ut
3.7
3.6
3.5
PPM
3.4
3.3

Figure 5.7 Contour plot of the HOHAHA experiment, showing the coupling pattern for Pro (3) δ protons, consistent with cis-trans isomerism. c = cis, t = trans.

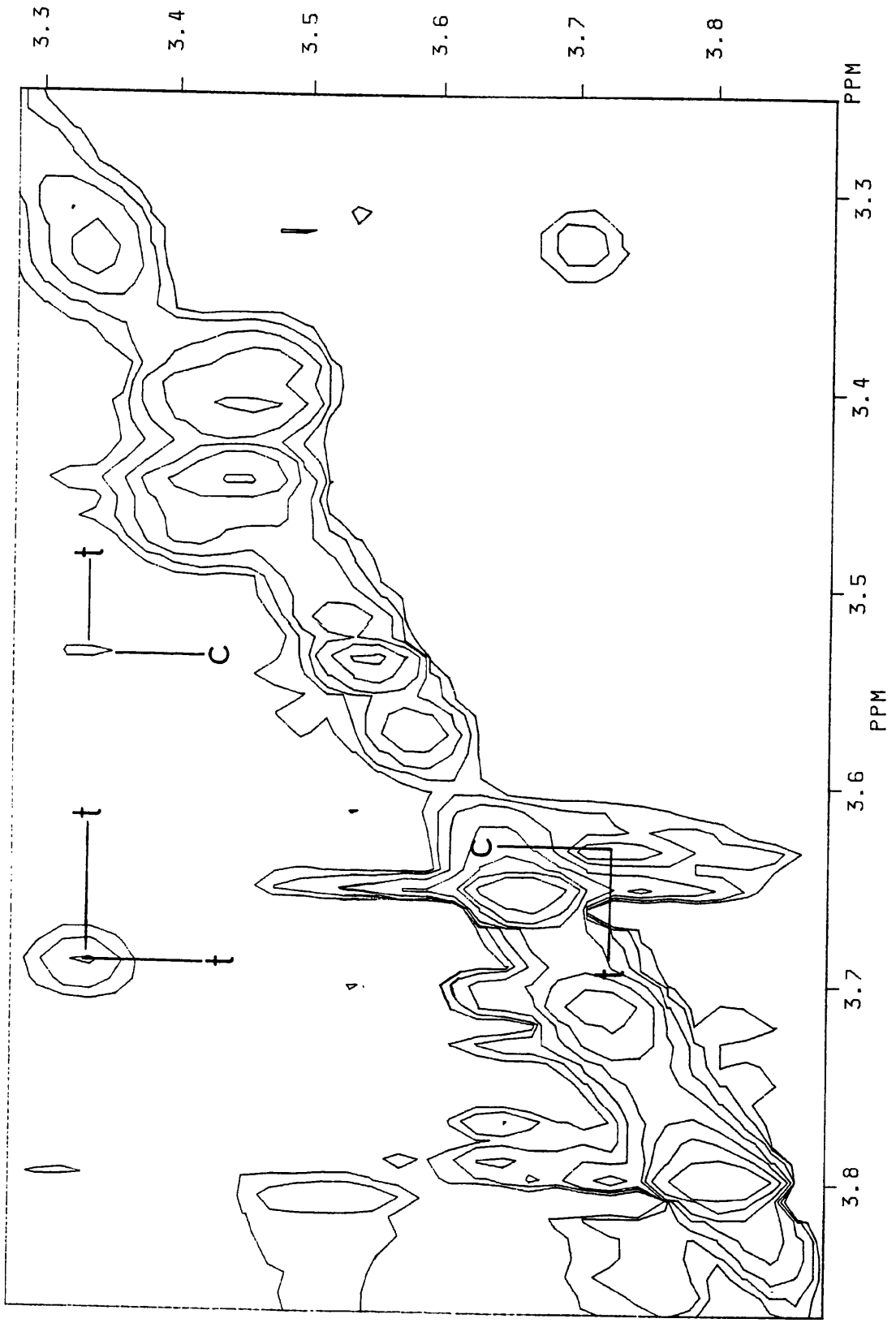
3.3
3.4
3.5
3.6
3.7
3.8
PPM
3.3
3.4
3.5
3.6
3.7
3.8
PPM
t
t
C
t
C
t

Figure 5.8 Contour plot to the ROESY experiment, in the region of the Pro δ protons. ROE and chemical exchange peaks are marked, in terms of cis and trans forms of the amide bond.

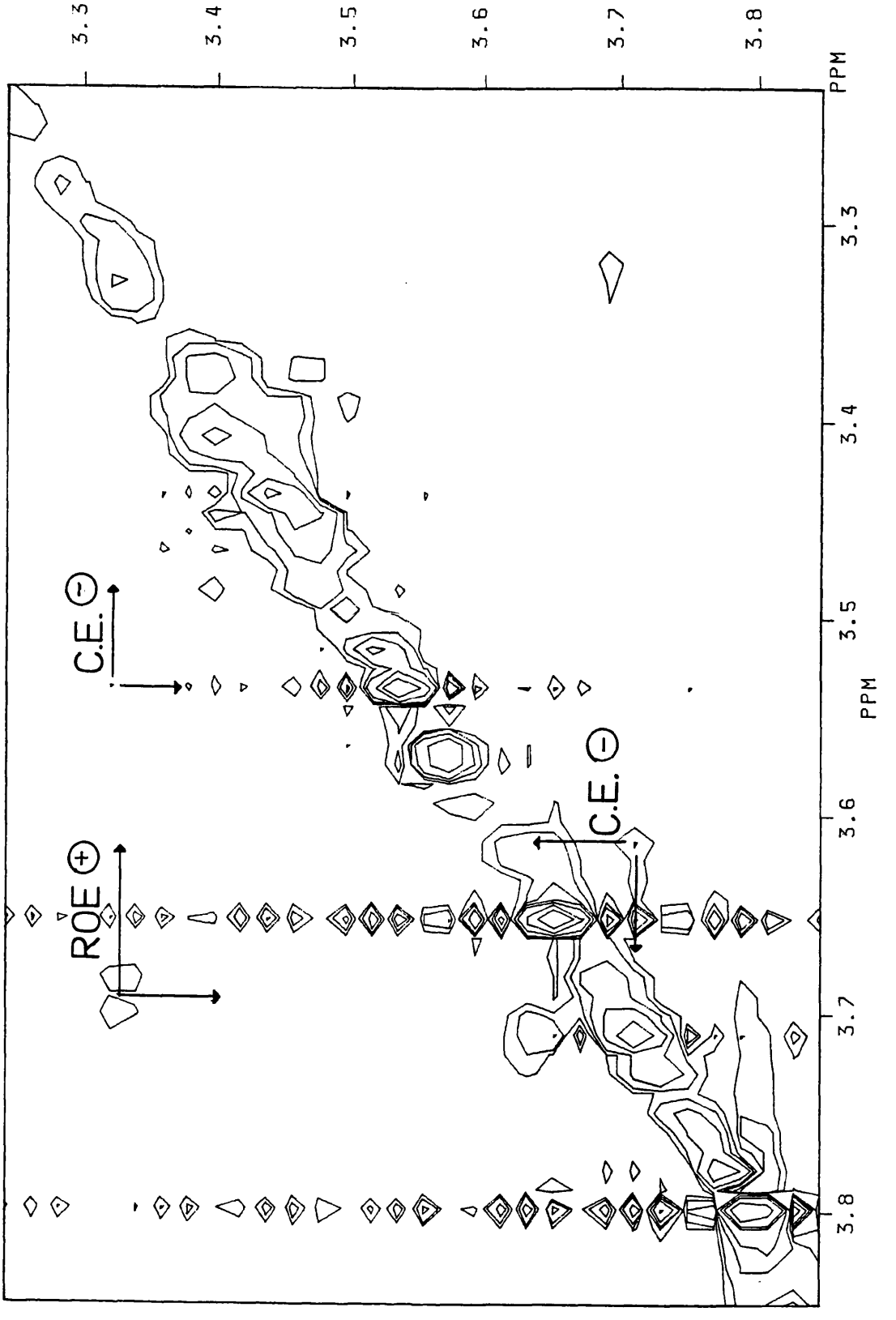
3.3
3.4
3.5
3.6
3.7
3.8
PPM
C.E. ⊖
C.E. ⊖
ROE ⊕
3.3
3.4
3.5
3.6
3.7
3.8
PPM

Figure 5.9 ROESY contour plot of the aromatic region of RIP, showing chemical exchange modulated peaks of the phenyl ring of residue 7.

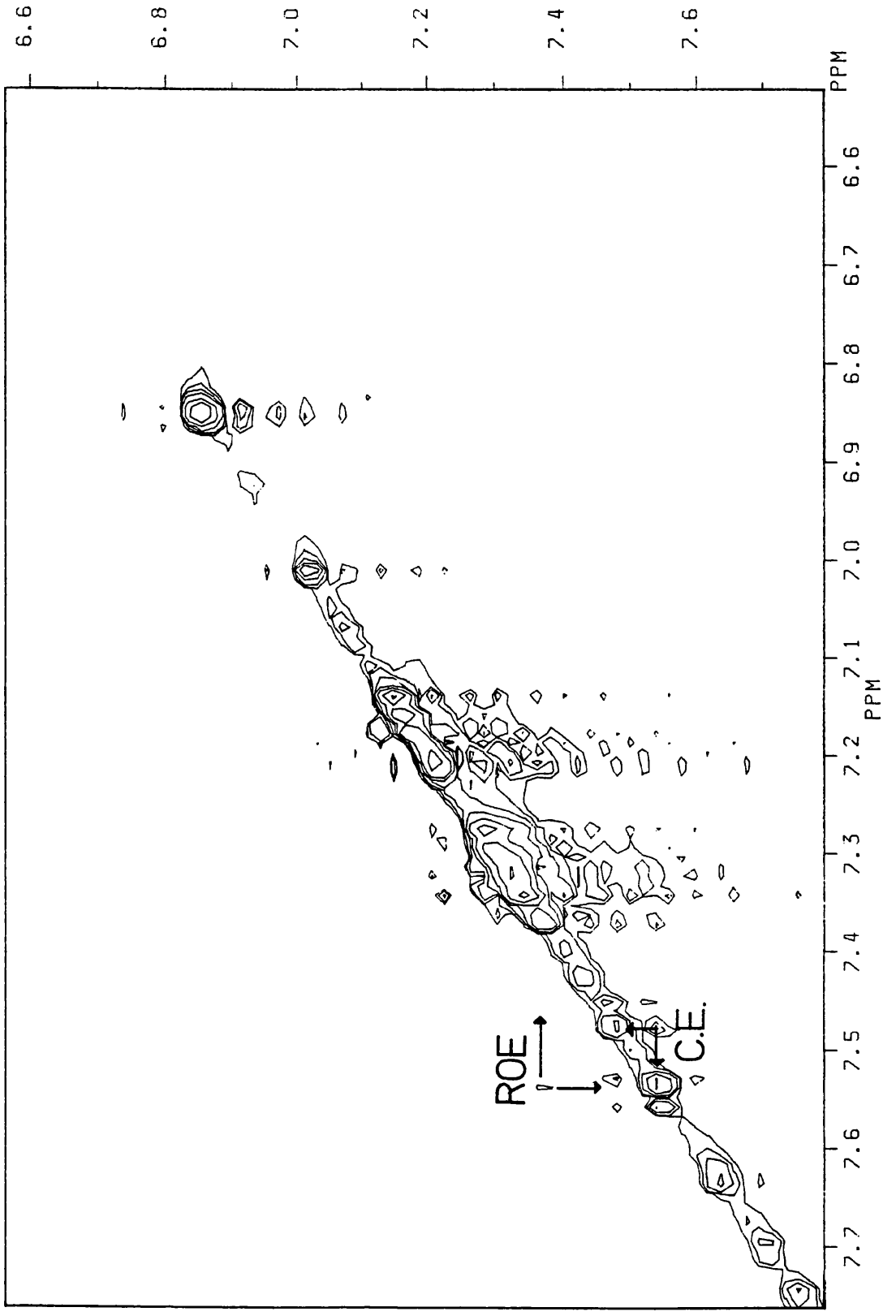
6.6
6.8
7.0
7.2
7.4
7.6
PPM
6.6
6.7
6.8
6.9
7.0
7.1
7.2
7.3
7.4
7.5
7.6
7.7
PPM
ROE
C.E.

Figure 5.10 Cross sections through several protons of RIP, showing intramolecular ROEs. These were consistent with a trans orientation of Pro (3) amide bond, and similar to the conformations found in H_2O.

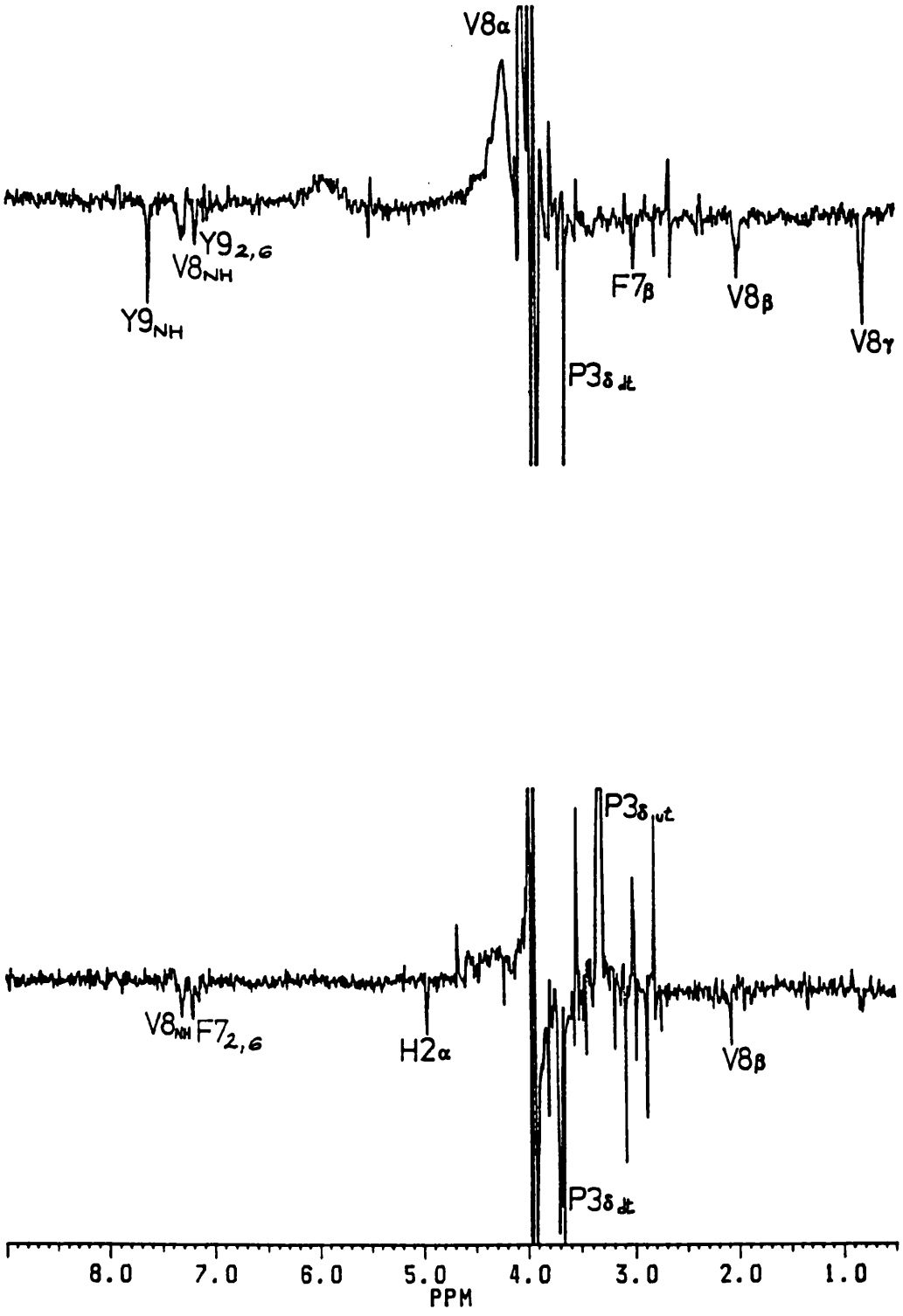
V8α
Y9 2,6
V8NH
Y9NH
F7β
V8β
V8γ
P3δ dt
P3δ ut
V8NH F7 2,6
H2α
V8β
P3δ dt
8.0
7.0
6.0
5.0
4.0
3.0
2.0
1.0
PPM

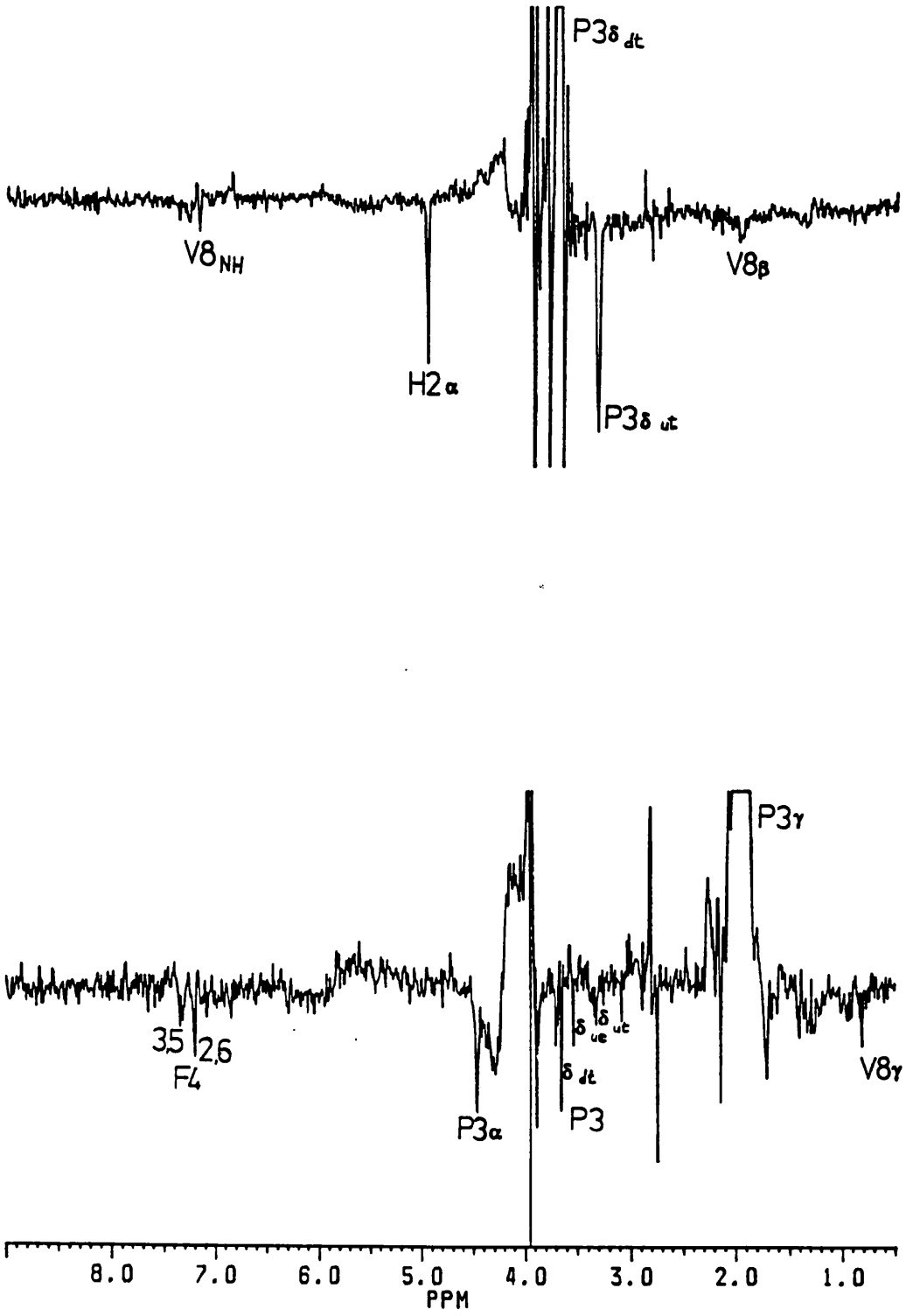
P3δ dt
V8NH
V8β
H2α
P3δ ut
P3γ
3,5
2,6
F4
P3α
δ ue
δ ut
δ dt
P3
V8γ
8.0
7.0
6.0
5.0
4.0
3.0
2.0
1.0
PPM

Figure 5.11 Cis form ROESY cross sections. Intramolecular ROEs were found which helped define the conformation of RIP in its 'other' form.

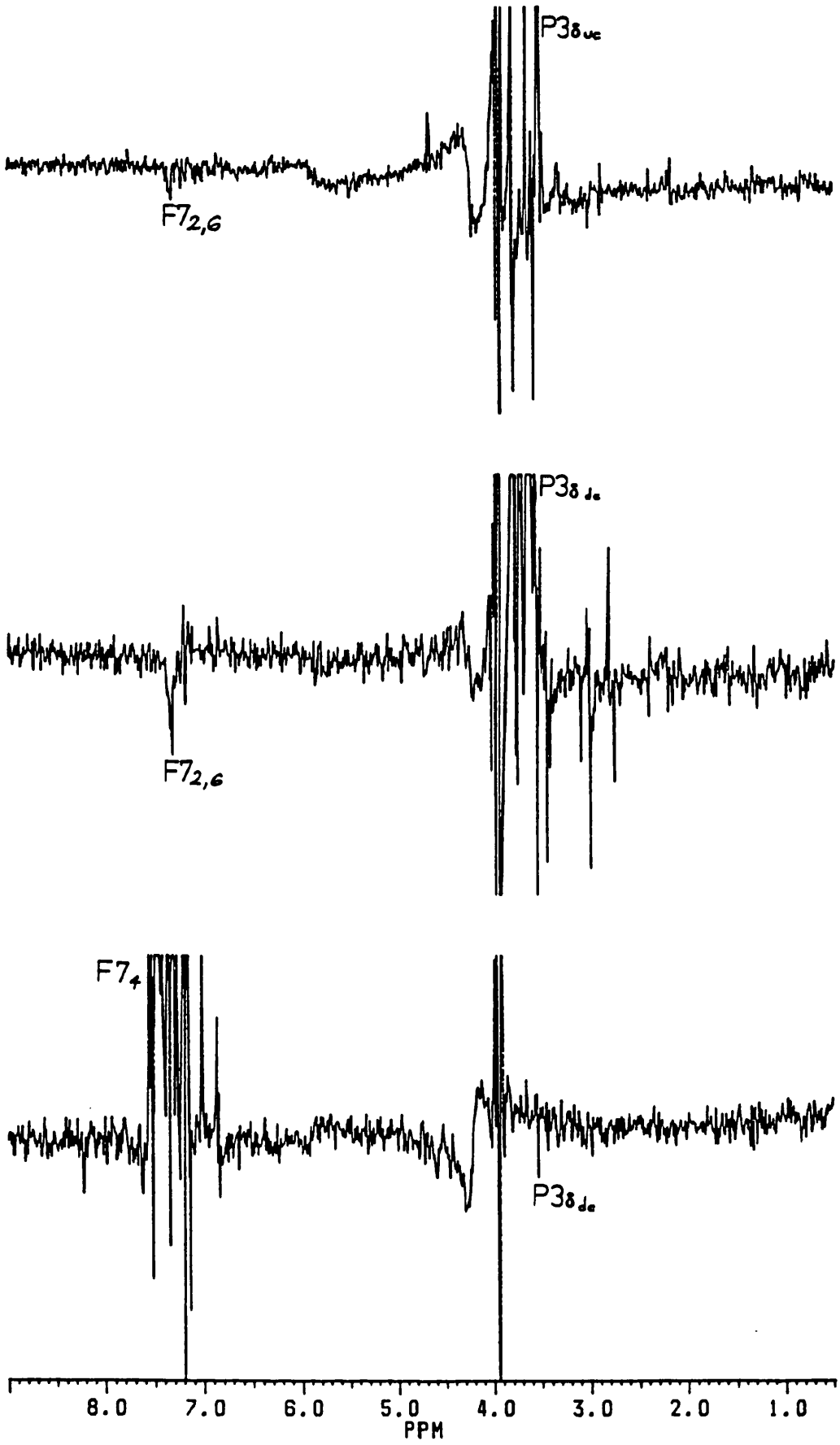
P3δ ue
F7 2,6
P3δ de
F7 2,6
F7 4
P3δ de
8.0
7.0
6.0
5.0
4.0
3.0
2.0
1.0
PPM

Chapter 6

NMR Studies of RIP in Methanol

6.1 Assignment of Proton Resonances

The 1-D ^1H spectrum of 4mg of RIP in 0.6 mls of methanol $-D^3$ (CD_3OH) is shown in Figure 6.1

A Homonuclear Hartmann-Hahn (HOHAHA) was carried out, the mixing time optimised to enhance small couplings, of 0.5Hz and upwards.

Seven of the eight amide protons were observed in the 1-D spectrum and cross-sections through each of these in the HOHAHA in turn were plotted to give correlations throughout the whole amino acid residue (Figure 6.2). Several amides overlapped slightly, but not enough to hinder interpretation. For the two Pro residues, cross sections were viewed through the α protons. As for RIP in H_2O and TFE, no cross peaks were observed between the β protons of

the three Phe residues and the protons of their aromatic rings. It was also not possible to obtain assignments around the Phe rings by this experiment. The rings represented a tight A-B-C system, and no cross-peaks could be observed , as all the resonances were very close in chemical shift.

A ROESY experiment, using a mixing time, τm, of 250 msec, was then carried out. Figure 6.3 shown a contour plot of the initial area of interests, the NH_i-$C\alpha_{i+1}$ connectivities, which allowed sequence specific assignments to be made. Initially, cross sections were taken throught the frequency of each NH proton (δ proton for Pro) (Figure 6.4). The sequence specific assignments were obtained for most of the protons in the peptide, from these cross-sections.

Figure 6.5 shows an expansion of the ROESY plot, the cross-peaks indicating connectivities between aromatic groups (Tyr, two His and three Phe) and their β protons. This confirmed the assignments for the Tyr residue, and also connected the two His imidazole rings to their β protons.

Also, it was possible to determine the resonance frequencies of the 2,6 protons of the Phe rings by cross-peaks to their β protons; this, in conjunction with the HOHAHA experiment , allowed sequence specific assignments for these resonances to be made.

However, His (2) had not been fully assigned as yet, nor had the three Phe ring protons.

In order to address both these problems of assignment, a long-range COSY was run, with solvent presaturation, and using a 45°

detection pulse instead of the normal 90°, to reduce the size of the diagonal and make the tight cross-peaks easier to observe.

Figure 6.6 shows a contour plot of the aromatic region of RIP, and the assignments which were possible. A reference back to the ROESY experiment, which showed aromatic β—cross-peaks, gave sequence specific assignments of these resonances.

Figure 6.7 shows the cross-peaks, in the long-range COSY, through 8.35ppm and 8.10ppm, the imidazole 4-protons. The connectivities to the imidazole 2-protons assigned unambiguously the remaining His(2) residue protons. The His(2) α proton was under the OH signal from methanol (See section 6.4) at ~ 4.93 ppm.

Table 6.1 shows the assignment obtained for RIP in methanol. Also tabulated are the $\Delta\delta$ values, the difference between the observed chemical shift and that obtained for a non-structural peptide. The distance to an aromatic ring, for protons with $\Delta\delta > 0.02$ppm., is also tabulated.

Coupling constants between NH_i-CH_i protons are shown in Table 6.2. These $^3J_{NH_i-CH_i}$ after correction for electronegativity effects, were related to the angle θ, and then ϕ_i, which could be used to define the backbone conformation(s).

6.2 Structural Information from ROEs

RIP in methanol existed as two interconverting forms; each conformation should give ROEs characteristic of its 3-D structure in that conformation. ^{1}H NMR studies in H_2O/D_2O characterised the predominant conformation in one form of the conformational

equilibrium, with the Pro(3) amide bond in the trans form. In methanol, CD results showed that there existed a ~ 50:50 mixture of the two components. However, the trans form of the component (in methanol) should have a similar structure to that determined in water by NMR and CD. The ROEs in methanol which therefore did not correlate with the general β-turn type of structure will probably have arisen from the other conformation, with the Pro(3) amide bond in a cis configuration.

Table 6.1 showed that a number of resonances had a significant chemical shift difference from the value in a non-structured environment. These protons may have been shifted upfield or downfield for a number of reasons; close proximity to the plane of aromatic rings (downfield shifts), lying above aromatic rings (upfield shifts), involvement in hydrogen bonding, shielding from solvent by folding of peptide chain etc.

No significant chemical shift differences were found for the benzene rings of residues 4 and 7. Previously, in H_2O, these appeared to have stacked, one on top of the other, causing ring-current shifts in both rings (Chapter 4). No ROEs were observed between these two residues in methanol; this lack of hydrophobic interaction may have been due to the changing of solvent polarity, from hydrophilic (H_2O) to more hydrophobic in nature (MeOH).

A number of rotating frame NOEs were observed between protons of residues which were far apart in terms of sequence, but were brought close together by folding of the peptide.

(i) 'Trans form'.

Figure 6.8 shows cross sections through different proton resonances on the diagonal of the ROESY experiment. These ROE cross-sections were consistent with the folding found in studies in water with a trans peptide bond i.e. a β-turn about the residues 4-7.

Indeed, cross-sections through the Pro(3) δ protons of the trans form (assigned from Section 6.3) showed ROEs to Val(8) α proton, as consistent with the 4-7 β-turn hypothesis.

The protons on the diagonal (in this section) showed no chemical-exchange peaks for the different ('cis') environment (except Pro(3)); the correct integral in the 1-D spectrum for these resonances was also observed. In both conformations, it appeared that similar chemical environments had been experienced by these protons, and as a result no chemical shift difference or exchange-peaks were found. This fact may infer a good deal of conformational flexibility of the molecule as a whole.

Pro(3) and Val(8) residues were brought close together by the chain-folding, perhaps because of the ionic interaction of the N and C termini; no ROEs were found between Pro(1) and Lys(10), unlike the case of water where many were seen. This may have been either a reflection of the smaller percentage of time which each residue spent in the charged form, or because the position of the conformational equilibrium had changed, and as a result the protons were not in the proximity of one another for long enough for ROEs to be observed. It was possible that a combination of these factors were responsible for the observation.

Similar to H_2O and TFE studies, in MeOH the Val(8) and Lys(10) residues were brought close together, perhaps by the presence of a hydrogen bond between Val(8) carbonyl and Lys(10) amide (See Chapter 7).

(ii) 'Cis' Form

Figure 6.9 shows the intramolecular ROEs obtained which were not consistent with the above structure, and so were hypothesised to result from the other component of the conformational equilibrium, with Pro (3) amide bond in the cis configuration.

The further downfield of the Pro(3)δc protons (at 3.73ppm) showed a ROE to Lys(10)δ protons, and vice-versa. From this ROE alone, it appeared that the peptide chain had undergone a shift, with the two ends of the chain moving in opposite directions.

The Tyr(9)NH - His(5)NH was also a good indication of this.

It was encouraging to note that the protons which were shifted in chemical shift by more than ± 0.2ppm from a non-structured environment were accounted for by the ROEs which had characterised the folding of the peptide.

In conclusion then, the ROEs found fitted into the hypothesis of a predominant two-state system, with the approximate structure in each state being defined.

These can be represented as:-

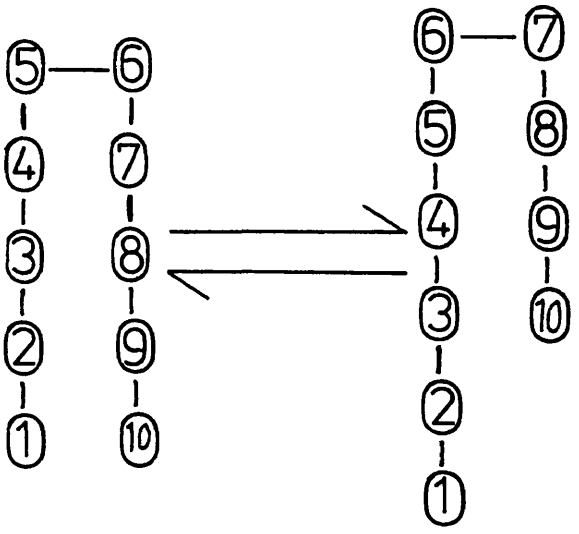

A series of NH_i - NH_{i+1} ROEs, consistent with neither states A or B were also observed for RIP in methanol. It may be that these were from state C, existing with an extended helix type of structure.

6.3 Chemical-Exchange and Cis-Trans Isomerisation

Figure 6.10 shows a contour plot of the long-range COSY experiment, in the region of the Pro δ protons. The cross-peaks between Pro(1) δu-δd was distinguishable and is marked. No other protons were in this region, and so the remaining four resonances arose from the Pro(3) δ protons.

As each proton existed in two separate distinct chemical environments, δ proton X coupled only to δ proton Y in its two environments. From this COSY experiment alone it was therefore possible to assign the chemical shift value for each δ proton in

each of the two environments. The cross-peak from the resonance at 3.63ppm to His(2) α proton (in the ROESY experiment) assigned this unequivocally to the trans configuration, and defined the other three resonances to two cis (3.73ppm and 3.67ppm) and trans (3.63ppm), by the coupling pattern.

Figure 6.11 shows a ROESY contour plot of the region of interest. The negative cross-peaks were ROEs, the positive were chemical-exchange modulated peaks. Chemical exchange occurred between the resonances at 3.73ppm - 3.63ppm and 3.67ppm - 3.57ppm indicating these protons were exchanging chemical environments, and the Pro(3) was undergoing cis-trans isomerisation about its amide bond. The exchange process, as previously, was slow relative to the NMR timescale, so that two separate resonance signals, reflecting each environment, were found.

Integration of peak areas to determine the percentage of cis and trans was possible (Figure 6.12), using Pro(1)δu as a calibration, because it was equivalent to one proton, and separated from the other Pro δ resonances. The integration of the peak at 3.57ppm (the 'trans' forms) integrated to 0.48 of a proton. The 'other' (cis) part of this proton was overlapped with the Pro(1)δD resonance, but accounted (by difference) for 52% of a proton. The ratio of trans:cis was therefore 48:52, which was remarkably close to that calculated from CD values, 47:53. (Chapter 3) This was very encouraging, and a good indication that the interpretation of the data was correct.

Once the presence of the cis:trans isomerisation had been confirmed, it was possible to interpret the broadening of selective resonances, namely His(2) and Phe(4) NH protons (see Figure 6.1).

It was anticipated that the relaxation of both protons would be modulated by the relatively slow isomerisation at Pro(3).

However, if no other low frequency mechanisms were present, both would be expected to have given two resonances signals in the correct ratio of cis:trans, as for Pro(3)δ protons. As both were broadened His(2) was so broad it was lost in the baseline and could not be assigned), another low frequency process must have acted on these protons. His(2) α proton was under the solvent resonance, and so pre-saturation may have relaxed adjacent His(2) NH proton. Another mechanism by which both protons were broadened was solvent exchange, both base and acid catalysed. His(2) NH in particular, because of its proximity to the charged N-terminal Pro(1) residue, would have experienced a greater rate of base-catalysed exchange, and as a result broadened more than the Phe(4) NH proton. The net result of these exchange processes acting simultaneously was a reduction in the T_2 value and a corresponding broadening of the signals.

6.4 Cryogenic ^{1}H NMR Studies

It was hoped to be able to study the 'freezing out' of the most thermodynamically stable conformation by NMR, in cryogenic solvents, in a manner similar to that for RIP in the CD studies. NMR should

give much more detailed information concerning the behaviour of the peptide than CD, as it was possible to study the change in the position of equilibrium by observing individual proton chemical shifts, rather than the peptide backbone and aromatic rings as a whole.

There are a number of intrinsic difficulties in studying molecules at low temperatures with NMR which are worth mentioning.

The sample was spun with N_2 (zero moisture) and cooled using liquid N_2. It was not possible to change the non-spinning shims below ~ 5°C, as moisture gathered on the probe head, turning to ice, and did not allow the sample to spin again.

Also, decreasing temperature, the strength of the lock signal decreased significantly, particularly below ~ -50°C, presumably because of the changing viscosity of the solvent. This change in lock-level would have had an effect on the quality of the spectrum obtained.

The change in chemical shift of some proton resonances, as well as being a reflection of changing peptide conformation, may also have been influenced by the changing of solvent viscosity, particularly for those protons which were exposed to the lattice. This would have had no significant effect when measuring CD spectra, but was a major factor for consideration of NMR data.

The biggest drawback with this type of experiment was perhaps the effect of slowing of the molecular tumbling as function of temperature. The spin-spin relaxation time (T_2) decreases with decreasing correlation time, τc, and as a result the spectral lines become increasingly broadened (as $\nu_{1/2} = \frac{1}{\pi T_2}$, where $\nu_{1/2}$ is the width of

the resonance peak at half-height). As a consequence., below ~ -90°C it was not possible to obtain any resonance signals from RIP, only solvent resonances were observed.

Figures 6.13 and 6.14 show the temperature variation, between +20°C to -89°C, of an RIP solution (16mM) in CD_3OD/glycerol - D8. In order to rule out the possibility of aggregation as a cause of the broad lines obtained, the experiment was repeated at several RIP concentrations, down to a concentration of 0.4 mM. The results obtained were consistent, ruling out aggregation as a major contributing factor to resonance broadening.

As the conformational equilibrium was slow relative to the NMR timescale, and two resonance signals were observed for each Pro(3) δ proton, lowering the temperature (and thus changing the equilibrium constant) should not in itself have caused broadening. The chemical shift values of each proton should have moved towards that value when the conformation was in the low temperature state; some protons, whose chemical environments were not affected, would show little changes with temperature, while others would have shown large movements until the low temperature state was 'frozen out'.

Figure 6.13 shows the temperature variation of aromatic protons between -20°C and -89°C. It was only possible to determine the temperature variation for four protons in this region because of the problems with many resonances overlapping, or moving into the middle of a crowded region. Figures 6.15 and 6.16 show the plots of chemical shift versus temperature for His(2) and His(5) 2-imidazole protons, and His(2) 4-imidazole and Tyr(9) 3,5 protons respectively.

Tyr(9) 3,5 protons showed no change in chemical shift with temperature, whereas His(2) 4-ring proton showed a slight movement, albeit over a range of only 25Hz. This indicated that the 4-imidazole proton of His(2) felt the effects of changing chemical environment more than that of the Tyr ring, due to either moving of the position of equilibrium, or solvent effects. However, relative to the dramatic shifts observed for His(2) and His(5) 2-ring protons (Figure 6.16), this change in chemical shift was relatively minor. These imidazole ring protons moved by 135Hz and 63Hz respectively, again in a regular manner, as seen by the straight lines obtained. It seemed likely that this effect was due to drastic changes in chemical environments rather than mere changes in solvent viscosity or exposure to solvent. His(2) was adjacent to the locus of conformational change (Pro(3)), and His(5) was at the position of the turn in the 'trans form' and so as a result these residues showed large changes relative to the Tyr residue. The movement of His(2) was greater than His(5), perhaps reflecting the fact that His(2) was next to the amide of Pro(3) and His(5) was further removed from it.

Figure 6.14 shows the temperature variation of the resonances between 5pm and 0.5ppm. Once again many protons were overlapping and so it was not possible to determine every proton's temperature variation. However, a number of protons were well enough separated to follow their chemical shift behaviour over the whole temperature range. Figure 6.17 shows the plot of chemical shift versus temperature for several hydrophobic side-chain protons. These appeared to show little or no variation in chemical shift.

However, at +1°C, while Pro(1) βd, Lys(10) δ, Lys(10) γ and Val(8) γ were still sharp, Pro(3) βd had broadened selectively. This may have indicated that this proton felt the slower molecular tumbling much more acutely than the other protons, and so was subsequently broadened, perhaps because of greater exposure to solvent. It was not until ~ -19°C that the other four protons had broadened to the same extent that Pro(3) βd had at +1°C.

Figure 6.18 shows the temperature variation of the chemical shift of three α protons which could be followed over the whole temperature range. His(2), Pro(3) and Val(8) α protons showed little variation with temperature, although all three showed a slight 'kink' in the plot, between -30°C to -50°C. It seemed likely that the same phenomenon was responsible for this variation, and effected almost no other parts of the molecule (hydrophobic side-chains or most aromatics). It was possible that the movement of a Phe ring (or rings) caused a ring current shift in these protons which had been brought close together by folding of the peptide chain (see Section 6.2). CD spectra had shown (Chapter 3) that at least one Phe ring may have shown a large variation in chemical environment with temperature, beginning at ~ -30°C. The chemical shift of these α protons then moved to their original values; it was possible that the Phe ring which had caused the shift had moved away from the proximity of these protons, due to movement of the peptide backbone.

In the aromatic region (Figure 6.13) one of the Phe rings began to move at ~ -30°C (labelled *), correlating well with CD results and the results obtained here. It was not possible to assign this

ring to a specific residue, because of the overlap with other proton resonances.

His(2) α proton was also assignable because of these low temperature studies; at room temperature the resonance appeared under the methanol —OH peak and was not observable.

In general then, these low temperature studies appeared to be dominated by the broadening of resonances due to the decreasing correlation time, but it was still possible to obtain useful information concerning the movement and mobility of specific resonances within the peptide, and the effects these movements had on other protons.

TABLE 6.1

Residue	Chemical Shift (ppm)		Obs.-Lit.	Distance to Aromatics (Å)
	α	4.32	-0.151	
	βu	1.96)	-0.012)	
	βD	2.36)	+0.065)	
Pro(1)	γ	1.96	-0.070	
	δu	3.46)	-0.193	
	δD	3.71)	+0.057	
	α	4.84	+0.210	
	βu	3.17)	-0.028)	
	βD	3.17)	-0.093)	
His(2)	NH	-	-	
	1m2	8.10	-0.02	
	1m4	7.23	+0.09	
	α	4.38	-0.091	
	βu	1.88)	-0.101)	
	βD	2.19)	-0.105)	
Pro(3)	γ	1.85	-0.180	
	δut	3.57)	-0.083)	
	δDt	3.63)	-0.023)	
	δuc	3.67)	+0.017	
	δDc	3.73)	+0.077	
	α	4.56	-0.103	
	βu	3.10)	+0.109)	
	βD	3.10)	-0.123)	
Phe(4)	NH	9.02	+0.792	4.10
	2.6	7.19	-0.099	
	3.5	7.25	-0.140	
	4	7.22	-0.119	
	α	4.48	-0.150	
	βu	3.12)	-0.078)	
	βD	3.12)	-0.143)	
His(5)	NH	8.18	-0.235	6.10
	1m2	8.35	+0.230	
	1m4	7.00	-0.140	

Residue		Chemical Shift (ppm)	Obs.-Lit.	Distance to Aromatics (Å)
	α	4.47	-0.193	
	βu	2.92)	-0.071)	
	βD	3.00)	-0.163)	6.30
Phe(6)	NH	8.05	-0.178	
	2.6	7.18	-0.109	
	3.5	7.26	-0.130	
	4	7.23	-0.109	
	α	4.57	-0.093	
	βu	3.01)	+0.019)	
	βD	3.14)	-0.083)	
Phe(7)	NH	8.16	-0.068	
	2.6	7.23	-0.059	
	3.5	7.29	-0.100	
	4	7.16	-0.179	
	α	4.01	-0.174	
	β	1.94	-0.190	
Val(8)	γu	0.76)	-0.182)	
	γD	0.84)	-0.129)	
	NH	7.69	-0.746	4.20
	α	4.53	-0.074	
	βu	2.82)	-0.057)	
	βD	3.07)	-0.102)	
Tyr(9)	NH	7.97	-0.213	6.30
	2.6	7.07	-0.079	
	3.5	6.67	-0.187	
	α	4.29	-0.068	
	βu	1.78)	+0.033)	
	βD	1.89)	+0.020)	
Lys(10)	γ	1.42	-0.051	
	δ	1.64	-0.068	
	ε	2.88	-0.143	
	NH	8.02	-0.388	5.20

TABLE 6.2

Residue	Coupling constant (Hertz)	Rotational Angle, Degrees
Lys (10)	J(NH-Cα) = 7.56.	θ = 13°, 149°;
	corrected = 8.26	ϕ = 47°, 73°, -89°, -151°
Tyr (9)	J(NH-Cα) = 7.88	θ = 6°, 151°;
	corrected = 8.59	ϕ = 54°, 66°, -91° -149°
Val (8)	J(NH-Cα) = 8.05,	θ = 152°,
	corrected = 8.77	ϕ = 92°, -148°
Phe (7)	J(NH-Cα) = 6.89	θ = 22°, 144°
	corrected = 7.50	ϕ = 38°, 82°, -84° -156°
Phe (6)	J(NH-Cα) = 7.39	θ = 16°, 148°;
	corrected = 8.06	ϕ = 44°, 76°, -88°, -152°
His (5)	J(NH-Cα) = 6.70	θ = 24°, 143°;
	corrected = 7.30	ϕ = 36°, 84°, -83° -157°

Figure 6.1 1-D spectrum of RIP in methanol (CD_3OH, 4mg in 0.6mls).

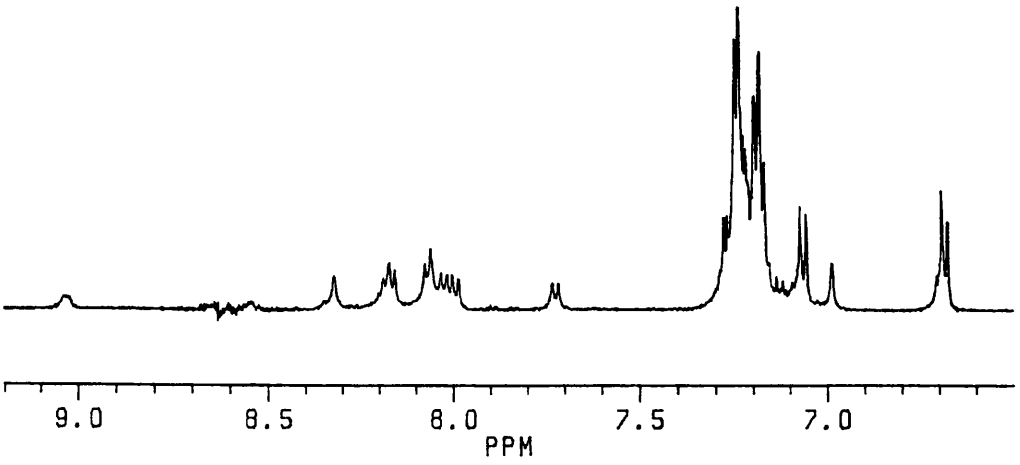
9.0
8.5
8.0
7.5
7.0
PPM

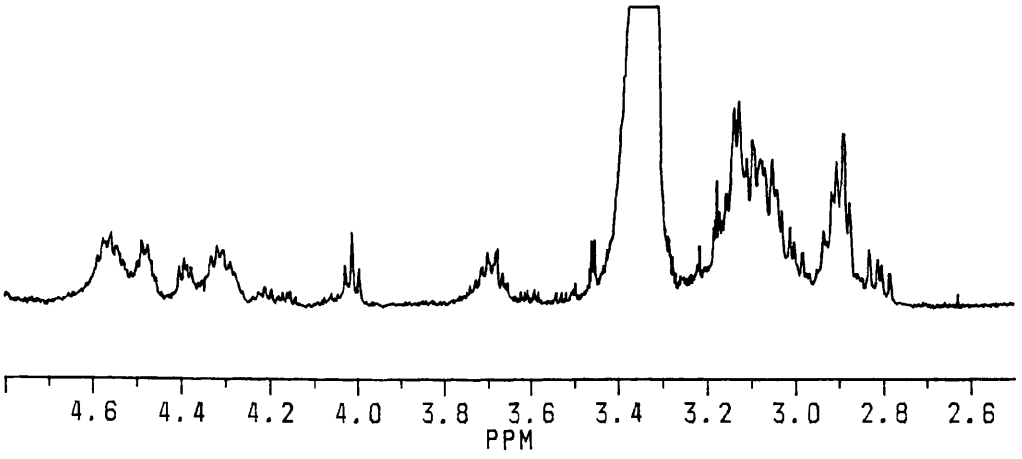
4.6
4.4
4.2
4.0
3.8
3.6
3.4
3.2
3.0
2.8
2.6
PPM

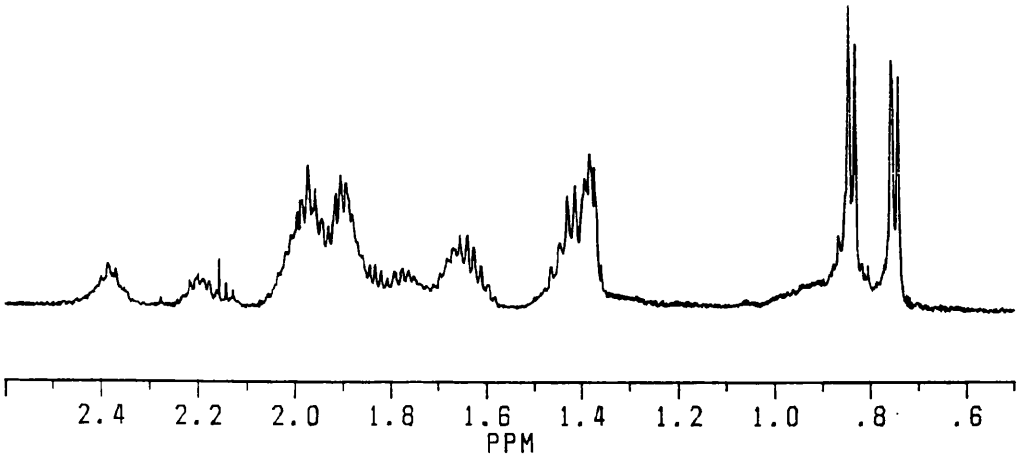
2.4
2.2
2.0
1.8
1.6
1.4
1.2
1.0
.8
.6
PPM

Figure 6.2 Cross sections through amide or alpha protons in the ROESY experiment, giving connectivities through the spin system of each amino acid residue.

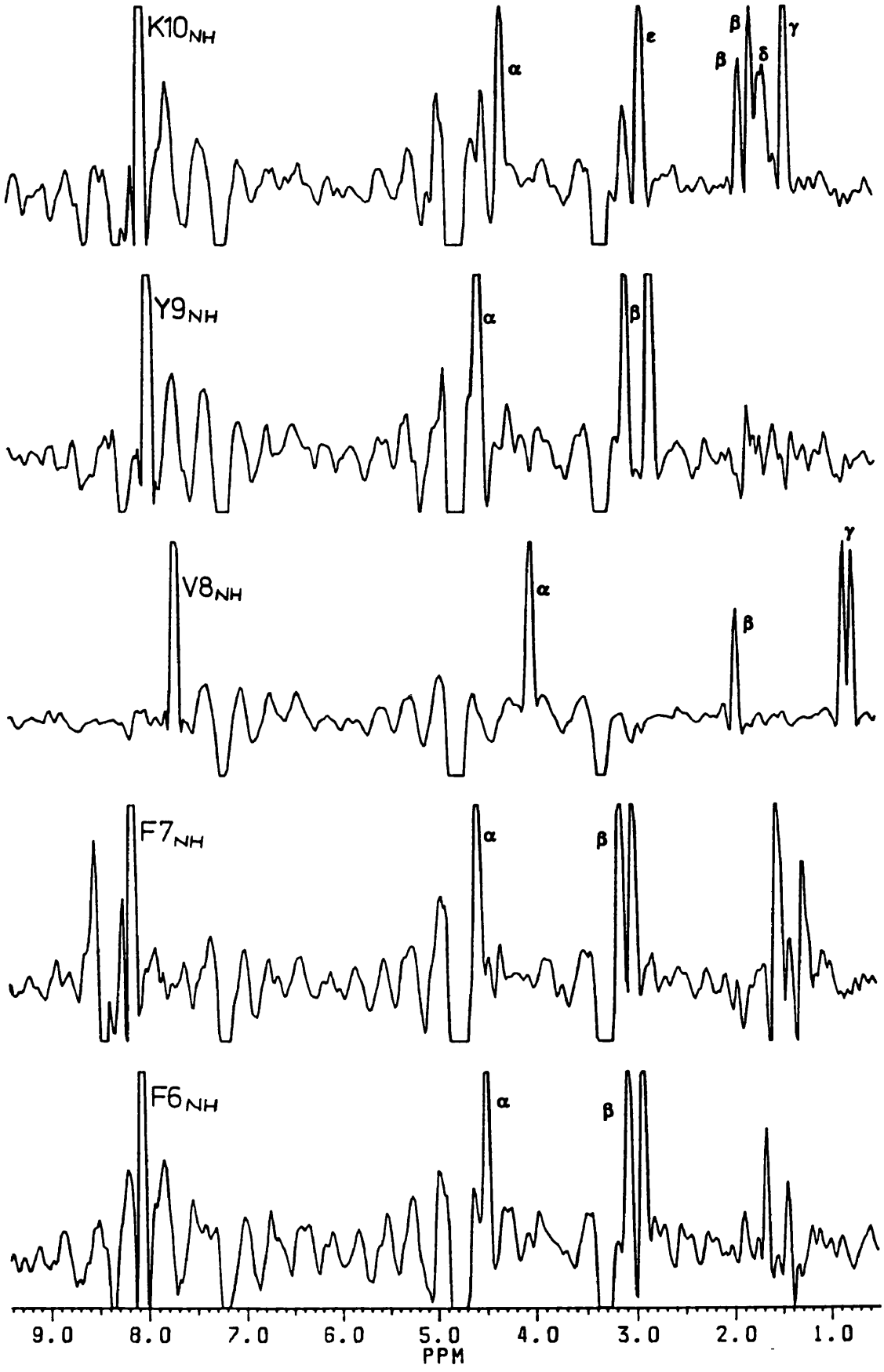
K10NH
α
ε
β
β
δ
γ
Y9NH
α
β
V8NH
α
β
γ
F7NH
α
β
F6NH
α
β
9.0
8.0
7.0
6.0
5.0
4.0
3.0
2.0
1.0
PPM

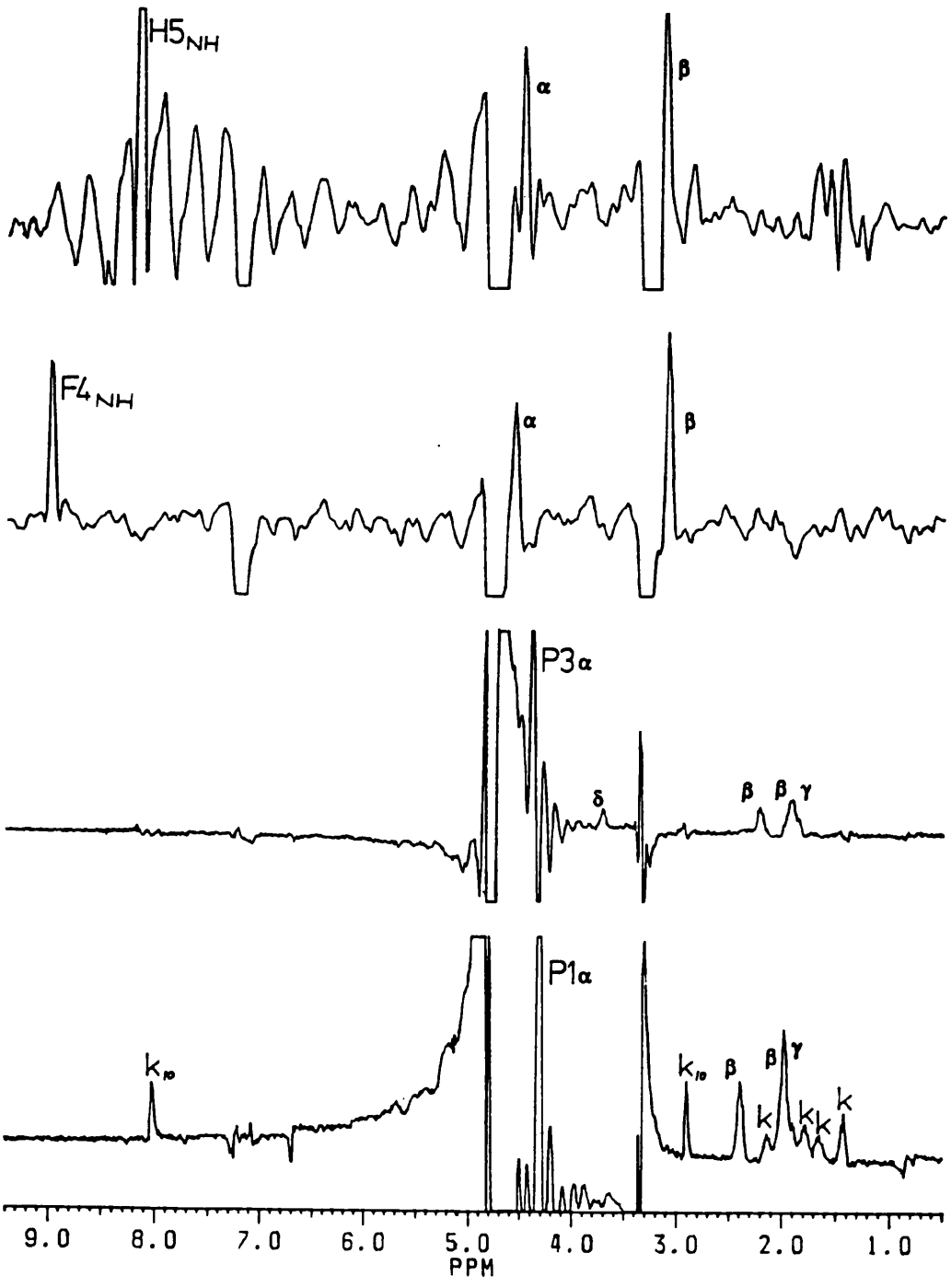
H5NH
α
β
F4NH
α
β
P3α
δ
β
β
γ
P1α
k10
k10
β
β
γ
k
k
k
k
9.0
8.0
7.0
6.0
5.0
4.0
3.0
2.0
1.0
PPM

Figure 6.3 Contour plot of the ROESY experiment, showing NH to α connectivities between adjacent amino acid residues.

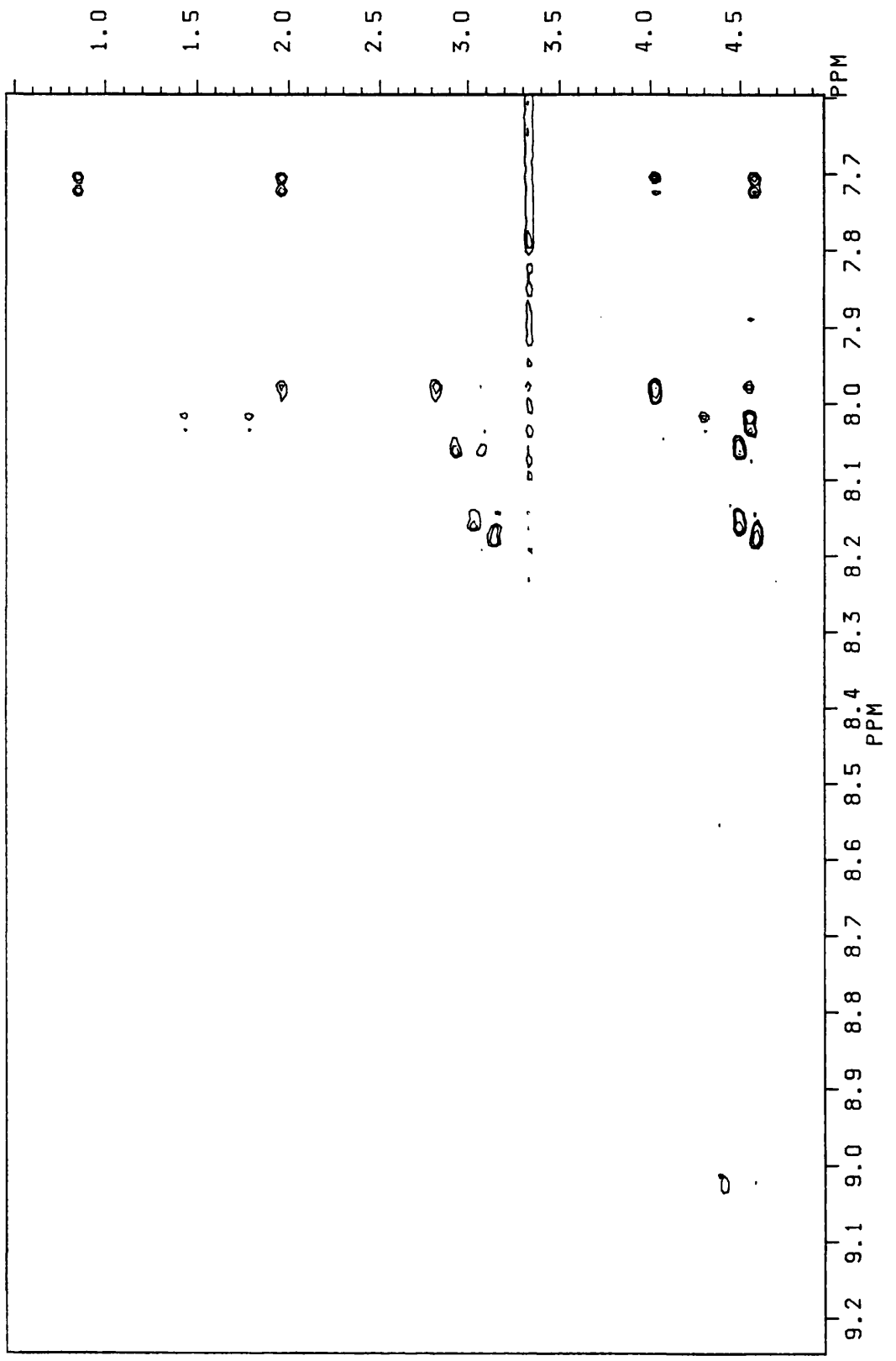
1.0
1.5
2.0
2.5
3.0
3.5
4.0
4.5
PPM
7.7
7.8
7.9
8.0
8.1
8.2
8.3
8.4
8.5
8.6
8.7
8.8
8.9
9.0
9.1
9.2
PPM

Figure 6.4 ROESY cross sections through amide or alpha protons, showing connectivities between adjacent residues.

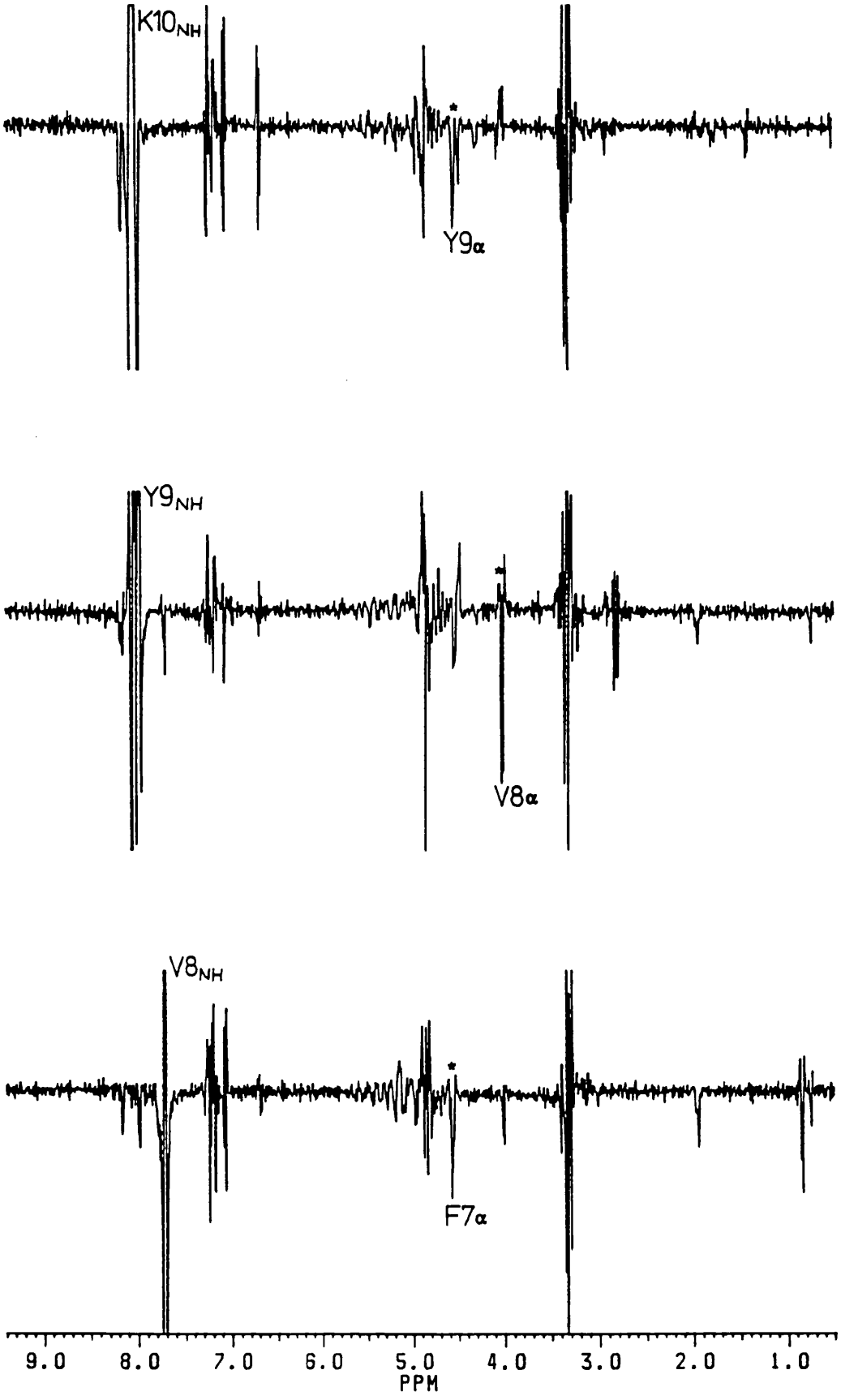
K10NH
Y9α
Y9NH
V8α
V8NH
F7α
9.0
8.0
7.0
6.0
5.0
4.0
3.0
2.0
1.0
PPM

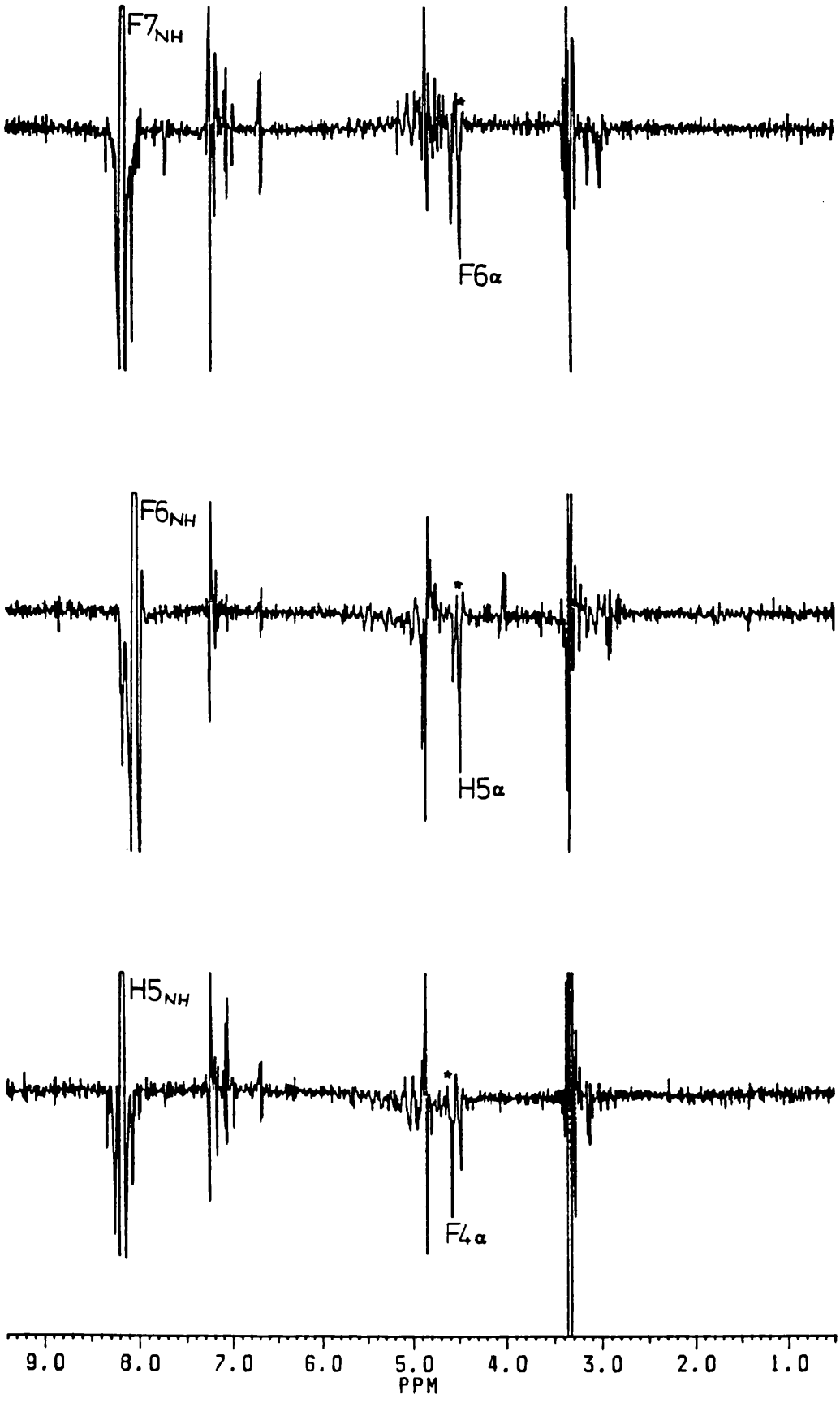
F7NH
F6α
F6NH
H5α
H5NH
F4α
9.0
8.0
7.0
6.0
5.0
4.0
3.0
2.0
1.0
PPM

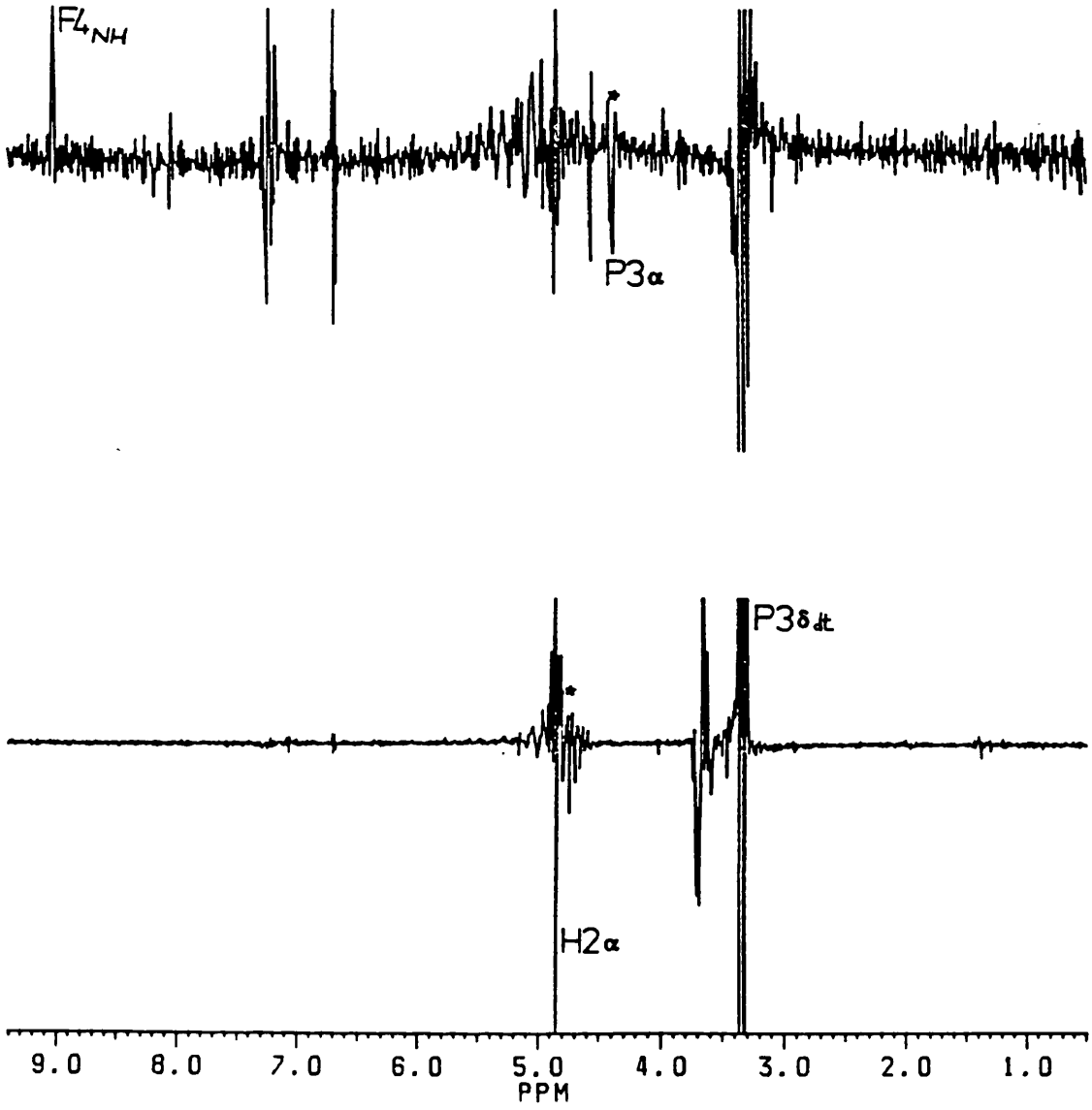
F4NH
P3α
P3δdt
H2α
9.0
8.0
7.0
6.0
5.0
4.0
3.0
2.0
1.0
PPM

Figure 6.5 Contour plot of the ROESY experiment showing aromatic to β proton couplings, allowing sequence specific assignments to be made, for Phe 4,6 and 7, and Tyr (9).

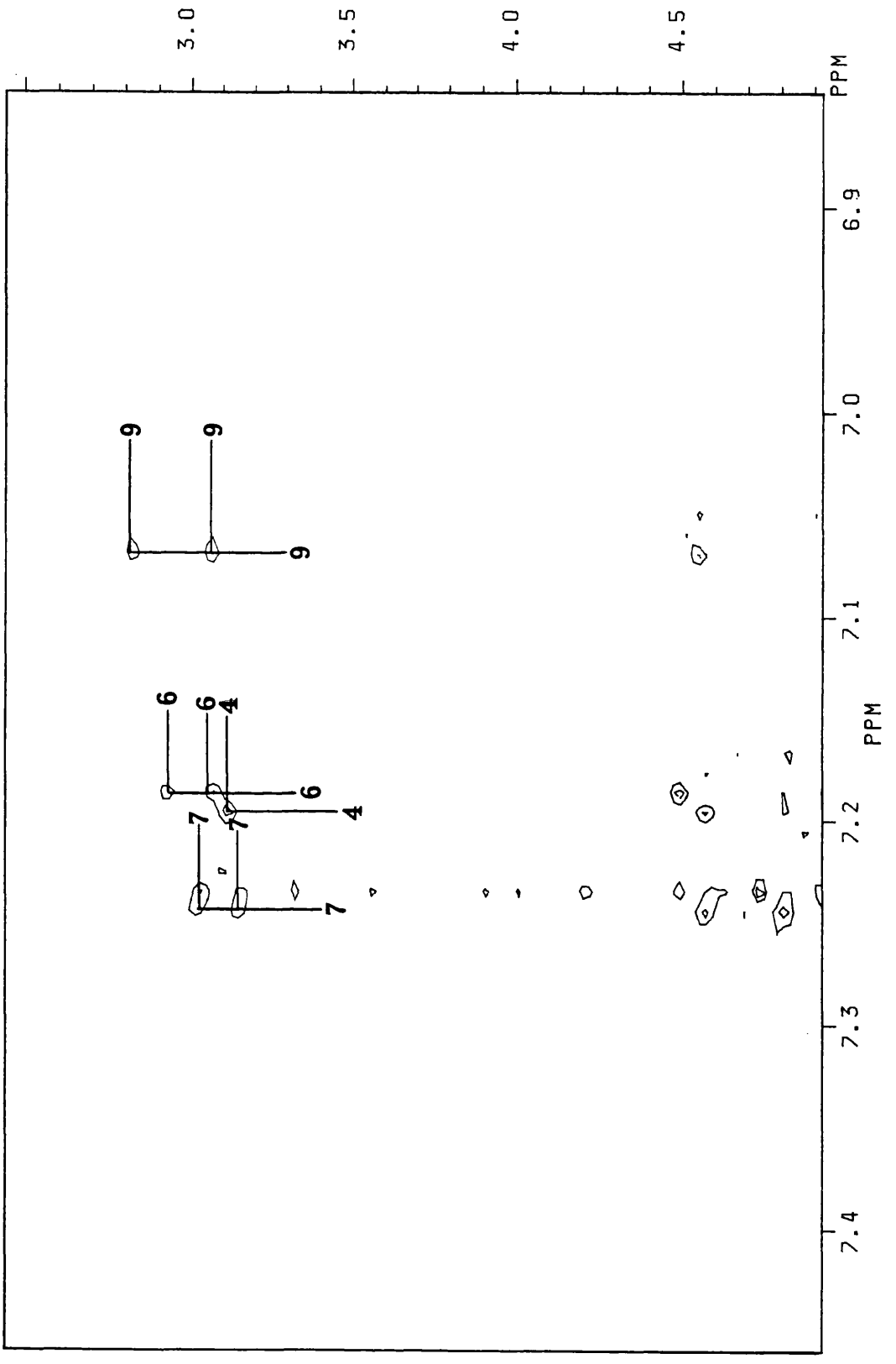
3.0
3.5
4.0
4.5
PPM
6.9
7.0
7.1
7.2
7.3
7.4
PPM
9
9
9
6
6
4
6
7
7
7

Figure 6.6 Contour plot of the aromatic region in the long-range COSY experiment, connecting the 2,6 protons to the 3,5 and 4 protons, for each of the three Phe residues.

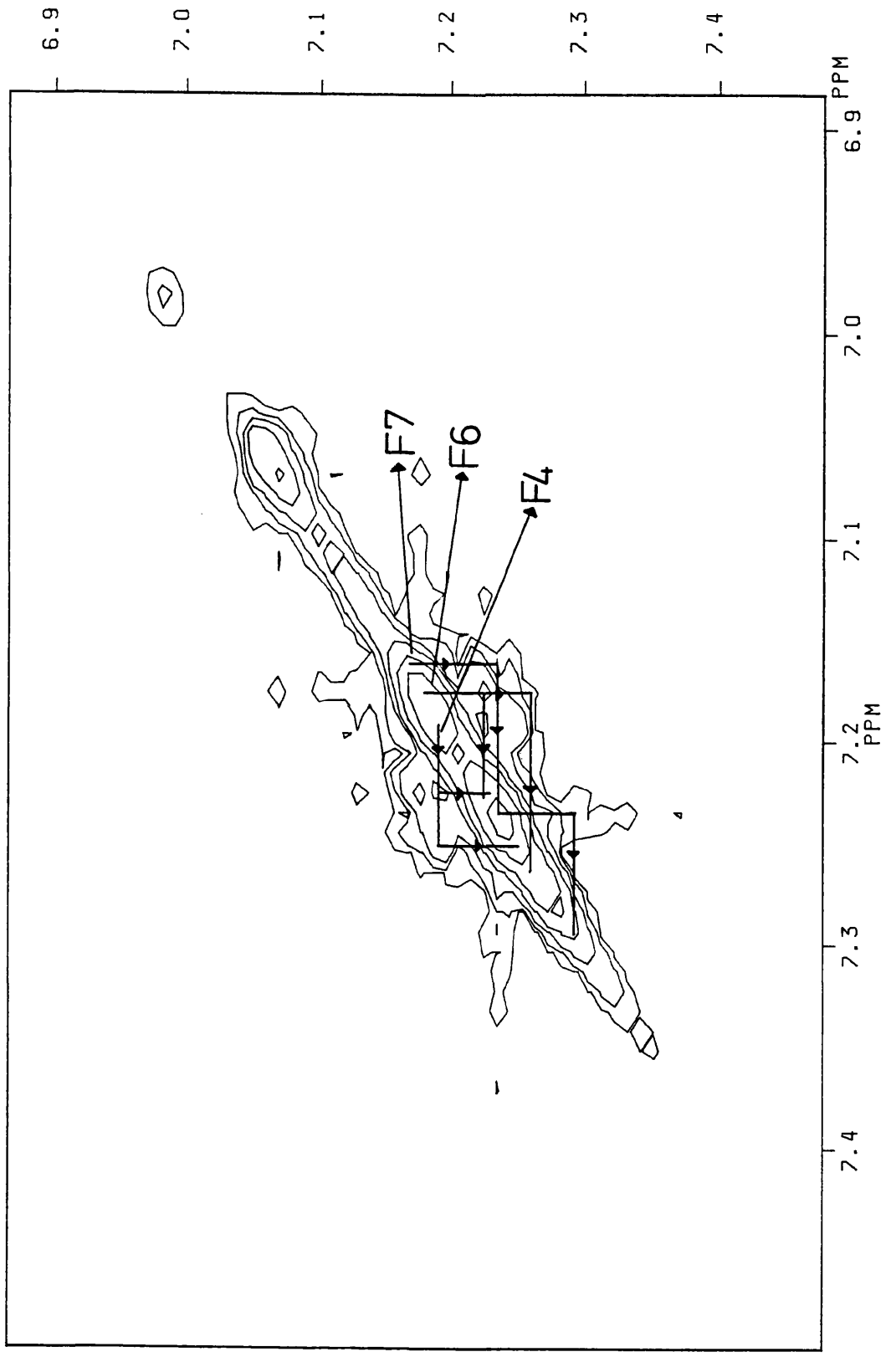
6.9
7.0
7.1
7.2
7.3
7.4
PPM
F7
F6
F4

Figure 6.7 Cross sections through the His imidazole 4-ring protons, showing connectivities to their 2-ring protons, in the long-range COSY experiment.

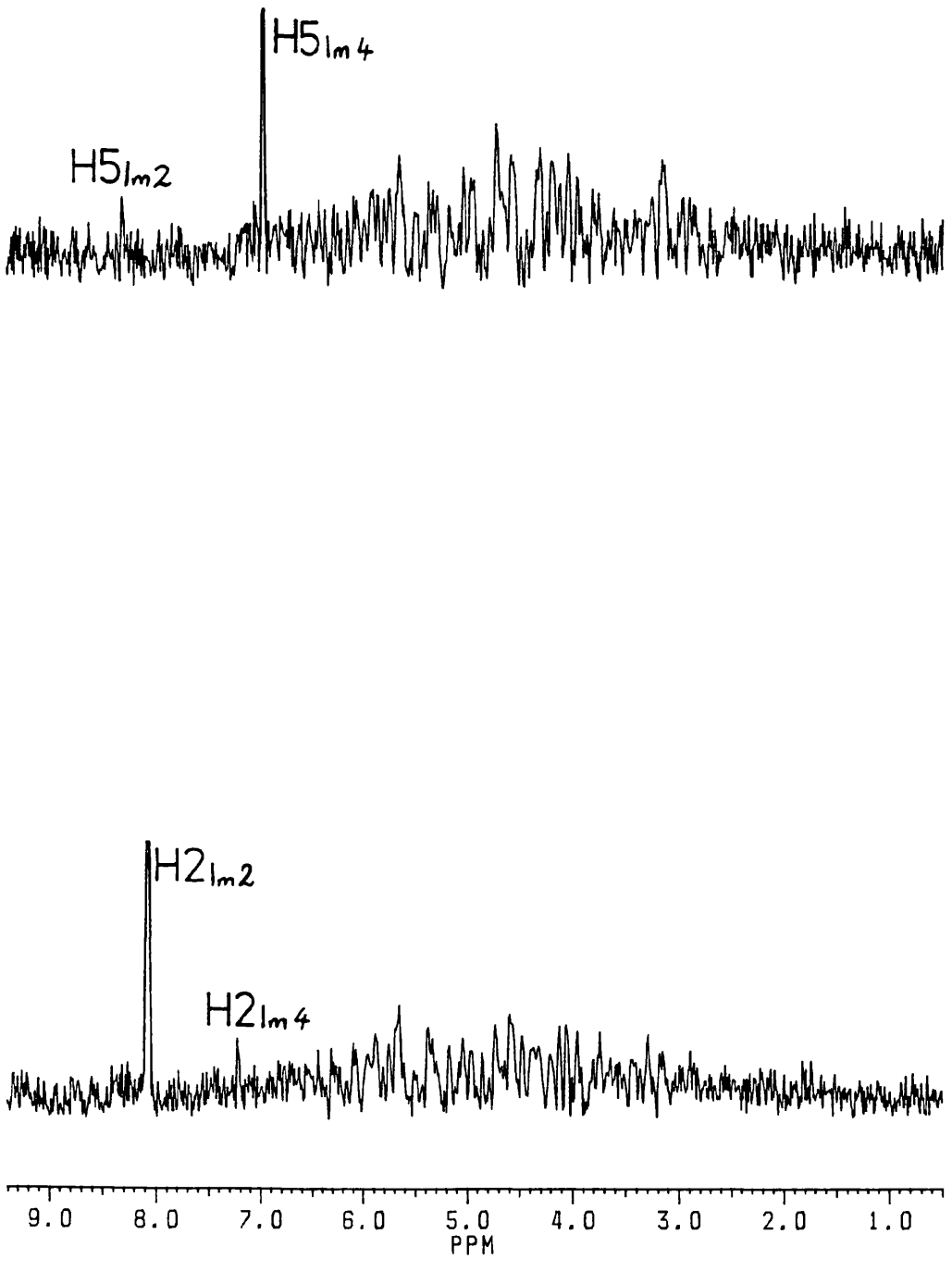
H5Im4
H5Im2
H2Im2
H2Im4
9.0
8.0
7.0
6.0
5.0
4.0
3.0
2.0
1.0
PPM

Figure 6.8 Cross sections through the ROSEY experiment. The intramolecular ROEs found were consistent with the conformation adopted by RIP in H_2O, with a trans Pro (3) peptide bond.

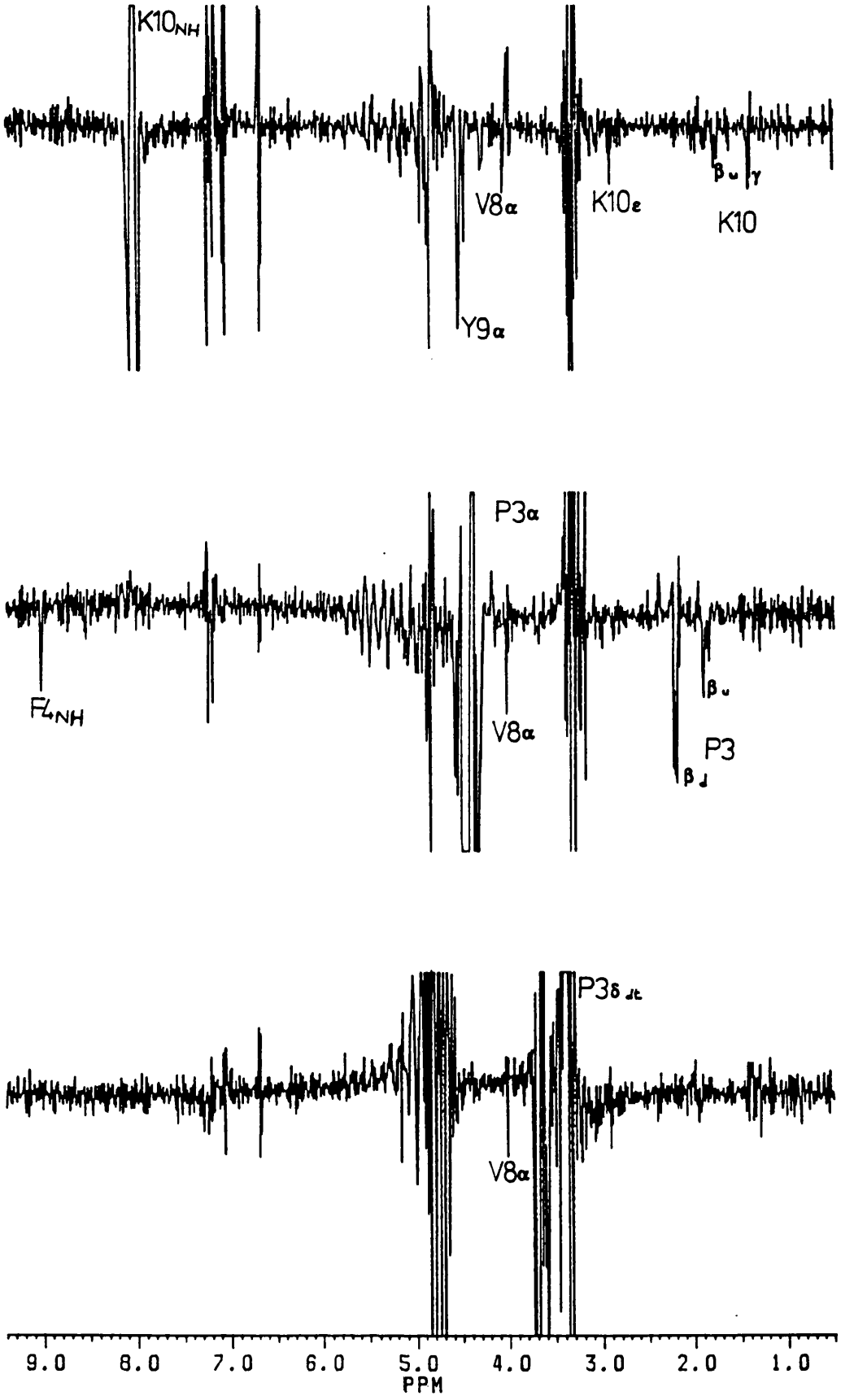
K10NH
V8α
K10ε
βu γ
K10
Y9α
P3α
FLNH
βu
V8α
P3
βd
P3δ dt
V8α
9.0
8.0
7.0
6.0
5.0
4.0
3.0
2.0
1.0
PPM

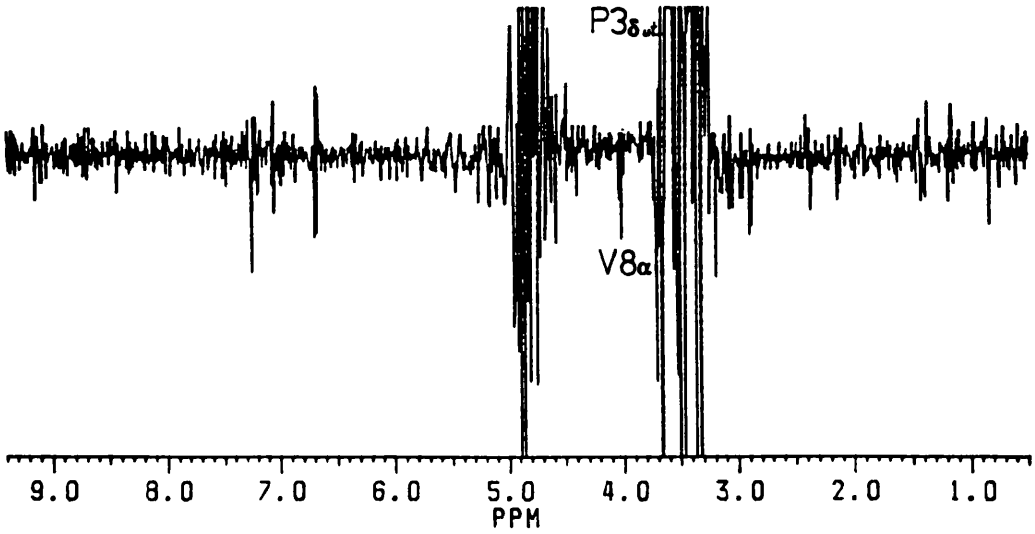
P3δ
V8α
9.0
8.0
7.0
6.0
5.0
4.0
3.0
2.0
1.0
PPM

Figure 6.9 Cross sections through ROESY experiment. These ROEs were not consistent with the ROEs found in H_2O, and resulted from state B (with a cis Pro(3) peptide bond). The NH_i - NH_{i+1} ROEs seen here were hypothesised to be from state C (See Chapter 8).

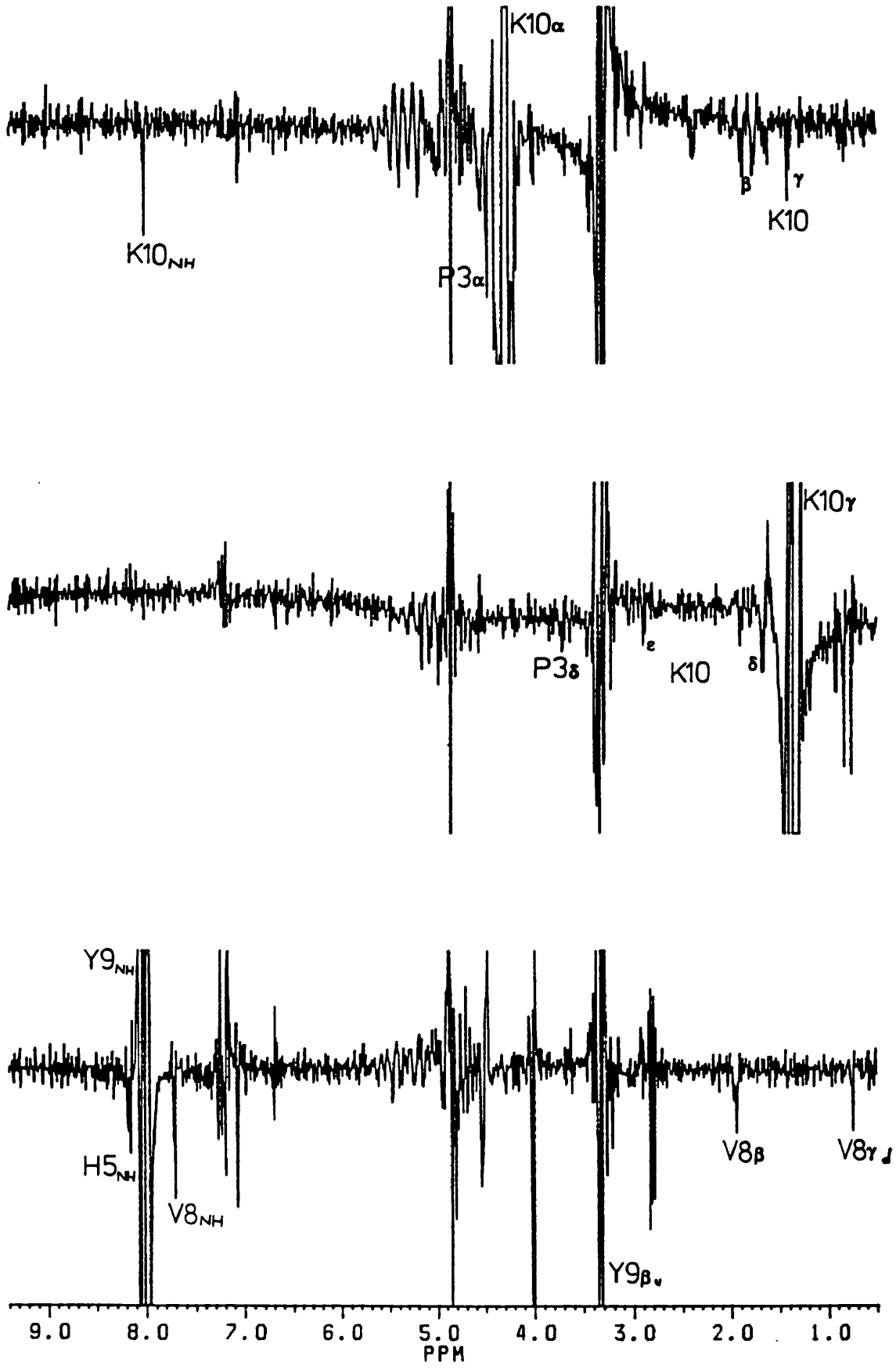
K10α
K10NH
P3α
β
γ
K10
K10γ
P3δ
ε
K10
δ
Y9NH
H5NH
V8NH
Y9βu
V8β
V8γ
9.0
8.0
7.0
6.0
5.0
4.0
3.0
2.0
1.0
PPM

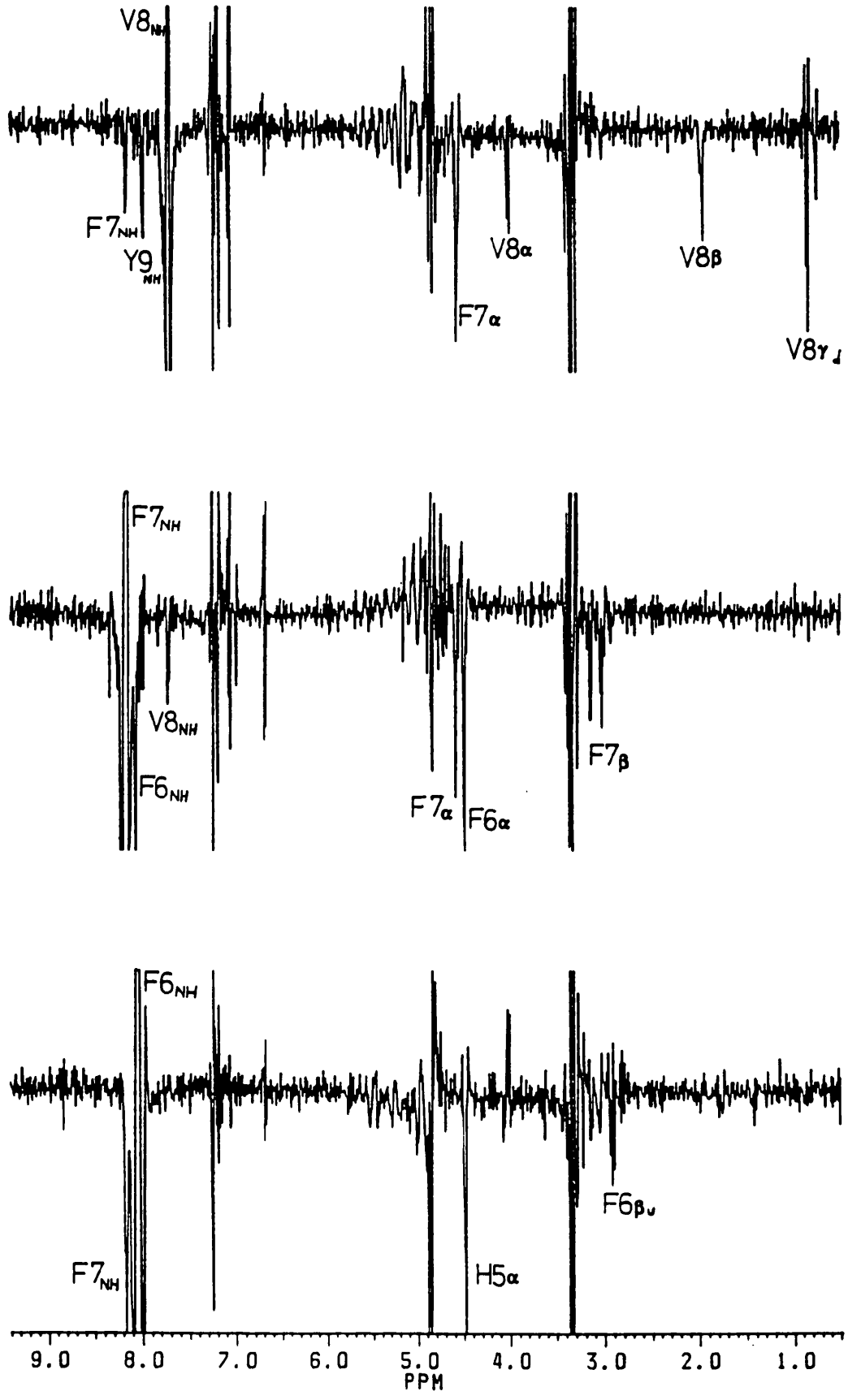
V8NH
F7NH
Y9NH
V8α
V8β
F7α
V8γ
F7NH
V8NH
F6NH
F7α
F6α
F7β
F6NH
F7NH
H5α
F6β
9.0
8.0
7.0
6.0
5.0
4.0
3.0
2.0
1.0
PPM

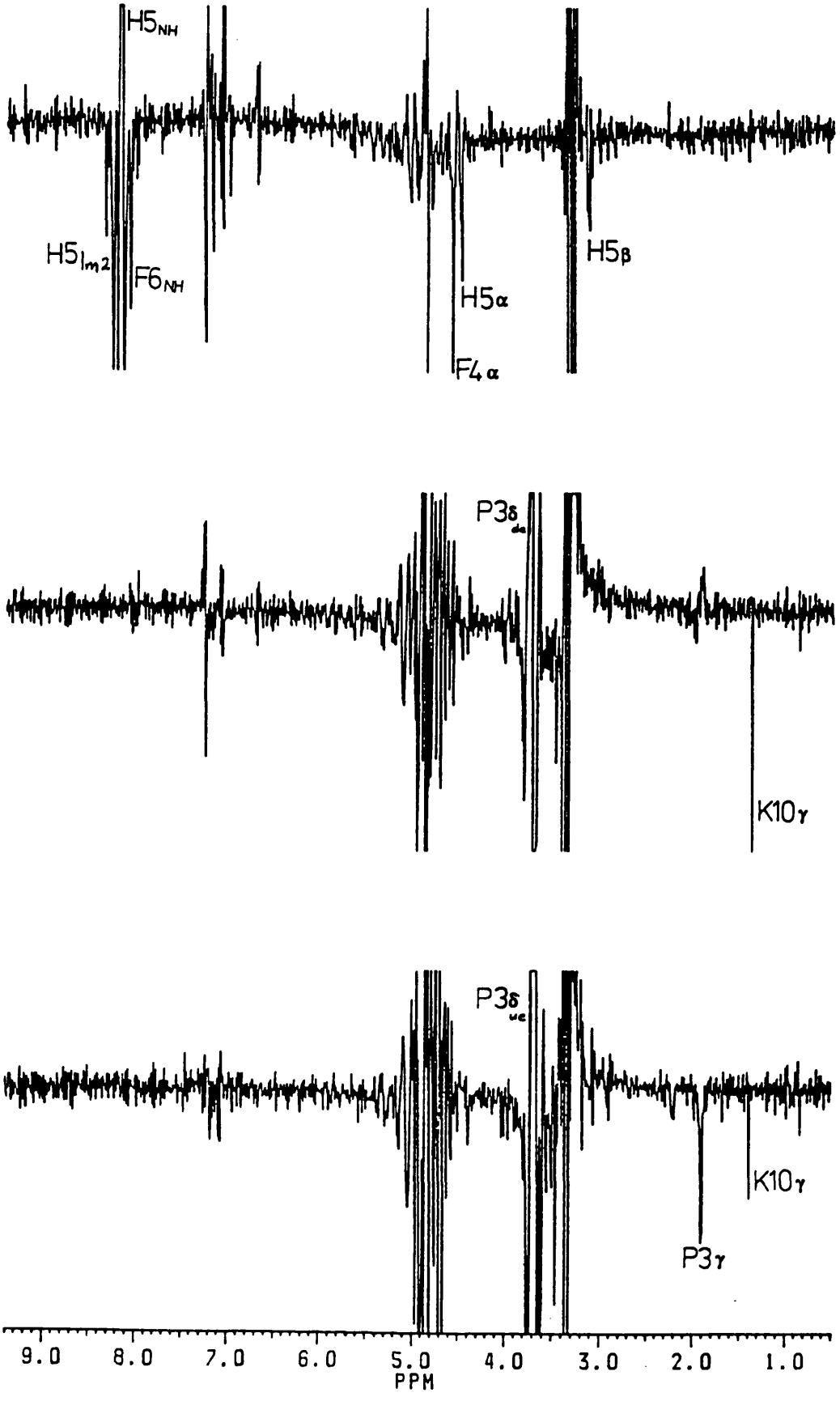
H5NH
H5Im2
F6NH
H5α
F4α
H5β
P3δde
K10γ
P3δue
K10γ
P3γ
9.0
8.0
7.0
6.0
5.0
4.0
3.0
2.0
1.0
PPM

Figure 6.10 Long-range COSY contour plot, showing the connectivities found for the four Pro (3) δ proton resonances.

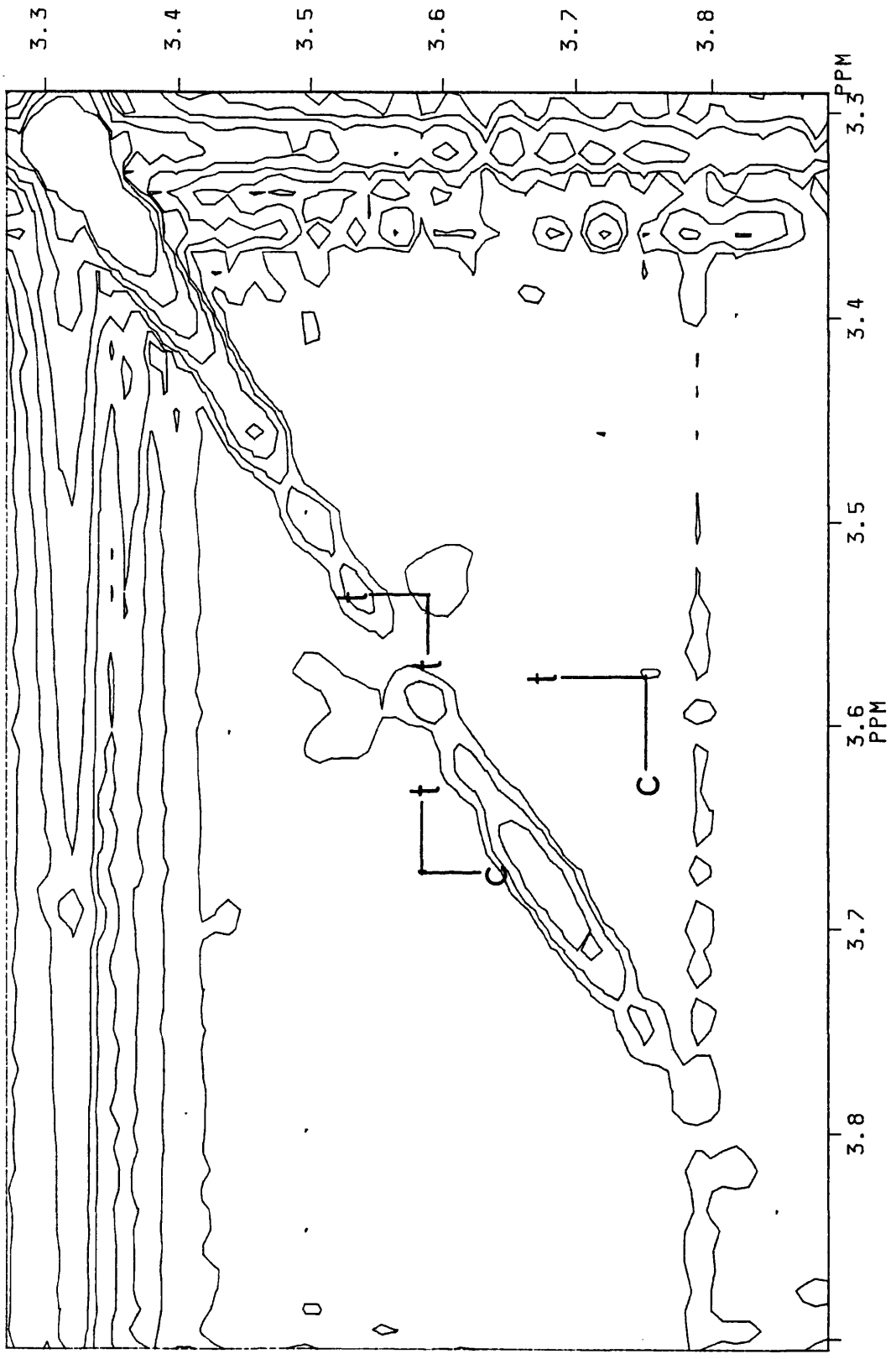
3.3
3.4
3.5
3.6
3.7
3.8
PPM
t
t
t
t
C
C

Figure 6.11 ROESY contour plot of the Pro (3) δ proton region. Indicated are the ROE (negative phase) cross peaks and the (positive phase) chemical exchange cross peaks, which confirmed the existance of isomerisation (cis-trans) at Pro (3).

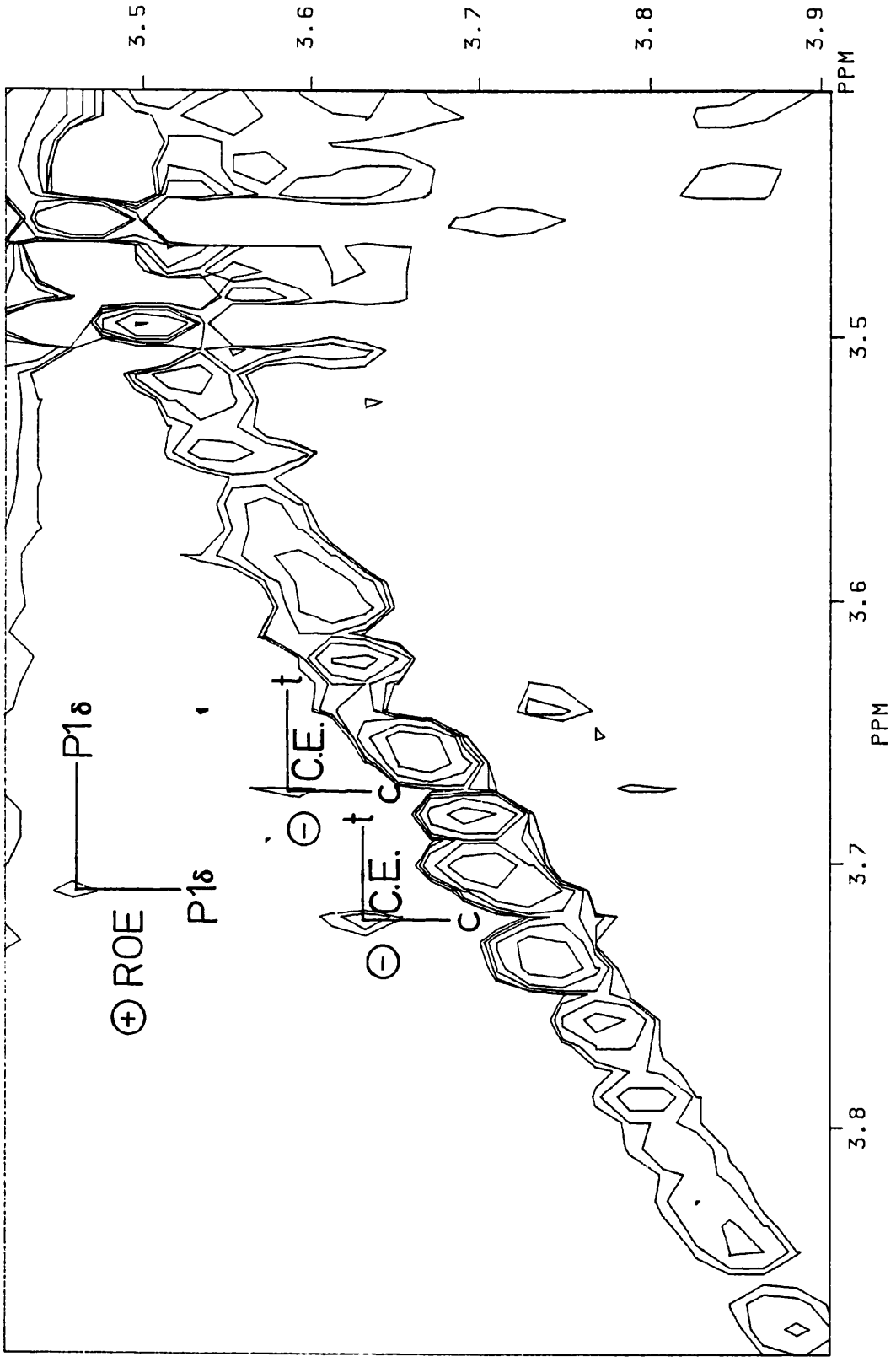
3.5
3.6
3.7
3.8
3.9
PPM
3.5
3.6
3.7
3.8
PPM
P1δ
P1δ
⊕ ROE
⊖ C.E.
t
c
⊖ C.E.
t
c

Figure 6.12 1-D plot of the Pro δ proton region for residues 1 and 3.

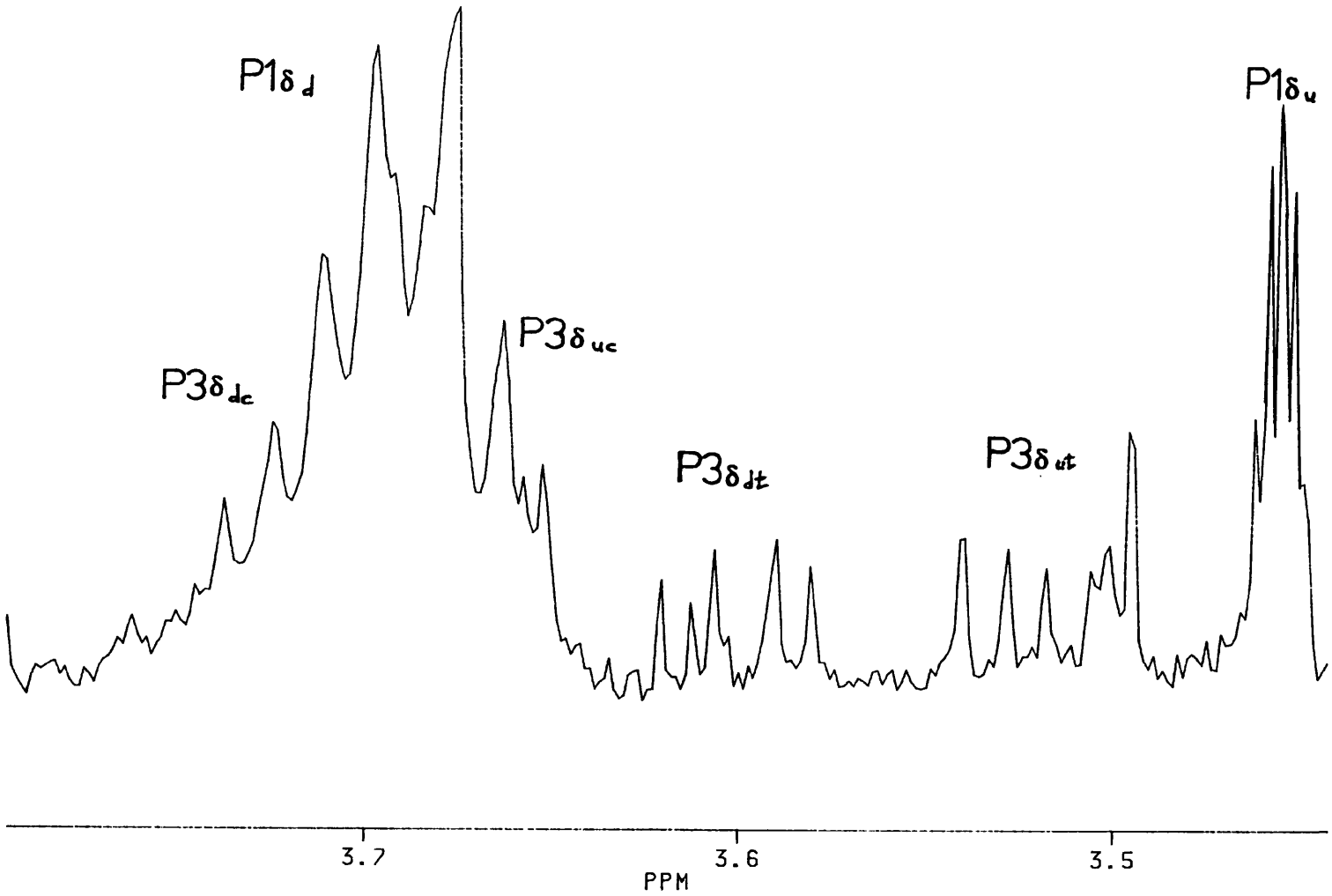
P1δ d
P1δ u
P3δ uc
P3δ dc
P3δ dt
P3δ ut
3.7
3.6
3.5
PPM

Figure 6.13 Plot of the aromatic region spectrum of RIP in methanol/glycerol (9:1) solution, at temperature between + 20°C to -89°C. An aromatic residue showed a large variation with chemical shift (marked *), and may correlate with CD results.

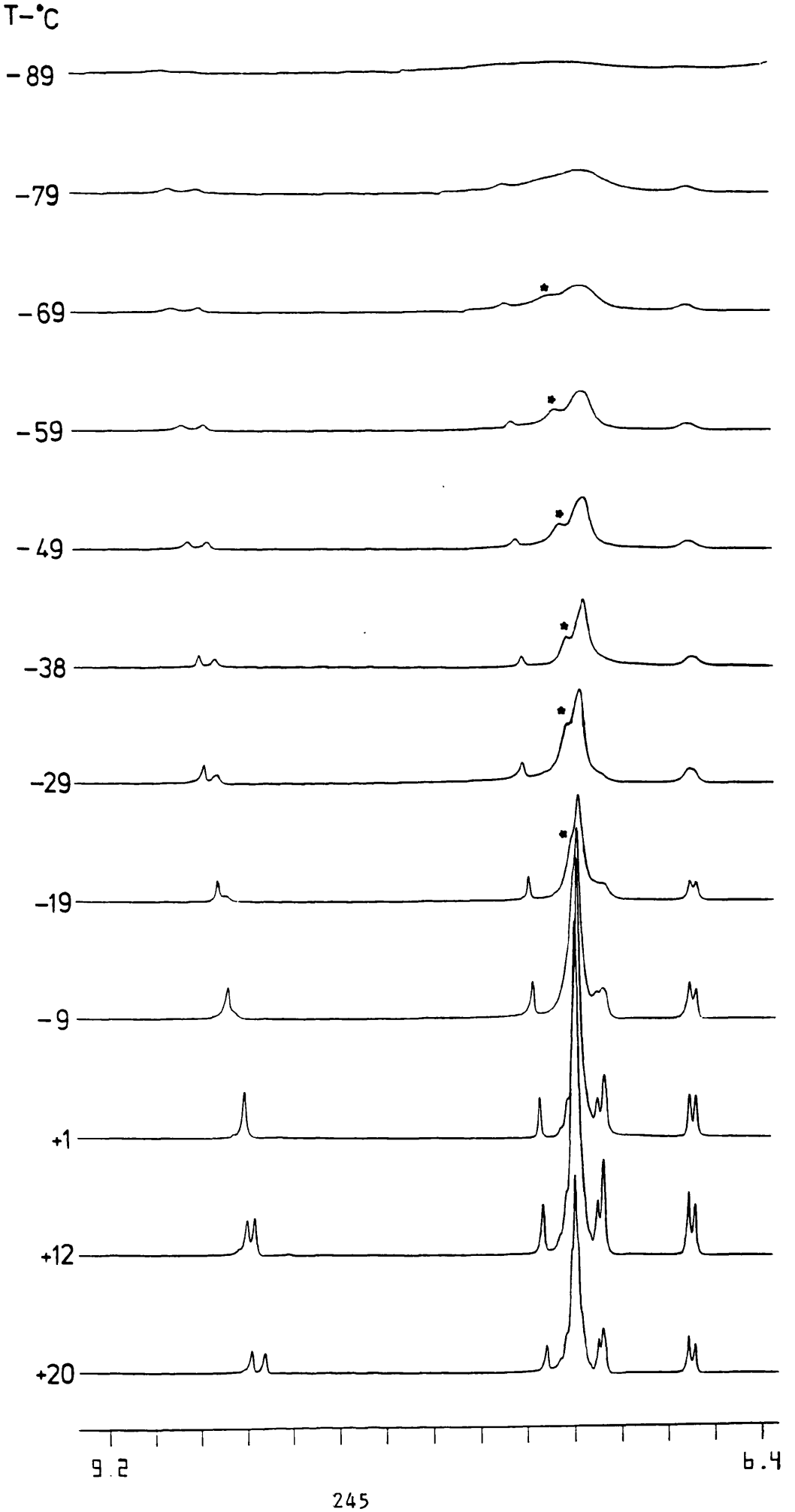
T-°C
-89
-79
-69
-59
-49
-38
-29
-19
-9
+1
+12
+20
9.2
6.4

Figure 6.14 1-D plots, between 5.1ppm and 0.5ppm. of RIP in methanol/glycerol (9:1) solution, at temperatures between +20°C to -89°C.

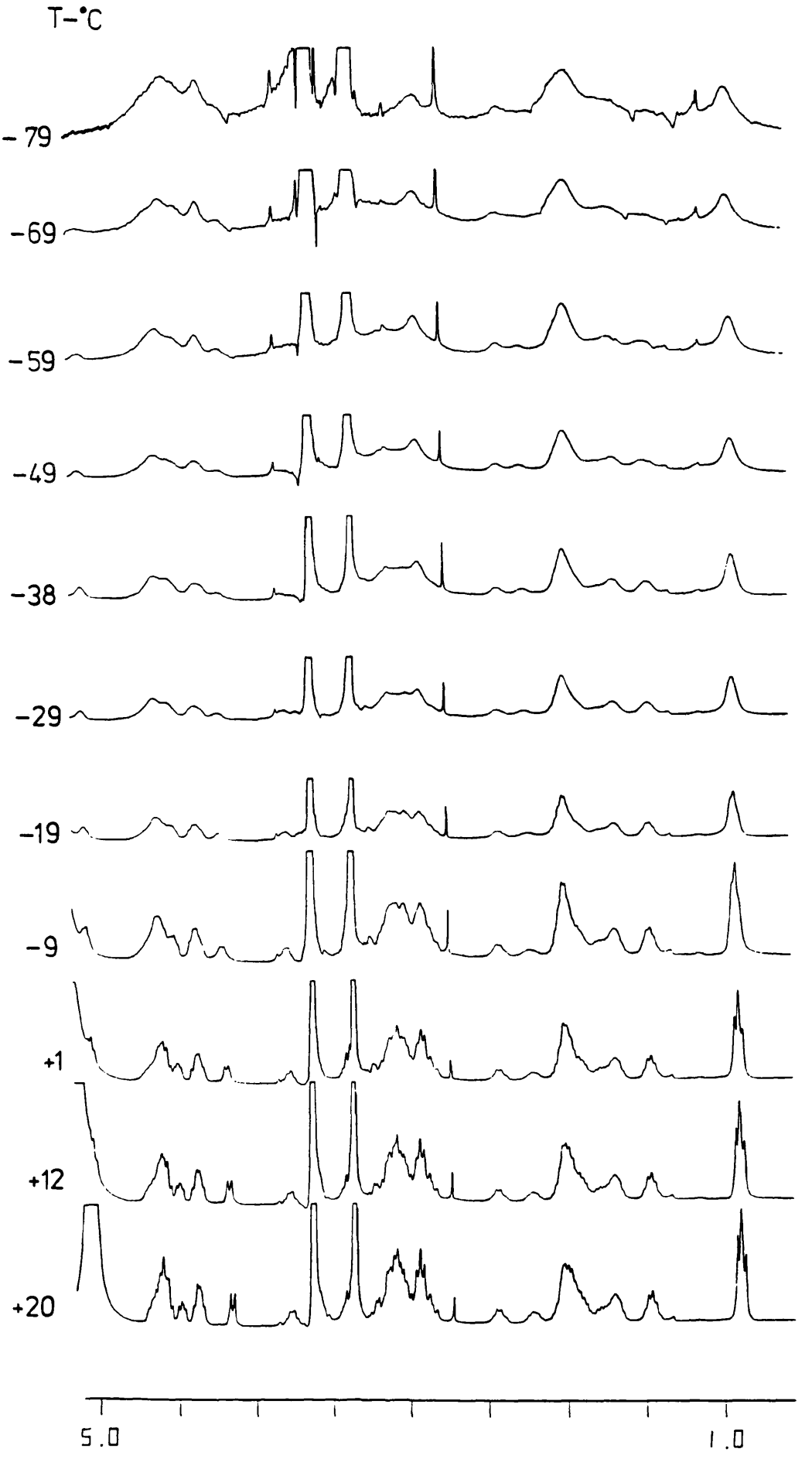
T-°C
-79
-69
-59
-49
-38
-29
-19
-9
+1
+12
+20
5.0
1.0

Figure 6.15 Plot of chemical shift versus temperature for His (2) and His (5) Im2 ring protons.

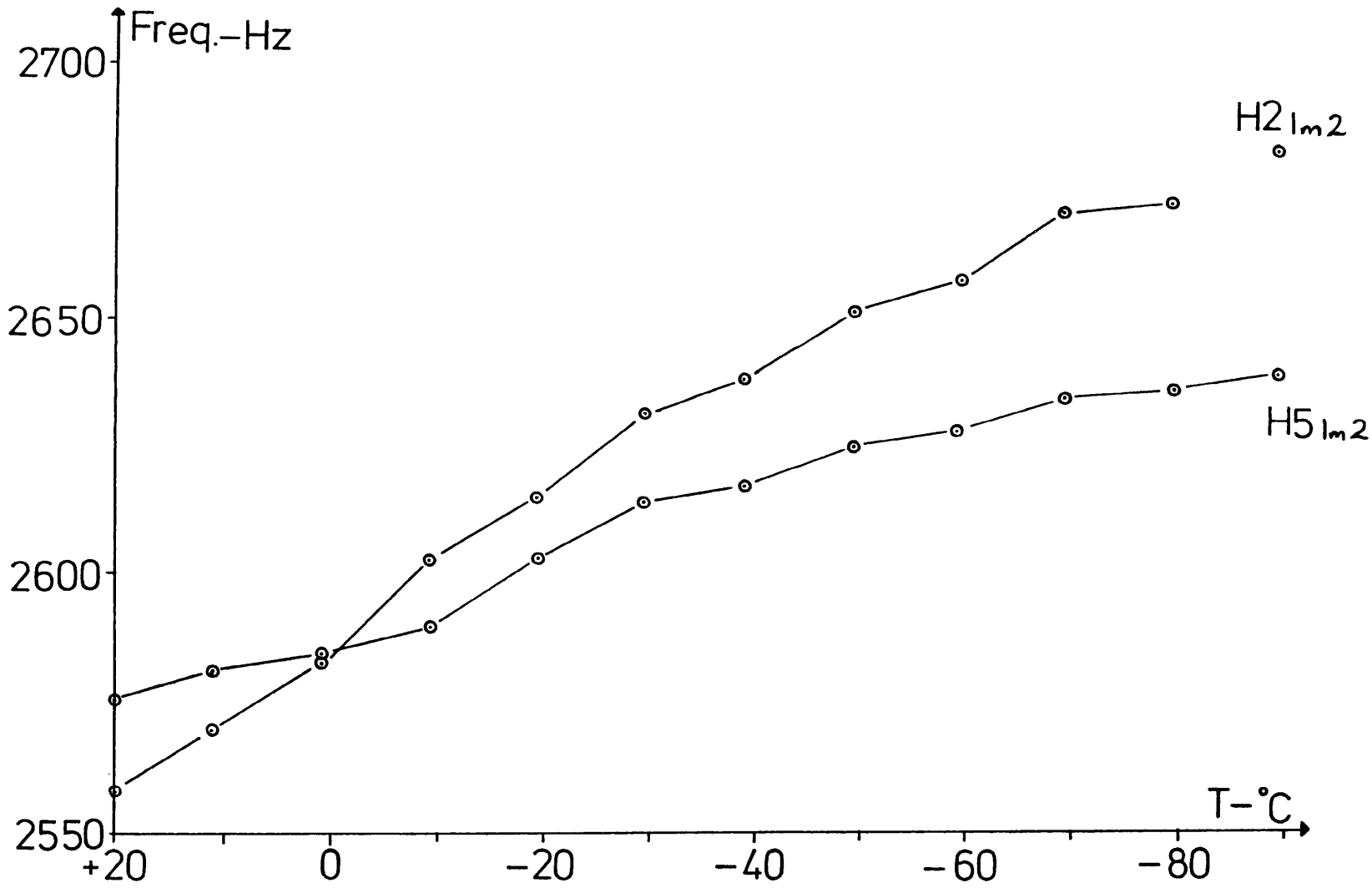
Freq.–Hz
2700
2650
2600
2550
H2 Im2
H5 Im2
T–°C
+20
0
–20
–40
–60
–80

Figure 6.16 Plot of chemical shifts versus temperature for His (2) Im4 and Tyr (9) 3,5 protons.

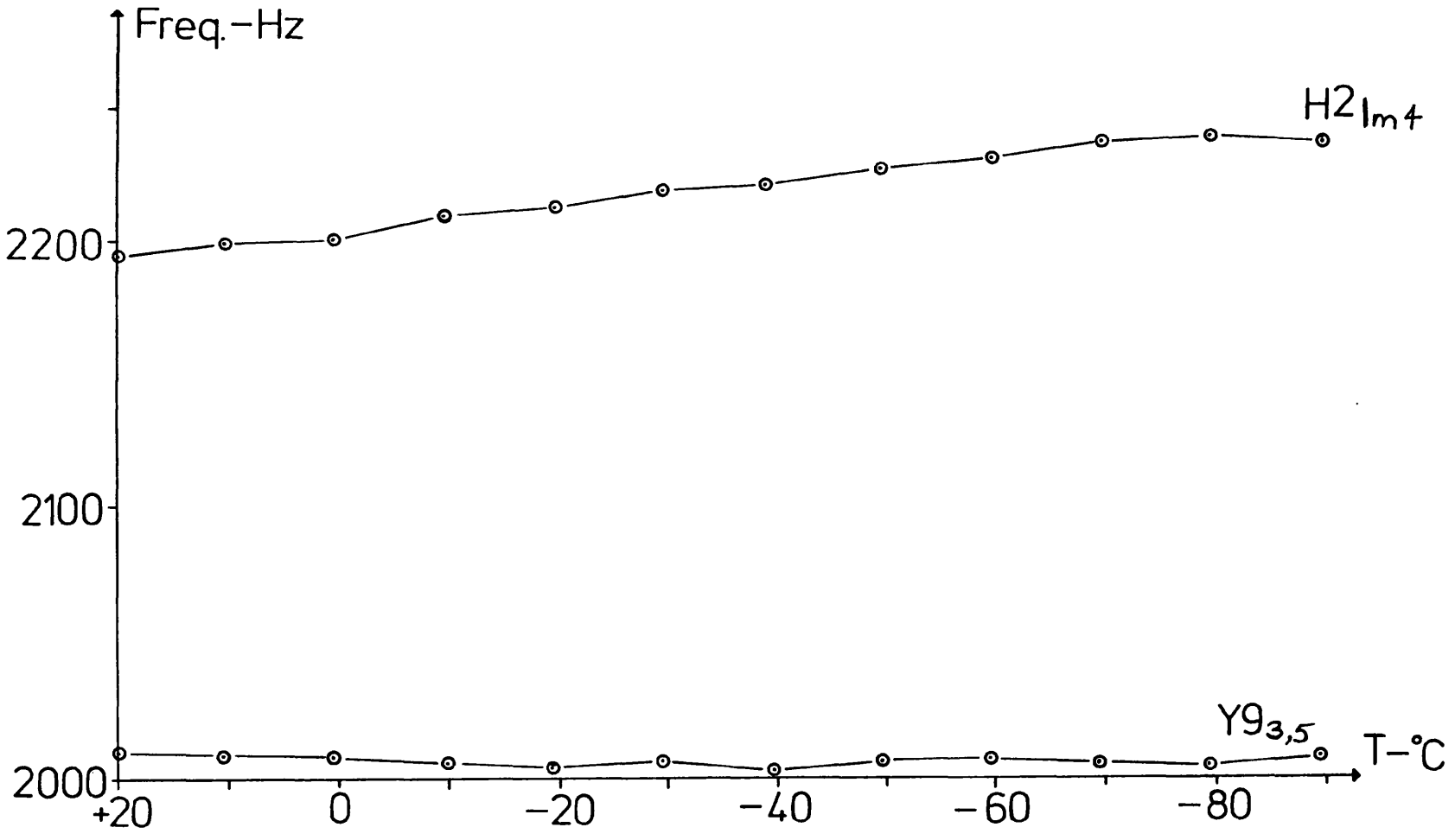
Freq.-Hz
H2 Im 4
2200
2100
Y9 3,5
T-°C
2000
+20
0
-20
-40
-60
-80

Figure 6.17 Plot of chemical shift versus temperature for Pro (1) β, Lys (10) δ and Pro (3) β protons.

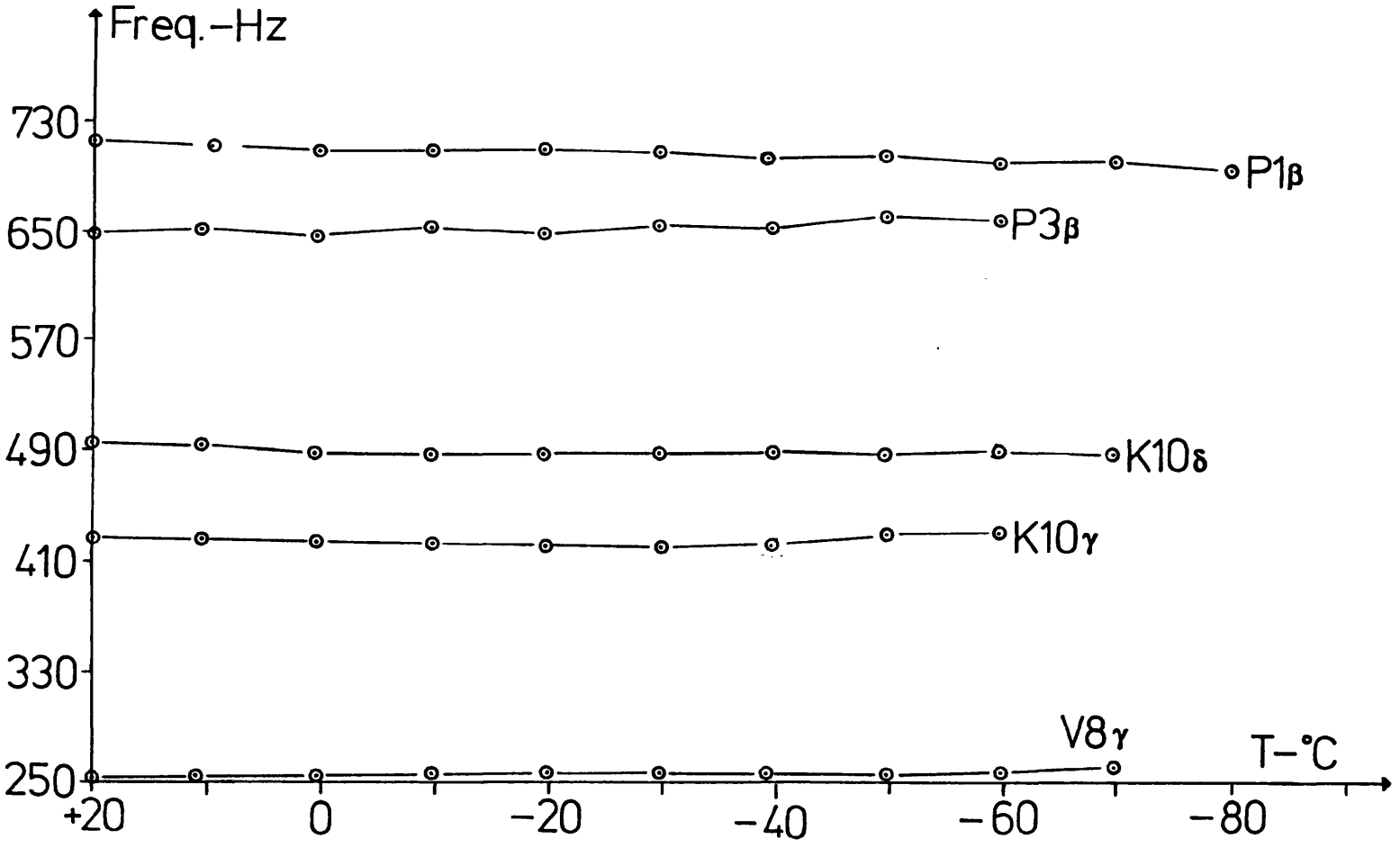
Freq.-Hz
730
650
570
490
410
330
250
P1β
P3β
K10δ
K10γ
V8γ
T-°C
+20
0
-20
-40
-60
-80

Figure 6.18 Plot of chemical shift versus temperature for His (2), Pro (3) and Val (8) alpha protons.

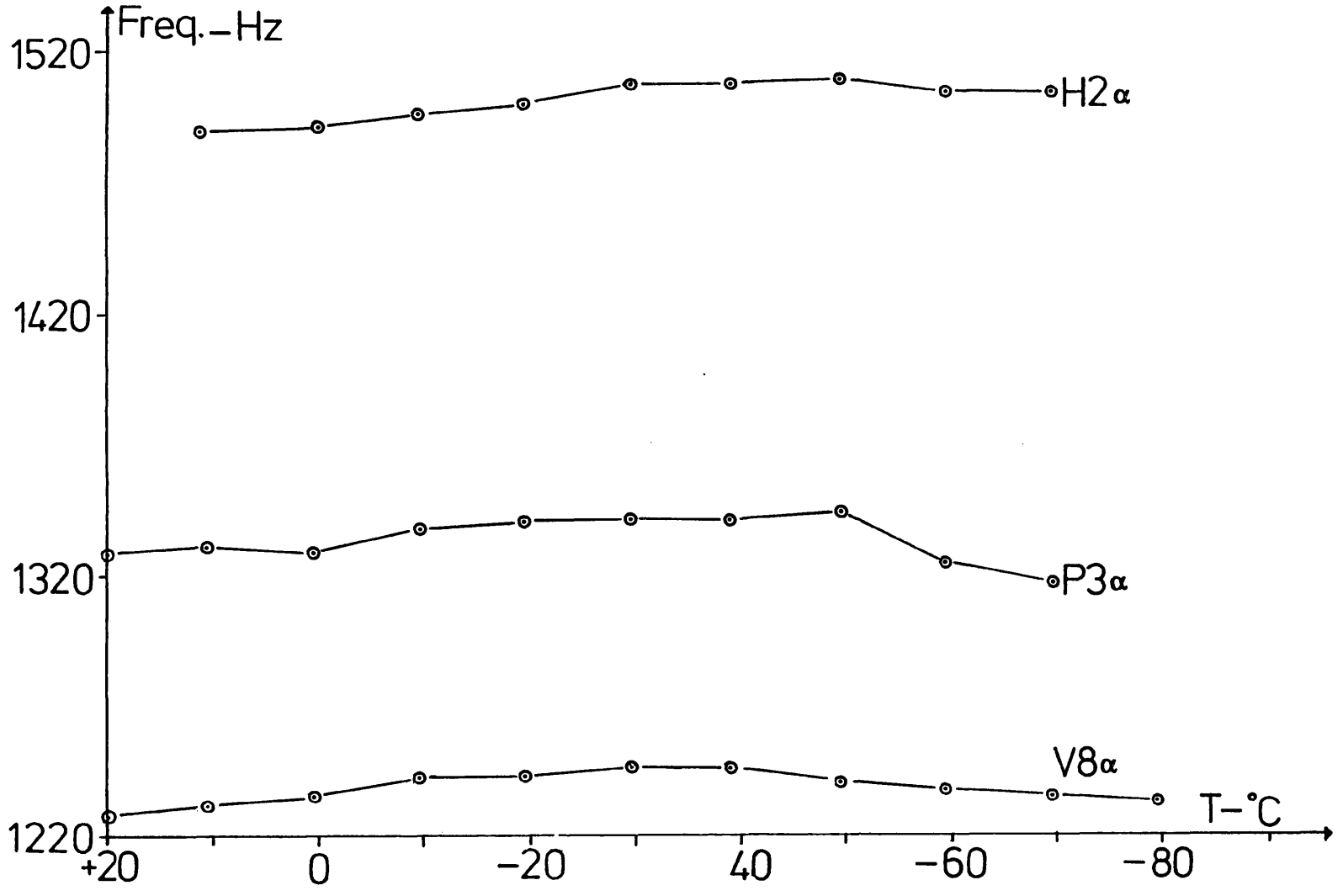
Freq.–Hz
1520
1420
1320
1220
H2α
P3α
V8α
T–°C
+20
0
–20
40
–60
–80

Chapter 7

7.1 Construction of An Approximate Inhibitor Structure

An approximate 3-D structure of RIP in solution was constructed using molecular modelling, based on the ROE distance constraints in H_2O/D_2O, with a trans amide bond. This was the most abundant conformation which existed and so the constraints used arose from one conformation or closely related set of conformers; the model obtained was therefore felt to be an accurate reflection of the structure of RIP with a trans Pro(3) amide bond.

The linear sequence was generated, based on the standard L-amino acid distances and dihedral angles. The structure thus obtained was a completely extended peptide chain with the correct sequence; the structure was then interactively moved to fit the ^1H NMR distances, by rotating about the ϕ_i ψ_i angles in turn. The ϕ_i angles had been calculated from $J_{NHi-CHi}$ coupling constants and were set to the value which best fitted the appropriate distance(s) and which minimised 'bad' contacts. Once the backbone had been altered

in this manner, side chains were rotated to fit both the distance constraints and coupling constant data (whether gauche or trans rotamers were more populated).

The structure of RIP was thus constructed by this interactive modelling procedure. The dihedral angles and the interproton distances of $\leq$ 7.0Å were calculated and inspected; these were found to be consistent with all of the available CD and NMR data.

7.2 Energy Minimisation of RIP Model.

The model of RIP constructed in section 7.1 contained a number of interactions which would have been energetically unfavourable; minimisation of this structure was carried out with no energy constraints added, so that distances were not constrained to their NMR values. These unfavourable elements could be removed while allowing RIP access a small part of the conformation space.

The resulting structure (Figure 7.1) was very similar to that previously calculated. The two Phe rings of 4 and 7 which stacked one on top of the other had moved slightly, to form more of an angle to one another. However, this would still have resulted in a shielding of each of the rings, as observed by ^{1}H NMR.

Distances and dihedral angles were inspected and found to be consistent with NMR data after these minimisation steps.

7.3 Molecular Dynamics Simulation

Using the energy minimised structure dynamics, a simulation at 289K was then carried out. This procedure consisted of three main steps. The first, heating raised the effective temperature from OK (where energy minimisation took place) to 298K over a period of 3 psec. The second step involved an equilibriation of RIP for 6 picoseconds. The simulation was the third step, and ran for a total of 10 picoseconds. During both heating and equilibration, little change was observed in the conformation of RIP, either in terms of backbone or side chain orientations.

Figure 7.2 shows the backbone (-NH-CH-CO-) behaviour of RIP during the 10 psec simulation, each conformation representing a time-step of 1 psec. During this simulation, both Phe rings of residues 4 and 7 moved away from their position of stacking on top of each other to protrude into solvent. Presumably it was energetically more favourable to do so in this instance, when not exposed to a hydrophyl solvent matrix. As a result of the backbone region at Phe(4) showed a large movement from the equilibrium position. The rest of the backbone, however, was fairly conserved in its conformation, and appeared to be moving about a fixed, energetically favourable structure, including the region of the proposed turn, at residues 4, 5, 6 and 7.

These structures obtained from energy minimisation and dynamics simulation can serve as the basis for the design of conformationally restricted analogues which have structures based on these derived solution conformations.

Figure 7.1 3-D model of the predominant conformation of RIP in aqueous solution after energy minimisation.

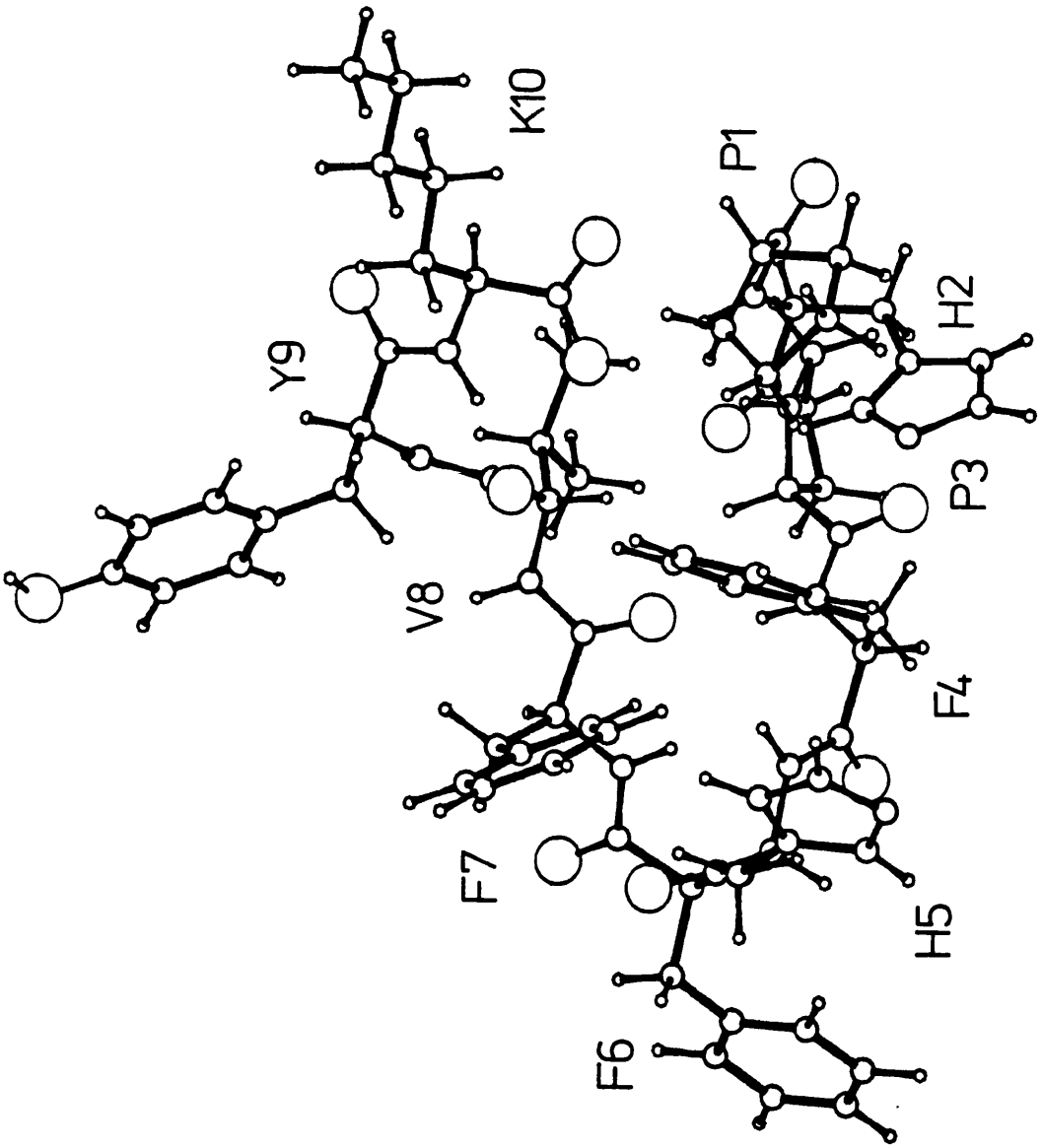
K10
P1
Y9
H2
P3
V8
F4
F7
H5
F6

Figure 7.2 The variation of the backbone of RIP during a molecular dynamics simulation. Each structure represents 1 picosecond, during a 10 picosecond simulation.

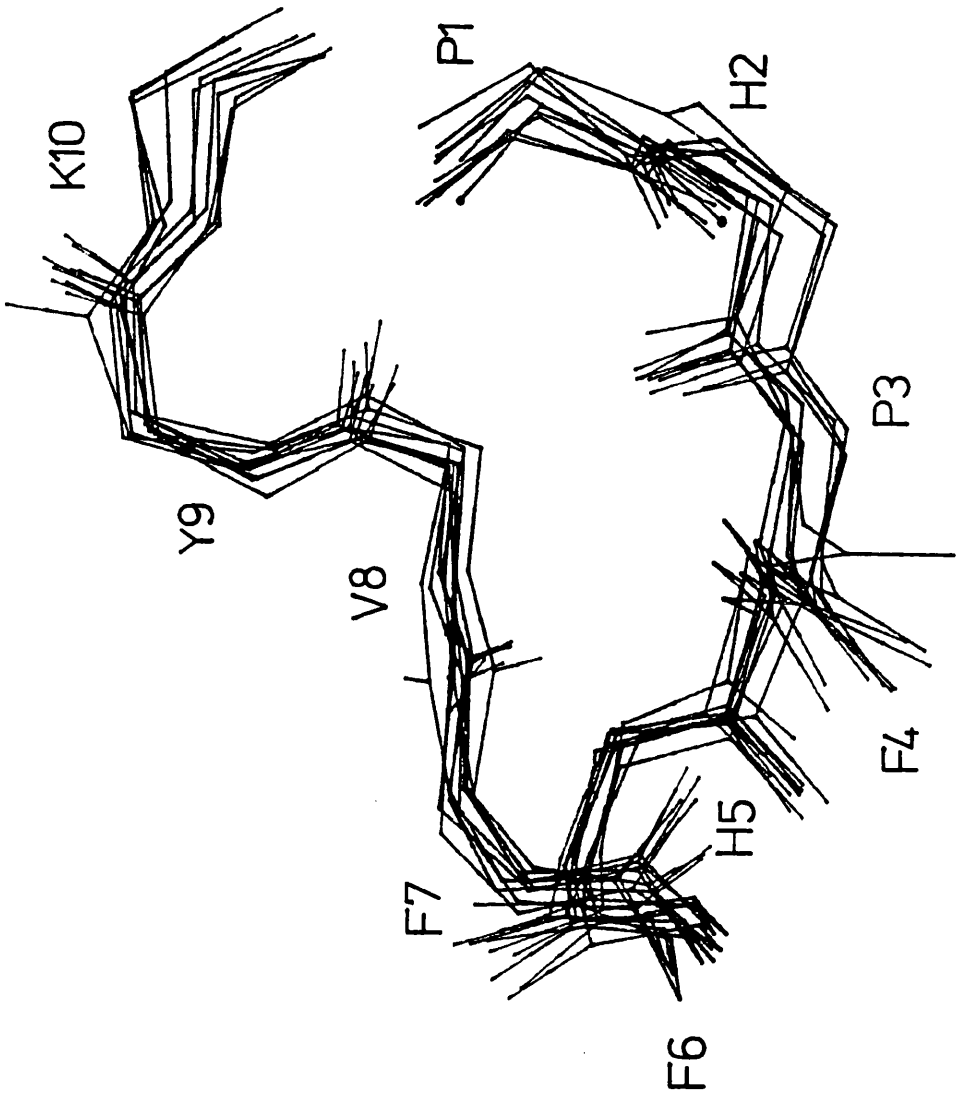
K10
P1
H2
Y9
V8
P3
F4
H5
F7
F6

Chapter8

CONFORMATIONAL ANALYSIS BASED UPON NMR AND CD PARAMETERS

8.1 Conformational Data From Circular Dichroism

8.1.1 Conformational Equilibrium

The conformations adopted by RIP in solution were dependent upon the solvent, as seen by the variation in CD spectrum as a function of solvent polarity. CD spectra recorded as a function of temperature in methanol/glycerol showed large variations until ~-140°C, where a conformational state containing a cis amide bond at Pro(3) was 'frozen out'.

Two isodichroic points were observed during a solvent titration between methanol and trifluoroethanol, proving the existence of a two conformational state equilibrium-state A with a trans Pro(3) amide bond, and a low temperature state, B, which had a cis Pro(3) amide bond. States A and B therefore existed simultaneously in methanol and TFE at room temperature.

In water, no detectable isodichroic points were observed when RIP was titrated with both methanol and trifluoroethanol.

In order to explain the conformational equilibrium in water, it was neccesary to evoke a third conformational state, C.

NMR data proved that states A and B were present in H_2O; state C was hypothesised to consist of a linear extended form of RIP. The presence of C altered the resultant water CD spectrum and meant that solvent titrations (to methanol and TFE) showed no isodichroic points.

The experimental error in measurement of CD spectra was ~10% in each case. It was therefore possible that a small percentage of state C was also present in TFE and methanol solutions of RIP, but was not detectable under experimental conditions.

The overall RIP conformational equilibrium was interpretable in terms of three conformational states, A,B and C. The folded forms A and B may interconvert via an extended conformation C.

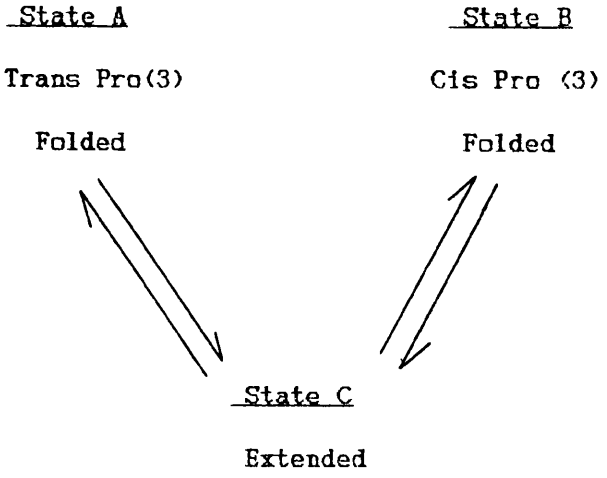

There were a number of other possible explanations (such as States A and B interconverting between one another via an extended conformation). However, the above scheme appeared to fit the available data best.

Solvent, Temperature	%A	%B	%C
TFE, room T	65	35	$\leqslant$10
MeOH, room T	47	53	$\leqslant$10
H_2O, room T	82	18	$>$10
MeOH/glycerol -142° C	0	100	$\leqslant$10

NB: Percentages of A and B were calculated from CD and NMR data without C being taken into account - the actual value of A and B would obviously be reduced by the presence of conformation C.

It was not possible, by CD, to determine the other locus (or loci) of conformational change, other than Pro(3).

8.1.2 Nature of Equilibrium Conformations.

Conformation A:

Simulation of CD spectra based on the known percentages of cis:trans isomerisation for TFE, led to the calculation of the spectrum corresponding to 100% state A, in which Pro(3) existed with a trans amide bond. The resultant spectrum bore some resemblance to that of a type III β-turn in terms of intensities, but showed variations in terms of positions of maxima and minima. This may be indicative of a conformation in which RIP had similarities to that of a β-turn.

Conformation B:

From CD alone nothing could be said regarding the conformations adopted by RIP as a whole, because at the lowest temperatures the CD spectrum was determined by contributions from the cis amide bond chromophore.

8.2. Conformational Data from NMR Parameters

8.2.1 Backbone Conformations

Conformation A:

Most information concerning conformational state A was found, as expected, in studies of RIP in water. Four Pro(3) δ proton resonances were observed; the ROEs from the two most intense of these, to His(2) α proton, confirmed the trans orientation of the peptide bond. Chemical exchange cross peaks, from protons experiencing different chemical environments on a slow timescale, were observed from the two most intense peaks to the two least intense peaks. This confirmed Pro(3) as one of the loci of conformational change (cis-trans isomerisation).

The intramolecular ROEs and dihedral angles, found by ^{1}H NMR in H_2O , were used to generate an energy minimised structure for RIP. A 3-D representation of the model was found in Chapter 7.

Table 8.1 shows the ϕ dihedral angles calculated from J(Cα-NH) coupling constants and those in the RIP molecular model, after removal of unfavourable interactions by energy

minimisation. Also tabulated are the calculated ψ and ω dihedral angles in the RIP model.

The good correlation between observed and energy minimised φ values was taken as an indication that the model was a fair reflection of the conformation adopted by RIP. The one case in which there was no correlation was the His(2) - the amide proton was broadened and the φ value calculated from it was merely an approximation.

Table 8.2 shows the intramolecular ROEs between pairs of protons which should have been observed, based upon the energy minimised RIP conformation; also shown is the distance between these protons, and whether the ROE was observed experimentally. The NH to CO values, for distances less than 3.5 Å are also tabulated.

Model building indicated that a turn occured around the residues Phe(4) - His(5) - Phe(6) - Phe(7), with the formation of a possible hydrogen-bonded structure. The conformation in this region was also determined by side chain considerations as well as that of the peptide backbone.

The dihedral angles at the position of the turn were

$\phi 5 = -78.89°$; $\psi 5 = +71.31°$; $\phi 6 = +47.65°$; $\psi = +32.95°$

These were not characteristic of any one particular turn conformation but were the only values for which the correct side chain orientations from ROE values were attainable. The turn was perhaps best described as a psuedo turn, which was non-ideal because of the effect of side chain stacking. The distance between Phe(4) α and Phe(7) α protons was 7.41Å, outside the

range (≤7.0Å) normally ascribed for residues at either side of a β-turn.

In the turn region there were close contacts between amide and carbonyl moieties which suggested the formation of two hydrogen bonds in this part of the molecule. Phe(7) CO and Phe(4)NH were within 2.94Å of each other, and this type of hydrogen bonded structure is a common feature in stabilisation at β-turn conformations (normally called the 1⟶4 hydrogen bond). The amide resonance showed little (-0.058 ppm) chemical shift variation from that expected in a non-ordered environment, however its close proximity to the phenyl ring of Phe(7) (within 2.98Å) may have offset any chemical shift effects due to hydrogen bonding. This turn region also appeared to be one of the loci of conformational change (see later) and the H-bond suggested by molecular modelling may have been short-lived; the lack of hydrogen bonding character, as determined by the amide chemical shift temperature variation, also suggested a fairly transient lifetime (if it existed at all).

Phe(4) CO and Phe(6) NH (separated by a distance of 2.73Å) may also constitute a hydrogen bond. In this instance, Phe(6)NH showed a movement of -0.398 ppm from the chemical shift of a random environment, and had been previously ascribed as having a degree of hydrogen bonding character.

There was, in general, a good agreement between the predicted rotating frame NOEs and those observed experimentally in the region of the turn. In particular

His(5) α → Phe(7)NH (4.48Å)

Phe(4) α → Phe(6)NH (4.41Å)

although observed as weak ROEs, were crucial in defining the backbone conformation around these four residues. The many backbone-sidechain ROEs were also very important in positioning the sidechain conformations.

There were, however, a number of ROEs which, based on the RIP model, should have been observed, but were not.

Phe(4)NH → Phe(6)NH (4.20Å)

Phe(4)NH → Phe(7)NH (2.82Å)

It was not expected to be able to observe every predicted ROE, because of the flexibility of the peptide backbone and the fact that two loci of conformational change were located within this sequence. Given these facts, the observed list of ROEs correlated well with those predicted.

The RIP model predicted a large number of ROEs between the N and C termini, and these were in general observed experimentally. This region was considered to be more rigid than the turn portion of RIP, because of the better correlation between predicted and observed ROEs.

The ROEs between

Pro(1) α → Lys(10) α (4.76Å)

Lys(10) γ (4.19Å)

in particular indicated the likelihood of an ionic interaction. The other ROEs from within this region supported this hypothesis

i.e. His(2) α → Val(8) γ (3.21Å)

His(2)1m2 → Val(8) α (4.41Å)

Pro(3) α → Val(8) α (2.76Å)

* This indicated an ionic interaction between the N and C termini.

as did the calculated ϕ angles, which were consistent with the RIP salt-bridged model.

A hydrogen bond between Val(8) CO and Lys(10) NH may be formed, as shown in the RIP model (2.75Å separation) Lys(10) NH had a chemical shift difference of -0.768 ppm from a random environment, much greater than the difference found for the corresponding Phe(6)NH and Phe(4)NH H-bonded protons. This may have indicated the formation of a stronger H-bonded due to a more rigid peptide backbone.

Interestingly, both His(2) and Pro(3) amide bonds appeared to have moved away from the energetically favourable value of ~180° (compare with the values for other amide bonds in the peptide, Table 8.1). In the case of Pro(3) (ω = +159.78°) this was perhaps understandable, as the conformation with a cis bond was obviously energetically stable (state B accounted for 18% of RIP solution conformations). However, for His(2) the situation was a little surprising (ω = -152.98°, assuming the modelled structure to be accurate). It may be that a movement away from 180° allowed the formation of a stronger $-NH_2^+ \ldots\ldots CO_2^-$ interaction*, the energy needed to distort the peptide bond being offset by the energy gained during salt-bridge formation.

In methanol and trifluoroethanol, the conformation adopted by RIP in state A was found to be similar to that in H_2O, as expected from CD studies. More of state B existed in these solvents, and it was thus possible to distinguish between the ROEs observed, by their similarities to those in H_2O (from state

A), or those which did not fit this general model (from state B or state C).

The dihedral angles in TFE and methanol were a reflection of the backbone conformation in all forms, and so were difficult to interpret in terms of single conformational states.

In TFE, no detectable backbone-backbone ROEs were observed in the Phe(4) - His(5) - Phe(6) - Phe(7) turn region, again reflecting its flexible nature relative to the terminal fragments.

P(3)δ_t ⟶ V(8) γ

⟶ V(8) β

⟶ V(8) NH

P(3)γ ⟶ V(8) γ

Phe(7)NH ⟶ P(3)δdt

V(3) α ⟶ P(3)δdt

These ROEs were observed in both TFE and H_2O solutions and showed that in the trans folded form, RIP adopted the same predominant conformation.

In methanol, a number of ROEs observed proved that RIP in State A again had a folded conformation very similar to that found in H_2O.

eg His(2)β ⟶ V(8) α

P(3)δt ⟶ V(8) α

P(3)α ⟶ V(8) α

V(8)α ⟶ K(10) γ

K(10)NH ⟶ V(8) α

Conformation B:

The strategy for the determination of conformation B was to observe ROEs not consistent with state A, then use these to construct an approximate structure. Of course, the ROEs assigned to this conformation had to be similar in all three solvents.

In H_2O, cross sections through the cis form Pro(3) δ protons showed no detectable ROEs; nor were any ROEs observed which were not consistent with the modelled RIP conformation. It was thus not possible to obtain any information on this cis form water structure.

In TFE, Pro(3) δc protons gave ROEs to Phe(7)4 proton, which was itself undergoing chemical exchange on the same time-scale as the cis-trans isomerisation. This ROE alone indicated a folded structure, with again an interaction across the chain, in a manner similar to state A. No other characteristic ROEs were detected which would further define conformation B.

~50% of conformation B was adopted in methanol and consequently most information was forthcoming in this solvent. The backbone ROEs

Tyr(9)NH $\longrightarrow$ His(5)NH

Lys(10) α $\longrightarrow$ Pro(3)α

Lys(10) γ $\longrightarrow$ Pro(3)δdc

were indicative of a structure in which the backbone turned back on itself. There appeared to be no salt-bridge in this

instance, as Lys(10) was lying opposite Pro(3), as compared with Pro(1) previously.

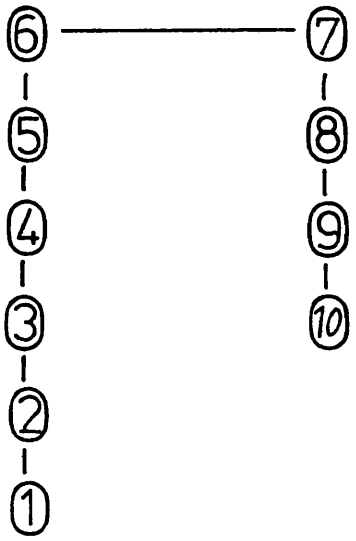

Although no ROEs were detected to confirm it, it seemed likely that the turn occured about the residues His(5) - Phe(6) - Phe(7) - Val(8).

There were therefore two loci of conformational change within RIP, apart from Pro(3),

- the turn region in the trans form, 4-5-6-7
- the turn region in the cis form, 5-6-7-8

which were present in all three solvent systems studied.

Conformation C:

In H_2O and TFE solutions, no detectable NMR evidence was found to confirm the presence of a third conformatinal state, C. In methanol however a number of ROEs, which were not consistent with either state A or B, were observed.

Although conformation C accounted for $\leqslant$10% of RIP conformational space in methanol, if dipole-dipole coupling was strong (close contacts between protons) characteristic ROEs would still be expected to be seen.

An extensive series of $NH_i \longrightarrow NH_{i+1}$ ROEs, from residues Tyr(9) through to Phe(6) showed the presence of a helical type of structure.

This evidence suggested that conformation C was an extended helical type of structure, between at least residues 6-7-8-9. Dipole-Dipole coupling may have been weaker in other parts of RIP, and so ROEs characteristic of state C not observed.

8.2.2 Sidechain Conformations.

For these studies in H_2O, it was felt that the ROEs and rotamer populations would have been a fair reflection of the predominant conformation (state A): in TFE and methanol the rotamer populations and ROEs were more likely a reflection of states A and B.

H_2O:

Table 8.3 shows the χ dihedral angles, taken from the energy minimised RIP molecular model. The rotamer populations calculated (where possible) from ^1H NMR studies are also tabulated for comparison (θ).

As anticipated, the angles calculated from CαH-CβH scalar couplings showed a little variation from the χ values in the RIP energy minimised RIP conformation, reflecting the greater degree of rotational freedom relative to the backbone. In order to

orientate the sidechains in the modelling to correlate with the observed ROEs, certain values of dihedral angles had to be used. For example, many ROEs were detected between Phe(4) and Phe(7) sidechains: the correct alignment of the two (from ring current shifts) was only obtainable with the ϕ, Ψ, χ values tabulated.

The predicted ROEs for this stacking correlated very well with the experimentally obtained ROEs.

e.g.

Phe(4)2,6	⟶ Phe(7)3,5	(3.12Å)
Phe(4)3,5	⟶ Phe(7)2,6	(3.28Å)
	⟶ Phe(7)3,5	(2.92Å)
	⟶ Phe(7)4	(4.34Å)

Also the ROEs

His(5)1m4	⟶ Phe(4)2,6	(3.16Å)
	⟶ Phe(4)3,5	(3.08Å)
	⟶ Phe(4)4	(4.86Å)
	⟶ Phe(7)3,5	(4.35Å)

were used to position this sidechain in the RIP model. Again after energy minimisation, good correlation was found between predicted and experimentally observed ROEs.

His(2) imidazole side chain was orientated towards Val(8), across the 'cyclised' structure. This correct orientation was obtained in the model

His(2)1m2	⟶ Val(8) α	(4.41Å)
	⟶ Val(8) α	(4.74Å)

obaining reasonable correlation between experimental and modelled χ dihedral angles.

Val(8) sidechain was orientated on the opposite side of the folded structure relative to the H5-F4-F7 stacking, to correlate with the weak ROEs observed to Phe(4) phenyl ring, (but not to Phe(7) sidechain)

Phe(4)2,6 → V(8) γ (4.55Å)

Phe(4)3,5 → V(8) γ (4.87Å)

The sidechains of Phe(6), Tye(9) and Lys(10) gave no detectable ROEs and were thus placed to make no close contacts in the folded RIP model, pointing away from the highly folded regions.

In conclusion then, the RIP model in water, although by no means a unique structure for the experimental parameters, held up under close scrunity, correlating well with the experimental NMR observations.

TFE and MeOH:

In TFE, Phe(7) sidechain experienced two different chemical environments one of which, the cis form, gave ROEs to Pro(3) δuc. Both Pro(3)δc resonances showed ROEs to Phe(7)2,6 protons. In state B, therefore, which may have existed with a turn at 5-6-7-8, Phe(7) sidechain lay across the turn, in proximity to Pro(3). In the trans form the lack of detectable ROEs from Phe(4)4 proton indicated the phenyl ring had most likely swung away from the folded turn region, and experienced a different chemical environment as a result.

ROEs from P(3)δut ⟶ Phe(4)2,6

P(3) γ ⟶ Phe(4)2,6

⟶ Phe(4)3,5

P(3)βd ⟶ Phe(4)2,6

indicated that, relative to RIP in water, Phe(4) phenyl group now faced away from the turn region and lay towards the back of the Pro(3) ring.

Lack of sidechain - sidechain and sidechain - backbone ROEs for His(2), Tyr(9) and Lys(10) were taken as an indication of their non-involvement in the folded regions of RIP.

RIP in methanol was characterised by a lack of sidechain ROEs, to either backbone or other sidechain protons. Of interest however was

His(5)1m2 ⟶ Phe(4)2,6

⟶ Phe(4)3,5

These ROEs indicated a distance of 5Å between these two sidechains. It was not possible to know, or predict, which conformational state (or states) was consistent with this interaction. His(5)1m2 showed a movement in chemical shift of +0.230 ppm from a random environment, a value indicative of ring current shifting due to the close proximity of aromatic residues. The positive sign showed deshielding effect, the imidazole proton being in the plane of the aromatic ring.

Table 8.1

Residue	ϕ (observed)	ϕ (model)
Lys (10)	-151°	-159.48°
Tyr (9)	+71°	+65.52°
Val (8)	-144°	-139.78°
Phe (7)	-152°	-166.44°
Phe (6)	+40°	+47.65°
His (5)	-92°	-78.97°
Phe (4)	-158°	-154.28°
Pro (3)	-	-58.08°
His (2)	-94°	+163.79°
Pro (1)	-	-

Table 8.1

Residue	¥ (model)	ω (model)
Lys (10)	-	-177.69°
Tyr (9)	-72.17°	-173.62°
Val (8)	-78.64°	+178.92°
Phe (7)	-172.55°	+179.05°
Phe (6)	+32.95°	-175.61°
His (5)	+71.31°	-173.66°
Phe (4)	-90.27°	+175.23°
Pro (3)	+135.00°	+159.78°
His (2)	+172.14°	-152.98°
Pro (1)	+3.42°	-

Table 8.2 √ = observed
x = not observed
- = unable to determine this ROE experimentally

ROE from	to	Model Distance Å	Observed
Pro(1) δ_1	F(4)β2	4.30	√
	F(4)2,6	3.41, 4.72	x
	F(4)3,5	4.32	x
	F(4)4	3.40	x
δ_2	F(4)2,6	4.65	x
	F(4)3,5	4.74	x
	F(4)4	3.12	x
α	K(10)α	4.76	√
	K(10)γ	4.19	√
γ1,2	F(4)2,6	4.63	x
	F(4)3,5	4.30, 4.92	√
His(2) NH	F(4)2,6	4.52	-
	F(4)3,5	4.22	-
	V(8)γ	4.70,3.69,3.22	-
	K(10)NH	4.33	-
	K(10)α	4.40	-
α	V(8)γ	4.33,4.35,3.21	√
β_1	F(4)β2	4.55	√
	V(8)γ	4.88	x
Im2	F(4)NH	4.47	√
	F(4)α	4.89	x
	F(4)2,6	3.93,3.27	√
	F(4)3,5	4.44,3.83	x
	F(4)4	4.38	x
	F(4)β1,2	4.42,3.04	√
	V(8)α	4.41	√
	V(8)γ	4.74	√

ROE from		To	Model Distance Å	Observed
	Im4	F(4)β1,2	4.97,3.95	-
		F(4)2,6	4.31	-
Pro(3)	δ_1	V(8)γ	4.85,4.38	✓
	δ_2	V(8)γ	4.57,4.40,3.95 3.65,3.05	✓
	α	F(7)NH	4.20	x
		F(7)α	4.97	x
		F(7)2,6	4.47	x
		V(8)NH	4.77	x
		V(8)α	2.76	✓
		V(8)β	4.53	x
		V(8)γ	4.63,4.31,3.65 3.46,3.09,1.92	✓
	β_1	V(8)γ	4.30	✓
	β_2	F(7)NH	4.99	-
		V(8)γ	4.87,4.32 4.24,3.02	-
	γ	V(8)γ	4.17,3.93,3,91 3,69,2.71	-
Phe(4)	NH	Phe(6)NH	4.20	x
		Phe(7)NH	2.82	x
		Phe(7)α	4.80	x
		Phe(7)2,6	2.98	✓
		Phe(7)3,5	4.41	x
		V(8)α	3.43	✓
		V(8)γ	4.90,4.77,3,81	x
	α	Phe(6)NH	4.41	✓
		Phe(7)NH	4.87	x

Table 8.2

ROE from	To	Model Distance Å	Observed
β_1	His(2)Im2	4.42	✓
	His(2)Im4	4.97	-
β_2	Phe(7)2,6	4.44	-/
	Pro(1)δ_1	4.30	✓
	His(2)Im2	3.04	✓
	His(2)Im4	3.95	-
2,6	Pro(1)δ1,2	4.72,4.65,3.41	x
	Pro(1)γ	4.63	x/
	His(2)Im2	3.93	✓
	His(2)Im4	4.31	x
	Phe(7)3,5	4.33,3.12	✓
	V(8)NH	4.73	✓
	V(8)α	2.80	✓
	V(8)γ	4.67,4.55	✓
3,5	Phe(7)3,5	4.16,2.92	✓
	Phe(7)2,6	3,28	✓
	Phe(7)4	4.95,4.34	✓
	Pro(1)δ1,2	4.74,4.31	x/
	Pro(1)γ	4.91,4.30	✓
	His(2)Im2	4.44,3.83	x
	His(2)NH	4.22	-/
	V(8)NH	4.27	✓
	V(8)α	2.81	✓
	V(8)γ	4.87	✓
	Y(9)β1,2	4.85,4.03	-/
	K(10)NH	3.55	✓
4	Pro(1)δ1,2	3.40,3.13	x
	His(2)Im2	4.38	x/
	Phe(7)3,5	3.50	✓
	Phe(7)4	4.03	✓
	K(10)NH	4.26	x

ROE from	To	Model Distance Å	Observed
His(5)NH	Phe(7)NH	3.54	x
	Phe(7)2,6	2.53	x
	Phe(7)3,5	2.19	✓
	Phe(7)4	4.49	x
α	Phe(7)NH	4.25	✓
	Phe(7)2,6	4.48	✓
	Phe(7)3,5	4.53	✓
β1,2	Phe(7)NH	4.40	x
	Phe(7)2,6	4.92,4.78,3.30	x
	Phe(7)3,5	4.36,4.08,2.45	✓
	Phe(7)4	4.62,3.14	✓
Im2	Phe(4)β1	3.76	x
	Phe(4)2,6	4.82	✓
Im4	Phe(4)β1	4.57	✓
	Phe(4)2,6	3.16	✓
	Phe(4)3,5	3.08	✓
	Phe(4)4	4.86	✓
	Phe(7)3,5	4.35	✓
	Phe(7)4	4.72	x
Phe(7) β1	Tyr(9)NH	4.37	✓
	Tyr(9)β1	4.25	-
	Tyr(9)2,6	3.75	-
Val(8) NH	Lys(10)NH	4.97	✓
α	Lys(10)NH	4.07	✓
β	Lys(10)NH	4.82	✓
γ	Lys(10)NH	3.77,4.85	✓
	Lys(10)α	3.84	

Residues	O ⊖ N Distance (Å)
Phe(4)CO.....Phe(6)NH	2.73
Phe(7)CO.....Phe(4)NH	2.94
Val(8)CO.....Lys(10)NH	2.75

Table 8.3

Residue	χ Model	Rotamer Population
Lys(10)	-167.46°	28% gauche
Tyr(9)	-114.30°	-
Val(8)	-171.03°	48% gauche
Phe(7)	+63.85°	-
Phe(6)	-82.57°	40% gauche
His(5)	-47.49°	28% gauche
Phe(4)	51.37°	-
Pro(3)	-27.20°	θ = 20°, 18°
His(2)	45.32°	26% gauche
Pro(1)	-23.01°	θ = 20°, 20°

References

Andreeva, N.S., Zdanov, A.S., Gutschina, A.E. and Fedorov A.E., 1984, J. Biol. Chem, 259, 11353.

Applequist, J. 1982, Biopolymers, 21, 779.

Arrowsmith, R.J., Carter, K., Dann, J.G., Davies, D.E., Harns, C.J., Morton, J.A., Lister, P., Robinson, J.A. and Williams, D.J., 1986, J. Chem. Soc., Chem. Comm, 755.

Ave, W.P., Bartholdi, E. and Ernst, R.R. 1976, J. Chem. Phys., 64, 2229.

Baron, J.S. and Hanson, G.J., 1986, European Patent Application 0, 202, 577.

Bartlett, P.A., and Kezer, W.B., 1984, J. Am. Chem. Soc., 106, 428.

Bax, A. and Davies, D.G., 1985, J. Mag. Res., 65, 355.

Bax, A. and Davies, D.G., 1988, J. Mag. Res., 77, 134.

Bax, A., Freeman, R. and Morris, G., 1981a, J. Mag. Res., 12, 164.

Bax, A., Freeman, R. and Morris, G., 1981b, J. Mag. Res., 44, 452.

Bax, A. and Lerner, L., 1986, Science, 232, 960.

Biollaz, J., Brunner, D.B., Burnier, M., Turrini, G.A., Porchet, M., Gomez, H.J., Jones, K.H., Ferber, F and Abrams, W.B., 1981, Clin. Pharmacol. Therap., 29, 665.

Birkenhager, W.H. and Reid, J.L., Handbook of Hypertension Vol. 3, Pharmacology of Hypertensive Drugs, Elsevier, Amsterdam.

Blaine, E.H., 1986, Fed. Proc., 45, 2375.

Blundell, T.L., Sibanda, B.L., and Pearce, L., 1983, Nature, 304, 273.

Boger, J., 1983, Pept., Struct, Funct., Proc. 8th Am. Pept. Symp., Pierce Chemical Co. Ill., 569.

Boger, J., 1985a, In Aspartic Proteinases and Their Inhibitors, Walter de Guyter, Berlin, 401.

Boger, J., Lohr, N.S., Ulm, E.H., Poe, M., Blaine, E.H., Fanelli, G.M., Lin, T.Y., Payne, L.S., Schorn, T., LaMont, B.I., Vassil, T.C., Stabilito, I.I., Veber, D.F., Rich, D.H. and Bopari, A.S., 1983, Nature, 303, 81.

Boger, J., Payne, L.S., Perlow, D.S., Lohr, N.S., Poe, M., Blaine, E.H., Ulm, E.H., Schorn, T.W., LaMont, B.I., Lin, T.Y., Kawai, M., Rich, D.H. and Veber, D.F., 1985b, J. Med. Chem., 28, 1779.

Bothner-By, A.A., Stephens, R.L., Lee, J.M., Warren, C.D. and Jeanloz, R.W., 1984, J. Am. Chem. Soc., 106, 811.

Bott, R., Subramanian, E. and DAvies, D.R., 1982, Biochem, 21, 6956.

Bouhnik, J., Galen, F.X., Menarol, J., Corvol, P., Seyer, R., Fehrentz, J., Nguyen, D.L., Fulcrand, P. and Castro, B., 1987, J. Biol. Chem., 262, 2913.

Brahms, S. and Brahms, J., 1980, J. Mol. Biol., 138, 149.

Bundi, A. and Wuthrich, K., 1979, Biopolymers, 18, 285.

Burton, J., Cody, Jr, R.J., Herd, J.A. and Haber, E., 1980, Proc. Natl. Acad. Sci., 77, 5476.

Eid, M., Evin, G., Castro, B., Menard, J. and Corvol, P. 1981, Biochem. J., 197, 465.

Burton, J., Hyun, H. and Tenbrink, R.E., 1983, Pept., Struct. Funct., Proc. 8th Am. Pept. Symp., Pierce Chemical Co. Ill., 559.

Bystrov, V.F., 1976, Prog. NMR Spec., 10, 41.

Campbell, I.D., Dobson, C.M. and Williams, R.J.P., 1985, Biochem. J., 231, 1.

Carlson, M., Karplus, M. and Haber, E., 1985, Hypertens., 7, 13.

Cody, R.J., Burton, J., Evin, G., Poulson, K., Herd, J.A. and Haber, E., 1980, Biochem. Biophys. Res. Comm., 97, 230.

Cushman, D.W., Cheung, H.S., Sabo, E.F. and Ondetti, M.A., 1977, Biochem., 16, 5484.

Dellaria, Jr., J.F. and Maki, R.G., 1986, Tet. Lett., 27, 2337.

Drake, A.F., Siligardi, G. and Gibbons, W.A., 1988, Biophys. Chem., 31, 143.

Dwek, R.A., 1973, NMR in Biochemistry, Applications to Enzyme Systems, Clarendon Press, Oxford, 48.

Dzau, V.J., Kopelman, R.I., Borger, A.C. and Haber, E., 1984, Am. J. Physiol., 246, H404.

Farrar. T.C. and Becker, E.D., 1971, Pulse and FT NMR, Academic Press, New York, 20.

Fearon, K., Spaltenstein, A., Hopkins, P.B. and Gelb, M.H., 1987, J. Med. Chem., 30, 1617.

Fehrentz, J.A., Heitz, A., Castro, B., Cazaubon, C. and Nisato, D., 1984, FEBS Lett., 167, 273.

Foundling, S.I., Cooper, J., Watson, F.E., Cleasby, A., Pearl, L.H., Sibanda, B.L., Hemmings, A., Wood, S.P., Blundell, T.L., Valler, M.J., Norey, C.G., Kay, J., Boger, J., Dunn, B.M.,

Leckie, B.J., Jones, D.M., Atrash, B., Hallett, A. and Szelke, M., 1987, Nature, 327, 349.

Franco-Morselli, R., Elghozi, J. and Joly, E, 1977, Brit. Med. J., 2, 1251.

Fray, J.C.S. 1980, Circ. Res., 47, 485.

Freelander, A.E. and Goodfriend, T.L., 1979, Methods of Hormone Immunoassay, 2nd Edition, Academic Press, New York, 889.

Freeman, R., 1988, Handbook of NMR, Wiley, New York.

Freidinger, R.M., Veber, D.F., Perlow, D.S., Brooks, J.R. and Saperstein, R., 1980, Science, 210, 656.

Gaillard, I., Fehrentz, J.A., Simon, D., Badovaille, G., Seyer, R., CAstro, B., Pau, B. and Corvol, P., 1986, FEBS. Lett., 207, 100.

Gould, A.B., Skeggs, L.T. and Kahn, J.R., 1966, Lab. Invest., 15, 1802.

Haber, E. and Burton, J., 1979, Fed. Proc., 38, 2768.

Haber, E., Koerner, T., Page, L.B., Kliman, B. and Purnode, A., 1969, J. Clin. Endocrin., 29, 1349.

Hanson, G.J., Baran, J.S., Lindberg, T., Walsh, G.M., Papaioannou, S.E., Babler, M., Bittner, S.E., Yang, P.C. and Corrobo, M.D., 1985, Biochem. Biophys. Res. Comm., 132, 155.

Hosoki, K., Miyazaki, M. and Yamamoto, K., 1977, J. Pharmacol. Exp. Therap., 203, 485.

Hui, K.Y., Carlson, W.D., Bernatowicz, M.S. and Haber, E., 1987 J. Med. Chem., 30. 1287.

Iimura, O., Shimamoto, K., Tanaka, S., Hosoda, S., Nishitani, T., Ando, T. and Masuda, A., 1986, Jap. J. Med., 25., 34.

Iizuke, K., Kamijo, T., Kubota, T., Akahane, K., Umeyama, H. and Kiso, Y., 1988, J. Med. Chem, 31, 701.

Ivanov, V.T., Filatova, M.P., Reissman, Z., Reutova, T.O., Effremov, E.S., Pashkov, V.S., Galaktionov, S.G., Grigoryan, G.L. and Ouchinnikov, Y.Aa., 1975, Pept. Chem. Struct. Biol., Proc. 4th Am. Pept. Symp., Ann Arbor, Michigan. 151.

James, M.N. and Sielecki, A.R., 1985, Biochem., 24, 3701.

Jeener, J., 19871, Ampere International Summer School, Basko Polje, Yugoslavia.

Jeener, J., Meier, B.H., Bachmann, P. and Ernst, R.R., 1979, J. Chem. Phys., 71, 4546.

Johnson, R.L., 1984, J. Med. Chem., 27, 1351.

Johnson, Jr., W.C., 1978, Ann. Rev. Phys. Chem., 29, 93.

Johnson, Jnr., W.C. and Tinico, Jr., I., 1972, Am. Chem. Soc., 94. 4389.

Jones, M., Suerias-Diaz, J., Szelke, M., Leckie, B.J. and Beattie, S., 1985, Pept. Struct. Funct. , Proc. 9th Am. Pept. Symp., Pierce Chemical Co., Rockford, Ill., 759.

Kessler,H., Griesinger, C., Kerssebaum, R., Wagner, K.,and Ernst, R.R., 1987, J. Am. Chem. Soc., 109, 607.

Kessler, H., Gehrke, M. and Griesinger, C., 1988, Agnew, Chem. Int. Ed. Eng., 27, 490.

Kobuku, T., Hiwada, K., Sato, Y., Iwata, T., Imamura, Y., Matsueda, Y., Yabe, R., Kogen, Y., Yamazaki, H., Iijima, Y. and Baba, Y., 1984, Biochem. Biophys. Res. Comm., 118, 929.

Kuo, M.C. and Gibbons, W.A., 1980, Biophys. J., 32, 807.

Leckie, B.J., Szelke, M., Atrash, B., Beattie, S.R., Hallett, A., Jones, D.M., McIntyre, G.D., Sueiras, J. and Webb, D.J., 1985, Biochem. Soc. Trans., 13, 1029.

Liepina, I., Nikiforovich, G.V., Paiva, A.C.M. and Antonio, C.M., 1984, Biochem. Biophys. Res. Comm., 122, 700.

Liu, C.F., Fehrentz, J.A., Heitz, A., LeNguyen, D., Castro, B., Heitz, F., Corelli, C., Galen, F.X. and Corvol, P., 1988, Tet., 44, 675.

Luly, J.R., Plattner, J.J. , Rosenberg, S.H. and KiFung, A., 1986, European Patent Application 0, 198, 203.

Luly, J.R., Plattner, J.J., Stein, H., Yi, N., Soderquist, J., Marcotte, P.A., Kleinert, H.D. and Perun, T.J., 1987, Biochem. Biophys. Res. Comm., 143, 44.

Madison, V. and Schellman, J., 1970, Biopolymers, 9, 511.

Marion, D. and Wuthrich, K., 1983, Biochem. Biophys. Res. Comm., 113, 967.

Morris, G.A. and Freeman, R., 1978, J. Mag. Res., 29, 433.

Navia, M., Springer, J.P., Poe, M., Boger, J. and Hoogsteen, K., 1984, J. Biol. Chem. 259, 12714.

Noggle, J.H. and Schirmer, R.E., 1971, The Nuclear Overhauser Effect, Academic Press, New York.

Olejniczak, E.J., Poulson, F.M. and Dobson, C.M., 1981, J. Am. Chem. Soc., 106, 1923.

Ondetti, M.A. and Cushman, D.W., 1978, Ann. Rep. Med. Chem., 13, 82.

Ondetti, M.A. and Cushman, D.W., 1982, Ann. Rev. Biochem., 51, 283.

Ondetti, M.A., Cushman, D.W. and Rubin, B., 1983, In Chronicles of Drug Discovery, Vol. 2, Wiley, New York, 1.

Pals, D.T., Thaisrivongs, S., Lawson, J.A., Kati., M., Turner, S.R., Degraff, G.L., Harris, D.W. and Johnson, G.A., 1986, Hypertens., 8, 1105.

Pearl, L.H. and Blundell, T.L., 1984, FEBS. Lett., 174, 96.

Plattner, J.J., Green, J., Fung, A.K.L., Stein, H., Kleinert, H.D., Sham, H.L., Smital, J.R. and Perum, T.J., 1986, Biochem. Biophys. Res. Comm., 139, 982.

Poorman, R.A., Palermo, D.P., Post, L.E. Murakami, K., Kinner, J.H., Smith, C.W., Reardon, I. and Heinrikson, R.K., 1986, Prot. Struct. Funct. Gen., 1, 139.

Powers, J.C., Harley, A.D. and Myers, D.V., 1977, In Acid Proteinases-Structure, Function and Biology, Plenum, New York. 141.

Rich, D.H., 1985, J. Med. Chem., 28, 263.

Rich, D.H., 1986, In Proteinase Inhibitors, Elsevier, Amsterdam, 179.

Rich, D.H., Bernatowicz, M.S. and Schmidt, P.G., 1982, J. Am. Chem. Soc., 104, 3535.

Rosenberg, S.H., Plattner, J.J., Woods, K.W., Stein, H.H., Marcotte, P.A., Cohen, J. and Perum, T.J., 1987, J. Med. Chem., 30, 1224.

Rotmensch, H.H., 1984, Fed. Proc., 43, 1333.

Sen. S., Smeby, R.R. and Bumpus, F.M., 1967. Biochem., 6, 1572.

Sen. S., Smeby, R.R. and Bumpus, F.M., 1968, Am. J. Physiol., 214, 337.

Sawyer, T.K., Pals, D.T., Mao, B., Maggiora, L.L., Staples, D.J., deVaux, A.E., Schostarez, H.J., Kinner, J.H. and Smith, C.W., 1988a, Tet. Lett., 44, 661.

Sawyer, T.K., Pals, D.T., Mao, B., Staples, D.J., deVaux, A.E., Maggiora, L.L., Affholter, J.A., Kati, W., Duchamp, D., Hester, J.B., Smith, C.W., Saneii, H.H., Kinner, J., Handschumacher, M. and Carlson, W., 1988b, J. Med. Chem., 31, 18.

Schriver, P.W., Berl, T. and Andersson, R.J., 1979, Am. J. Physiol., 23, F321.

Sham, H., Rempel, C., Plattner, J.J., Stein, H., Cohen, J. and Perum, T.J., 1986, Abstracts, 191st Meeting of the American Chemical Society, New York, MEDI 8.

Sibanda, B.L., Blundell, T., Hobart, P.M., Foogliano, M., Bindra, J.S., Dominy, B.W. and Chirgwin, J.M., 1984, FEBS. Lett., 174, 102.

Siligardi, G., Drake, A.F., Mascagni, P., Neri, P., Lozzi, L., Niccolai, N. and Gibbons, W.A., 1987, Biochem. Biophys. Res. Comm., 143, 1005.

Skeggs, L.T., Dorer, F.E., Levine, M., Lentz, K.E. and Kahn, J.R., 1980, In The Renin Angiotensin System, Plenum, New York, 1.

Skeggs, L.T., Lentz, K., Kahn, J.R. and Hochstrasser, H., 1968, J. Exp. Med., 128, 13.

Smith, C.W., Saneii, H.H., Sawyer, T.K., Pals, D.T., Scahill, T.A., Kamdar, B.V. and Lawson, J.A., 1988, J. Med. Chem., 31, 1377.

Sprague, P.W. and Powell, J.R., 1985, In Ann. Rep. Med. Chem., 20, 61.

Stein, H., Cohen, J., Tricarico, K., Sham, H., Rempel, C., Perum, T.J. and Plattner, J.J., 1986, Fed. Proc., 45, 869, Abstract 4151.

Stewart, J.M. and Young, J.D., 1984, Solid Phase Peptide Synthesis, Pierce Chemical Co., Rockford, Ill.

Swales, J.D. 1979, Pharmacol. Ther., 7, 173.

Szelke, M., Jones, D.M., Atrash, B., Hallett, A and Leckie, B.J., 1983, Pept., Struct. Funct., Proc. 8th Am. Pept. Symp. Pierce Chemical Co., Rockford, Ill., 579.

Tang, J., 1979, Molec. Cell Biochem., 26, 93.

Tenbrink, R.E., Pals, D.T., Harris, D.W. and Johnson, G.A., 1988, J. Med. Chem., 31, 671.

Thaisrivongs, S., Pals, D.T., Kati, W.M., Turner, S.R., Thomasco, L.M. and Watt, W., 1986, J. Med. Chem., 29, 2080.

Thaisrivongs, S., Pals, D.T., Lawson, J.A., Turner, S.R. and Harris, D.W., 1987, J. Med. Chem., 30, 536.

Thaisrivongs, S., Pals, D.T., Turner, S.R. and Kroll, L.T., 1988, J. Med. Chem., 31, 1369.

Turcotte, J.G., Yu, C., Lee. H. and Pavanarum, S.R., 1975, J. Med. Chem., 18, 1184.

Vallotton, M.B., 1987, TIPS, 8, 69.

Veber, D.F., Bock, M.G., Brady, S.F., Ulm, E.H., Cochran, D.W., Smith, G.M., Lamont, B.I., DiParolo, R.M., Poe, M., Freidinger, R.M., Evans, B.E. and Boger, J., 1984, Biochem. Soc. Trans., 12, 956.

Wakerlin, G.E. 1958, Circulation, 17, 653.

Wider, G., Macura, S., Kumar, A., Ernst, R.R. and Wuthrich, K., 1984, J. Mag. Res., 56, 207.

Wood, J.M., Gulati, N., Forgiarini, P., Fuhrer, W. and Hofbauer, K.G., 1985, Hypertens., 7, 798.

Wood, J.M., Heusser, C., Gulati, N., Forgiarini, P. and Hofbauer, K.G., 1985, Hypertens., 8, 600.

Woody, R.W., 1974, Pept., Polypept. and Prot., Wiley, New York, 339.

Woody, R.W., 1978, Biopolymers, 17,1451.

Woody, R.W., 1985, Pept., Anal. Synth. Biol., Vol 7, 29.

Wuthrich, K., 1986, NMR of Proteins and Nucleic Acids, Wiley, New York. 117.

Wyvratt, M.J. and Patchett, A.A., 1985, Med. Res. ReEv., 5. 483.